Assessing the Performance and Climate Effects of Future Supersonic Transport

M.P. den Boer

TU Delft

Assessing the Performance and Climate Effects of Future Supersonic Transport

by

M.P. den Boer

in partial fulfillment of the requirements for the degree of

Master of Science
in Aerospace Engineering

at the Delft University of Technology
to be defended publicly on Wednesday June 12, 2019 at 15:00

Project duration:	February 3, 2018 – June 12, 2019	
Thesis supervisor:	Ir. J. A. Melkert, TU Delft	
Thesis committee:	Prof. dr. ir. L. L. M. Veldhuis	TU Delft, chairman
	Ir. J. A. Melkert	TU Delft, supervisor
	Prof. dr. V. Grewe	DLR & TU Delft

Cover image by Johnathan Safford taken (#0413742) from airliners.net
A digital version of this thesis is available at https://repository.tudelft.nl/

TU Delft

Acknowledgments

This report describes the effort that was put into the evaluation of the (environmental) performance of new supersonic transport aircraft through the creation of a new design program. It is the result of nearly twelve months of work, and is part of the Master's thesis project at TU Delft, which forms the capstone of my education in aerospace engineering. All this would not have been possible without the help of others, who I want to thank here.

First of all, I want to thank my supervisor Joris Melkert for his continuous enthusiasm and support, showing me that compromises sometimes need to be made in order to achieve the optimal end results, and always being available for questions. I would also like to thank my thesis co-student Jordy Nijsse for helping me with building the supersonic design program, and Roelof Vos for assisting us with the structuring of the design program modules, to ensure that we were on the right track.

My environmental results would not have been possible without the help of Volker Grewe and Irene Dedoussi. Through meetings about the use of climate models (AirClim) and climate functions for the climate impact analysis of supersonic aircraft, as well as providing useful literature, my understanding of the topic and the quality of work has greatly improved. Additionally, I want to thank Dan Rutherford and Tim MacDonald for answering my questions about the reference engine emission index method in a recent study, and for having a discussion about the clean-sheet design for new supersonic aircraft engines. I also want to thank Paul Roling for allowing me to use the full version of the Piano-X program so that I was able to gather the required subsonic aircraft reference data.

Furthermore, I want to thank the team behind the ParaPy software for helping me solve several issues I encountered while using their software, in particular in assisting me with the creation of the functions used to determine the cross-sectional area distribution of the 3D aircraft geometry. As a special mention I would like to thank Egbert Torenbeek for showing me the key factors that contribute to the design of supersonic aircraft through his past experiences, as well as providing me with useful literature not (widely) available to students.

Last but not least, I want to thank my parents and brother, other relatives, and friends for supporting me during the (almost) six years that I spent at the faculty of Aerospace Engineering. Being a student at the TU Delft has taught me many new things, and provided me with a solid basis with which I can go into the next stage of my career. Therefore, in my final words of appreciation I want to thank Delft University of Technology for giving me the opportunities to improve myself.

M.P. den Boer
Delft, June 12 2019

Executive Summary

In recent years, the world has become more aware of climate change, and aims to reduce global emissions. Aviation is an important contributor to climate change because its emissions are produced at higher altitudes where their impact is enhanced. Despite this, air traffic is expected to grow at 3-5% annually in the coming decades, further increasing its climate change contribution. In this landscape, several companies plan to launch new supersonic transport (SST) aircraft. Because the current civil supersonic environmental regulations are based on experiences with Concorde, which was built in the 1960s and last flew in 2003, the International Civil Aviation Organization (ICAO) has requested that an investigation be performed to determine what can be expected of new supersonic aircraft. Results found will then be used to evaluate the current environmental regulations and locate problems, so that they can be studied in-depth in the future. Because of the amount of effort required, two theses are produced, this one with a focus on the design program and climate effects, and the second with a focus on design sensitivity and noise.

To generate the supersonic aircraft, a design program was coded in Python, where several modules were integrated into a single program. Some of the modules use object-oriented programming so that they can be replaced or extended with relative ease in future research. The design modules in the current program are the Class I, wing loading, engine design, aircraft design, aerodynamics, and Class II analyses.

The Class I module uses the fuel fraction method to estimate the fuel weight fraction, which with an operating empty weight found from a curve fit or the Class II module, allows for takeoff weight estimation. The module was tested on the Concorde, Tu-144, and ten design studies, and showed an average error of 5.6% for takeoff weight prediction. Using the module it was also shown that supersonic aircraft are very sensitive to the specific fuel consumption and aerodynamic efficiency, which is the result of their low payload fraction.

The wing loading analysis uses 12 constraints to find the feasible design region and the design point. Combined with the known takeoff weight, the wing area and takeoff thrust are then estimated. The engine thrust, together with engine data such as the component efficiency values, overall pressure and bypass ratio, is then used to perform engine cycle calculations, both for the takeoff sizing condition, and off-design subsonic cruise segments. The current off-design method does not work for the supersonic cruise and low-thrust settings. Next, using the sized engine and known wing area, as well as several user inputs like the wing aspect ratio, the aircraft geometry is produced which is built up from a fuselage, double delta wing, and horizontal and vertical tail. More information about these modules can be found in the second thesis.

Following this, the aerodynamics module evaluates the low-speed performance of the aircraft through the Polhamus method for delta wings. Together with a low-fidelity high-lift device sizing routine, the maximum lift coefficients are estimated for the landing and takeoff configuration. Additionally, the lift- and drag routines for the supersonic and subsonic cruise are executed to estimate the L/D-ratios for all Class I mission segments. An error of less than 5% was found for the supersonic L/D-ratio after testing it on past designs.

The Class II module is the component in the main design routine, and estimates the weight of a large number of aircraft components to get a more reliable estimate of the operating empty weight. Before this, the ultimate load factors are estimated through a gust analysis to generate a flight envelope. The operating empty weight is broken down into four main groups: structures, propulsion, equipment, and operations items. The best functions for each component were selected and calibrated by using data from Concorde. To correct for improvements in technological and materials science, technology factors are selected and added.

After providing the program with the top-level requirements for a supersonic aircraft design, as well as some additional inputs like the aircraft name and storage location, it will iterate over the different modules in the order discussed above, until the Class I takeoff weigh has converged to within 0.1% of the one or more successive iterations. The design program was tested by trying to create aircraft similar to those in design studies by using similar inputs and requirements. This showed that the aircraft takeoff weight was predicted to within less than 5% of the reference weight on average, which given the low fidelity of the program is very good. It also manages to produce these aircraft designs with runtimes of less than five minutes. With the program completed, five designs were produced for a range of 4,600-5,000 NM, and a capacity of 18 to 250 passengers, which fly at Mach 1.6. These requirements were selected to cover the full range of potential aircraft designs, even though a 250 passenger aircraft is considered unlikely for the near future.

The resulting supersonic transport (SST) designs show that the supersonic aircraft have lower payload fractions than comparable subsonic aircraft, and are also heavier, requiring more fuel to travel the same distance. Compared to the Gulfstream G550, a supersonic business jet will require about 2.5 times as much fuel for a 4,600 nautical mile stretch while carrying 12 passengers. Similarly, the SST250 will use about 3.6 times as much fuel as a Boeing 787-8 on a 5,000 nautical mile mission while carrying 212 passengers. From comparing designs subject to the same requirements at different Mach numbers it is also found designing for Mach 1.6 often results in the lowest takeoff weight. Changing the design ranges shows that especially the smaller SSTs takeoff weights are more sensitive to range increases because of their lower payload fractions. For the SST50 aircraft it is also found that a four-engine configuration is better than a two-engine configuration, since it has a 4.2% lower takeoff weight, and less powerful engines.

For the environmental analyses, three studies are included, the landing and takeoff (LTO) cycle emissions, CO_2 certification, and a set of climate functions for estimating the global temperature change. Given that no LTO data for new SST engines are available, several subsonic engine series are used to estimate the emission index values using the known engine overall pressure ratio. Both the sub- and supersonic definition of the LTO cycle, as well as the sub- and supersonic regulations are used. The results show that the supersonic aircraft can meet the subsonic LTO regulations, although NO_x will be the most difficult. It is also found that the current supersonic LTO regulations are outdated, and that there is a small difference between the results found when using the sub- and supersonic LTO cycle definition.

The CO_2 certification results are less promising, as none of the supersonic aircraft are capable of meeting the regulations, with a minimum exceedance of over 70% for the supersonic business jet. Meanwhile, most in-production subsonic aircraft can meet the regulations. This shows that the CO_2 regulations would have to be modified for supersonic aircraft, because their specific air range values are much lower than for subsonic aircraft. Additionally, using the supersonic designs produced, a set of best fits is created which can allow others to get a first estimate for the CO_2 metric value when the takeoff weight or span loading are known.

For the global climate impact functions, a supersonic fleet is created and its revenue passenger kilometers (RPKs) and total cruise fuel consumption is estimated for the year 2050. To allow for comparison, an equivalent subsonic fleet is created with a similar RPK using cruise data from the Piano-X program. Due to the limitation of the engine module off-design calculations, it is not possible to predict the cruise NO_x emission index value using direct prediction methods. To overcome this issue, three scenarios are defined with 5, 10 and 18 g/kg NO_x production at cruise. The findings show that a fleet of supersonic business jets will result in a global temperature increase which is 2.7 to 3.5 times larger than that of a subsonic fleet which offers the same amount of RPK, depending on the NO_x emission index value. The temperature change is smallest for the lowest emission index of 5 g/kg, so NO_x emissions should ideally be minimized. For the largest SST250 the temperature increase is 4-5.1 times greater than a subsonic fleet, which shows that supersonic transportation is substantially worse for the climate.

In conclusion, a low-fidelity supersonic aircraft design program has been produced to generate supersonic aircraft designs. The performance of these designs has shown that the supersonic aircraft cannot meet the CO_2 regulations, and that their relative climate impact is much larger than that of subsonic aircraft. It is therefore questionable whether the time gains from supersonic transportation are worth the additional impact on the climate, given the increased importance of climate to the general public. To this end, further research should be performed with more advanced models and better fleet and network definitions.

List of Figures

List of Tables

Contents

Nomenclature

Acronyms

APU	Auxiliary Power Unit
AVL	Athena Vortex Lattice
BC	Black Carbon
BFFM2	Boeing Fuel Flow Method 2
BWB	Blended Wing Body
CAD	Computer-Aided Design
CAEP	Committee on Aviation Environmental Protection
CFC	Chlorofluorocarbon
CFD	Computational Fluid Dynamics
CFR	Code of Federal Regulations
CO	Carbon monoxide
COREL	Conical Relaxation
CORSIA	Carbon Offsetting and Reduction Scheme for International Aviation
DARPA	Defense Advanced Research Projects Agency
DATCOM	Data Compendium
DLR	Deutsches Zentrum für Luft- und Raumfahrt
DNS	Direct Numerical Simulation
EASA	European Aviation Safety Agency
ECS	Environmental Control System
EEA	European Economic Area
EHA	Electro-hydraulic adctuators
EIS	Entry Into Service
ETOPS	Extended-range Twin-engine Operational Performance Standards
ETS	Emissions Trading Scheme
FAA	Federal Aviation Administration
FAR	Federal Aviation Regulation
FEM	Finite Element Modeling
FLOPS	Flight Optimization System
GE	General Electric
GSP	Gas Turbine Simulation Program
HASA	Hypersonic Aerospace Sizing Analysis
HELESA	High-Efficient Low-Emission Supersonic Aircraft
HISAC	Environmentally-friendly High Speed Aircraft
HLD	High-lift device
HPC	High pressure compressor
IAE	Instruments, Avionics and Electronics
IATA	International Air Transport Association
ICAO	International Civil Aviation Organization
ICCT	International Council on Clean Transportation
IDE	Integrated Development Environment
IFR	Instrument Flight Rules
ISA	International Standard Atmosphere
KBE	Knowledge Based Engineering
LE	Leading edge
LEAP	Leading Edge Aviation Propulsion

LES	Large Eddy Simulation
LOSU	Level of Scientific Understanding
LPC	Low pressure compressor
LPP	Lean Premixed Prevaporized
LTO	Landing and Takeoff
MDAO	Multidisciplinary Design, Analysis, and Optimization
MEA	More Electric Aircraft
NACA	National Advisory Committee for Aeronautics
NASA	National Aeronautics and Space Administration
NLR	Nederlands Lucht- en Ruimtevaartcentrum
NO_x	Nitrogen oxides
nvPM	Non-volatile Particulate Matter
OAW	Oblique All Wing
OEI	One Engine Inoperative
OFW	Oblique Flying Wing
OML	Outer Mold Line
OpenVSP	Open Vehicle Sketch Pad
PANAIR	Panel Aerodynamics
PFCU	Power Flying Control Unit
PW	Pratt & Whitney
RAM	Random-access Memory
SAI	Supersonic Aerospace International
SCENIC	Scenario of Aircraft Emissions and Impact Studies on Atmosphere and Climate
SCOPE11	Smoke Correlation for Particle Emissions-CAEP11
SSBJ	Supersonic Business Jet
SST	Supersonic Transport
SU2	Stanford University Unstructured
SUAVE	Stanford University Aerospace Vehicle Environment
TAPS	Twin-Annular Pre-mixing Swirler
TE	Trailing edge
UAV	Unmanned Aerial Vehicle
UHC	Unburned hydrocarbons
USAF	United States Air Force
UV	Ultraviolet
YEIS	Year of Entry Into Service

Greek Symbols		**Unit**
ω	Specific humidity	–
α	Angle of attack	degree
β	Mach compressibility $\beta = \sqrt{M^2 - 1}$	–
δ_{flap}	Flap deflection angle	degree
η	Airfoil efficiency	–
Λ	Sweep angle	degree
π_{oo}	Overall pressure ratio	–
Π_{ATM}	Technology development factor from Isikveren	–
ρ	Density	kg/m^3
$\overline{\sigma}$	Suction parameter	–

Roman Symbols		
A	Aspect ratio	–
BPR	Bypass ratio	–
b	Span	m

C_D	Drag coefficient	–
C_{D_W}	Wave drag coefficient	–
C_f	Skin friction coefficient	–
C_L	Lift coefficient	–
C_{L_α}	Lift curve slope	rad^{-1}
$\Delta C_{l_{max}}$	2D high-lift device lift contributions	–
c	Chord length	m
c_j	Specific fuel consumption	lb/lbf·hr
D	Drag (force)	N
d	Diameter	m
E	Endurance	s
EI(X)	Emission index of species X	g/kg
e	Span efficiency factor	–
FC	Fleet cruise fuel consumption	kg
F_{oo}	Takeoff engine thrust	kN
f	Slenderness ratio	–
K_D	Design lift to cruise lift coefficient ratio	–
K_g	Gust alleviation factor	–
K_p	Polhamus potential-flow contribution coefficient	–
K_v	Polhamus vortex contribution coefficient	–
L	Lift (force)	N
L_{cabin}	Cabin length	m
l	Lifting length	m
M	Mach number	–
M_{ff}	Mission fuel fraction	–
MTOM	Maximum Takeoff Mass	kg
$\dot{m}_f$	Fuel flow	kg/s
n	Load factor	–
OEW	Operating Empty Weight	kg
OPR	Overall Pressure Ratio	–
p_{cr}	Cruise altitude pressure	hPa
q	Dynamic pressure	Pa
R	Range	m
Re	Reynolds number	–
RF	Radiative Forcing	W/m^2
RGF	Reference Geometric Factor	–
RPK	Revenue Passenger Kilometer	pax·km
r_s	Area ratio	–
S	Area	m^2
SAR	Specific Air Range	km/kg
SFC	Specific Fuel Consumption	lb/(lbf·hr)
SN	Smoke Number	–
S_{NO_x}	NO_x severity parameter	–
s/l	Box ratio	–
T	Thrust	N
ΔT	Temperature change	mK
Δt	Segment time	s
TAS	True Airspeed	m/s
TIT	Turbine Inlet Temperate	K
T/W	Thrust loading	–
t	Thickness	m

t/c	Thickness-to-chord ratio	–
U_e	Equivalent gust speed	ft/s
V	Flight speed	m/s
W	Weight	kg
WAR	Water-to-air ratio	–
W/S	Wing loading	N/m^2
w_f, w_{ff}	Fuel flow, Corrected fuel flow	kg/s
w_{max}	Maximum width	m

Subscripts

0.25/0.25c	Quarter-chord
0.5/0.5c	Semi-chord
3	Engine station 3 at combustor entry
amb	Ambient
APU, lr/APU, sr	Auxiliary power unit for long/short range
calc	Calculated
cont	Contingency
cr	Cruise
des	design
div	Diversion
e	End of segment
eff	Effective
eng	Engine
exp	Exposed
F/f	Fuel
fuse	Fuselage
HL	Hinge line
HT/ht	Horizontal tail
inb	Inboard
lam	Laminar
LE	Leading edge
LG	Landing gear
ltr	Loitering
max	Maximum
mid	Mid-segment
OE	Operating empty
outb	Outboard
PL	Payload
ref	Reference
req	Required
s	Start of segment
TE	Trailing edge
TO	Takeoff
turb	Turbulent
VT/vt	Vertical tail

1 Introduction

In the coming decades passenger air traffic is expected to grow by 3-5% annually [1]. According to the International Air Transport Association (IATA) the expected growth will result in 7.8 billion passengers being transported in the year 2036[1]. On the other hand, the world is increasingly aware of global climate change, and looking to reduce emissions to meet targets stipulated in the Paris Agreement [2]. While aviation is not the biggest contributor to climate change at roughly 4.9% (including contrail cirrus) of the anthropogenic radiative forcing [3], it cannot be ignored, in particular since aircraft emit their greenhouse gases much higher in the atmosphere. With the future growth in air traffic it is expected that the contribution of aviation will increase by a factor 3-4 in 2050 [3], which is undesirable for a sustainable future.

One of the large challenges in aviation is to provide the required air traffic capacity in the future, while reducing the climate impact. The industry will need to find solutions to improve the efficiency of aircraft, which could be done through radically different configurations, newer engines and optimized flight trajectories. Also, airlines will need to work with new regulations such as the European Emissions Trading Scheme (ETS)[2] and the International Civil Aviation Organization's (ICAO) Carbon Offsetting and Reduction Scheme for International Aviation (CORSIA)[3] program. Note that ETS is already effective for intra-EEA (European Economic Area) flights and might be revised or (partially) replaced by CORSIA which starts a pilot in 2021.

At the same time, a revival of supersonic transportation is taking place with several companies looking to launch civil supersonic aircraft in the next decade. Historically, the few supersonic aircraft which have been operated were less efficient, and emitted their greenhouse gases at higher altitudes than subsonic aircraft. With the increased focus on climate impact it is questionable whether supersonic transportation is an acceptable option for the future. To get a clearer picture, an investigation into the current regulations and expected performance of new supersonic aircraft was requested by ICAO. This investigation will form the focal point of this report. However, before discussing the goals of the investigation, Section 1.1 provides some more historical background information on supersonic travel, and Section 1.2 gives insight on some key benefits and issues associated with supersonic transportation. These are linked to the research goals and questions in Section 1.3, after which Section 1.4 shows the thesis structure.

1.1. History of supersonic flight

To get a better understanding of the supersonic transport industry it is beneficial to briefly discuss the history and the renewed interest, which provides a good background for the research goals.

1.1.1. Twentieth century

In 1947 Chuck Yaeger became the first recorded human to break the speed of sound in the Bell X-1 aircraft[4]. This achievement was fueled by the urge of mankind to go ever faster and in the years following, increasingly faster (military) aircraft were built and operated. The technological developments also sparked the idea of supersonic civil transportation. This led to a large number of projects, of which the Anglo-French Concorde and the Soviet Tu-144 were the only ones to fully materialize. Especially the former is still considered an icon in aviation history. Both aircraft were capable of cruise flight at just over twice the speed of sound. However, neither aircraft became a success with the Tu-144 only flying passengers commercially 55 times[5],

[1] *2036 Forecast Reveals Air Passengers Will Nearly Double to 7.8 Billion*, https://www.iata.org/pressroom/pr/Pages/2017-10-24-01.aspx, October 2017 (accessed March 6 2018)

[2] https://ec.europa.eu/clima/policies/transport/aviation_en (accessed February 27 2019)

[3] *Historic agreement reached to mitigate international aviation emissions*, https://www.icao.int/newsroom/pages/historic-agreement-reached-to-mitigate-international-aviation-emissions.aspx, October 6 2016 (accessed February 27 2019)

[4] https://airandspace.si.edu/collection-objects/bell-x-1 (accessed April 4 2019)

[5] *Tu-144*, http://www.tupolev.ru/en/aircrafts/tu-144 (accessed December 27 2018)

and Concorde only having a fleet of 14 aircraft. Concorde flew for the last time in 2003, and there has been no supersonic civil transportation since.

(a) Concorde[6]

(b) Tu-144[7]

Figure 1.1: Past supersonic transport aircraft

The main reasons that led to Concorde's failure were the environmental concerns of airport noise, sonic boom and its emissions and climate impact. Additionally, the sonic boom restrictions in combination with its limited range and payload capabilities, constrained the Concorde by only allowing a few city pairs to be operated on profitably, and as such it never made up for its development costs. At the same time, Boeing succeeded by opting to go for the larger 747 aircraft, which had much better payload-range performance and better suited the hub-and-spoke network structure which rose to fruition in the following decades. Another important contribution was the crash of Air France flight 4590 in 2000 which ended its 27 year period without a fatal incident, which made Concorde one of the safest aircraft according to some experts[8].

1.1.2. Renewed interest

Despite the failures of the Concorde and Tu-144, research into supersonic transport aircraft never ceased, and over the years there have been a large number of projects (see [4, 5] for overviews) as well as technological developments in both civil and military aircraft design [6]. These developments include the introduction of Multidisciplinary Design, Analysis, and Optimization (MDAO) which allows for computerized design of aircraft so that more aircraft designs can be investigated and optimized for various performance characteristics.

More recently, some of the design projects have begun to transform into commercial (start-up) companies looking to offer supersonic civil transportation in the near future like Boom Supersonic[9] and Aerion[10]. Both companies aim to launch their aircraft in the next five to ten years. Larger companies like Airbus and Boeing do work on design projects for supersonic aircraft, but have not announced any aircraft to go into production. It is possible that they are waiting for the smaller companies to test the waters, and for regulations to be updated. However, Boeing did recently announce a partnership with Aerion[11] which could be to have a head start in case supersonic transportation becomes a success.

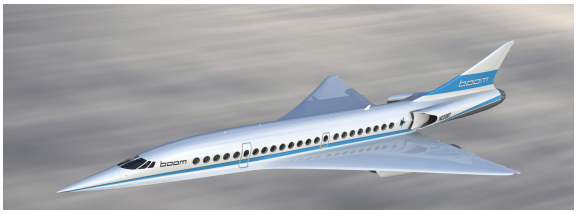

(a) Boom SST[9]

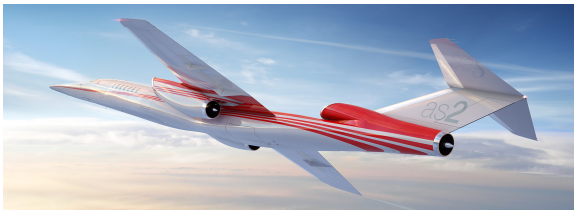

(b) Aerion AS2 SSBJ[10]

Figure 1.2: Current SST designs

An important market segment which these companies target are the premium passengers who value time more strongly and would be willing to pay more for reduced travel times. Additionally, the business jet market is growing, which also includes people that value time as business jets are sometimes referred to as 'time-

[5] taken from https://www.baesystems.com/en/heritage/bac-concorde (accessed May 25 2018)
[6] taken from http://www.tu144sst.com/ (accessed May 25 2018)
[8] *Concorde's Stellar Safety Record*, Ruppe, D.,https://abcnews.go.com/International/story?id=83069 (accessed February 27 2019)
[9] https://boomsupersonic.com/ (accessed December 27 2018)
[10] https://www.aerionsupersonic.com (accessed December 27 2018)
[11] Bogaisky, J., *Boeing To Help Aerion Develop Supersonic Jet As Lockheed Martin Exits*, www.forbes.com, February 5 2019 (accessed February 26 2019)

machines'. Furthermore, the rise of airlines, such as Emirates, and more efficient and cost-efficient wide-body aircraft has resulted in a shift towards point-to-point transportation which is served by smaller aircraft than the 747 and A380. While this segment of 200-300 passenger aircraft is less realistic, it is still seen as an opportunity that could be investigated.

1.2. Supersonic benefits and issues

As shown, the interest in supersonic transportation never really disappeared. This is because of the speed benefit offered compared to subsonic aircraft, which allows for flying the same stretch 2-3 times faster. While little time is saved during climb and descent because they are performed at subsonic speeds, the overall time savings from supersonic cruise are still in the order of several hours for Transatlantic flights. For city pairs across the Atlantic/Pacific for example, this could enable an airline to service some city pairs twice a day using a single aircraft. This could also enable passengers to fly one way in the morning, have an important meeting, and be back home the same day, although this does depend on distance and timezones.

The level of flight comfort that can be provided by supersonic aircraft is improved compared to subsonic aircraft because at the higher supersonic cruise altitude, the atmosphere is more stable. As a result, there is a lower probability of aircraft encountering strong gusts (turbulence) during cruise flight. Over the Atlantic, the aircraft can also largely avoid the influence of the jet streams which is beneficial when they oppose the flight direction, as they would otherwise increase the flight time and fuel burn. Additionally, the airspace in the lower stratosphere is much less crowded which could allow for more direct flying from origin to destination.

While flying at supersonic speeds has a number of benefits, it also introduces new problems and enhances those associated with subsonic aircraft. The airport noise is enhanced because of the lower bypass ratios, which results in higher jet exhaust velocities and jet noise. Note that compared to the Olympus turbojet engine of Concorde, modern supersonic turbofan engines with low bypass ratios will produce less noise. Also, for aviation, the climate impact of aircraft has become increasingly important given the global warming phenomenon and the push to reduce it, while still supporting the large passenger growth expected. For supersonic aircraft, which fly at higher altitudes, the impact of the different species (e.g. NO_x) increases, resulting in a larger climate impact for the same emissions, which is an important issue.

A problem not applicable to subsonic aircraft is the so-called sonic boom, which is generated by the shockwave that is produced when an aircraft flies faster than the speed of sound. The shockwave will, upon reaching the ground, cause vibrations by interacting with objects which are perceived by the population as a 'boom'. In most of the world, it has led to a ban on overland supersonic flight, reducing the potential of flying supersonic when compared to subsonic aircraft on overland stretches.

These problems are well-known to the aircraft designers and solutions have been thought of which can at least partially mitigate some of the issues, but they often require changes to the existing regulations, and further investigations. The latter is needed because it is necessary to determine whether the changes made result in aircraft designs that can be considered acceptable.

1.3. Thesis goal and research questions

As shown in the first paragraphs, the environmental impact should be investigated before new supersonic aircraft can enter the market. There are issues however since the majority of the regulations currently applicable to supersonic civil aircraft are based on experiences with the 'old' Concorde, which was designed and built in the sixties and seventies, and is therefore no longer deemed representative. Since no other supersonic transport projects other than the Tu-144, which was also designed in the sixties, ever performed commercial flights there is no strong basis from which updated regulations can be derived. Without such a basis, new regulations might not adequately support the arrival of new commercial supersonic transportation in a sustainable manner, which could cause them to fail like Concorde. It may also be that supersonic transport is not desirable. This is the reason that ICAO has requested an investigation to determine what can be expected of new SSTs, and forms the foundation of this thesis. Based on the request of ICAO, the following research objective was defined for the thesis:

Provide the International Civil Aviation Organization (ICAO) with information about the design and (environmental) performance of supersonic aircraft with Entry Into Service (EIS) in the period 2020-2025 through the creation of a low-fidelity design program, and by comparing the designs to current subsonic aircraft, so that statements and recommendations can be made about the environmental regulations and acceptability of future supersonic transportation.

The main areas of interest in this investigation are the environmental concerns of airport noise, sonic boom, and emissions and their climate effects. Before these topics can be investigated, it is necessary to have a method by which representative aircraft designs can be created. Altogether, this results in a very broad topic, which makes it difficult to properly cover all areas. Consequently, the research is performed by two students and the level of detail is limited.

The goal set forth for this thesis is twofold, and can be phrased as follows:

- *To investigate the design process of supersonic aircraft, and create a program capable of producing a range of supersonic aircraft designs for different requirements.*
- *To investigate the climate impact of supersonic aircraft designs which meet the anticipated market demands, and evaluate current regulations.*

Since the design program consists of several modules, which each require considerable effort, the modules were divided among the two students, and upon completion are combined into a single program. In terms of results, the other student will focus more on the sensitivity of the designs to different parameters by using the design program, and investigate the airport noise and sonic boom environmental concerns. The report elaborating on the findings from this study can be found as [7].

Using the two goals listed above, the research was further broken down by creating a set of research questions which form the guide to accomplish the goals. These questions are the following:

1. How accurate are the results provided by each of the design program modules?
2. Can a supersonic aircraft design program be produced which is capable of providing sufficiently accurate results with the resources available?
3. What are the requirements for state-of-the-art supersonic aircraft?
4. How are the performances of the best designs which meet the requirements, and how do they compare to subsonic aircraft?
5. What is the climate performance of the best supersonic designs, and how do they compare to subsonic aircraft?

Of these questions, the third was already partially answered through a literature study [8]. However, the requirements were not yet fully detailed, and only considered small supersonic transports (SSTs) and supersonic business jets (SSBJs). Also, some new developments have taken place since, such as the unveiling of the new Affinity turbofan engine by General Electric (GE) to be used on the Aerion AS2[12].

It should be noted that the end result of the thesis is not a definitive statement of whether supersonic transport is acceptable or not in terms of climate impact. Instead, it will provide the results, comparing different scenarios and showing how they perform and compare the performance to subsonic aircraft. The findings can be used as a starting point for further investigations about regulations and aid decision making processes.

1.4. Thesis structure

Now that the goals of the thesis have been described, the last step is to provide an overview of the content in this report, starting with describing the main program used to produce the supersonic aircraft designs in Chapter 2. Following this, the different modules comprising the design program are individually presented and tested, starting with the Class I analysis in Chapter 3. Following this, a summary of the wing loading analysis, and engine and aircraft geometry design process is provided in Chapter 4. After this, the aerodynamics and Class II weight estimation modules are discussed in Chapters 5 and 6, respectively. Then, Chapter 7 will show the different expected aircraft designs as found by the design program and evaluate their performance. Next, Chapter 8 details the climate evaluation methods used, and Chapter 9 discusses the climate performance of the supersonic designs. Based on all previous findings, Chapter 10 will provide the final conclusions from the investigation, after which Chapter 11 will provide a set of recommendations for future research to improve the design program, but also to improve the accuracy and thereby quality of the climate impact results.

To limit the complexity and size of the main texts, most chapters have supporting texts located in appendices, which will be referred to in the appropriate locations.

[12] Phelps, M., *Aerion Unveils Stage 5 GE Affinity Engine for Supersonic AS2*, www.ainonline.com (accessed December 27 2018)

2
Design program description

This chapter will discuss the creation of the design program and the choices that were made during production. However, before that is done, Section 2.1 provides some background for the typical aircraft design process in the aviation industry. Section 2.2 will then elaborate on the decisions made during the production of the supersonic aircraft design program. Following this, the structure of the program is discussed in Section 2.3. As a last step Section 2.4 gives a more detailed breakdown of the data flow within the program.

2.1. Aircraft design

In aircraft design there are several stages which have to be completed before the aircraft can go into production and operation. First, the requirements have to be defined for which it has to be designed. This often involves a detailed market survey and forecast to predict whether there are enough potential aircraft sales to warrant the required investments. Once this is completed and shows sufficient market potential, three design stages are defined [9]:

1. Conceptual design: Using the design requirements from the market survey, a large number of different aircraft concepts are studied by using relatively low-fidelity design programs. It is also possible to make use of some form of optimization to find the best designs. These are then compared through a trade-off study to determine which one is best. The end result is a conceptual aircraft configuration and layout capable of meeting all of the requirements set at the start.

2. Preliminary design: The design produced in the conceptual stage is further analyzed and adjusted where needed while ensuring it still meets the design requirements. At this point more advanced analysis methods will be implemented such as wind tunnel testing for aerodynamics, and detailed Finite Element Modeling (FEM) to evaluate the structural integrity of the design. Towards the end of this stage, it is necessary for the company to make the decision whether to continue the project or cancel it (or put it on hold temporarily while waiting for future technological developments).

3. Detailed design: prior to this stage most major design choices have been made. The focus shifts to the design of the smaller details of the aircraft which are needed for the production process such as the individual structural components (e.g. spars, ribs), nuts and bolts, but also items like software. Once the level of detail is sufficient, construction and (flight) testing can also commence.

After testing, the aircraft is type certified if all regulations are met, after which it can be shipped to the customers (e.g. airlines). Note that the three design stages discussed above do not show the full picture since the amount of effort and resources that go into each stage are not distributed evenly. Instead, the distribution is more in the range 1%-9%-90% [10]. However, the conceptual design stage already defines a large part of the design that is worked on in the preliminary and detailed design stages, reducing the freedom of designers. This shows that the conceptual design is quite possibly the most important design stage.

In the early days of aviation aircraft design was largely performed by trial-and-error, which allowed for new knowledge to be gathered. This knowledge could then be used for new designs and to define simple (empirical) rules and equations for others to apply. With the introduction of more powerful, smaller, and cheaper computers the focus has begun to shift from empirical methods to computerized design using mathematical models. Like in the early days, trial-and-error is still applied by investigating a large variety of designs, but the key difference is the that the level of detail is much higher. Also, in the time required for the production of a simple design in the early days of aviation, hundreds if not thousands of designs can be analyzed through modern computerized design routines. It should be noted however, that the creation of such mathematical models and a single design program combining them does require a large amount of resources initially.

Two important fields in the current aircraft design industry are Knowledge Based Engineering (KBE) and Multidisciplinary Design, Analysis, and Optimization (MDAO). The former is engineering by application of specialized software for manufacturing and production design. The basis of KBE software is created by experts in the respective fields of interest, and allows for less experienced users to accurately analyze those expert fields. The KBE software can also be used as a means to support computer-aided design (CAD). MDAO is the field of engineering which applies optimization methods to find solutions to design problems which require the inclusion of various disciplines through separate analysis modules. Note that for both of these fields different and more complex definitions exist.

Within TU Delft, effort has already been put into the creation of an aircraft design program called the Initiator [11, 12]. It is capable of designing aircraft with various configuration options: the conventional, canard, three-surface, Prandtl and Blended-Wing-Body, but it currently cannot be used in the supersonic domain and therefore cannot be applied without modifications.

2.2. Pre-production decisions

Before building the program, it was necessary to make several decisions which are partially related to the previous section. The first step was to decide on whether to produce an automated design program. Given the added complexity that comes with the supersonic flight regime, much lower fidelity could be achieved through manual design, and fewer designs could be analyzed, so the decision was made to create an automated design program.

Next, it was necessary to select an aircraft design stage for the program. Since the main goal of the research is to provide information on the environmental impact of supersonic aircraft, rather than to create the most advanced (and detailed) design possible, the conceptual design stage level of fidelity is considered sufficient. Still, even for a conceptual design the fidelity level will be relatively low, given the limited resources, and the lack of dedicated literature for supersonic aircraft design which are more readily available for subsonic aircraft. The program will also have to be iterative to allow for designs to be adjusted if constraints are violated.

This led to the next decision, whether to use an already existing program for the design process or to build our own. Out of existing programs two key options were considered, the Initiator program [11, 12] of TU Delft, and Stanford University's Aeronautical Vehicle Environment (SUAVE) program[1]. For the former, a meeting was held with one of the responsible staff members to discuss the possibilities. From this meeting, it was concluded that it would not be possible to make use of the Initiator program. SUAVE, an open source program, was also looked at but was not found to be optimal as its process was complex, and required additional effort to fully comprehend the intricacies of the system. This led to the decision to create a new program for the conceptual design of supersonic aircraft.

After this decision, the last step was to choose the programming language to be used for the program. The two candidates considered were Matlab and Python, as both languages have been used in the Master phase, and using them will allow others to make modifications more easily in the future. Additionally, both have been used for existing design programs, with the Initiator being Matlab-based and SUAVE Python-based. To make a decision between the two, a trade-off was performed based on several items as listed below:

- Programming experience: Both languages have been used during the Master phase of the study, but Python was used more often by both creators so it is seen as the preferred option.
- Base functionality & extensions: For this item there is some difference, primarily in the base functionality. Whereas Matlab is a program that contains a large range of features in the base version, Python's base version has fewer features. However, Python allows for expanding its library by installing thousands of different packages created by other users, giving it more options than Matlab.
- Open-source: This item is important to consider because Matlab[2] is a program that requires a paid license to download and use it. Python on the other hand is open-source, which is part of the reason why there are many additional packages available to extend its functionality.

Based on the items above, it was decided to use Python for the program. An added benefit of this was that it was possible to use the KBE package ParaPy[3] to generate a 3D geometry with relative ease, which could then be used for area ruling and visualizing the designs.

[1] http://suave.stanford.edu/ (accessed December 16 2018)
[2] available through https://mathworks.com/products/matlab.html (accessed May 6 2019)
[3] https://www.parapy.nl/ (accessed December 27 2018)

In order to further improve the program, it is also possible to introduce an optimization routine such that the design process can be optimized (steered) based on specific performance parameters in an objective function. This was not implemented for the full program as of yet, because it would require much additional effort, and is expected to function better once more modules are included such as stability and cost estimation to add more versatility to the optimization targets. Note that a small optimization routine is included in the engine design process, to find the required air mass flow at the design point.

2.3. Program modules and integration

The full program consists of a set of different modules which are each responsible for the analysis of specific aspects of the aircraft design and its performance. Because of the large amount of work, the research was performed by two students, and the modules were divided such that working independently was possible before combining them. The modules are listed and briefly described below, along with indications of where more information can be found. To better understand the connectivity Figure 2.1 can be studied.

- Requirements and design inputs: Before anything can be done, the top-level requirements for the aircraft should be defined. These follow from a market study and are defined in Section 7.3. Aside from this, estimates of some aircraft design and aerodynamic parameters have to be provided so that the initial Class I and wing loading analyses can be performed, and the aircraft geometry generated. More information about this is provided in Appendix A.2.

- Class I weight estimation: This is the starting point for the iterative design loop. Using the top-level requirements and a set of initial estimates for factors such as the lift-to-drag-ratio (L/D) and specific fuel consumption, this module will provide the user with a first estimate of the main aircraft weight groups. These are the takeoff weight, operating empty weight and fuel weight. For each subsequent iteration, the takeoff weight is again calculated. A more detailed description of this is provided in Chapter 3.

- Convergence checker: This system can be seen as a simple check where the difference between the takeoff weight from two successive Class I weight analyses is determined. As long as this difference is larger than a set margin, the program will continue the iteration process ('while' loop). Depending on user settings the program will stop iterating once the weight has been stable for a certain number of successive iterations (default is two). After this, the iterative process is stopped and the output writer program is executed. Alternatively, if no convergence is achieved by the program, it will continue until a user-defined maximum number of iterations has been completed, and then stop.

- Wing loading diagram: In the wing loading analysis several aircraft performance requirements (e.g. takeoff distance, cruise speed, stall speed) are used to define a feasible region on a wing loading diagram, where all constraints are satisfied. From this feasible region, the point with the best engine and wing size is selected. This can then be used with the Class I takeoff weight to determine the wing area and required engine thrust. A summary of the method is given in Section 4.1.

- Propulsion: So far, the aircraft design has been created by mostly using statistics, requirements and a set of other design input parameters. However, to better substantiate the results, the aerodynamic and propulsion system performance should be properly analyzed. So far, the engine performance was based on reference aircraft. Its real performance is more complex, and depends on factors such as bypass and pressure ratios, but also the engine configuration, inlet and nozzle shape and dimensions. The method used is summarized in Section 4.2.

- Geometry creation: Using the wing area estimated in an earlier step, and several other user-defined design inputs, the aircraft geometry is produced. This includes the calculation of values such as the wing areas, sweep angles, and exposed areas. A summary of the method is provided in Section 4.3.

- Aerodynamics: Apart from propulsion, the aerodynamics module is also important. Among other things, this module looks at the low-speed lifting performance and high-lift device (HLD) sizing, as well as the determination of L/D-ratios for the flight segments in the Class I analysis. A detailed description is given in Chapter 5. Note that after the aerodynamics module is run, a check is performed to ensure that the aircraft HLD system is capable of providing the maximum lift coefficient values used in the wing loading analysis. If it is found that the system is incapable of meeting the requirements, the lift coefficient values are reduced and the program will once again start with the wing loading analysis.

- Class II weight estimation: The operating empty weight used in the first Class I analysis is estimated using statistical data from past aircraft. As the aircraft weight is the sum of its component weights, it is beneficial to estimate the weight of each individual component so that the operating empty weight value becomes more reliable and accurate. This also allows for including correction factors to account for technological developments in materials and systems for specific components. The method used is detailed in Chapter 6.
- ParaPy image creator: This module falls outside of the iterative design loop because it is a rather time and computational effort intensive process compared to the other modules. It produces several images of the resulting aircraft design created by the iterative design process.
- Climate analysis: This module is added to help answer some of the research questions and includes the evaluation of different certification regulations applicable to new aircraft (i.e. LTO cycle emissions and CO_2), but also to provide an indication of the potential global temperature change caused by a supersonic fleet. It is an optional module which is only run if the user requests it. More details about the module can be found in Chapter 8.
- Noise analysis: Aside from the climate impact, the noise impact (i.e. airport noise and sonic boom) is also important for new aircraft as discussed earlier. The methods used for this analysis are described in [7]. As with the climate analysis, it is an optional program.
- Output writer: This is currently the last main module in the aircraft design program. It will use the results from the different modules found during the final design iteration, and combines them into a pdf document which provides the user with an overview of the resulting design and its performance characteristics. An example output file is shown in Appendix G.

After the output writer is run, the program is terminated. All outputs will then be moved to a folder location set by the user. To support the above explanation, the flow chart shown in Figure 2.1 was produced.

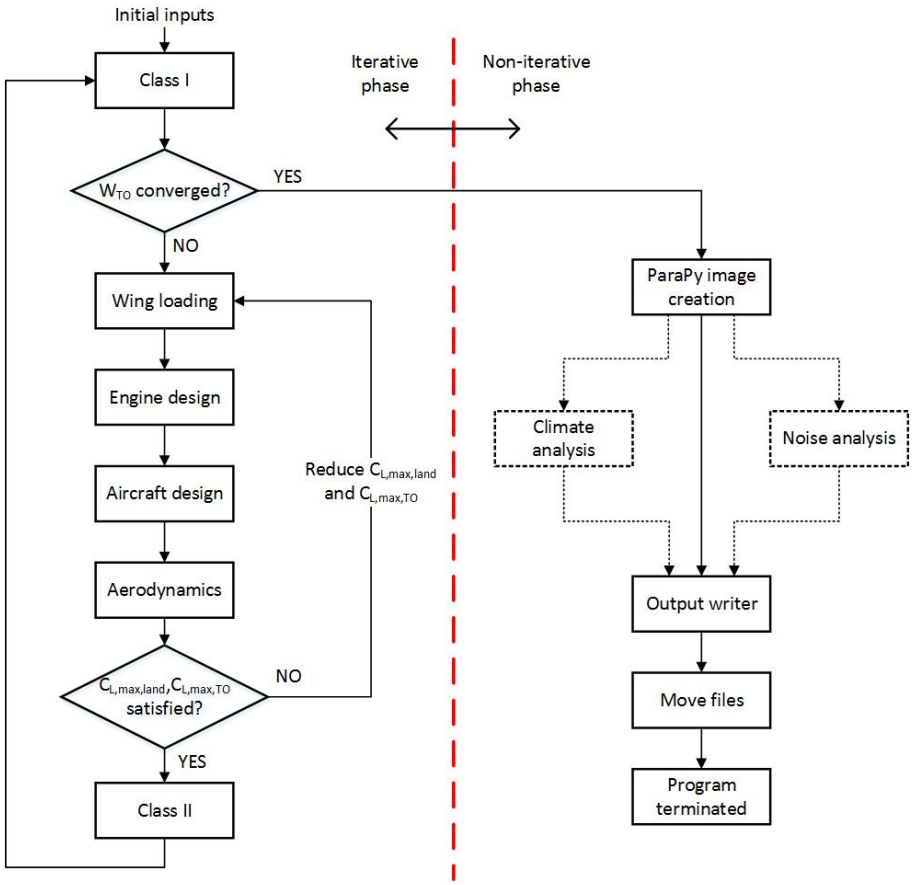

Figure 2.1: Design program flow chart

The flow chart shows the two iterative loops left of the red dashed line, with the main loop being the one with the takeoff weight convergence check following the Class I analysis. The second smaller loop is for the maximum lift coefficients of the aircraft to ensure that the design is indeed feasible. More detailed information about the items being passed on between modules can be found in Section 2.4.

Parts of the design program are programmed in an object-oriented manner, meaning that (where possible) the module uses a class-structure, where instances of the modules can be coupled to a single aircraft object. This way, the aircraft object can call the coupled class functions which will use the instance variables, allowing for multiple aircraft designs (i.e. objects or dictionaries) to exist and be analyzed concurrently. Using an object-oriented programming approach also allows for new modules to be added or old ones to be replaced with relative ease, which increases the flexibility.

A last important aspect of the program is the linking of the different modules, since a module might require outputs produced by preceding modules. These links become more clear in the next section, and currently the focus is on the method used for linking. Because of the mutable character and clear structuring of the values, dictionaries were selected as the means to store and pass on inputs and outputs. A dictionary allows for assigning a value, or values (or other data types like numpy arrays) to a key. This key can then be used to extract the corresponding values at a later stage. For example, assigning takeoff weight to a key "W_TO" means that later modules can simply call the key "W_TO" to get the corresponding value. A dictionary is mutable because a value corresponding to a key can be overwritten, or removed entirely.

Within the program, a master dictionary is created which contains sub-dictionaries created by the individual modules. For example, there are sub-dictionary containing the operating empty weight breakdown (Class II module), aerodynamic values (aerodynamics module), and engine characteristics (engine module). This master dictionary is passed on to each subsequent module, and within that module, the necessary sub-dictionaries are extracted, and the required values are used by selecting the proper sub-dictionary keys in the functions. For each new iteration, the values of the sub-dictionaries are overwritten either by overwriting the full dictionary, or by simply assigning a new value to specific dictionary keys. Note that there is an important attribute of dictionaries that should be kept in mind, which is described in Appendix A.1.4.

2.4. Program N^2-diagram

In order to better visualize the structure of the full program and show the links and dependencies between modules, a so-called N^2-diagram was produced which is shown in Figure 2.2. In the chart, the different modules discussed previously are located along the main diagonal and contained in thick red boxes. To visualize the part that represents the iterative design process, the corresponding boxes are given a black outline.

The N^2-diagram provides an overview of the main parameters that are passed on from one module to the next (note that these are not the dictionaries discussed earlier). The entries above the main diagonal show values which are passed down to the next module in the system. Meanwhile, entries below the main diagonal are values which are being fed back to a previously run module and allow for the iterative process (e.g. the specific fuel consumption values are fed back from engine design to the Class I analysis). This direction of data flow is also visualized by the two arrows. Note that not all parameters being passed on are listed, but just the most important ones.

Looking at the diagram, it can also be seen that the Initial setup module only provides inputs to all other modules, and that the Output writer does not return anything. Note that the convergence checker determines whether the iterative process ends through the takeoff weight values, so only if it finds that there is no convergence, will the iteration loop modules following Class I get executed. If it is found after the Class I analysis that the weight has converged, the remaining modules in the iterative process are skipped and the ParaPy image creation, optional environmental analyses, and output writer are run. The program is terminated once the output writer module has been run successfully.

Initial setup	n_{pax}, R_{des}, speeds, altitudes, SFC, L/Ds, reserve fuel settings, setup	s_{land}, s_{TO}, h_{land}, h_{TO}, speeds, altitudes	Efficiencies, BPR, pressure ratios, YEIS	AR, speeds, Airfoil names	Settings (plots), Flight conditions	Setup data, cruise data, n_{pax}, n_{crew}, tech factors			Output name and settings
	Class I	W_{TO}		$W_{fuel,max}$	W_{TO}, a/c weight during flight segments	W_{TO}, Weight during flight segments, W_{MZF}		Weight per segment	W_{PL}, W_{TO}, W_{OEW}, Payload-range data
		Wing loading	T_{eng}	Wing area	$C_{Lmax,TOreq}$, $C_{Lmax,landreq}$				W/S-T/W diagram with design point, W/S, T/W
	SFC values	n_{eng}	***Engine***	Engine dimensions		Engine characteristics		Engine characteristics	Engine characteristics
				Aircraft design	Dimensions (wing, fuselage, HT, VT, engine)	Dimensions (wing, fuselage, HT, VT, engine)	Dimensions (wing, fuselage, HT, VT, engine)	Dimensions (wing, fuselage, HT, VT, engine)	Dimensions (wing, fuselage, HT, VT)
	L/D values	$C_{Lmax,TO}$, $C_{Lmax,land}$, $C_{Lmax,clean}$, $C_{D,0}$ and K-values			***Aerodynamics***	CL-alpha, CL,max, LE_{HLD}-trigger		L/D values	L/D curves
	W_{OEW}					***V-n diagram & Class II***			Weight breakdown, Gust diagrams
							ParaPy Image creation		Images, Area distribution
								Environmental Analyses (Climate, Noise)	Climate data, Noise data
									Output writer

Figure 2.2: Design program N^2-diagram. Note that the parts representing the iterative design process are contained in black boxes. For those reading the report in black and white, these are the boxes from the Class I to the V-n diagram & Class II modules.

3
Class I weight estimation

During the first step in the aircraft design process the takeoff weight should be estimated. Before the weight estimation method is explained it is necessary to define the mission profile (see Figure 3.1). The mission begins with engine startup, taxiing to the runway, and takeoff. After this, the aircraft will climb to roughly its subsonic cruise altitude, where it could perform a subsonic cruise segment if supersonic flight is prohibited in that airspace. Next, the aircraft accelerates through the transonic regime at an optimal altitude with the least drag, and climbs to its higher supersonic cruise altitude. During supersonic cruise the aircraft will continue to climb either continuously or stepwise. After the supersonic cruise, the aircraft will decelerate and descent to the subsonic cruise level, which can be slightly higher than before supersonic cruise, given the aircraft fuel burn. If no subsonic cruise is needed the aircraft will descend and land. Additionally, to account for unforeseen conditions contingency, diversion, loiter (holding), and final reserve segments are included.

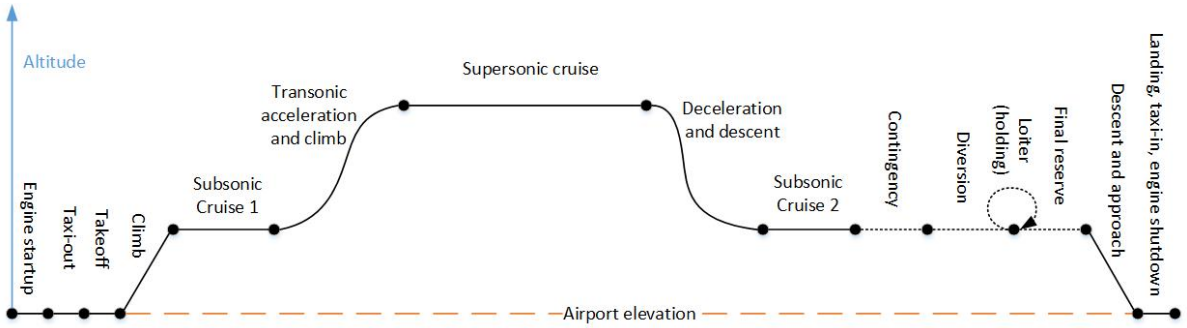

Figure 3.1: Mission profile (note cruise climb not shown)

Now that the mission has been defined, the weight estimation can be performed. The Class I method is explained in Section 3.1. Validation of the method is shown in Section 3.2, and the calculation of some additional weights in Section 3.3. Sections 3.4 and 3.5 then discuss input sensitivity and payload-range calculations, respectively.

3.1. Class I methodology

In the Class I calculations the aircraft takeoff weight is broken down as shown in Equation (3.1).

$$W_{TO} = W_{PL} + W_{OE} + W_F \tag{3.1}$$

where W_{PL} is the payload weight, W_{OE} the operating empty weight, and W_F the total fuel weight. The method used is a mix of that described by Roskam [13] and Sadraey [9] and is centered on the fuel-fraction method. The takeoff weight of the aircraft is computed by using Equation (3.2).

$$W_{TO} = \frac{W_{PL}}{1 - \frac{W_{OE}}{W_{TO}} - \frac{W_F}{W_{TO}}} \tag{3.2}$$

This equation is used while iterating a guess for the takeoff weight until it has converged to within 0.1% of the previous iteration guess. Figure 3.2 shows the convergence trend for the Concorde analysis. The payload weight calculation is discussed in Section 3.1.1. The operational empty weight estimation and the fuel fraction methods are explained in Sections 3.1.2 and 3.1.3, respectively.

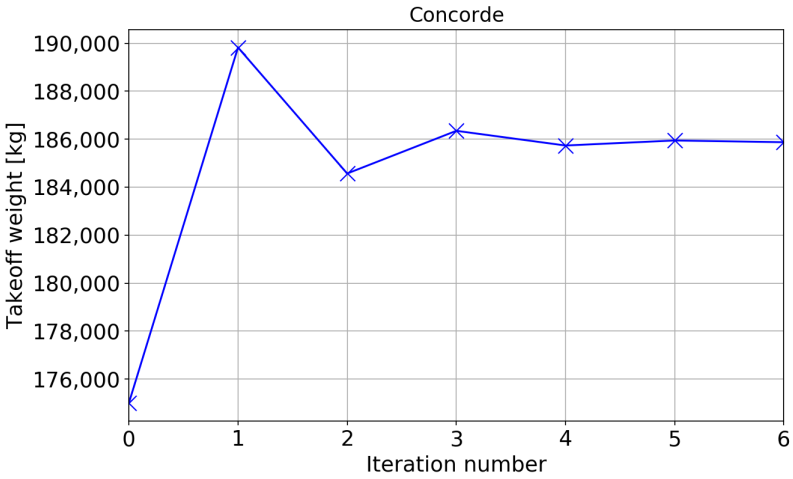

Figure 3.2: Concorde takeoff weight convergence history

3.1.1. Payload weight

The payload weight is the first term that needs to be determined and in this case consists of passengers and their luggage. There exists some variation in the definition of the passenger weights used by airlines and over the years they have been subject to change. The values used in this research are largely based on a survey funded by the European Aviation Safety Agency (EASA) [14]. There, it was found that the average passenger weight is 88 kg, including carry-on luggage and the weight of any infant below two years of age carried by an adult on a single seat. For luggage an average weight of 17 kg was found, but this number also includes domestic and intra-European flights, which are less likely to be operated by supersonic aircraft. Looking at the detailed breakdown in the report, the mean weight of luggage for long-range flights (>5000 km) during winter is 18.9 kg. Winter was chosen as it is the critical season for luggage weight [14]. To this value, the 95% confidence range of 0.18 kg was added, and then rounded up to make the weight 20 kg. It should be noted that for supersonic aircraft, which are likely to be more commonly used by businessmen on short trips, the fraction of passengers with separate luggage for the belly will be less. This percentage is assumed to be 50-75%, which amounts to an average passenger weight of 98-103 kg including luggage, but can be changed easily.

3.1.2. Operating empty weight

The operating empty weight can be broken down into the empty weight, crew weight, and weight of operating items. The operating empty weight of aircraft is often related to the takeoff weight for Class I analyses. In order to find this relationship a database was built containing reference aircraft designs from the past. As for several studies the empty weight was provided and not the operating empty weight, the assumption was made that the operating empty weight is 1.05 times the empty weight. This 1.05 was found by looking at several weight breakdowns and taking the average operating-empty-weight-to-empty-weight ratio. The operating empty weight of the designs were then plotted against their takeoff weights on a logarithmic scale to find a fit. The logarithmic plot showed a good fit (R^2_{log} = 0.989) using 30 data points, and is shown in Figure 3.3. The values and sources of the individual data points are listed in Table B.2.

Based on this fit, the operating empty weight is related to the takeoff weight by Equation (3.3):

$$W_{OE} = 10^{\log_{10}(W_{TO})\cdot a+b} = 10^{\log_{10}(W_{TO})\cdot 0.41394-0.1690} \tag{3.3}$$

The figure shows that there are two main clusters in which supersonic aircraft fall, with the left one being mostly SSBJs and the other cluster larger SSTs. An attempt was also made to create a fit through the SSBJs and SSTs separately, but this resulted in worse fits and was therefore deemed inferior to the fit using both aircraft types.

3.1.3. Fuel weight

In order to estimate the fuel weight of the aircraft, the fuel fraction method is used. For this a mission is broken down into a series of segments, and for each of them a fuel fraction is either assumed or calculated. The fuel fraction for each segment is defined as the ratio of the weight at the end over that at the start of the

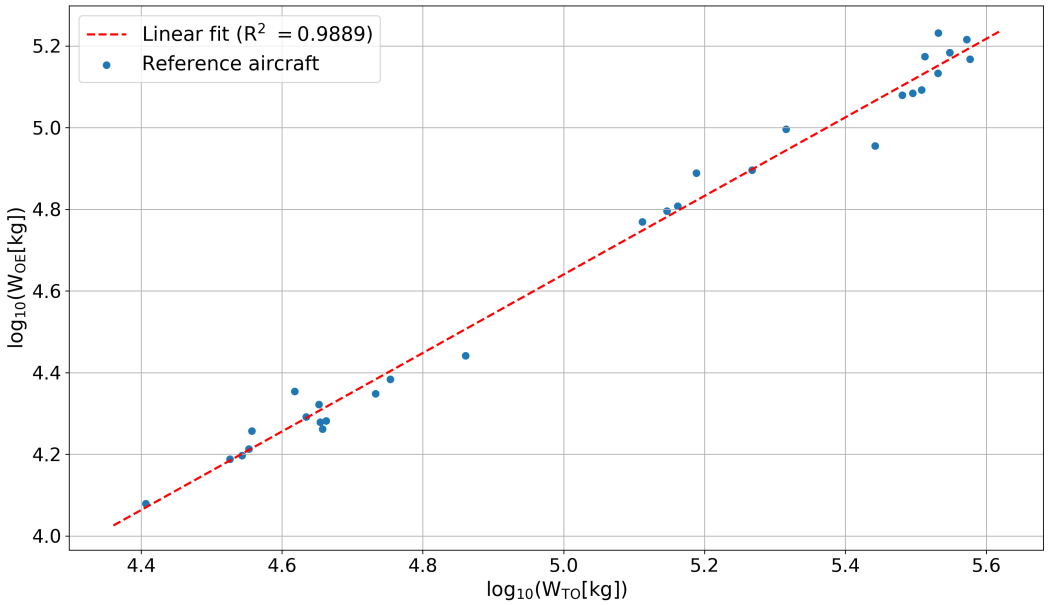

Figure 3.3: Operating empty weight regression

segment [13]. Following the calculation of all fuel fractions, the mission fuel fraction M_{ff} is defined as the product of the individual fractions:

$$M_{ff} = \Pi_{i=0}^{i=15} \frac{W_{i+1}}{W_i} \tag{3.4}$$

where in this case i=0 is the ramp weight and i=15 the end of mission weight. As the main interest is in the takeoff weight, and not the ramp weight, the first two segments (engine startup and taxi-out) are not included. The fuel-to-takeoff-weight ratio is then computed by using Equation (3.5).

$$\frac{W_F}{W_{TO}} = (1 - M_{ff}) = \left(1 - \Pi_{i=2}^{i=15} \frac{W_{i+1}}{W_i}\right) \tag{3.5}$$

For cruise segments the Breguet range equation for jet aircraft is used to determine the fuel fractions [13]:

$$R = \frac{V}{c_j} \cdot \left(\frac{L}{D}\right)_{cr} \cdot \ln\left(\frac{W_{st}}{W_{end}}\right) \tag{3.6}$$

where R is the segment range, V the cruise speed, c_j the specific fuel consumption and L/D the lift-to-drag ratio. The Breguet equation assumes that the aircraft is performing a cruise climb at constant speed and angle of attack, which has been used by several past supersonic design studies. Also, at the flight level where supersonic aircraft operate, the traffic density is very low so it is expected that there is a bigger potential for continuous cruise climbs. To still account for the effect of traffic limitations, the segment range is multiplied by 1.02, which increases the fuel required for the segment as found by Hale [15]. Also, in the calculations it is assumed that the there is no wind, which is quite a strong assumption, but at the higher altitudes where supersonic aircraft operate, this is more reasonable, since the atmosphere is more stable.

It should also be noted that due to the aircraft altitude, some other changes should be kept in mind as explained by Ruijgrok [16]. In the lower stratosphere, where the speed of sound is constant, a constant airspeed also results in a constant Mach number, and aerodynamic ratio. Given the small angle of attack, force equilibrium can be assumed and thrust is written as $T = C_D \cdot \frac{1}{2} \cdot \rho \cdot V^2 \cdot S$. This indicates that the thrust is directly proportional to the air density, and that the ratio T/ρ is also constant. In turn, this means that the engine setting will also be constant, and consequently that the specific fuel consumption is also fixed. The Breguet range equation could then be rewritten to the form shown below [16]:

$$R = \frac{1}{c_j} \cdot \sqrt{\frac{T}{S} \cdot \frac{2}{\rho} \cdot \frac{C_L^2}{C_D^3}} \cdot \ln\left(\frac{W_{st}}{W_{end}}\right) \tag{3.7}$$

From this rewritten equation it can be seen that in order to maximize the range of an aircraft in the lower stratosphere, the ratio of C_L^2/C_D^3 should be maximized, when the engine setting is constant. This is different

from the situation in the troposphere, where C_L/C_D should be maximized. Note that in this study L/D is maximized as this was also done in other studies and to limit complexity.

For the loiter (holding) segment the Breguet endurance equation for jet aircraft is used [13]:

$$E = \frac{1}{c_j} \cdot \left(\frac{L}{D}\right)_{ltr} \cdot \ln\left(\frac{W_{st}}{W_{end}}\right) \tag{3.8}$$

with the endurance E representing the time spent loitering, c_j the specific fuel consumption, and L/D the loitering lift-to-drag ratio. The values used in the equations will be shown later when the results are analyzed.

The first mission segment, takeoff, is assumed to have a fuel fraction of 0.995 as suggested in [13]. Next is the climb segment, which is assumed to include the transonic acceleration and uses the correlation shown in Figure 3.4.

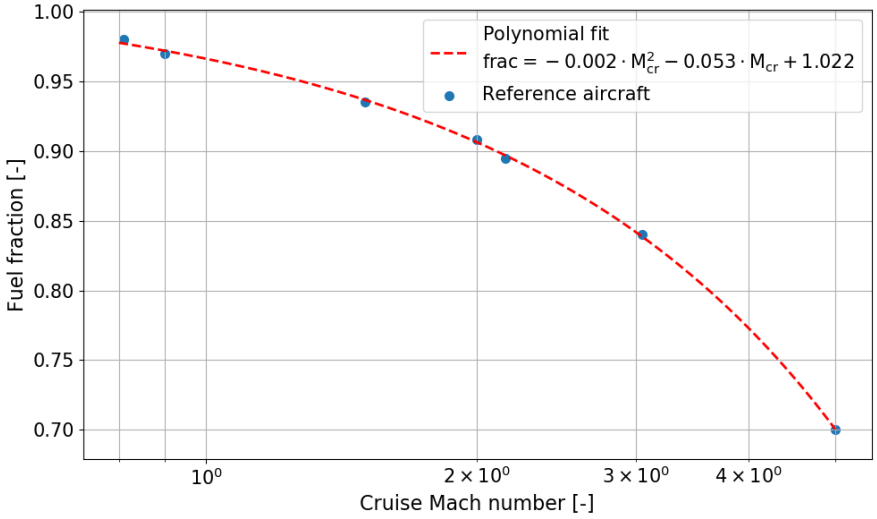

Figure 3.4: Climb segment fuel fraction as function of cruise Mach number [17]

Based on the cruise Mach number, the fuel fraction is found by evaluating the second-order polynomial fit. If a subsonic cruise segment precedes supersonic cruise, then the fuel fraction is split into two segments. For the climb to subsonic cruise the ratio is found by evaluating the polynomial. For the climb and acceleration from sub- to supersonic cruise the ratio is then computed using the following equation:

$$\frac{W_{end}}{W_{st}}\left(M = M_{sub} \rightarrow M_{sup}\right) = \frac{\frac{W_{end}}{W_{st}}\left(M = 0 \rightarrow M_{sup}\right)}{\frac{W_{end}}{W_{st}}\left(M = 0 \rightarrow M_{sub}\right)} \tag{3.9}$$

During the climb and transonic acceleration, as well as during the deceleration and descent, distance is traveled, which is subtracted from the supersonic cruise range. The method used for determining these distances is explained in Appendix B.1.

For the subsonic cruise segments it is possible to either define their distances as a fraction of the total range or as absolute values. These distances are then also subtracted from the supersonic cruise range. The supersonic and two subsonic cruise segments utilize the Breguet range equation shown earlier to compute their fuel fractions. Following this the descent fuel fraction is assumed to be 0.985 as suggested by Roskam [13], with the deceleration fraction from super- to subsonic speeds being 0.99 and the subsonic descent fraction approximately 0.995. Then, the last segment is landing, taxi, and shutdown for which a fuel fraction of 0.992 is used [13].

This concludes the main mission, but to meet the regulations several extra mission segments are added:

- Contingency fuel: the contingency fuel is used to compensate for unforeseen conditions. Regulations by ICAO stipulate that it should be 5% of the trip fuel or five minutes of flight, whichever is larger [18]. In virtually all situations, the former will be larger. In Federal Aviation Administration (FAA) regulations (91.167), however, it is stated that apart from the trip and alternate fuel, there should be enough fuel for a 45 minute extension at cruise conditions in instrument flight rule (IFR) conditions[1]. Since the loiter and final reserve fuel are not mentioned, it is assumed that they are included in this 45 minute period. Also, according to [19], the FAR (Federal Aviation Regulation) 141.645 rule for international flight, the

[1] www.ecfr.gov (accessed August 17 2018)

contingency should allow for flying 10% of the mission time. Since loiter and final reserve fuel fractions are included in the mission for a total loiter time of one hour, it is deemed sufficient to use 30 minutes of flight time in subsonic cruise configuration for the contingency segment. In the cases investigated this will result in contingency fuel being 3-7% of the trip fuel. The corresponding fuel fraction is computed using the Breguet range equation in subsonic configuration and subsonic cruise altitude.

- Alternate fuel: the alternate fuel is used to divert to a different airport, and includes a climb, cruise and descent segment. For the module it is defined as a subsonic cruise segment of 250 nautical miles, which is used in several other supersonic design studies as well. The Breguet range equation is again used to calculate the fuel fraction.
- Loiter: fuel reserved for loitering en-route to the arrival airport in case of traffic. Defined to be 30 minutes of flight time in the loiter (holding) configuration near the airport [18]. The holding altitude is assumed to be 6,500 m with a holding speed of 280 kts according to ICAO [20]. For this situation the Breguet endurance equation is applied.
- Final reserve fuel: the last reserve fuel component which should be used only in special circumstances, allows for 30 minutes of flight at holding speed, which is 230 kts at an altitude of 1,500 ft under standard conditions as defined by ICAO [18, 20]. The Breguet endurance equation is used for this segment.

There is also the option to include additional and discretionary fuel fractions, but these are typically at the discretion of the pilots flying the aircraft, and therefore not implemented.

3.1.4. Verification

After the different steps were completed a verification was performed by checking the individual calculations through unit testing. Additionally, an example Class I analysis from Roskam [13] was used to verify that when the same inputs are provided, the results found are similar. Here, it was found that there was a deviation of less than 0.1%, which was caused by round-off differences, so that the module could be considered verified.

3.2. Validation

Since the weight estimation method described above is based on relatively simple equations and assumptions on aerodynamics and engine performance, combined with top level requirements, validation is needed. For the validation of the module only two aircraft can be used that actually flew, the Concorde and Tu-144, of which the former has the most information available. Despite this, assumptions have to be made for various performance parameters. The two aircraft are supplemented with ten supersonic aircraft design studies. Again, in these studies, certain values will often not be available like the loiter L/D or specific fuel consumption. In such situations scaling will be used with other similar aircraft, or values are assumed such that the aircraft weight becomes reasonably similar to that found by the study. Note that the values assumed are always checked to be in the range provided by Roskam for SSTs [13], as well as the values of comparable supersonic aircraft in the database. The aircraft and inputs used to analyze them are shown in Table 3.1.

For each aircraft a single design mission is used, as for most only a single mission is available in literature. The design point used for Concorde is that with maximum fuel, 8,550 kg of payload and a range of 3,550 NM. Similarly, for the Tu-144, the mission selected is at its maximum payload of 15 tonnes, and a range of 5,330 km. If no design payload weight was indicated by the sources, as was the case for the Edge SST, the payload is calculated as described in Section 3.1.1. Using the module, the estimated takeoff weight and operating empty weight were calculated for the 12 aircraft, and plotted against the reference values found in literature. To better show the accuracy, lines for ±10% and ±25% deviation are also included. The results are shown in Figures 3.5 and 3.6, and listed in Table 3.2.

To determine the delta (or deviation) the following equation is used:

$$\text{delta [\%]} = \frac{\text{computed value} - \text{reference value}}{\text{reference value}} \cdot 100\% \tag{3.10}$$

Note that the two aircraft (8 and 9) indicated with red triangles (▷) in the two figures use inputs that deviate from the literature values. This was done to prevent the mission from becoming impossible, as the payload weight would become negative for too high fuel fractions.

Table 3.1: Class I validation aircraft characteristics

Aircraft	R_{mis} [NM]	n_{pax} [-]	W_{payl} [kg]	M_{sup} [-]	h_{sup} [m]	L/D_{sup} [-]	$c_{j,\,sup}$ [lb/lbf.hr]	M_{sub} [-]	h_{sub} [m]	L/D_{sub} [-]	$c_{j,\,sub}$ [lb/lbf.hr]	L/D_{hold} [-]	$c_{j,\,hold}$ [lb/lbf.hr]	Source
1. Concorde	3,550	88	8,850	2.02	18,300	7.14	1.195	0.95	9,000[2]	11.5	0.913[3]	9.27	1.020 [4]	[5] [6][21, 22]
2. Edge	5,750	250	-	2.4	18,300	9.6	1	0.70	10,700	11.3	0.78	9.4[7]	0.76	[23]
3. Low boom SSBJ	4,000	10	1,021	2	18,000	7	1.03[8]	0.92	11,000	11.24[9]	0.782[9]	8.48[9]	0.968[9]	[24]
4. Cranfield SSBJ	4,320	19	2,000	1.6	18,000	8	0.856[9]	0.90	10,000	10.6	0.65[10]	9.1[4]	0.805[9]	[25]
5. HELESA	4,000	18	1,890	1.6	15,000	7.1	0.83	0.92	12,000	11.4	0.63	8.6[4]	0.78[4]	[26]
6. Tu-144	2,878	150	15,000	2	18,000	7	1.23	0.95[11]	11,000	11.27[12]	0.94	9.09[12]	1.10[4]	[13] [14]
7. McD AST	3,968	292	27,682	2.62	19,500	8.92	1.35	0.95[15]	11,000[15]	13.20[16]	1.032[12]	10.64[16]	1.152[12]	[27, 28]
8. NASA M2.4[17]	6,500	250	24,968	2.4	19,500	9[18]	0.91	0.90	9,500	17.6	0.85	16.8	0.8	[29]
9. 1080-874	5,000	279	26,576	2.4	18,500	8.89	1.12[19]	0.90	10,500	14.43	0.876[19]	12.0[20]	0.978[19]	[30]
10. NLR M1.6	5,500	250	23,750	1.6	16,000	11.1[18]	0.98[21]	0.95	9,450	12.8	0.8	12.1	0.9	[31]
11. N+1 overwater	3,720	128	16,354	1.3	14,020	8.72	0.81[22]	0.95	12,200	12.76	0.59[23]	11.2[4]	0.68[4]	[32]
12. NASA N+3	4,850	100	9,752	1.6	15,200	8.7	0.881	0.90	9,500	12.75[24]	0.613[24]	11.2	0.7	[33]

[2] initial cruise altitude, after supersonic cruise optimum altitude is 10,700 m
[3] scaled using Tu-144 engines
[4] assumed between super- and subsonic conditions
[5] http://www.concordesst.com (accessed April 24 2018)
[6] IHS Markit, *Concorde*, https://janes.ihs.com/JAWAInServices/Display/1336723 (accessed June 26 2018)
[7] assumed in between 7.6 at takeoff and 11.3 subsonic
[8] value significantly lower than 1.2 indicated in source, but this prevented mission from being possible, so 1.03 was selected
[9] scaled using HELESA
[10] IHS Markit, *Rolls-Royce RB199*, https://janes.ihs.com/AeroEngines/Display/1306206 (accessed June 15 2018)
[11] assumed same as Concorde
[12] scaled using Concorde
[13] http://www.tu144sst.com/index.html (accessed April 24 2018)
[14] IHS Markit, *Saturn RD-36-51*, http://janes.ihs.com/AeroEngines/Display/1306317 (accessed April 24 2018)
[15] assumed flight condition same as Tu-144
[16] scaled using Concorde with 0.92 factor as otherwise L/D larger than maximum value
[17] many changes had to be made compared to source, or design would not be possible. These include operating at maximum L/D and over 30% reduced supersonic SFC.
[18] maximum L/D assumed to make mission possible
[19] 85% of value found in source
[20] scaled using Edge
[21] reduced wrt cruise start value of 1.05 to account for weight loss, and make mission possible
[22] should be in range 0.8-0.9 according to specific range values
[23] should be in range 0.574-0.67 according to specific range values
[24] scaled using N+1 values

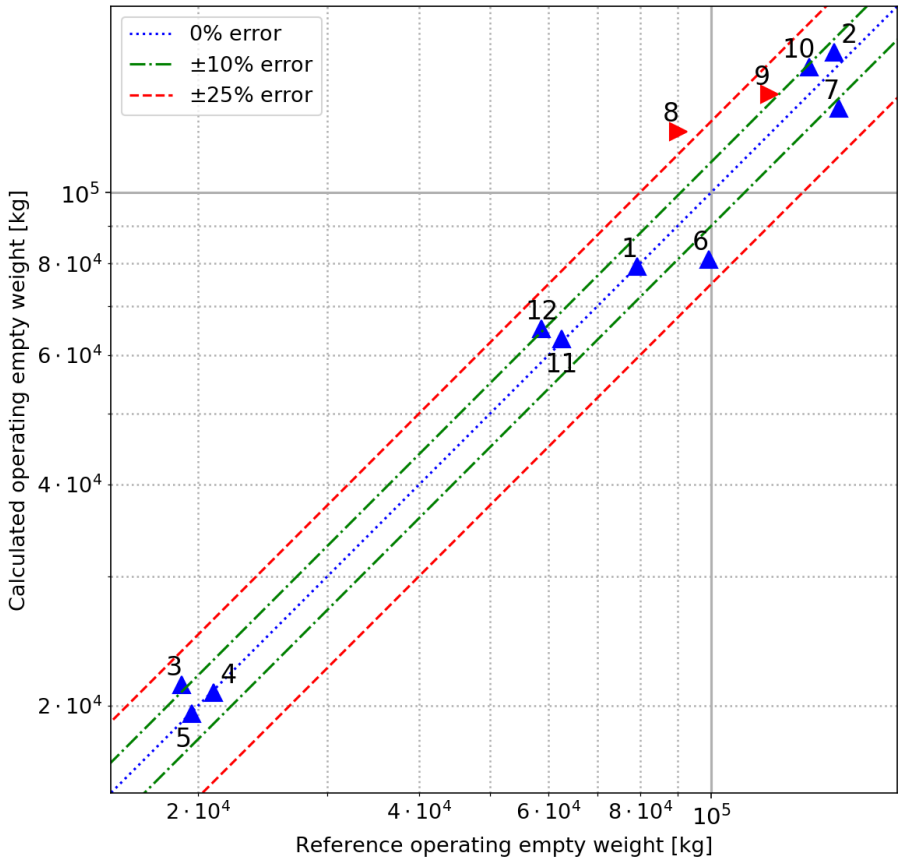

Figure 3.5: Operating empty weight comparison between Class I results and reference for 12 aircraft

From the operating empty weight results it can be seen that there is quite some variation in the deviation from the reference values. Still, only in one case the difference is more than 25%, and the absolute average deviation is 9.90%. For the Tu-144, the difference is quite large because the aircraft was relatively heavy, in comparison to the Concorde, where different construction methods were used. Also, in case of the NASA M2.4 SST, a large number of technology factors (see Section 6.4) were applied to the different components to account for further weight reductions, which are not captured by the operating empty weight fit. This can to some extent explain why the deviation is over 30%.

For the takeoff weight, the deviations are smaller, with only one aircraft (N+3) having more than 10% difference, and an absolute average deviation of 5.57%. Part of the differences in takeoff weight comes from the variation of the operation empty weight, which is in turn caused by the fit that is used to relate it to the takeoff weight. In the case of large deviations as seen for the Tu-144 and NASA M2.4 aircraft, they also represent larger outliers in Figure 3.3. Consequently, if the takeoff weight calculated is closer to the reference value, the operating empty weight will have a larger deviation. Also, as a result of the operating empty weight deviation, the fuel weight will deviate. So, for the NASA M2.4 where the operating empty weight is 34.12% larger than the reference value, the fuel weight calculated is almost 40,000 kg lower than its reference value.

These errors will also affect new aircraft as long as a statistical relationship is used to link the operating empty weight and takeoff weight. It should be noted that the reserve fuel fractions used in the design module are based on the regulations stipulated by ICAO, while for some aircraft designs, the mission profile featured different reserve fuel segments. The effect of this is that the fuel fraction calculations deviate, with the consequence that the takeoff weight can also deviate. However, because the reserves represent a smaller part of the total fuel fraction, the impact is limited. Despite these issues, given that the absolute deviations for both weights are less than 10%, the Class I module is considered accurate enough for this stage of the design process.

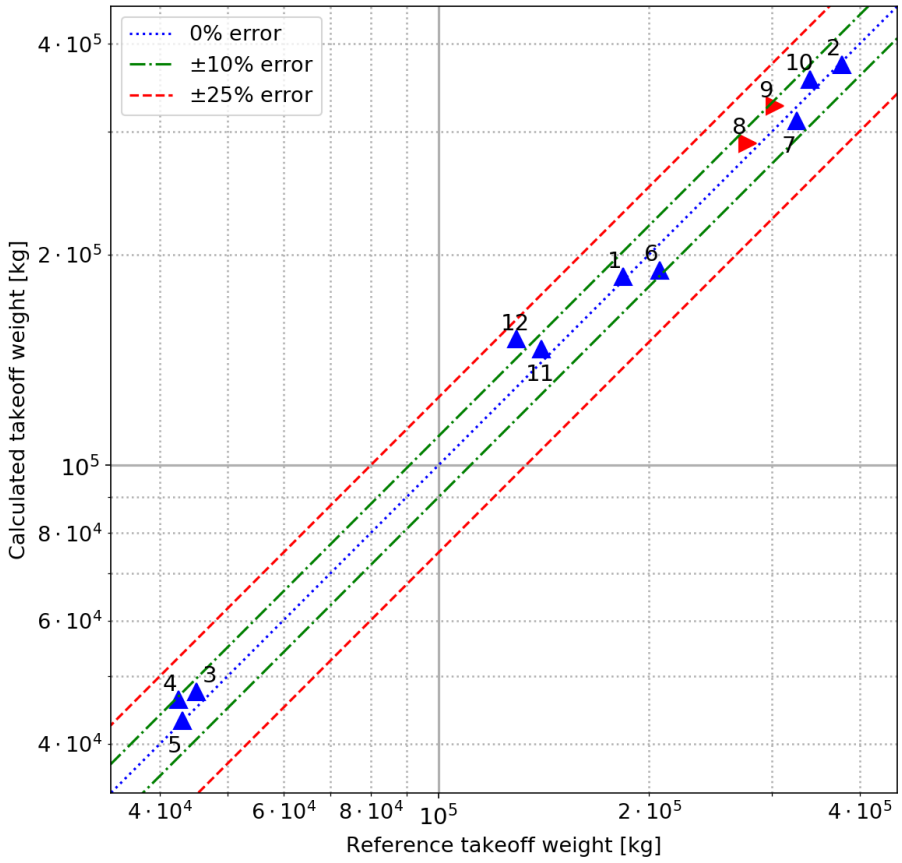

Figure 3.6: Maximum takeoff weight comparison between Class I results and reference for 12 aircraft

Table 3.2: Class I validation results for 12 aircraft

Aircraft	**OEW_{ref} [kg]**	**OEW_{calc} [kg]**	**Delta [%]**	**$MTOW_{ref}$ [kg]**	**$MTOW_{calc}$ [kg]**	**Delta [%]**
1. Concorde	79,264	79,362	+0.12	185,066	185,914	+0.46
2. Edge	147,186	155,341	+5.54	377,389	373,753	-0.96
3. Low boom SSBJ	18,998	21,354	+12.40	45,103	47,479	+5.27
4. Cranfield SSBJ	21,000	20,815	-0.88	42,500	46,239	+8.80
5. HELESA	19,577	19,492	-0.43	43,100	43,188	+0.20
6. Tu-144	99,199	81,052	-18.29	206,974	190,031	-8.19
7. McD AST	149,448	130,169	-12.90	325,679	310,982	-4.51
8. NASA M2.4	90,332	121,154	+34.12	276,889	288,619	+4.24
9. 1080-874	120,255	136,115	+13.19	302,481	325,786	+7.70
10. NLR M1.6 airliner	136,000	148,195	+8.97	340,000	355,900	+4.68
11. N+1 overwater	62,489	63,133	+1.03	140,160	146,564	+4.57
12. N+3	58,766	65,175	+10.91	129,267	151,490	+17.20
Absolute average	-	-	**9.90**	-	-	**5.57**

3.3. Additional weights

Aside from the takeoff weight of the aircraft, there are several other weights that might be interesting to the designer. The first is the aircraft ramp weight, which is the weight at the gate before the aircraft starts its engines. In order to compute the ramp weight, the fuel fractions of the two first segments, being engine start and taxi-out, are used. For the engine start and warmup, the fuel fraction is assumed to be 0.990, and for taxi-out 0.995, as suggested in [13]. The ramp weight is then found by the following equation:

$$W_{ramp} = \frac{W_{TO}}{0.990 \cdot 0.995} \approx 1.015 \cdot W_{TO} \tag{3.11}$$

This will result in a ramp weight that is approximately 1.5% greater than the takeoff weight. Aside from this, it is also possible to estimate the aircraft maximum landing weight, which will also be used later on during the wing loading analysis. For this Equation (3.12) from Torenbeek [34] is used:

$$W_{MLW} = \left[0.2 + 0.9 \cdot e^{-\frac{R_B}{R_{ref}}}\right] \cdot (W_{TO} - W_{MZF}) + W_{MZF} \tag{3.12}$$

where R_B is the design range for maximum payload in nautical miles, R_{ref} is 1,000 nautical miles, and W_{MZF} is the maximum zero fuel weight. The maximum zero fuel weight is the aircraft weight when it is at its maximum payload weight without any mission fuel on board. In the current Class I calculations, where only a single design point is used, it is simply the sum of the operating empty and payload weights. For Concorde, the maximum landing weight is found to be 110,274 kg, which is 0.77% less than the actual value of 111,130 kg[25]. For the Tu-144 the maximum landing weight is calculated to be 119,605 kg, which is 0.33% lower than the actual value of 120,000 kg[26]. This shows that the maximum landing weight calculations are also accurate, and can be used in the wing loading analysis.

3.4. Input variation and sensitivity

In Section 3.2 it was shown that the module created is capable of performing Class I weight analyses of supersonic aircraft with sufficient accuracy for this stage of the design process. Aside from the operating empty weight and takeoff weight already shown, another factor is important to aircraft design, namely the payload weight fraction. For the twelve aircraft analyzed earlier, the payload fractions are shown in Table 3.3.

Table 3.3: Supersonic aircraft payload weight fractions for 12 supersonic aircraft

ID	Aircraft	Percentage [%]	ID	Aircraft	Percentage [%]
1	Concorde	4.76	7	McD AST	8.90
2	Edge	8.10	8	NASA 2.4 SST	8.65
3	Low boom SSBJ	2.15	9	1080-874	8.16
4	Cranfield SSBJ	4.32	10	NLR M1.6	6.67
5	HELESA	4.38	11	N+1 overwater	11.16
6	Tu-144	7.89	12	NASA N+3	6.44
Average			**6.80**		

This shows that the average payload weight fraction is 6.80%. Looking at the Concorde and Tu-144 it can be seen that the Tu-144 has a larger payload fraction. This is because for Tu-144 the sizing mission is at maximum payload, while for Concorde the maximum payload situation was not used. The reason for this difference is that the missions used were listed in literature, and could therefore be used more reliably. Compared to subsonic aircraft which have payload fractions of around 15-25% (see also Table B.3) the value is low, and to a large extent this is caused by the higher fuel fraction which reduces the payload fraction. Note that for business aircraft the relative payload fraction is smaller, such as the Gulfstream G650 with about 6.5%[27] (not for maximum range). As a result of the high fuel fraction, a small change in the input parameters can result in a large increase of the fuel quantity. If the takeoff weight is fixed, this means that the payload has to be reduced by the same amount as the fuel increase. Since the payload fraction is smaller than for subsonic aircraft, an equal reduction in payload will have a larger impact on a supersonic aircraft. In turn, this will affect the profitability, and therefore market potential, so it is interesting to look at the design sensitivity.

Looking at the inputs used (Table 3.1), it can be seen that there is quite some variation in the values. To better understand this, an attempt was made to find correlations for the inputs, of which the supersonic lift-to-drag ratio and specific fuel consumption are the most important, because their segment represents the majority of the mission fuel. Note that some more aircraft have been added for which insufficient information was available to perform a Class I analysis. Starting with the supersonic lift-to-drag ratio, a correlation was sought with the year of design as shown in Figure 3.7.

[25] IHS Markit, *Concorde*, https://janes.ihs.com/JAWAInServices/Display/1336723 (accessed June 26 2018)
[26] http://www.tu144sst.com/index.html (accessed April 24 2018)
[27] Gulfstream G650 brochure www.gulfstream.com (accessed October 11 2018)

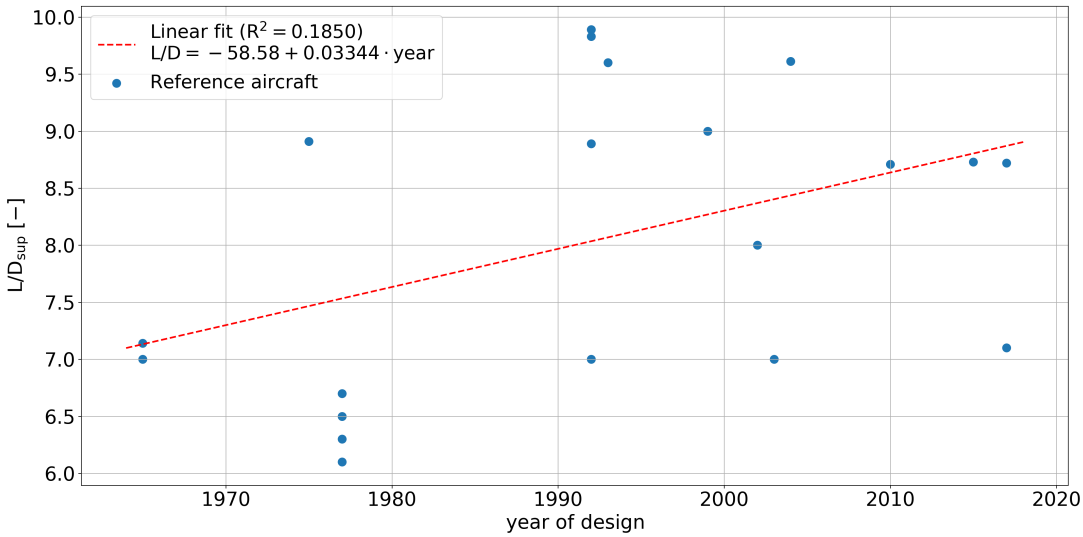

Figure 3.7: Supersonic L/D regression

From this no good fit was found, but a small trend was discerned with the lift-to-drag ratio increasing over time. The variation in the L/D-ratios shown in the plot can be explained by the fact that some design projects used advanced analysis tools, while others made use of simpler (semi-)empirical relationships. The trend of increasing L/D can to some extent be explained by the development of more advanced models, like Computational Fluid Dynamics (CFD) and windtunnels, which allow for a better understanding and prediction of the supersonic flow phenomena, and for shaping the aircraft to improve L/D. Also, more advanced wing and fuselage structures can be built and modeled in KBE tools, which allows for reducing factors such as wave drag. The average value of the supersonic lift-to-drag ratio is 8.04 and its standard deviation is 1.249.

A similar analysis for the supersonic specific fuel consumption ($c_{j,sup}$) resulted in Figure 3.8.

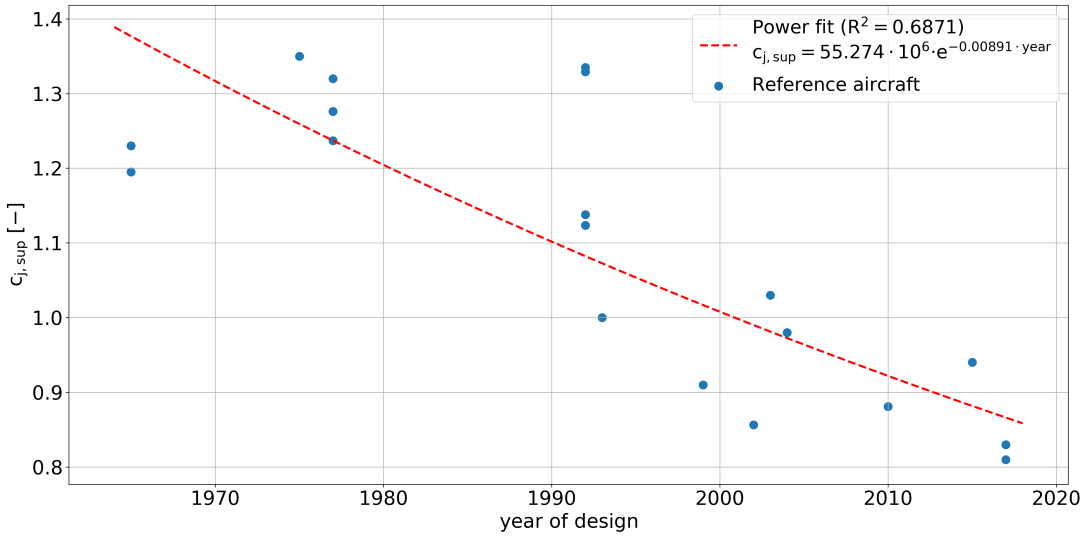

Figure 3.8: Supersonic specific fuel consumption regression

For the specific fuel consumption, an exponential trend was found with a fit of R^2 = 0.687. It shows that over time the specific fuel consumption values have decreased. This decrease can largely be explained by improvements in engine design, like the introduction of more heat resistant and lighter materials, which allow for higher pressure ratios, as well as improvements in fuel burn efficiency. However, since the engines for most projects are based on models, some small variations could still affect the values, but they will not drastically alter performance.

To better understand the impact of the inputs, the lift-to-drag ratio and specific fuel consumption for several aircraft will be changed by ±10%. Note that the impact of the L/D and specific fuel consumption change on takeoff weight will be the same (e.g. a 10% increase in L/D results in the same change as a 10% reduction of

specific fuel consumption) because of the Breguet range equation definition. A percentage change is chosen instead of several standard deviations because it will impact all aircraft equally, while a standard deviation will affect a lower L/D more than a higher value. Three situations will be looked at:

1. Unchanged mission (payload and range constant), with just a change in L/D.
2. Payload altered to get the takeoff weight to be within ±0.25% of the original takeoff weight found using the inputs in Table 3.1.
3. Range altered to get the takeoff weight to be within ±0.25% of the original takeoff weight found.

Since the amount of data would be too large to properly display for all aircraft, and would not add much more information, four aircraft are used. The Concorde and Tu-144 represent the only operated supersonic transport aircraft, NASA's N+3 represents future SSTs and the Cranfield SSBJ represents future SSBJs. The results are shown in Table 3.4.

Looking at the results, it can be seen that for an increase in L/D (or decrease of specific fuel consumption), the performance of all aircraft improves, as can be expected given that the supersonic cruise fuel fraction and thereby the total fuel fraction decreases. This results in a decrease of the maximum takeoff weight if the range and payload remain unchanged. On average, the reduction in takeoff weight is 21.79%. It can also be seen that for aircraft with higher original payload ratios (Tu-144, N+3), and consequently smaller fuel ratios, the impact of the change is smaller, because the relative fuel fraction improvement is also smaller. This is also visible when comparing the change in payload ratios, where given the fixed payload weight, a larger reduction in takeoff weight will result in a bigger improvement.

Since the takeoff weight decreased when the lift-to-drag improved (or sfc reduced), there is room to add more payload, while keeping the takeoff weight close to the original value. For the four aircraft this results in an average payload weight increase of 36.09%. The absolute increase in payload corresponding to this percentage is the same amount as the absolute decrease in fuel weight because of the way in which the takeoff weight is computed (see Equation (3.13)).

$$W_{TO} = W_{PL} + \frac{W_{OEW}}{W_{TO}} \cdot W_{TO} + \frac{W_f}{W_{TO}} \cdot W_{TO} \tag{3.13}$$

The operating empty weight fraction is a function of the takeoff weight only, so if the takeoff weight is within 0.25% of the original value, the operating empty weight will also be similar. The fuel fraction decrease is then compensated for by the increase in payload, showing that the absolute payload increase mathematically equals the fuel weight decrease. In real-life however, this is not true because the larger payload will require a larger fuselage or different seating configuration to transport the increased payload. In turn, the aircraft design has to be altered and the operating empty weight will likely increase. Consequently, the payload weight will still increase but not by the 36.09% stated earlier. The exact increase that can be achieved cannot be estimated for this scenario, and requires an iterative design process to include all effects of the payload increase.

Alternatively, the payload can be fixed but now be transported over a larger distance, with an average range increase of 8.45% (or 333 NM). To visualize the impact of this, a circle of 330 NM is drawn around London Heathrow (LHR) as shown in Figure 3.9.

Figure 3.9: 330 NM range circle around London Heathrow (LHR)[28]

[28] Great Circle Mapper, http://www.gcmap.com (accessed August 14 2018)

This shows that the improvement in range will allow the aircraft to fly from London to Amsterdam (AMS), Cologne (CGN), Dublin (DUB) or Paris (CDG), meaning that the potential route network increases.

The same analysis has also been performed with a 10% reduction of the aerodynamic efficiency (or 10% increase in sfc). This performance decrease results in an average maximum takeoff weight increase of 39.21%, which is about 1.8 times as much as the weight reduction shown earlier. As expected, for a smaller original payload fraction, the relative increase in takeoff weight is larger, since the relative fuel fraction increase resulting from the performance drop has more impact. To keep the maximum takeoff weight close to the original value, the average payload reduction needed is 38.20%, but again, this is an overestimation and in reality the aircraft would become smaller, reducing the relative payload decrease. The average range reduction for the same takeoff weight is 7.73%. The values are close to their respective increases achieved when the aircraft performance is improved.

Similar behavior was identified for seven of the other eight aircraft. The one exception was the Low boom SSBJ (aircraft 3), for which in the case L/D is reduced (or sfc increased) by 10%, the aircraft becomes unfeasible if no other changes are made. This is caused by the increased fuel weight fraction, which, combined with the already low payload-to-weight fraction, will lead to the denominator in Equation (3.2) becoming negative. A means to remedy this would be to reduce the operating empty weight, or reduce the fuel reserves. This case is also a clear indicator that the sensitivity of supersonic transport aircraft, with their lower payload fraction, should not be underestimated and be kept in mind during the design process.

For the subsonic and loitering (holding) conditions, the effect of changes to the parameters can also be investigated. Because these segments represent a smaller part of the total mission fuel, the impact of variations are not as large as with the supersonic segments. However, all the above calculations have been performed under the assumption that the entire cruise segment of the main mission is performed in supersonic configuration. Given the current regulations on sonic boom this is not always possible, and this will be investigated by analyzing the same missions, except now with 20% of the original design mission range being flown in subsonic cruise configuration. The 20% is split equally over the two subsonic cruise segments in Figure 3.1. This is done for the same four aircraft, and the results are shown in Table 3.5

It can be seen that the reduction of the supersonic segment length results in small weight changes for three of the four aircraft, with only the N+3 showing a change of more than 2%. For the Tu-144 and Cranfield SSBJ the changes are such that they could be seen as negligible, and Concorde only shows a reduction of 1.56%. Consequently, the changes in payload ratio are also small, and almost equivalent to and in opposite sign of the takeoff weight increase or reduction. These small changes are expected given the values used in the Breguet range equation where the following ratio in the exponent is important for the fuel fraction as a function of range R:

$$\frac{R \cdot c_j}{L/D \cdot V} \qquad \text{in:} \qquad \frac{W_{end}}{W_{st}} = e^{-\frac{R \cdot c_j}{L/D \cdot V}} \tag{3.14}$$

Looking at the ratio of the constants c_j, L/D and the cruise speeds for subsonic and supersonic cruise it was found that for three of four aircraft (not N+3), the difference between the ratio for sub- and supersonic cruise is very small, meaning that in terms of fuel fraction, it does not really make much difference whether the aircraft flies sub- or supersonic. In turn, the mission fuel fraction does not change much and the takeoff weight will remain close to the original value. However, looking at the total time spent in cruise flight, there is an average increase of 21.9%, which reduces the attractiveness of supersonic flight from a passenger perspective. Also, when comparing the performance of supersonic aircraft in subsonic flight to current subsonic transport aircraft, their performance is much worse (e.g. subsonic aircraft L/D about 17-23 vs 10-14 for supersonic aircraft flying subsonic). Clearly, supersonic aircraft should be operated in supersonic configuration whenever possible.

Table 3.4: Class I L/D sensitivity analysis results

Change	Situation	Original				Unchanged mission		Payload change			Range change	
	Aircraft	W_{TO} [kg]	R_{mis} [NM]	W_{PL} [kg]	W_{PL}/W_{TO} [%]	W_{TO} [kg]	W_{PL}/W_{TO} [-]	W_{TO} [kg]	W_{PL} [kg]	W_{PL}/W_{TO} [-]	W_{TO} [kg]	R_{mis} [NM]
L/D +10%	Concorde	185,914	3,550	8,845	4.76	142,345 -23.44%	6.21 +30.61%	185,933 +0.01%	12,370 +39.85%	6.65 +39.84%	185,815 -0.05%	3,842 +8.23%
	Tu-144	190,031	2,878	15,000	7.89	161,643 -14.94%	9.28 +17.56%	190,036 +0.00%	18,135 +20.90%	9.54 +20.90%	190,032 +0.00%	3,102 +7.78%
	N+3	151,490	4,850	9,752	6.44	117,736 -22.28%	8.28 +28.67%	151,475 -0.01%	13,175 +35.10%	8.70 +35.11%	151,188 -0.20%	5,284 +8.95%
	Cranfield SSBJ	46,239	4,320	2,000	4.32	33,991 -26.49%	5.88 +36.04%	46,272 +0.07%	2,970 +48.51%	6.42 +48.40%	46,249 +0.02%	4,702 +8.84%
L/D -10%	Concorde	185,914	3,550	8,845	4.76	265,429 +42.77%	3.33 -29.96%	185,840 -0.04%	5,120 -42.11%	2.76 -42.09%	185,901 -0.01%	3,284 -7.49%
	Tu-144	190,031	2,878	15,000	7.89	232,008 +22.09%	6.47 -18.09%	190,032 +0.00%	11,670 -22.20%	6.14 -22.20%	189,946 -0.04%	2,672 -7.16%
	N+3	151,490	4,850	9,752	6.44	211,521 +39.63%	4.61 -28.38%	151,432 -0.04%	6,160 -36.83%	4.07 -36.81%	151,536 +0.24%	4,453 -8.19%
	Cranfield SSBJ	46,239	4,320	2,000	4.33	70,444 +52.35%	2.84 -34.36%	46,208 -0.06%	975 -51.25%	2.11 -51.21%	46,216 -0.05%	3,970 -8.09%

Table 3.5: Class I analysis results for partial subsonic cruise

Change	Situation	Original					Unchanged mission			Payload change			Range change	
	Aircraft	W_{TO} [kg]	R_{mis} [NM]	W_{PL} [kg]	W_{PL}/W_{TO} [%]	t_{cruise} [hr]	W_{TO} [kg]	W_{PL}/W_{TO} [%]	t_{cruise} [hr]	W_{TO} [kg]	W_{PL} [kg]	W_{PL}/W_{TO} [-]	W_{TO} [kg]	R_{mis} [NM]
20% of mission subsonic config	Concorde	185,914	3,550 (710)	8,845	4.76	2.52	183,010 -1.56%	4.83 +1.59%	3.18 +26.11%	185,944 +0.02%	9,035 +2.15%	4.86 +2.13%	186,029 +0.06%	3,565 +0.42%
	Tu-144	190,031	2,878 (576)	15,000	7.89	1.97	189,933 -0.05%	7.90 +0.05%	2.53 +28.17%	190,039 +0.00%	15,010 +0.07%	7.90 +0.06%	190,097 +0.03%	2,879 +0.04%
	N+3	151,490	4,850 (970)	9,752	6.44	4.76	135,536 -10.53%	7.20 +11.77%	5.54 +16.40%	151,540 +0.03%	11,180 +14.64%	7.38 +14.60%	151,456 -0.02%	5,017 +3.44%
	Cranfield SSBJ	46,239	4,320 (864)	2,000	4.33	4.19	46,307 +0.15%	4.32 -0.15%	4.89 +16.92%	46,210 -0.06%	1,990 -0.50%	4.31 -0.43%	46,210 -0.06%	4,316 -0.08%

3.5. Payload-range analysis

In the previous sections, the focus has mostly been on the design point where the payload and takeoff weight are maximized. However, for airlines and aircraft manufacturers it is also interesting to look for other flight scenarios, where payload is exchanged for additional fuel. This allows the airline to transport (fewer) passengers over a greater distance. To visualize the dependency of range and payload, a so-called payload-range diagram can be created. An exemplary diagram is shown in Figure 3.10.

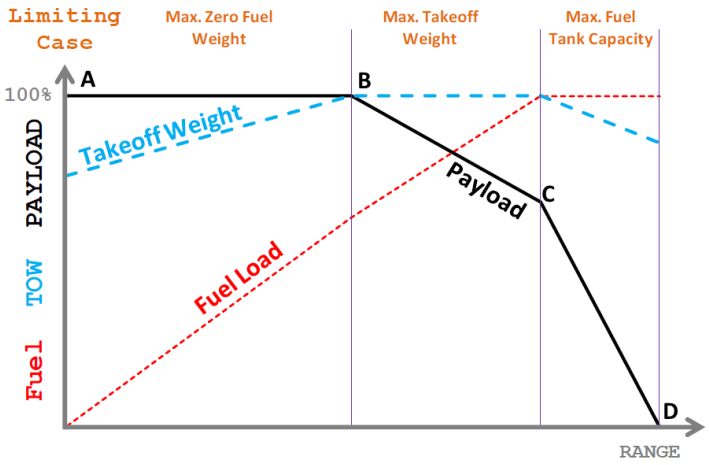

Figure 3.10: Example payload-range diagram [35]

In this diagram four points are shown:

- A: Aircraft is at maximum payload, but with no fuel on board. As a result, the range is zero.
- B: The range corresponding to this point is also known as the harmonic range. It is defined as the range where the payload is still the maximum, while being at the maximum takeoff weight.
- C: Between points B and C, payload is exchanged for extra fuel until the maximum amount of fuel is on-board. To attempt to estimate the maximum amount of fuel a small database was created in Appendix B.4, which shows the ratio of the maximum fuel to the harmonic range fuel. From the database an average ratio of 1.242 was found with a standard deviation of 0.152. Looking at Concorde and Tu-144, the ratios are smaller, so a standard deviation was subtracted for the supersonic aircraft and a ratio of 1.089 is used. It should be noted that only for Concorde, the design point used earlier during the module validation is not the harmonic range.

  Because of the smaller payload and higher fuel fractions of supersonic aircraft, it is possible that the payload weight becomes zero before the fuel has reached the maximum predicted amount. In that case, there is no point C and the maximum fuel load ratio is less than the assumed value of 1.089.
- D: Beyond point C, any remaining payload is reduced to zero at point D, where the aircraft is no longer transporting any payload. Since the fuel weight is still at maximum, the takeoff weight can be less than the maximum takeoff weight. The range corresponding to this point is often termed the 'ferry range'. For the ferry range, the operating empty weight and fuel weight combine to form the takeoff weight. From this, a fuel fraction can be computed, and this fraction can be used to estimate the total range that can be flown.

Now that the diagram has been discussed, the method for the range calculations will be described. It uses the same fuel fraction method described earlier, but in a different manner. Instead of computing the fuel weight fraction from the segments, the supersonic segment is analyzed from the known fuel fraction, which can be computed from the fuel and takeoff weights for points C and D. These fractions are then converted to M_{ff}, which represents the product of all segment fuel fractions. Next, it is assumed that the only segment that is extended by the extra fuel is the supersonic cruise, meaning that for all other segments the weight ratios remain unchanged from those found for the harmonic mission. Then, the supersonic cruise weight ratio is computed as follows:

$$\frac{W_7}{W_6} = \frac{M_{ff}}{\prod_{i=2}^{5} \frac{W_{i+1}}{W_i} \cdot \prod_{i=7}^{15} \frac{W_{i+1}}{W_i}} \tag{3.15}$$

Next, by making use of the rewritten Breguet range equation, the range is computed (with 2% correction to account for cruise step climb):

$$R_{sup} = \ln\left(\frac{W_7}{W_6}\right) \cdot \frac{V \cdot \frac{L}{D}}{c_{j,sup} \cdot 1.02} \tag{3.16}$$

The difference between this value and the value found in the harmonic range calculations then represents the range increase. In order to show the results of payload-range diagram calculations, the Tu-144 and HELESA aircraft were analyzed, and the results are shown in Figure 3.11.

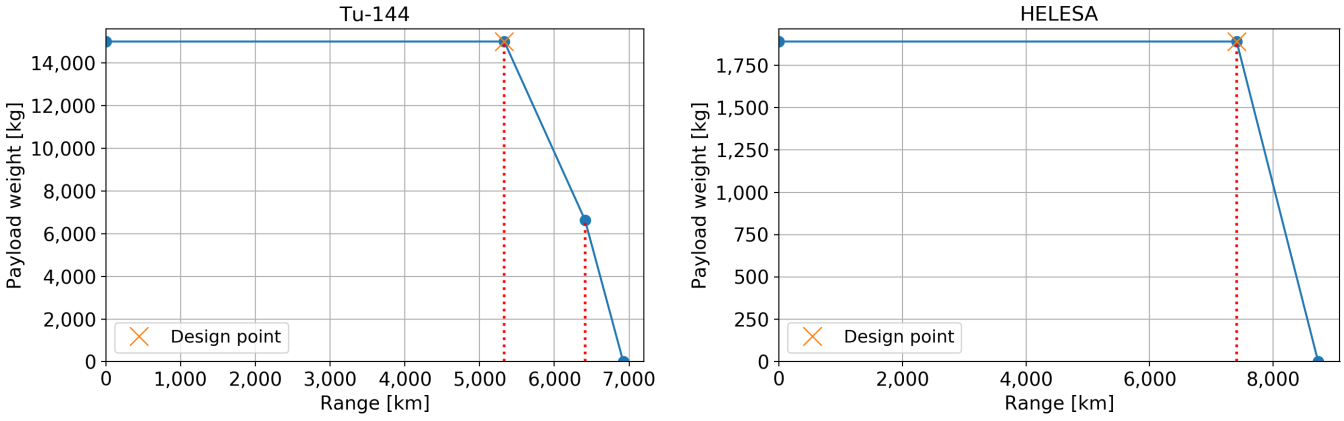

(a) Tu-144

(b) HELESA

Figure 3.11: Payload-range calculation example results for two supersonic aircraft

Looking at the result for the Tu-144 it can be seen that the range at point C is 6,410 km, which represents an increase of 1,305 km (20.3% increase) over the harmonic range at a payload of 6,635 kg (55.8% reduction). The ferry range is 6,921 km, which is a 1,591 km improvement (29.8%) over the harmonic range. For HELESA, there is no point C, only the harmonic and ferry range exist, which shows a 17.8% range improvement. To show the range improvements for the other aircraft the values are listed in Table 3.6. Note that Concorde is not included because it was lacking data on the harmonic range.

Table 3.6: Payload-range data for 11 supersonic aircraft

Aircraft	Harmonic		Point C		Ferry	Change C		Change D
	Range [km]	Payload [kg]	Range [km]	Payload [kg]	Range [km]	Range [%]	Payload [%]	Range [%]
Edge	10,649	30,282	12,917	13,538	14,037	+21.3	-55.3	+31.8
NASA Low-Boom SSBJ	7,408	1,021	-	-	8,069	-	-	+8.9
Cranfield SSBJ	8,000	2,000	-	-	9,428	-	-	+17.9
HELESA	7,408	1,890	-	-	8,727	-	-	+17.8
Tu-144	5,330	15,000	6,410	6,635	6,921	+20.3	-55.8	+29.9
McD AST	7,349	27,682	8,975	14,053	9,988	+22.1	-49.2	+35.9
NASA M2.4	12,038	24,968	14,282	12,285	15,595	+18.6	-50.8	+29.5
1080-874	9,260	26,576	11,108	12,061	12,041	+20.0	-54.6	+30.0
NLR M1.6	10,186	23,750	12,075	7,377	12,596	+18.5	-68.9	+23.7
N+1	6,889	16,354	8,027	10,384	9,176	+16.5	-36.5	+33.2
N+3	8,982	9,752	10,553	2,938	10,957	+17.5	-69.9	+22.0
Average						**+19.4**	**-55.1**	**+25.5**

The table shows that the average increase in range achieved at point C is 19.4% at the expense of a 55.1% payload reduction. At the ferry range (point D), the average range increase is 25.5%. This shows that there is quite some room for the aircraft operators to adjust their flight routing using the increased range, albeit with lower payload. It can also be seen that for the three SSBJ aircraft, there is no point C. This is because their payload weight at harmonic range is less than the fuel increase of 8.9% assumed for point C, meaning that the aircraft would exceed the maximum takeoff weight if it were operating at maximum fuel. Consequently, they only have a ferry range where the payload is zero. The SSBJs also show that for smaller payload ratios, the amount of range increase that can be achieved is less than it is for the larger SSTs.

4
Wing loading and aircraft generation

Now that the aircraft weight has been estimated by the Class I method discussed in the previous chapter, the next step in the conceptual design process is the wing loading analysis. The wing loading method is briefly discussed in Section 4.1. From the wing- and thrust loading found, it is possible to estimate the wing area and engine thrust by using the Class I takeoff weight. Since the required engine thrust is now known, a low-fidelity engine design can be produced through the method outlined in Section 4.2. Given that the wing area and payload requirements are known, as well as inputs like the wing aspect ratio, it is possible to calculate the geometrical characteristics of the aircraft design. A short overview of the method is provided in Section 4.3. For detailed descriptions of the methods applied and results that were found, the reader is referred to [7].

4.1. Wing and thrust loading

The wing- and thrust-loading method revolves around the different requirements the aircraft design has to meet. These include requirements like the landing and takeoff distances, stall speed, cruise speed and altitude, and critical load factors. Each requirement can be represented by a mathematical equation which returns a curve or line as a function of wing loading (W/S). The equations used for this purpose can be found in sources such as [9, 13]. The curves can all be combined into a single figure (i.e. the wing loading diagram) with the wing loading on the x-axis and thrust loading on the y-axis, as shown in Figure 4.1. The following constraints are used in the current version of the design program:

1. Stall speed (clean and landing configuration)
2. Landing distance
3. Takeoff distance
4. Cruise speed (subsonic)
5. Cruise speed (supersonic)
6. Climb gradient for six scenarios defined in FAR25 [36] (e.g. OEI climbout)

Constraints for supersonic and subsonic turns with load factors of more than 1.5 were also considered for the analysis, but intermediate results showed that especially the supersonic turn constraint would result in too high design T/W values. If such a turn is to be performed, the aircraft cannot be assumed to be in level flight, and will lose altitude to overcome the thrust shortage. For the same reason, and because they are not considered primary objectives for a passenger aircraft, the constraints for the cruise, service and absolute ceiling altitudes were also left out.

It is important to note that engine thrust varies with altitude, and that this variation should be taken into account by correcting the thrust loading. The first correction accounts for thrust lapse due to air density changes, and involves multiplying the thrust by the product of two density ratios. The first ratio is for altitudes up to 11 km and has an assumed exponent of 0.7 because of the bypass ratio expected, and the second ratio is the density at the constraint altitude divided by that at 11 km altitude in the standard atmosphere [37].

$$\text{density factor} = \left(\frac{\rho_{11\text{km}}}{1.225}\right)^{0.7} \cdot \frac{\rho_{\text{h}}}{\rho_{11\text{km}}} \tag{4.1}$$

When operating below 11 km, the second term becomes one and the numerator of the first term equals the density at the constraint altitude. Additionaly, there are corrections for the inlet pressure variation and bypass ratio as detailed in [7]. The product of the density, pressure and bypass ratio correction factors forms the full thrust correction factor.

Aside from the thrust correction for altitude and Mach number, it is also necessary to include the effect of the weight change during flight. At the start of supersonic cruise, the aircraft will have already burnt thousands of kilograms of fuel to climb and accelerate. Since the wing loading value on the x-axis uses the takeoff weight, it is necessary to multiply the thrust loading values found for supersonic cruise by the ratio of the supersonic cruise weight and takeoff weight. This is done for all curves that represent a situation in which the aircraft is no longer at its takeoff weight, with the weight ratio depending on the conditions.

Now that all constraints have been evaluated and corrected, the curves originating from the different top-level requirements are combined into a single wing loading diagram. An example diagram from the program is shown in Figure 4.1 for a sample Mach 1.6 four-engine supersonic aircraft.

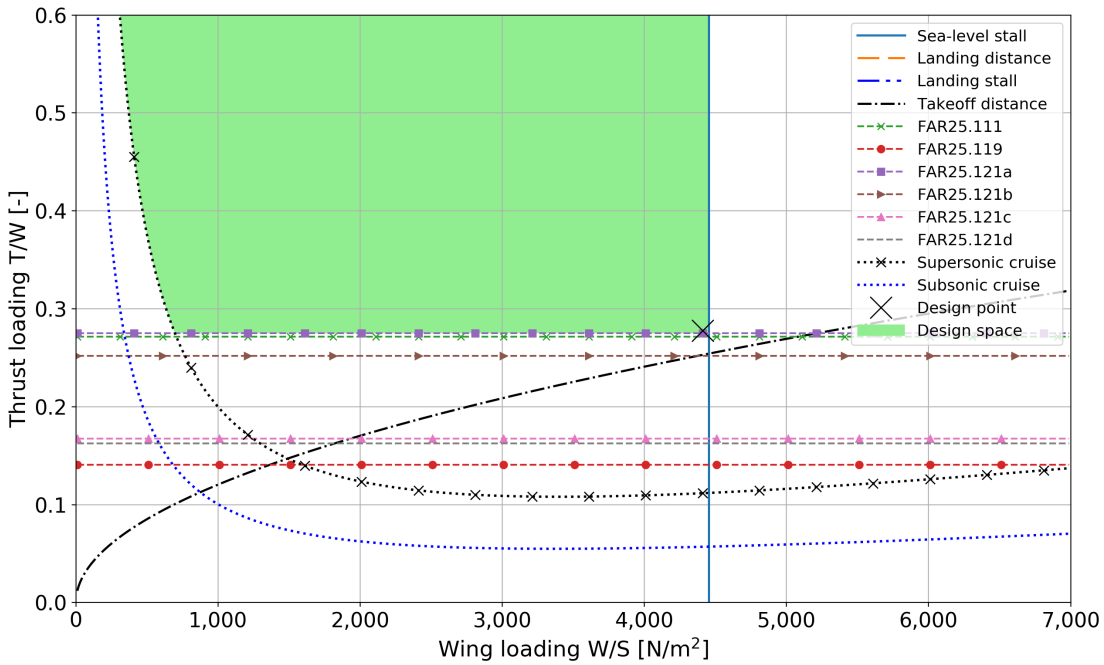

Figure 4.1: Wing loading diagram example for four engine aircraft (note design point with margins of 1%)

With the diagram it is possible to find the region where a design is feasible, meaning that it meets all constraints that have been set. This region is called the 'design space' and is highlighted in the figure by the green area, and used to select the design point. For turbojet-powered aircraft the design point is often located as far down and to the right as possible within the design space. This ensures that the aircraft has the smallest wing possible with a low power engine. In turn, this makes for a less complex engine which can be designed more easily and which will likely cost less to build and operate. Note that in some cases, it might be better to select a different point with a larger wing and/or engine, but for the current module this is assumed to not be necessary. An investigation into the effect of the design point selection will be included in [7]. Because the design point is considered too close to the edge of the feasible region, a small margin is introduced by selecting a slightly lower wing- and higher thrust loading value. This margin is a 1.0% increase of the design thrust loading, and 1.0% reduction of wing loading.

Because some of the constraints are dependent on the aerodynamic performance and weight of the aircraft, the diagram changes for each iteration. For example, the maximum lift coefficient at landing affects the landing stall constraint. For each iteration this can result in a different wing and engine size, which will affect the overall engine and aircraft design. By using the design point values together with the known takeoff weight, the wing area and takeoff engine thrust are determined and passed on to the engine and aircraft design modules.

4.2. Engine design

Now that the takeoff thrust at sea-level is known, it is possible to design the engine. Before performing the engine cycle calculations, a set of parameters for each engine component has to be defined. These include the efficiency of the intake, compressors, turbines and combustion chamber, but also factors like the engine

bypass and overall pressure ratio. For the bypass ratio, it is assumed that the engines have a bypass ratio in the range 2-3.5. This is still a relatively low ratio, but represents an improvement over Concorde and can aid in meeting the airport noise regulations. Also, fuel characteristics and compressor stage pressure ratios are provided. The values of these ratios as well as the component efficiencies are estimated by using past engine data and literature such as [38].

In the first step of the sizing calculations, the engine thrust is determined by dividing the total thrust by the user-defined number of engines. The engine count can be two or four, but not three. The three-engine configuration is currently not considered as it requires additional structural and aerodynamic considerations for the center engine, which is likely to be positioned in the rear part of the fuselage as with the Boom SST, or in the vertical tail as with the Aerion AS2 (see Figure 1.2). The benefit of three engines over two is that they can be less powerful which could aid in meeting noise requirements. New noise regulations that come into effect in 2020 were a reason for Aerion to switch from two modified JT8D engines[1] to three (GE Affinity) engines.

At this point most parameters needed for simple engine cycle calculations (see [39] for example calculations) are available, except for the air mass flow, turbine inlet temperature and compressor pressure ratios.

To determine the latter the compressor configuration has to be defined. Looking at the new GE Affinity engine, the decision was made to use a fan with two or more stages, and a high pressure compressor. For each separate stage, a pressure ratio of 1.4 is assumed based on literature [38, 40]. Using the overall pressure ratio, and starting with a two-stage fan, the number of HPC stages is determined. If the number of HPC stages is greater than ten, a third stage is added to the fan section, and the number HPC section stages is again increased until the OPR is reached. Note that the HPC stage pressure ratio is reduced when the OPR is higher than the user-defined value to ensure that the OPR is accurate.

For the turbine inlet temperature estimation it was decided to make use of a function with the engine certification year as variable. Note that other variables and methods were also considered but these were either not providing a good fit, or too complex. The turbine inlet temperature value used by the engine design program uses the following fit (output in Kelvin) [7]:

$$TIT = 454.545 \cdot \log_{10}\left(0.1632 \cdot \left(engineyear - 1950\right)\right) + 1000 \tag{4.2}$$

Note that it is also possible for the user to define the turbine inlet temperature manually to account for technological developments, instead of using the fit.

For the determination of the final unknown, the air mass flow, a constrained optimization routine is introduced. The objective function of the optimization is the engine specific fuel consumption, which is minimized by the system. To ensure that the results are realistic an equality constraint is introduced: $T_{calc} - T_{req} = 0$. This is done to ensure that the engine can deliver the required thrust at takeoff conditions, and is not under- or oversized. Also, bounds are inserted to make sure that the air flow is not excessively small or large although they are quite broad, currently set to ensure the air flow is between 30 and 1,300 kg/s. The optimization routine has been tested and was found to produce results that were within the ranges found for other aircraft engines. Again, more information about this is provided in [7].

Now that the engine has been sized for the design condition at takeoff, it is possible to also calculate the engine performance at off-design conditions. For the Class I weight estimation these are the different segments comprising the design mission. As for each segment, different altitudes, speeds and thrust settings apply, the values of the specific fuel consumption will vary. Because the amount of knowledge available on the compressor and turbine off-design performance (e.g. compressor and turbine maps) is low, the method in [41] is used since it does not require turbomachinery maps. Note however, that for the supersonic conditions, this method does not work properly in its current form. Instead, for supersonic cruise the specific fuel consumption is estimated by simply scaling the subsonic cruise specific fuel consumption by 1.24 [7]. This factor was found using engine data from past aircraft design studies. Additionally, the off-design method does not function for the lower thrust settings of the LTO cycle, which means that it can not be used for the LTO cycle emissions analysis.

Apart from the overall engine performance, the different dimensions of the engine are also needed for the aircraft design. The dimensions are estimated by using a set of statistical relationships set up using data from past turbojet, and turbofan engines, and are similar to the example shown for the engine mass. For the Class II weight estimation module the weight of a single engine has to be estimated so that the propulsion system weight can be determined. For this, Equation (4.3) is used which depends on the takeoff thrust of a single engine, and is based on the fit shown in Figure 4.2 [7].

[1] Trimble, S., *DUBAI: Aerion continues search for US assembly site*, https://www.flightglobal.com/news/articles/dubai-aerion-continues-search-for-us-assembly-site-418885/, November 10 2015 (accessed February 28 2019)

$$W_{eng} = 0.01621 \cdot T_{eng} + 346.0 \tag{4.3}$$

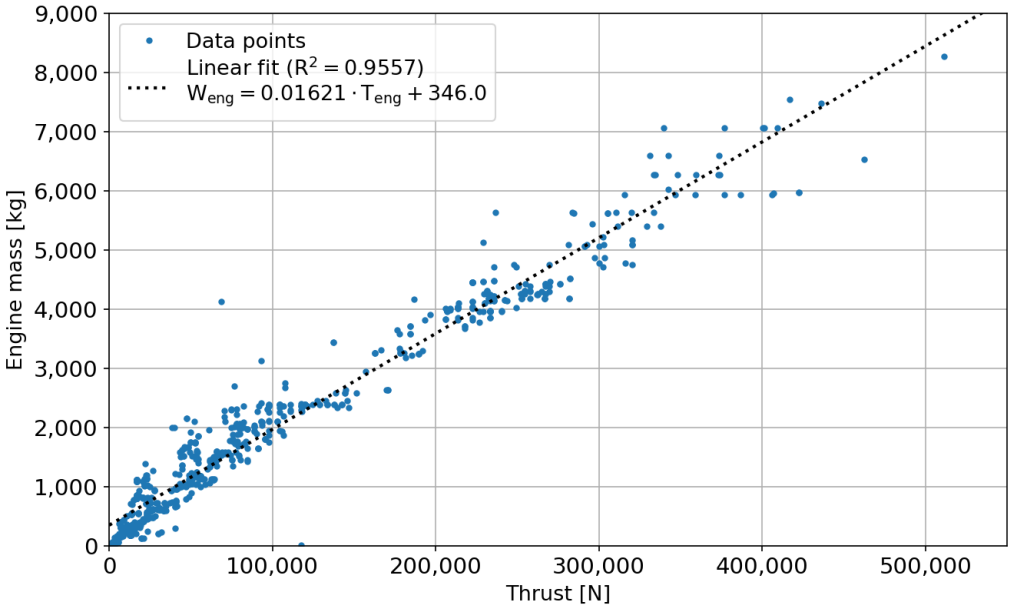

Figure 4.2: Engine mass estimation fit based on findings in [7]

The thrust is provided in Newtons, and the resulting engine mass is in kilograms. Because the graph above groups all engines together it is not possible to distinguish between engine groups. To resolve this, a second graph was created which splits the engines into four groups based on their OPR and bypass ratio values, as shown in Figure 4.3. It shows that the majority of the engines with an OPR of less than 30 have a thrust level that often does not exceed 100 kN, while ones with an OPR greater than 30 and a bypass ratio greater than three often produce more than 130 kN of thrust. More information can be found in [7]. Note also that the graph below includes fewer engines because for some engines in Figure 4.2 the OPR or bypass ratio is unknown.

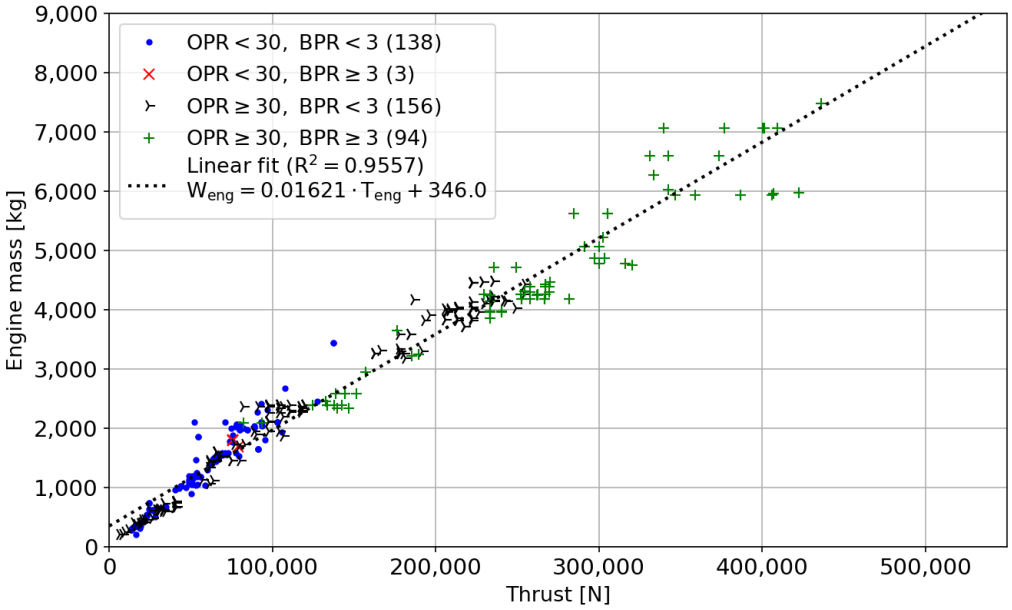

Figure 4.3: Engine mass estimation fit with engines groupes by OPR and BPR, with number of engines in each group listed between breackets [7]

As the last step it is necessary to indicate whether a variable geometry inlet is used as well as its shape and dimensions so that the air induction (inlet) system mass can be estimated. For cruise Mach numbers greater

than 1.7, a variable inlet is implemented, while below Mach 1.7 a fixed inlet is used. This concludes the engine design process, and the different dimensional parameters are passed on to the aircraft geometry design module.

4.3. Aircraft geometry design

The aircraft geometry is important to the design routine because it provides the necessary inputs for the aerodynamics and Class II analysis modules. The simplified aircraft used in this program is built up from four components: the fuselage, double delta wing, vertical tail and horizontal tail. This breakdown is visualized in Figures 4.4 and 4.5 along with several key dimensions.

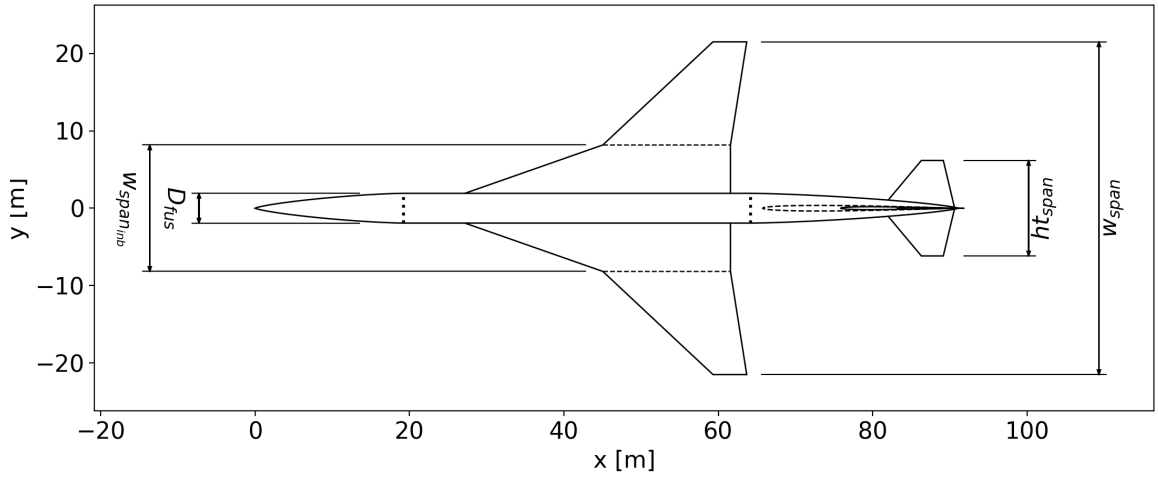

Figure 4.4: SST250 aircraft geometry top view with some dimensions

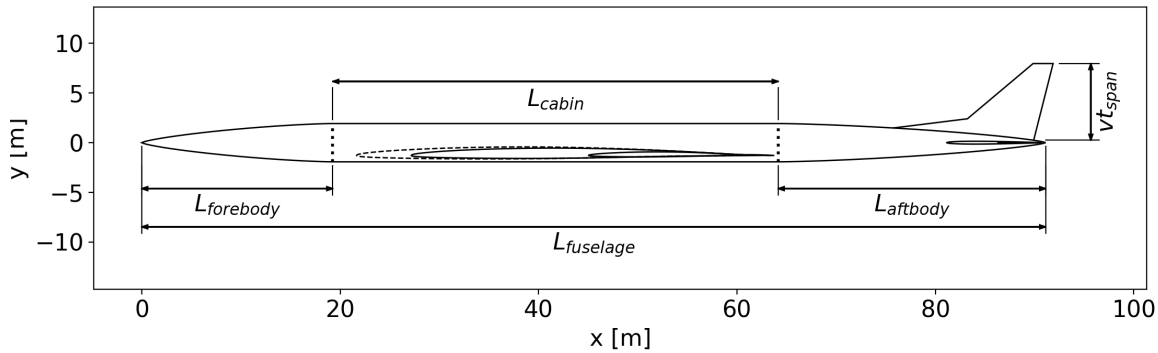

Figure 4.5: SST250 aircraft geometry side view with some dimensions

Starting with the fuselage, it is assumed that it is composed of three parts, a conical nose section, a constant diameter cylinder, and a conical tail section. These division of these three sections can be seen in the top- and sideview with the thick dotted lines inside the fuselage. The conical sections are assumed to have a shape similar to a Sears-Haack body, and require a slenderness ratio and maximum radius (or diameter) to be defined. The diameter is equal to that of the cylindrical section, and the slenderness ratios are taken from statistics of other supersonic aircraft which show a typical range of 6 to 8 [42]. Note that for the nose section, the slenderness range used is 5-7. The cockpit is assumed to be located in the nose section, while the cylindrical section houses the passengers, lavatories and galleys. Note that some of the galleys and lavatories are placed in the tail section. Based on the number of passengers, the seating arrangement is selected, which combined with the seat pitch and room for galleys and lavatories, results in a cabin length. Combined with an aisle width, seat pitch and seat width, the cylinder diameter is then computed. The fuselage also has an upsweep angle which is assumed to be about four degrees, but it is not included in the current ParaPy aircraft because it resulted in strange distortions of the aircraft object for some sets of inputs.

Looking at the double delta wing, the leading edge sweep angles are important since they should be selected such that the majority of the leading edge is subsonic in supersonic flight as is shown later in Chapter 5. To this end, the quarter chord sweep angles of the inboard and outboard wing sections are selected such that the full wing leading edge is positioned inside the Mach cone. For this reason, high supersonic design Mach numbers (>2) will result in unrealistic wing designs, unless the subsonic leading edge fraction is reduced by the user. For the inboard wing section, the trailing edge sweep angle is assumed to be zero to allow for the high-lift devices to function optimally. Next, by using the kink location and other dimensional parameters (e.g. aspect and taper ratio, wing position, dihedral angle) which are either user-defined or constants, the other dimensional parameters of the wing are calculated (e.g. chord lengths). A more detailed view of the wing is shown in Figure 4.6.

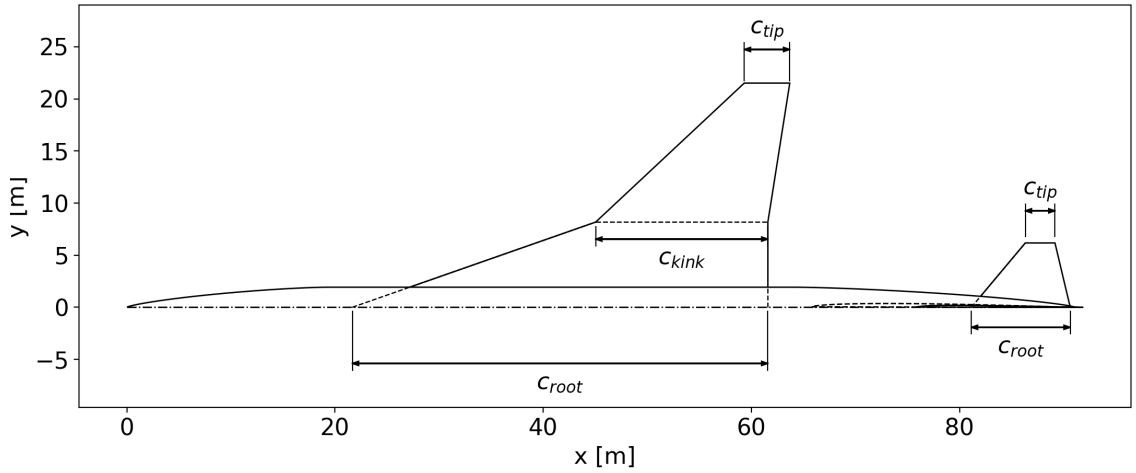

Figure 4.6: SST250 aircraft wing geometry top view with some dimensions

For the horizontal tail, the design is kept simple by assuming that it is a single trapezoidal surface with a constant leading edge sweep angle of about 40-50°. The vertical tail is a bit more complex as it features a dorsal fin section at the root, which increases the sideslip limit for the vertical tail and allows for a thicker root. The areas of the tail surfaces are determined by using statistical volume coefficients. Other dimensional parameters such as the aspect and taper ratios are selected based on statistics from other (supersonic) aircraft, or calculated from available dimensions. The tail surfaces are positioned near the end of the fuselage tail section to increase their moment arm, and to be similar to other supersonic aircraft designs, as will be shown in [7].

For each of the components, it is also possible to calculate other dimensions such as the wetted and exposed areas. Another important attribute of the aircraft is its ability to store the fuel required to fly the design mission. To this end, several locations have been identified to store fuel, the main wing, the horizontal tail, part of the main fuselage, and part of the aft fuselage section. Of the latter component, 60-80% of its volume is assumed to be available for fuel storage, although it is primarily used for SSBJs because of their smaller wing fuel volume. For larger SSTs, the tail fuel volume is often not used. For the wing and horizontal tail, the fuel volume is assumed to be the volume in between top and bottom skin, and front and rear spars, which for their positioning depend on the presence of control and high-lift surfaces. Common positions are 10-20% of the chord for the front and 60-75% for the rear spar. Also the tip region of the main wings hold no fuel to reduce lightning strike risks, and correction factors have been added to account for fuel expansion and the volume occupied by fuel system components.

Together with the engine dimensions from the engine sizing module, all necessary aircraft dimensions are now known, and they are passed on to the subsequent design modules. It should be noted that for each new iteration a new aircraft is created. For more information on the methodology and several validation cases look at [7].

5
Aerodynamics

For the aircraft Class I sizing calculations shown in Chapter 3, the initial aerodynamic performance of the aircraft is estimated using statistics from past supersonic designs. However, as was also shown, the supersonic aircraft designs are very sensitive to the aerodynamic efficiency of the aircraft, so these values should be estimated using aerodynamic theories instead of statistics, to improve the reliability of the results. Other areas that will benefit from the aerodynamic analyses are the wing loading analysis for which the low-speed lift performance is needed, and the Class II weight estimation which requires lift data for the gust calculations.

Before looking at the full aircraft, it is beneficial to look into the airfoil type that could be used for the wing. This is discussed in Section 5.1. After this, the lifting performance of the full aircraft is analyzed in Section 5.2, which also includes the low-speed scenarios of takeoff and landing. Drag is the second factor required to estimate the aerodynamic efficiency of the aircraft and the method used is discussed in Section 5.3. To close off the chapter, some remarks are made about the module in Section 5.4.

5.1. Airfoil selection

For aerodynamics, the first item that has to be discussed is the airfoil selection. For this, the leading edge condition is important because for a subsonic leading edge, more standard airfoils can be applied, while for a supersonic leading edge it is beneficial to select different airfoils like diamond airfoils. Currently, it is assumed that the wing leading edge will be subsonic to prevent this problem. To ensure this, the wing leading edge is positioned behind the Mach cone originating from the inboard wing leading edge in the aircraft design routine. Also, because not a large amount of resources were available, the airfoil selection was simplified by looking at reference aircraft, which in this case are fighter aircraft, and some other supersonic design studies. The airfoils used in those designs are listed in Table 5.1.

Table 5.1: Supersonic airfoil overview

Aircraft	Airfoil	Source
F16	NACA 64A204	[9, 43]
Concept	NACA 66-series t/c 3-6%	[44]
Concept	NACA 65A(1.5)04/0.3	[45]
F20	65A004.8	[43, 45]
F18	65A005/65A003	[43, 45]
F15	64A006.6/64A003	[9, 43]

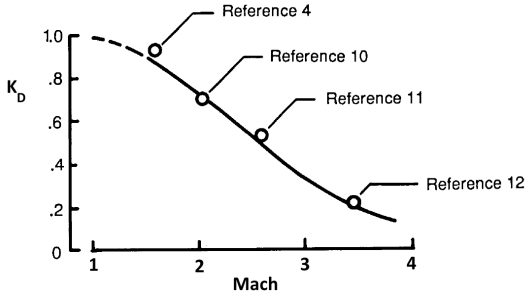

Figure 5.1: Design lift-to-cruise lift coefficient ratio K_D as function of cruise Mach number [46]

The airfoil families that will be used for now are the NACA 65A-series, and the NACA 64A-series. To reduce the wave drag generated by the wings, the thickness will be relatively low in the range 2-5% t/c. The airfoil coordinate files are generated by using a program from NASA [47]. This program can generate NACA 6- and 6A-series airfoils and requires at least a series identification (e.g. 65A), maximum thickness ratio, chord length, design lift coefficient, and mean chordwise loading (0.8 for 6A-series airfoils [47]). For the design lift coefficient, the cruise lift coefficient is used in combination with the findings from [46], which show the ratio of the design-to-cruise lift coefficient ratio (K_D) as a function of cruise Mach number. The plot is shown in Figure 5.1 and indicates that for Mach 2.0, the design lift coefficient is approximately 0.74 times the cruise lift coefficient. The cruise lift coefficient can be estimated using the aircraft conditions at its cruise start. For Concorde the value was estimated to be about 0.17, so that the design lift coefficient for cruise would be about 0.13.

It should be noted that more airfoil series could be added in the future to enhance the capabilities of the module. To show that the airfoil coordinate files generated are accurate, a NACA 64A010 and 64A012 airfoil were created and their lift curves were predicted using XFoil. These were then compared to the findings in [48] and the results are shown in Figure 5.2.

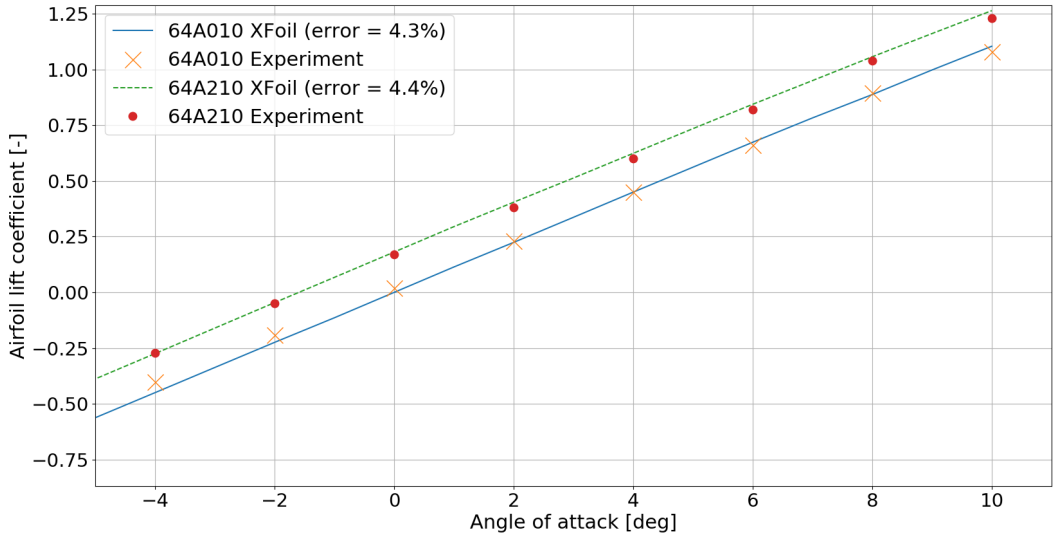

Figure 5.2: NACA 64A010 and 64A210 airfoil comparison XFoil and experiment [48]

Using the values from the two sources, the average absolute error of the XFoil prediction for both airfoils is just over 4%. The figure shows that the prediction for the symmetrical NACA 64A010 is very closely captured by XFoil with some values being slightly below and some above the reference, while for the cambered 64A210, the lift curve slope is consistently slightly overestimated by XFoil. This can be partially caused by small errors in the boundary layer displacement prediction of XFoil. However, the values are still quite close showing that the airfoils are properly represented by the coordinates from the airfoil generation program [47]. Note however that it was found that for the airfoil series listed in the above table, the digital DATCOM method results for the supersonic lift curve slope do not change for a change in airfoil. This means that the type of airfoil does not affect the supersonic lifting performance. Still, the airfoil thickness and geometry are used for fuel volume and cross-sectional area calculations.

5.2. Lift analyses

The first aerodynamic parameter that is described is lift, for which a different method is applied depending on the speed regime. Before starting, it should be kept in mind that the purpose of the aerodynamics module is to compute the lift-to-drag ratio at specific conditions, and the maximum lift coefficient for low speeds. As a result, the lift curves do not have to be perfect for the higher speeds, although it should be checked that the cruise angles of attack are not too large. Additionally, for low speed flight high-lift devices will be needed if insufficient lift is available at the angles of attack associated with approach and takeoff.

5.2.1. Lift analysis method

For subsonic conditions the DATCOM method is applied which is a function for the lift curve slope that depends on the wing aspect ratio A, semi-chord sweep angle $\Lambda_{0.5c}$ and Mach number (through β) [49]. It is a common method that is referred to in other sources such as Raymer [50]:

$$C_{L_\alpha} = \frac{2 \cdot \pi \cdot A}{2 + \sqrt{4 + \frac{A^2 \cdot \beta^2}{\eta^2} \cdot \left(1 + \frac{\tan \Lambda_{0.5c}{}^2}{\beta^2}\right)}} \tag{5.1}$$

In this equation another factor is included, η, the airfoil efficiency. In [19, 31] it is assumed to be 1.0, while sources such as Raymer [50] indicate a value of 0.95. For the current design process an intermediate value of 0.98 is applied. Note that the sweep angle used is the effective sweep angle of the wing that is found by multiplying the sweep angles for the inboard and outboard part with their respective areas, and dividing it by the total area:

$$\cos\Lambda_{0.5c} = \frac{\cos\Lambda_{0.5c,inb}\cdot S_{inb} + \cos\Lambda_{0.5c,outb}\cdot S_{outb}}{S_{inb} + S_{outb}} \tag{5.2}$$

Additionally, in [19] it is indicated that Equation (5.1) does not account for transonic lift divergence, and that for a transonic airliner at maximum flight speed it underestimates the wing lift gradient by 5-10%. To account for this, the wing lift curve slope value will be multiplied by a factor 1.08 for Mach numbers above 0.9. Between Mach 0.75 and 0.9 the contribution is increased linearly from 1.0 to 1.08.

The lift curve slope that is then found does not yet represent the full aircraft lift curve slope because part of the wing is located inside the fuselage. To correct for this the lift curve slope is multiplied by the ratio of the exposed wing area to the reference wing area. Additionally, the fuselage will produce lift. To account for this a correction factor F from Raymer [50] is used:

$$F = 1.07\cdot\left(1+\frac{d}{b}\right)^2 \tag{5.3}$$

where d is the fuselage diameter and b the wing span. The final equation for the aircraft lift curve slope in the subsonic regime is as follows:

$$C_{L_\alpha} = \frac{2\cdot\pi\cdot A}{2+\sqrt{4+\frac{A^2\cdot\beta^2}{\eta^2}\cdot\left(1+\frac{\tan\Lambda_{0.5c}{}^2}{\beta^2}\right)}}\cdot\frac{S_{exposed}}{S_{ref}}\cdot F \tag{5.4}$$

For the supersonic regime (M>1.4), the digital DATCOM[1] [51] is used to estimate the lift curve slope. This program requires a set of wing geometrical characteristics, as well as an airfoil designation. Additionally, the program needs to know for what conditions to analyze the wing, such as a set of Mach numbers with corresponding altitudes, and a set of angles of attack. An example input file is shown and discussed in Appendix C.1.

An important limitation of the digital DATCOM is that for the analysis of a double delta wing, it can only feature a single airfoil along the entire span, meaning that the thickness cannot be varied. While this will affect the results, the thickness variation along the span for supersonic aircraft is smaller than that for subsonic aircraft, reducing the overall effect of this limitation. Still, it should be kept in mind when looking at the results. An attempt was made to quantify the effect by using the digital DATCOM, but it was found that for the supersonic regime, the airfoil type has no effect on the computed lift curve slope. Only when switching from a 'regular' airfoil to a diamond shaped airfoil, does the lift curve value change. This signifies another shortcoming of the digital DATCOM method. From a study in [52], it was found that for thin supersonic airfoils (e.g. double wedge), the effect of thickness on the lifting performance can be ignored. While the subsonic airfoils have a different shape, it is assumed that this finding can be extended to them. However, thicker airfoils will cause an increase of the drag-due-to-lift, reducing the lifting efficiency [53].

Another limitation of the digital DATCOM is that it can only compute the supersonic lift curve slope for the linear lift region, and only returns a single value, rather than an individual lift coefficient for each angle of attack. This is not considered to be a problem, as it is assumed that the aircraft will not operate outside of the linear lift region in supersonic flight. The lift curve slopes found are used to generate the lift curves for the aircraft in supersonic conditions by also assuming that the zero-lift angle of attack is approximately zero degrees, as can be expected for a thin wing in supersonic flow. As with the subsonic calculations, the lift curve slope found by the digital DATCOM is multiplied by the exposed-to-reference-wing area ratio, and fuselage lift correction factor.

The transonic regime represents a bit more of a problem as the digital DATCOM cannot estimate the lifting performance in that region. Therefore, a different method had to be applied. Up to the drag divergence Mach number, which is close to one, Equation (5.4) can be used [50]. Using this equation, the lift curve slopes at Mach 0.9 and 0.95 are computed. At Mach 1.0, it is assumed that the lift curve is about 0.5% greater than that at 0.95. This percentage was found by looking at the changes between Mach 0.9 and 0.95. Then, a third-order polynomial is fitted through these three points (0.9, 0.95, 1.0) and the lift curve slope at Mach 1.4 from the digital DATCOM. While not ideal, this will give an indication of the lift curve slopes that can be expected.

5.2.2. Validation and calibration

In order to determine whether the prediction of the lift curves is accurate enough two reference aircraft designs and their lift curves were used. Based on information found in literature, comparable geometries were created for each aircraft, and the results were then compared. Note that the airfoil data for both aircraft was

[1] http://www.pdas.com/datcom.html (accessed April 2 2019)

not known exactly and that therefore it was decided to use a NACA 64A103 airfoil. It was indicated earlier, that for the supersonic regime the airfoil type does not influence the result. The same also applies to the subsonic calculations in Equation (5.4). In case of the a more detailed aircraft design the airfoil will be more precisely designed for the particular design lift coefficient, e.g. if the design coefficient is 0.13 the airfoil would be 64A(1.3)03 which will have a slightly different shape and lift curve slope, primarily in the subsonic regime. Given the relatively small differences (e.g. NACA 64A103 instead of NACA 64A(1.3)03) and low thickness, the effect that the small deviation in airfoil is expected to be much smaller (at most a few percent) than that originating from design variations like the aspect ratio. The effect of these variations is captured by the (digital) DATCOM methods.

The first aircraft used for checking the accuracy of the results is Concorde, for which the low speed performance is compared in Table 5.2.

Table 5.2: Lift coefficient comparison between subsonic method and measurements of Concorde [54] (assumed M=0.25)

Angle of attack	$C_{L,ref}$	$C_{L,calc}$	Deviation
0°	0.0	0.0	0.00%
5°	0.192	0.1953	+1.72%
10°	0.417	0.3906	-6.33%
15°	0.696	0.5859	-15.8%
20°	0.979	0.7812	-20.2%
Average			**-8.13%**

This table shows that the low-speed lifting performance of the Concorde aircraft is slightly overestimated for low angles of attack, and underestimated for higher angles of attack. The deviation can be explained by a combination of factors not considered by the subsonic method used. The first is that the Concorde wing features a very complex spanwise and lengthwise twist, which will affect the lifting performance of the aircraft. Second, the lift contribution of the fuselage is simply a correction factor applied to the wing lift, which could cause the difference to become larger or smaller, depending on the real-life contribution. Lastly, the increase in difference between the predicted and actual lift as the angle of attack is increased can be explained by the additional vortex lift generated on the Concorde wing. This vortex lift is not considered by the current subsonic method. Still, all things considered, the values are seen as acceptable given the low fidelity of the method, although for higher angles of attack some extra correction might be beneficial.

The second case that was used for checking the accuracy was the NLR (Nederlands Lucht- en Ruimtevaartcentrum) conceptual design from [31]. This was chosen because it contained a clear description of the design, including its geometry, as well as lift curve graphs for a range of flight speeds. It should be noted that the NLR conceptual design is largely based on semi-empirical relations, but given that the methods applied here are also based on semi-empirical relations and graphs, this was not seen as a problem. The lift curve for Mach 0.25 was estimated by the module and compared to the reference values, as shown in Table 5.3.

Table 5.3: Subsonic (M=0.25) lift coefficient comparison between subsonic method and source [31]

Angle of attack	$C_{L,ref}$	$C_{L,calc}$	Deviation
0°	0.0	0.0	0.00%
2°	0.094	0.0944	+0.47%
4°	0.187	0.189	+1.01%
8°	0.392	0.378	-3.61%
12°	0.631	0.567	-10.2%
14°	0.761	0.661	-13.1%
Average			**-4.24%**

This shows that for low speed flight, the subsonic lift curve method provides accurate results, although the deviation does start to increase for higher angles of attack as was the case for Concorde. This deviation can be again be caused by the additional vortex lift that is used in the NLR report, but also the fuselage correction factor and wing area ratios, as these were not used in the reference source. Because both aircraft showed large deviations for high angles of attack, it was decided that a correction or alternate method had to be introduced to improve the accuracy of the lift prediction at low speeds.

To this end several methods were studied and tested, as is elaborated upon in Appendix C.3. The method

that was found to be best was the Polhamus suction method described in [55], which also accounts for vortex lift. It revolves around the following equation, where the first term accounts for the potential-flow contribution and the second for the vortex lift contribution. Note that there is no correction for the fuselage or exposed wing area included.

$$C_L = K_p \cdot \sin\alpha \cdot \cos^2\alpha + K_v \cdot \sin^2\alpha \cdot \cos\alpha \tag{5.5}$$

The values of the coefficients K_v and K_p can be estimated based on graphs as described in Appendix C.3. With the new method, the results in Table 5.4 were found for the two aircraft.

Table 5.4: Subsonic (M=0.25) lift coefficient with corrected method compared to references [31, 54]

Concorde				NLR			
Angle of attack [deg]	$C_{L,ref}$ [-]	$C_{L,polh}$ [-]	Deviation	Angle of attack [deg]	$C_{L,ref}$ [-]	$C_{L,polh}$ [-]	Deviation
0°	0.0	0.0	0%	0°	0.0	0.0	0%
5°	0.192	0.201	+4.90%	4°	0.187	0.186	-0.53%
10°	0.417	0.442	+6.02%	8°	0.392	0.405	+3.29%
15°	0.696	0.708	+1.72%	12°	0.631	0.648	+2.63%
20°	0.979	0.982	+0.31%	14°	0.761	0.775	+1.84%
Average			**+2.59%**	Average			**+1.45%**

This shows that for Concorde, the average deviation is now positive, and at most 6%, while the average is 2.6%. For the NLR design, the deviation is now also reduced, which could be expected as their aircraft low-speed lift performance was analyzed using the Polhamus method. With this improved method, the low-speed performance can be estimated more accurately than using the original method, and it is deemed accurate enough for this stage of the design process.

For the supersonic calculations, the data from the NLR report were used as a basis for the comparison. Using the digital DATCOM method with lift corrections for the fuselage and exposed wing area, the lift curve for Mach 1.6 and 1.8 was estimated, as is shown in Table 5.5.

Table 5.5: Supersonic lift coefficient comparison between digital DATCOM and source [31]

	M=1.6			M=1.8		
Angle of attack	$C_{L,ref}$	$C_{L,calc}$	Deviation	$C_{L,ref}$	$C_{L,calc}$	Deviation
0°	0.0	0.0	0.00%	0.0	0.0	0.00%
2°	0.088	0.089	+1.34%	0.077	0.082	+5.98%
4°	0.179	0.177	-1.04%	0.156	0.163	+4.69%
6°	0.278	0.266	-4.24%	0.238	0.245	+2.82%
Average			**-0.99%**	Average		**+3.37%**

The supersonic table shows that the lift curve slope is slightly underestimated by the digital DATCOM for Mach 1.6, and slightly overestimated at Mach 1.8. In part this is the result of the digital DATCOM using a constant thickness airfoil along the span, while the NLR aircraft features a thickness variation from 3% t/c at the root to 2.8% at the kink, and to 2% at the tip. Another factor is the fuselage lift contribution which can result in an additional deviation. It is also possible that the airfoil used in the reference is of a different type than the one used in the calculations. Furthermore, the lift curve of NLR is estimated by a set of methods taken from literature and is therefore also an approximation. Given these potential causes of the differences, the results are assumed to be accurate enough for the level of detail desired at this stage.

To show the results from the method where the transonic region is interpolated, the lift curve slope values were computed for the sub- and supersonic regime using the NLR aircraft design, and plotted in Figure 5.3. The transonic region line is indicated as a dashed line with the interpolation points indicated by crosses. This shows that the peak for the lift curve slope is near Mach one, and that as the Mach number is increased in the supersonic regime, the lift curve slope decreases. Note that there are two kinks in the curve. The first is at Mach 0.75 after which a correction factor is introduced for the transonic lift divergence as explained in Section 5.2.1. The second is at Mach 1.4 and is the result of the transition from interpolated data for the transonic regime to the digital DATCOM data for the supersonic regime.

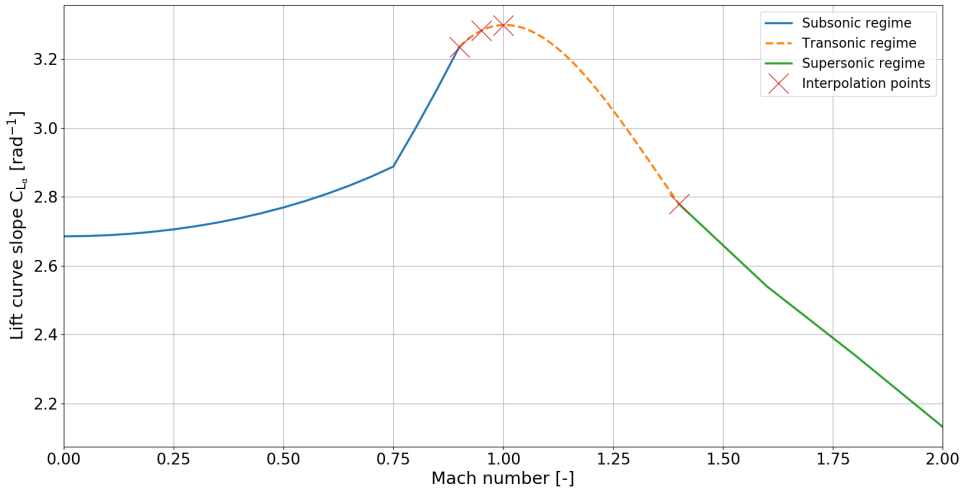

Figure 5.3: Lift curve slope variation with Mach number for NLR design

5.2.3. Takeoff and landing

While the above has shown how the clean lift curves are being estimated, past studies indicated that supersonic aircraft, with their low aspect ratio and thin wings, often require additional high-lift systems to improve their low-speed lifting performance. Without them, the aircraft might not be able to meet top-level requirements such as the takeoff and landing distances.

Starting with the takeoff run, the aircraft will still have its wheels on the ground, or at least be close to the ground. As a result of the aircraft being close to the ground, a 'cushion' of air is formed under the aircraft wings which improves its lifting performance (i.e. "ground effect"). An investigation on the Concorde aircraft (Figure 5.4) showed the impact to be considerable, with the lift coefficient increasing by about 50% for an angle of attack of 10° with wheels on the ground. This angle of 10° is assumed to be the maximum angle at which the aircraft can lift off, as higher angles would require increasingly longer landing gear struts to prevent tailstrikes.

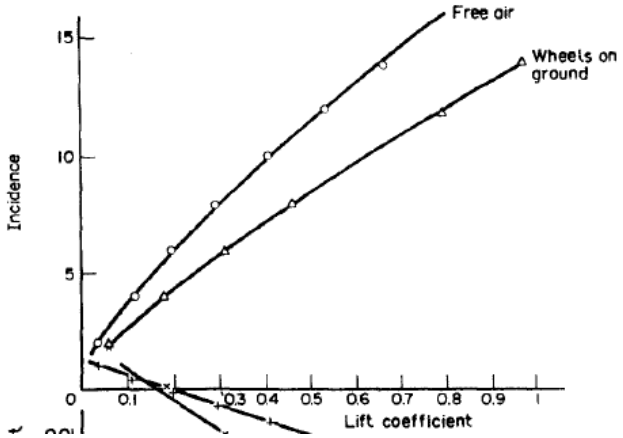

Figure 5.4: Concorde low-speed lift curve with and without wheels on ground (incidence in degrees) [54]

For the aircraft design created by the module, it is assumed that for the 10° angle of attack used at takeoff, the lift coefficient found in clean conditions can be increased by 40%. This is less than the improvement found for Concorde but introduces a safety margin and accounts for some of the downforce generated by the horizontal tail. From static tests on the XB-70, a large supersonic bomber, the ground effect at a height of 0.3 times its span was found to be about 27-28% [56], meaning that with the wheels on the ground it will likely be larger. This source also contains ground effect measurements for fighter aircraft, but these are considered less representative for SSTs. For landing no ground effect is included because the aircraft is at a height of more than a wingspan. Note also that the ground effect does not only improve the lifting capability of the aircraft, but that it can also reduce the amount of lift induced drag (see Chapter 18 of [57]).

Next, the amount of extra lift required to meet the landing and takeoff requirements can be determined by calculating the difference between the maximum lift coefficient used in the wing loading analysis and that which is achieved in clean flight at 12° (landing), and with wheels on the ground at 10° (takeoff). For landing the angle of attack is assumed to be limited to 12° because otherwise, the pilot visibility would become an issue and might require a rotating nose as was the case for Concorde. The increase in lift resulting from high-lift devices is estimated using Equation (5.6), and the change in zero-lift angle of attack by Equation (5.7). The latter is not used however, as it is assumed that the maximum lift coefficient increment applies to the angle of attack for the takeoff and landing constraints, which is one of the reasons that lift penalties are added later on.

$$\Delta C_{L_{max}} = \Delta C_{l_{max}} \cdot \frac{S_{flapped}}{S_{ref}} \cdot \cos \Lambda_{HL} \tag{5.6}$$

$$\Delta \alpha_{L=0} = (\Delta \alpha_{L=0})_{airfoil} \cdot \frac{S_{flapped}}{S_{ref}} \cdot \cos \Lambda_{HL} \tag{5.7}$$

The approximate lift contribution $\Delta C_{l_{max}}$ is dependent on the type of high-lift device (HLD) being used as listed in Figure 5.5.

Table 12.2 Approximate lift contributions of high-lift devices

High-lift device	$\Delta C_{l_{max}}$
Flaps	
Plain and split	0.9
Slotted	1.3
Fowler	1.3 c′/c
Double slotted	1.6 c′/c
Triple slotted	1.9 c′/c
Leading edge devices	
Fixed slot	0.2
Leading edge flap	0.3
Kruger flap	0.3
Slat	0.4 c′/c

Figure 5.5: Approximate lift contributions of high-lift devices [50]

In the table, the entry c'/c stands for the ratio of the flapped chord length (with HLD deployed) and the clean chord length (with HLD retracted). The flapped area is the area of the part of the wing that is located in front of a trailing edge HLD, or behind a leading edge HLD, as shown in Figure 5.6. Λ_{HL} represents the sweep angle of the HLD hinge line. This hinge line sweep angle is dependent on the ratio of the HLD chord to that of the wing section. It can be that the flap chord has a constant length, which would result in an increase of the HLD-chord-to-wing-chord-ratio along the span. The presence of the hinge line sweep angle also shows that especially for the leading edge devices of highly swept delta wings, the relative lift contribution is much smaller than that at the less swept trailing edge. Therefore, the primary HLDs will be positioned at the trailing edge. It should also be noted that during takeoff, the high-lift devices will have a lower deployment angle, which results in a lower lift increase. It is assumed that during takeoff, the lift increment is 72% of the value computed using the equations above. This falls within the range 0.6-0.8 advised in [50].

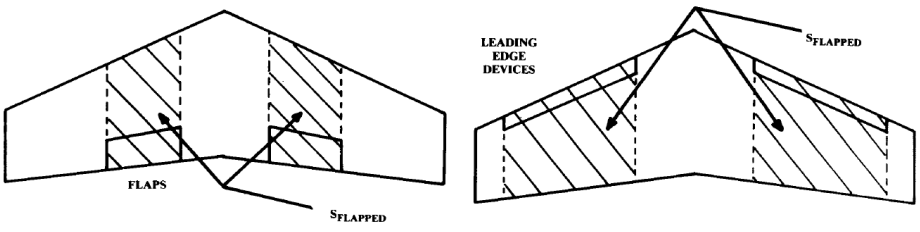

Figure 5.6: Flapped area definition [50]

Because it was found that for SSTs, the low-speed takeoff and landing lift performance is important, a detailed discussion of the calculation method used to find the required HLD lift increments, flapped areas and chord ratios is provided in Appendix C.4. To see whether the high-lift analysis returns reliable values, it was decided to apply the module to the Concorde wing geometry. It was found that the flapped area for trailing-edge

devices is about 181 m^2, split over two stretches, which is just over half of the wing reference area. For the leading edge devices, about 178 m^2 can be flapped. The trailing edge inboard hinge line angle is zero degrees, and for the outboard section it is about 23.2°, assuming that 25% of the chord is a flap. Depending on the type of HLD the following results are found:

- Slotted flaps provide an increment of 0.551 for landing and 0.441 for takeoff
- Single slotted fowler flaps provide an increment of 0.616 for landing and 0.485 for takeoff
- Double slotted flaps provide an increment of 0.749 for landing and 0.579 for takeoff
- Leading edge flap provides an increment of 0.057 for landing 0.045 for takeoff

The results show that the lift increase provided by trailing edge high-lift devices is much larger than that provided by the leading edge devices. This can be explained by the 75% lower base value of $\Delta C_{l_{max}}$ for the leading edge devices. Additionally, the hinge line sweep angle for the leading edge devices is very large because of the high sweep of supersonic wings. For a sweep angle of 55° it resembles a factor of 0.57. Together, this results in the leading edge device being $0.25 \cdot 0.57 \approx 0.14$ times as effective as leading edge devices. Even with the larger flapped area this cannot be compensated for. From past studies it was found that LE HLDs can help improve the L/D of delta wings for downward deflection, and the lift, but also drag for an upward flap deflection [58]. Thus, it can be used for low-speed operations as well as for supercruise as shown in [59].

Because of the low complexity of the flap system the lift increments are not very large in absolute terms (order 0.4-1.0). During the sizing routine the module will either use a specific combination of HLDs defined by the user, or cycle over the different options to find which one is capable of providing the required maximum lift coefficient. If the HLD system(s) analyzed cannot meet the requirements, the maximum lift coefficients are reduced and the wing loading analysis is run once again as shown in Figure 2.1.

5.3. Drag analyses

For the drag calculations, the different drag components which are required will be discussed separately in individual subsections. A drag breakdown diagram is shown in Figure 5.7 and indicates the subsections where they are discussed. Note that for the supersonic volume and lift-induced drag two methods are discussed which is why those blocks have two subsections listed.

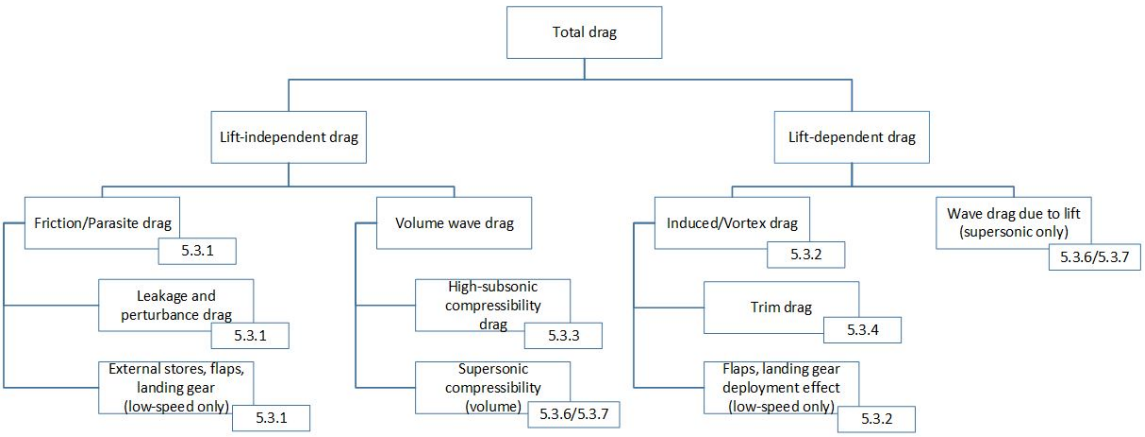

Figure 5.7: Drag breakdown diagram

5.3.1. Friction drag

The first drag component that is determined is the parasite or friction drag. For this step, the component buildup method as described by Raymer [50] is applied, where each component is analyzed separately and then combined into a single drag coefficient:

$$C_{D,f} = \frac{\sum C_{f_c} \cdot FF_c \cdot Q_c \cdot S_{wet_c}}{S_{ref}} + C_{D,\,misc} + C_{D,\,L\&P} \tag{5.8}$$

For each component the first step is to compute the flat-plate skin friction coefficient C_{f_c}, which depends on the flight conditions, Reynolds and Mach number. Depending on whether the flow is laminar of turbulent, the friction coefficient is calculated by using Equations (5.9) and (5.10), respectively.

$$C_{f,lam} = \frac{1.328}{\sqrt{Re}} \tag{5.9}$$

$$C_{f,turb} = \frac{0.455}{\left(\log_{10} Re\right)^{2.58} \cdot \left(1 + 0.144 \cdot M^2\right)^{0.65}} \tag{5.10}$$

Based on the fraction of the surface with laminar flow, a weighted average friction coefficient can be calculated for each component. For subsonic flight, laminar flow can be achieved on 5-20% of the wings and tail, and if the design is shaped properly this percentage could be improved. For the fuselage and engine nacelles, the flow is assumed to be fully turbulent, which also partially offsets any potential underestimation of wing and empennage friction drag contributions. During supersonic flight the amount of laminar flow is much smaller and set to be in the range 0-4%, meaning that the flow is almost completely turbulent.

The second factor FF is the form factor of a component and adds a correction for the component based on its geometry. For the wing and empennage components Equation (5.11) is used, while the fuselage and nacelle use Equations (5.12) and (5.13), respectively [50]:

$$FF_{wing} = \left[1 + \frac{0.6}{x/c_m} \cdot \frac{t}{c} + 100 \cdot \left(\frac{t}{c}\right)^4\right] \cdot \left[1.34 \cdot M^{0.18} \cdot \cos \Lambda_m{}^{0.28}\right] \tag{5.11}$$

$$FF_{fuse} = \left(1 + \frac{60}{f^3} + \frac{f}{400}\right) \tag{5.12}$$

$$FF_{nac} = 1 + \frac{0.35}{f} \tag{5.13}$$

where f represents the slenderness ratios of the particular components. Also, for the horizontal and vertical tail, an additional contribution has to be added to account for the gap between the tail and control surfaces. This contribution is assumed to be 10% as suggested by Raymer [50].

The third parameter, Q, is the component interference factor, which accounts for the mutual interference between the different components. For the main wing, the interference factor is one, assuming that the wing is well-filleted [50]. Also, for the fuselage the factor is assumed to be one. The tail surfaces have an interference factor of about 1.04. For the nacelle, the interference factor is more important, particularly when it is mounted directly underneath the wing. In that case, the value of Q is about 1.5. Only when the engines are mounted more than one engine diameter away from the wing, will the interference factor be equal to one [50].

To correct for other drag factors which are not included such as leakage and protruding (L& P) items a 4% margin is added to the total aircraft friction drag. Apart from the component friction drag, there are other contributions to the zero-lift-drag, which are stored under the miscellaneous term. This includes drag from external stores such as missiles and bombs, which are not applicable to the current design. The effect of the upsweep of the aft fuselage however, can affect the drag, and is accounted for by the following equation [50]:

$$C_{D,\ upsweep} = \frac{3.83 \cdot u^{2.5} \cdot A_{max}}{S_{ref}} \tag{5.14}$$

where u is the upsweep angle in radians, A_{max} the maximum fuselage cross-sectional area, and S_{ref} the main wing reference area.

For low-speed flight in the landing and takeoff configuration, additional friction drag contributions should be included for the landing gear and flaps. For the landing gear, the friction drag coefficient is assumed to fall in the range 150-250 counts indicated in [13], with most designs having 175-200 drag counts. Much lower values are not expected because the landing gear struts are expected to be slightly longer than for subsonic aircraft, which results in a larger drag. More detailed estimates are not possible because landing gear geometry details are unknown. For the trailing edge flap drag, the following function from [50] is used:

$$C_{D,flap} = 0.0023 \cdot \frac{b_{flapped}}{b} \cdot \delta_{flap} \tag{5.15}$$

where the span fraction indicates what part of the wing span features a flap, and δ_{flap} is the flap deflection in degrees. This deployment angle will be about 10°-20° for takeoff settings and 30°-40° for landing configuration. For the leading edge high-lift devices, 5 drag counts are added for takeoff, and 7 for the landing configuration, which falls in the range 4-8 counts listed for slats in [60].

For supersonic flight conditions, the values of the form and interference factors are one, and a new drag contribution is added, the wave drag due to volume which accounts for the drag resulting from shock formation. This term is explained further in Sections 5.3.6 and 5.3.7. To determine whether the values found are in the proper range, a comparison was performed using the results from [31] as shown in Table 5.6.

Table 5.6: Friction drag coefficient comparison [31]

Mach number [-]	0.3	0.95	1.6	2.0
Altitude [m]	0	9,000	15,000	16,500
$C_{D_f,\,ref}$ [cts]	69.4	61.9	56.4	51.2
$C_{D_f,\,calc}$ [cts]	58.4	59.1	58.2	53.6
Deviation [%]	-15.9	-4.5	+3.2	+4.7

This shows that for low subsonic speed, there is a substantial deviation between the value found by NLR and that found by the friction module. The difference can be explained by the module using a friction coefficient that depends on the amount of laminar flow, while the NLR calculations assume a fully turbulent flow. Also, a different method is applied to determine the friction coefficient and Reynolds number. Additionally, the nacelle friction, fuselage upsweep and miscellaneous drag contributions in this module are not used in the NLR calculations, which also explains some of the difference for supersonic conditions. For the supersonic conditions it is also assumed that a very small portion of the wing and empennage (2-4%) is subjected to laminar flow, which was not done for the reference design. Potentially, more laminar flow can be achieved as was shown by Aerion and NASA with their supersonic natural laminar flow research [61]. The high-subsonic and supersonic values show only small deviations, so the module can be used to calculate the friction drag coefficients. It should also be noted that for the high-subsonic flight condition (M=0.95), the high-subsonic compressibility drag coefficient of 2.9 drag counts should still be added to find the zero-lift drag coefficient, reducing the deviation from -4.5% to -0.5%.

5.3.2. Lift induced drag

The second subsonic drag component is the lift induced drag. For this drag component the following equation is often applied:

$$C_{D,i} = \frac{C_L^2}{\pi \cdot A \cdot e} \tag{5.16}$$

Here, the lift coefficient is varied, and the aspect ratio is known from the aircraft geometry. The last unknown factor 'e' is the Oswald span efficiency factor. It is an indicator of how closely the lift distribution of the wings approximates an elliptical distribution. For most aircraft the value of the Oswald factor is in the range 0.7 to 0.85 in clean configuration. In [62], an overview of methods for estimating 'e' was provided, along with a proposed solution which was created by combining several methods. An attempt was made to apply this method to the NLR aircraft and Concorde, but the method uses a Mach dependent factor in the calculations which becomes negative for high subsonic Mach numbers (M>0.85), and therefore returns a negative value for 'e'.

Instead, it was decided to apply the method used in SUAVE which is based on the method of Kroo [35]:

$$e = \frac{1}{e_{inviscid} + \pi \cdot A \cdot K \cdot C_{D,0}} \tag{5.17}$$

Here, $e_{inviscid}$ is the span efficiency factor that would apply for inviscid flow. As in SUAVE, its value is assumed to be 0.8 [35]. While it would be better to not assume a value, not enough resources are available to determine what method would be best to estimate this value. A is the aspect ratio, K represents a correction factor which was found to be 0.38 [35], and $C_{D,0}$ is the parasite drag coefficient.

For subsonic flight, a vortex will form over the wing at high angles of attack, increasing the amount of lift-induced drag. However, for the high-subsonic flight where L/D is to be determined, the aircraft will under normal circumstances operate at relatively low angles of attack (<6°) and as such the wing is not expected to be generating a (strong) vortex. Consequently, this drag contribution is ignored for now.

A last key contribution to the induced drag is caused by the change in span efficiency factor resulting from flap deflection. To get a rough estimate for this change, the results from [60] are used where for wing-mounted engines the average increase of e was found to be 0.0026 times the flap deflection in degrees. Since supersonic aircraft have less effective HLDs, this value is reduced to 0.0023, which means that the following contribution is added to the clean wing factor (note δ_{flaps} in degrees):

$$\Delta e_{flaps} = +0.0023 \cdot \delta_{flaps} \tag{5.18}$$

5.3.3. High-subsonic compressibility drag

For flight at high-subsonic Mach numbers close to Mach one, local shocks can form on the aircraft geometry. These shocks will lead to an increase in the drag experienced by the aircraft. To determine whether this drag should be taken into account it is necessary to estimate the drag divergence Mach number. For this, the Delta method [63] and its charts were used, which is elaborated on in Appendix C.5. The aircraft is a supersonic configuration with relatively thin wings (effective t/c < 0.04), and a design lift coefficient in the range 0.1-0.3 during supersonic flight. The uncorrected 2D drag divergence Mach number is then expected to be in the range 0.81-0.84. After adding corrections for the quarter chord sweep angle which is expected to be over 50°, and the low aspect ratio, the resulting 3D wing drag divergence Mach numbers are in the range 1.0 and above.

While the expected high subsonic cruise Mach number of 0.9-0.95 is slightly below the drag divergence Mach number, there is still some drag increase expected. To estimate this drag increase the method from Shevell [64] is used which needs the crest-critical Mach number, which is about 0.06-0.07 below the divergence Mach number for high sweep angles. In SUAVE [35] it is assumed for Concorde that the value is 0.93, which given the estimated values of the divergence Mach number is a good assumption, and is also used in this module. Then, using this crest-critical and the freestream Mach (M_0) numbers, their ratio can be calculated. For a cruise speed of Mach 0.95 it is 1.02. Then, using Figure 5.8 the value of the ratio $\Delta C_{D_C} / \cos^3 \Lambda_{0.25}$ can be determined. The wave drag increment is then estimated using Equation (5.19).

$$\Delta C_{D,c} = \frac{\Delta C_{D_C}}{\cos^3 \Lambda_{0.25}} \cdot \cos^3 \Lambda_{0.25} \quad (5.19)$$

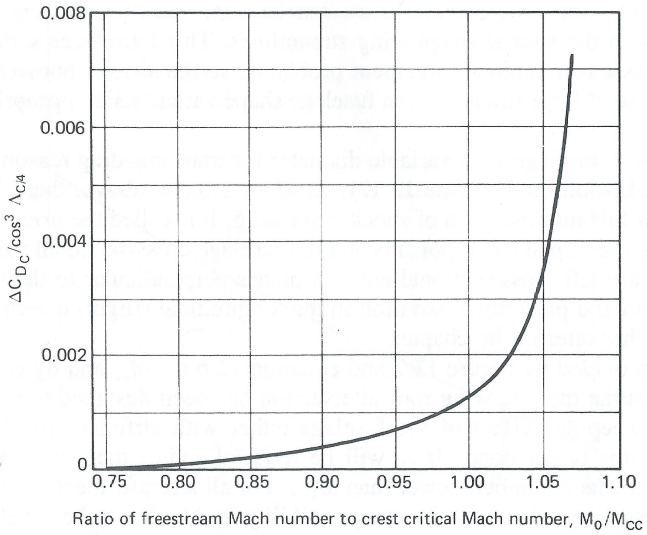

Figure 5.8: High-subsonic compressibility drag fit [64]

For a ratio of 1.02, the fraction value is about 0.002. With a quarter-chord sweep angle of 58°, the compressibility drag coefficient is about 2.5 drag counts ($2.546 \cdot 10^{-4}$). Another method that was looked at was to apply the data from the F-106 fighter in Roskam [42] as a reference for the SSTs. For a cruise Mach number of 0.95 this would result in a drag increase of roughly 4.4 drag counts. However, in Roskam [42] it is stated that the method should not be applied for aircraft with a cruise speed of 0.9 and above, so it was decided not to use that method. Still, it shows that the value found from the method by Shevell is of the same order of magnitude.

5.3.4. Trim drag

In normal flight, the aircraft has to be trimmed to ensure that it remains stable as it becomes lighter. For aircraft with a regular horizontal tail, its surface will often generate a download, which reduces the overall aircraft lift. To compensate for this, the main wing has to produce some more lift, which will increase its lift induced drag (trim drag). Ideally, the amount of trim drag can be calculated by performing a detailed stability analysis to determine the amount of trim lift required. However, in the current research not enough resources are available to do this, so a different assumption is made.

In Kroo [65], it is indicated that when no information is available about the center of gravity position, the results from more reliable detailed computations for other aircraft can be used. These showed that the trim drag can represent about 1-2% of the total aircraft drag. In this research a conservative value of 2% is used for low-speed flight and added to the total drag coefficient. For high-subsonic and supersonic flight, it is assumed that there is a negligible amount of trim drag because the aircraft is designed for that regime. Also, using automated fuel transfer systems contributes to this assumption by trimming out the aircraft.

5.3.5. Subsonic drag calculation

By combining the three drag components discussed previously it is now possible to generate a lift-to-drag curve by combining it with the lift calculations from Section 5.2. The resulting drag curve equation is Equation (5.20).

$$C_D = C_{D,0} + C_{D,i} + C_{D,c} = C_{D,f} + \frac{C_L^2}{\pi \cdot A \cdot e} + \Delta C_{D,c} + C_{D,trim} \tag{5.20}$$

Using this equation, it is possible to generate a lift-to-drag curve for the aircraft at different subsonic speeds and configurations as a function of the lift coefficient. Note that for Mach numbers below the critical Mach number of 0.9, the compressibility drag contribution is zero.

5.3.6. NLR Supersonic drag method

The primary method applied in the aerodynamics module for the supersonic drag prediction is the method used by NLR in [31]. In this method, the first important consideration is the zero-lift wave drag caused by volume, which is first described. After that, the complete drag curve equation is provided. A more detailed discussion of the method can be found in Appendix C.6.

Zero-lift wave drag

For the zero-lift wave drag calculations, the total drag coefficient is estimated by summing the contributions of the fuselage, main wing, and horizontal and vertical tail. The nacelles are ignored at this stage because they are more complex to model. It should be noted that this method is not optimal, and that it will only provide a rough estimate of the volume wave drag. Still, for this stage of the research the level of fidelity is deemed to be sufficient. An option to improve the accuracy would be to make use of the supersonic area rule instead, but this is more difficult to implement.

Starting with the fuselage, its contribution is estimated by approximating it as that of two Kármán ogives (with length l_n) which represent the forebody and aftbody, and have a constant diameter cylinder (D_n) in between them. Their contribution is computed by using Equation (5.21). To account for interference between the two ogives a 2% increase is added to the aftbody contribution [31]. The drag contribution for the fuselage is corrected for the flight Mach number. The drag coefficient found is multiplied by the fuselage frontal area (area of the cylinder) and divided by the main wing reference area to correct it for the full aircraft [31].

$$C_{D_{Wfus}} = \left(\frac{D_n}{l_n}\right)^2 \tag{5.21}$$

For calculations of the wing volume drag contribution a method used for delta wings is applied. For this reason, the double delta main wing needs to be approximated by an equivalent single delta wing with an equivalent leading and trailing edge sweep angle (see Appendix C.2). Then, the following equation is used which closely approximates slender-body theory, where Λ_{LE} is the equivalent leading edge sweep angle [31]:

$$K_{SH} = 1.18 \cdot \frac{1 + 0.6 \cdot \beta \cdot \cot \Lambda_{LE}}{1 + 2.4 \cdot \beta \cdot \cot \Lambda_{LE}} \tag{5.22}$$

Following this, the wave drag for the full wing is computed using the following equation:

$$C_{D_{WV}} = K_{WV} \cdot A \cdot \left(\frac{t}{c}\right)^2 \qquad \text{with} \qquad \mathrm{K_{WV}} = \frac{\mathrm{r_s}^2}{3} \cdot \frac{128}{\pi} \cdot \mathrm{K_{SH}} \tag{5.23}$$

Here, r_s is the ratio of the wing area to the enclosing rectangular area (see Appendix C.2). For many wing sections its value will be close to 0.7, and for the horizontal and vertical tail it is assumed that this is true. For the main wing, the ratio will be computed by using its dimensions. The coefficients found are then multiplied by the exposed area of each component and divided by the main wing reference area.

By summing the four components the total volume wave drag coefficient is found. In [31], supersonic area ruling was also applied to the same aircraft model in order to determine what the difference was between the two methods. Here, it was found that the drag predicted by the supersonic area rule was only 70% of that computed using the method above. To correct for this, a 0.85 correction factor was added to the sum of the wave drag contributions, as is also be done in the current module.

Supersonic drag model NLR

The supersonic drag curve that is used in [31] assumes that there are two regions, the region with a lift coefficient below, and with a lift coefficient above the design lift coefficient. This design lift coefficient was defined earlier and is dependent on the supersonic cruise Mach number, and lift coefficient at the design cruise altitude. As a first step, the design drag coefficient is estimated using Equation (5.24).

$$C_{D_{des}} = C_{D_0} + \left(1-\overline{\sigma}\right)\cdot\frac{C_{L_{des}}^2}{C_{L_\alpha}} + \overline{\sigma}\cdot(1+\delta)\cdot\frac{r_s\cdot\beta\cdot C_{L_{des}}^2}{4\cdot\pi}\cdot\left[\left(\beta\cdot\frac{s}{l}\right)^{-1} + 2\cdot\beta\cdot\frac{s}{l}\right] \tag{5.24}$$

where the majority of the terms are the same as those defined previously. C_{D_0} represents the summation of the friction drag and zero-lift wave drag. δ accounts for the non-ellipticity of the wing lift and is assumed to be 0.1 [31]. Additionally, $\overline{\sigma}$ is a representation of the design suction parameter that applies to the wing. While it can be estimated by using methods in [66, 67], it is assumed that for the design lift coefficient, it is approximately equal to the fraction of the wing leading edge that is subsonic. Then, using the design lift coefficient as a boundary, the drag curve is built up from the following two functions.

$$\text{for} \quad C_L \le C_{L_{des}} \qquad C_D = C_{D_{des}} + (1+\delta)\cdot\frac{r_s\cdot\beta}{4\cdot\pi}\cdot\left[\left(\beta\cdot\frac{s}{l}\right)^{-1} + 2\cdot\beta\cdot\frac{s}{l}\right]\cdot\left(C_L^2 - C_{L_{des}}^2\right) \tag{5.25}$$

$$\text{for} \quad C_L > C_{L_{des}} \qquad C_D = C_{D_{des}} + \frac{\left(C_L^2 - C_{L_{des}}^2\right)}{C_{L_\alpha}} \tag{5.26}$$

The full method explained above was applied to the aircraft design of NLR, which led to the lift-drag curve shown in Figure 5.9.

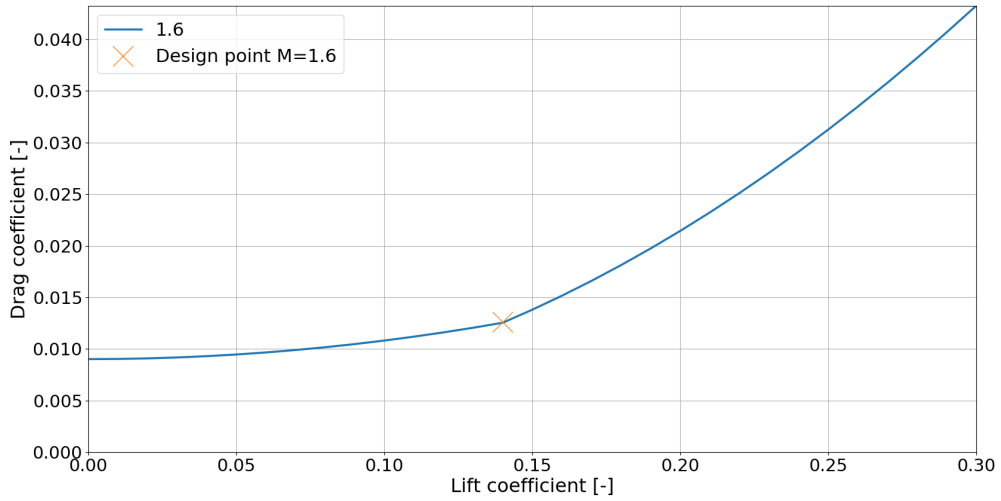

Figure 5.9: NLR supersonic L/D method applied to aircraft design [31]

As expected, there is a kink in the curve at the design lift coefficient. The sharpness of the kink is dependent on the value of the lift curve slope in the supersonic regime. At the design lift coefficient and Mach number of 1.6, a lift-to-drag ratio of 11.16 was found, which is within 0.54% of the value of 11.1 indicated in [31]. Since the method showed a good match to the report, the next step was to make an attempt to apply it to Concorde aircraft. Its design point is assumed to be the midpoint of its supersonic cruise at about 18.3 km altitude at Mach 2.02 and a weight of 138,132 kg. The results of this analysis are shown in Figure 5.10.

In this case, the kink at the design lift coefficient is much less clearly visible, which is the result of the value found for the lift curve slope (1.971 rad^{-1}). Because Concorde is operating at a higher cruise Mach number of 2.02 not the entire exposed wing is assumed to feature a subsonic leading edge as was the case for the NLR design, so that $\overline{\sigma}$ is set to be about 0.8. The lift-to-drag ratio at the design point is found to be 7.887 which is assumed to be the maximum L/D-ratio. The cruise lift-to-drag ratio used in the Class I calculations was 7.14, which when divided by 0.866 will return the approximate value of the maximum L/D-ratio as approximately 8.24. The value found using the NLR method is 4.28% less than this reference value. Again this is an acceptable deviation for the level of fidelity sought, but it should be noted that the method was found to be rather sensitive to factors like the cruising altitude.

Therefore, despite the fact that for both cases investigated the deviation between the value computed and the value from references is small, the accuracy of the method is not optimal. In most cases it is expected that the deviation will be within 10% of the true value, but this can only be said with certainty if additional cases are investigated. At this stage however, it is not possible to investigate a much larger range of aircraft due to time constraints.

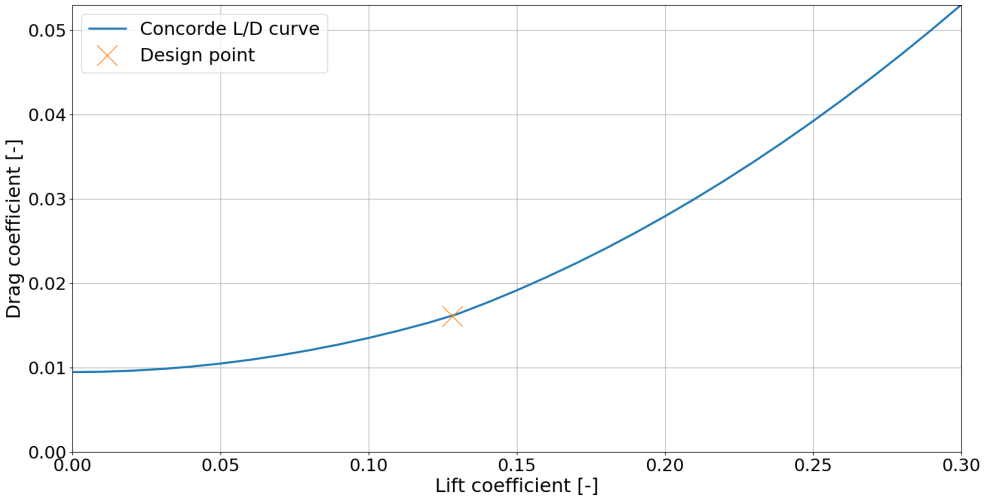

Figure 5.10: NLR supersonic L/D method applied to Concorde

5.3.7. Raymer supersonic drag model

As a second option, the method explained by Raymer [50] was also implemented in the program. This method can be used if the previous method returns unrealistic values and could be seen as a back-up method.

Zero-lift wave drag

For the volume-dependent wave drag component the method in Raymer requires that the aircraft area distribution along its length is determined. The method used to determine this cross-sectional area distribution is explained in Appendix C.7. From this distribution it is possible to determine what the maximum cross-sectional area is, as well as the fraction of the aircraft that features a constant cross-sectional area. Due to local area ruling and small variations in the geometry, this last fraction is assumed to be equal to or at least close to zero. Using the maximum cross-sectional area and the corresponding length, an equivalent Sears-Haack body is created for which the drag can be computed by Equation (5.27).

$$C_{D,\,SH} = \frac{9 \cdot \pi}{2} \cdot \left(\frac{A_{max}}{l} \right)^2 \tag{5.27}$$

Then, using this value, for Mach numbers greater than 1.2 a correlation is added to the function to approximate the aircraft volume wave drag. This correlation is as follows:

$$C_{D,\,wv} = E_{WD} \cdot \left[1 - 0.386 \cdot (M - 1.2)^{0.57} \cdot \left(1 - \frac{\pi \cdot \Lambda_{LE}^{0.77}}{100} \right) \right] \cdot C_{D,\,SH} \tag{5.28}$$

Here E_{WD} is an empirical wave-drag efficiency factor indicating how closely the aircraft shape approximates that of a Sears-Haack body. If the shapes match perfectly, then E_{WD} is one, but this is often not the case. Typical SST designs can be expected to have an efficiency factor in the range 1.4-2 assuming they have a clean design with a smooth area distribution. The drag coefficient found should then still be divided by the wing reference area to scale it to the actual aircraft. From the method outlined, it can be concluded that reducing the maximum area will have a larger positive effect than increasing the aircraft length to smooth out the distribution.

Raymer total supersonic drag

The second supersonic drag component is the lift-induced drag. For this Raymer [50] provides a simple empirical equation, which can be used to get a quick estimate of the induced drag factor K.

$$K = \frac{A \cdot \left(M^2 - 1 \right)}{4 \cdot A \cdot \sqrt{M^2 - 1} - 2} \cdot \cos \Lambda_{LE} \tag{5.29}$$

Note that this will provide a rough estimate for K and that it is advised to make use of the leading edge suction method, but for this stage of the design process it is accepted as the method of choice. The method has been used in a conceptual design project where a conceptual Mach 2.2 airliner was designed [68]. The combined drag curve values are then computed by using Equation (5.30).

$$C_D = C_{D_0} + C_{D_i} = C_{D_f} + C_{D_{wv}} + K_{sup} \cdot C_L^2 \tag{5.30}$$

5.3.8. Supersonic methods compared

To compare the methods, both the NLR and Raymer method were applied to the NLR design, resulting in the graph shown in Figure 5.11.

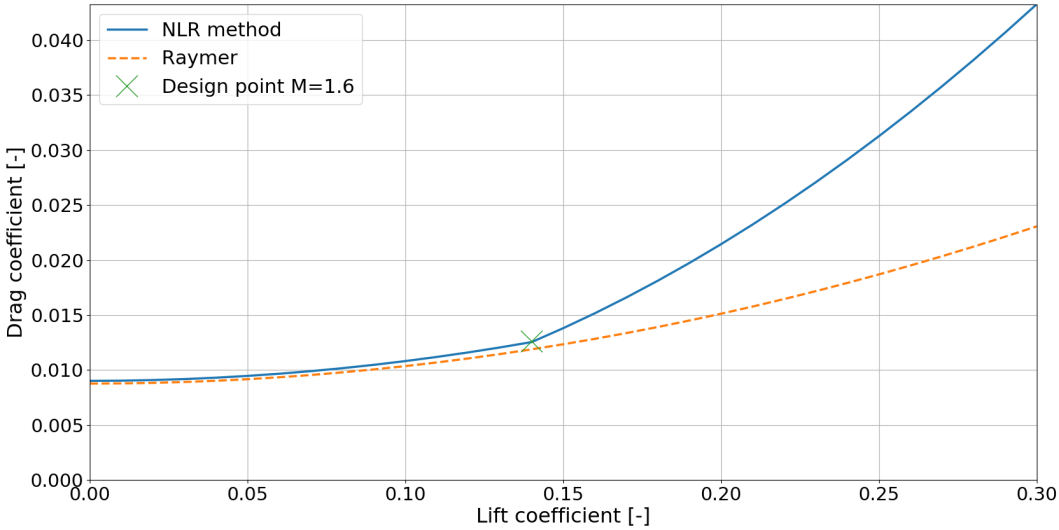

Figure 5.11: Supersonic L/D method comparison on NLR design

From this graph it can be seen that the Raymer method will result in a slightly better L/D-ratio for the same design lift coefficient (11.78 vs 11.16). Also, the Raymer method has a continuous curve, while the NLR method has a kink at the design lift coefficient. It should be noted that there is some variation possible in the Raymer method values because the maximum area is not exactly known due to the lack of knowledge about the inlet area. Consequently, the Sears-Haack body might have a slightly different drag coefficient. Additionally, it was assumed that the value of E_{WD} was 1.8. Given that the NLR method incorporates a larger number of design parameters in the calculation of the drag values, and has been shown to be sufficiently accurate for both Concorde and the NLR aircraft, it is selected as the main method of the aerodynamics module.

Additionally. during the validation process of the full design program, it was found that the Raymer method for supersonic drag often resulted in too high L/D values during supersonic cruise. Consequently, the takeoff weights became too low. Some attempts were made to resolve this issue such as including a correction factor for the cross-sectional area to increase the drag. However, these did not work for all aircraft designs and deviations remained too large. This further supports the decision to use the NLR method for supersonic drag.

5.4. Aerodynamics remarks

The number of options available for the analysis of aerodynamics of subsonic and (low-)transonic aircraft is already quite large, and can be complex. For supersonic aircraft, which operate in three flight regimes, this can cause issues since many methods used for subsonic conditions will not work in supersonic flight.

During the investigation, due to a limited amount of resources, a number of more accurate methods that were encountered could not be sufficiently studied, implemented and tested. As a result, the accuracy of the module is anticipated to be acceptable for conceptual design, although improvements can definitely be made, should additional research be requested. For these potential future investigations, a number of methods and ideas were found. These are elaborated on in Appendix C.8.

6
Class II

Through the Class I and wing loading analyses, an aircraft has now been created which has a known layout and dimensions as was shown in Section 4.3. Additionally, the engine has been sized and aerodynamic performance is known. However, during the first Class I calculations the operating empty weight was estimated by using a statistical relationship, which does not account for technological developments. In order to come up with a better estimate it is now possible, with the more evolved aircraft design, to perform a Class II weight estimation. During the Class II analysis, the weights of aircraft components are estimated such as the wing and fuselage, but also the air conditioning and de-icing systems.

It should be noted that with these calculations the results are still based on statistical relationships, but do allow for distinguishing between components. This can be beneficial if the impact of new developments applying to one particular component have to be evaluated. In order to perform the Class II calculations, first a flight envelope needs to be created so that the limiting load factor of the aircraft design is known. This process is shown in Section 6.1. Following this, the Class II breakdown and sizing relations are elaborated on in Section 6.2. The module is calibrated in Section 6.3, and in Section 6.4 technological developments are applied. Lastly, Section 6.5 looks at the sensitivity of the operating empty weight to technological developments.

6.1. V-n diagrams

There are two types of V-n diagrams, the maneuver diagram, and the gust diagram. The former is used in the creation of the latter, and to produce the total aircraft V-n diagram (i.e. flight envelope), the two are laid on top of each other. From the resulting figure, the limit load factors can be found as the highest and lowest load factors. An example containing both V-n diagrams is shown in Figure 6.1. Note that the velocities are all converted to an equivalent airspeed in knots.

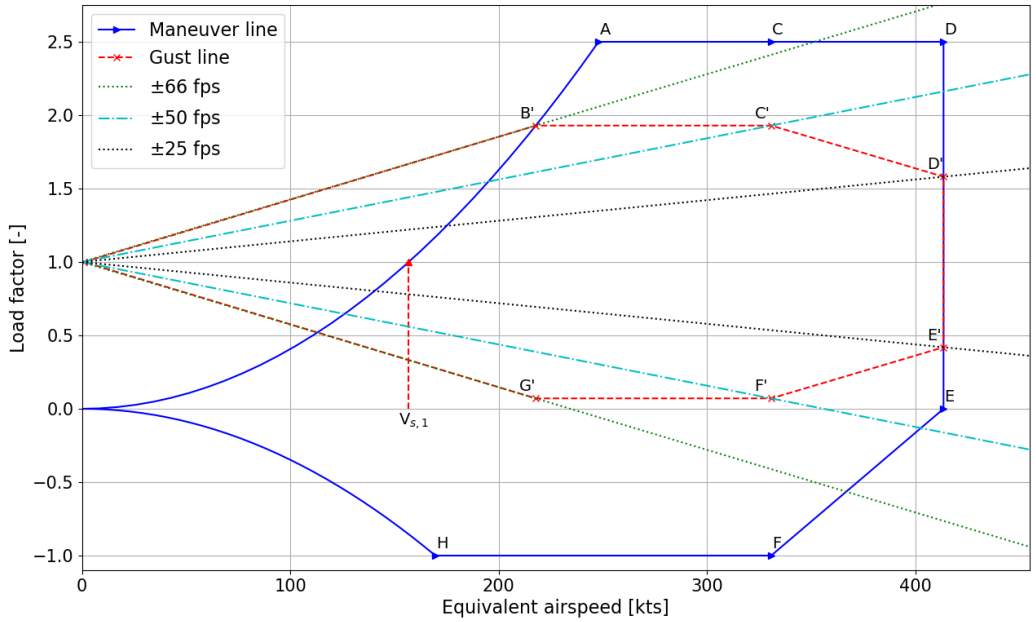

Figure 6.1: Example V-n diagram (for h < 20,000 ft)

Starting with the maneuver diagram, the first point of interest is the stall speed $V_{s,1}$ at $C_{N,max}$, where the load factor is one. The point is indicated by the red triangle, and $V_{s,1}$ by the vertical dashed line. Point A lies further along the stall line, and its speed corresponds to that at which the limiting load factor is reached while operating at $C_{N,\,max}$. $C_{N,\,max}$ is assumed to be 1.1 times the maximum lift coefficient, and the limiting (positive) load factor is calculated by the following equation (with takeoff weight in pounds) [69].

$$n_{lim,\,pos} = 2.1 + \frac{24,000}{W_{TO} + 10,000} \tag{6.1}$$

For most commercial transport aircraft this limiting factor will be 2.5. V_C (point C) and V_D (point D) represent the cruise and dive speed, respectively. The cruise speed is defined by the load case being investigated, while the dive speed is computed based on the cruise speed. For subsonic cruise conditions, the dive speed is 25% higher than the cruise speed, while for supersonic cruise the dive Mach number is assumed to be 0.2 higher than the cruise Mach number [70]. For both points the aircraft is operating at the limiting load factor.

On the lower side of the V-n diagram there is also negative stall which should be considered. The limiting negative load factor is assumed to be -1 as indicated by Roskam [69]. Then, using the maximum negative lift coefficient, the velocity V_H is calculated at which the limiting negative load factor is reached (point H). This maximum negative lift coefficient is assumed to be -0.85 times the maximum positive lift coefficient as was found by looking at the positive and negative stall points in [71] for several altitudes. From point H until V_C is reached (point F), the load factor remains minus one. At V_D (point E), the load factor is zero, and between those two points the load factor is assumed to vary linearly. This concludes the maneuver diagram, and the next step is to discuss the gust diagram.

The method used to set up the gust diagram is similar to that explained in [65, 69]. First, to determine the load factor resulting from a gust, Equation (6.2) is used, and it forms the basis of the entire method.

$$n = 1 \pm \frac{K_g \cdot C_{L_\alpha} \cdot U_e \cdot V_e}{498 \cdot (W/S)} \tag{6.2}$$

A number of factors are included in this equation (note Imperial units). The first is the gust alleviation factor K_g, which is included to account for the cosine-like intensity of gust loads on aircraft, and is computed by using Equation (6.3) or Equation (6.4), depending on the Mach number [50, 70].

$$K_g = \frac{0.88 \cdot \mu}{5.3 + \mu} \qquad \text{if} \quad M < 1 \tag{6.3}$$

$$K_g = \frac{\mu^{1.03}}{6.95 + \mu^{1.03}} \qquad \text{if} \quad M > 1 \tag{6.4}$$

where μ is defined as follows:

$$\mu = \frac{2 \cdot (W/S)}{\rho \cdot g \cdot \bar{c} \cdot C_{L_\alpha}} \tag{6.5}$$

C_{L_α} is the lift curve slope, which depends on the flight conditions, and U_e is the equivalent reference gust speed, which is taken from Table 6.1 for the point investigated.

Table 6.1: V-n diagram equivalent gust speeds [65]

Altitude	0-20,000 ft	>50,000 ft
V_B	66 fps	38 fps
V_C	50 fps	25 fps
V_D	25 fps	12.5 fps

It should be noted that between 20,000 and 50,000 ft, the gust speed is varied linearly between the limiting values. V_e is the equivalent airspeed of the aircraft in knots, and W/S is the aircraft wing loading.

For the gust diagram, the velocity V_B is the first parameter that needs to be found, to place point B'. It represents the design speed for the maximum gust intensity, and is the airspeed where the positive stall curve and the line from Equation (6.2) intersect. To this, an additional constraint is added by regulations [36], namely that V_B cannot be less than the value found by evaluating Equation (6.6).

$$V_{B,\,min} = V_{S_1} \cdot \sqrt{1 + \frac{K_g \cdot C_{L_\alpha} \cdot U_e \cdot V_e}{498 \cdot W/S}} \tag{6.6}$$

Should V_B be less than this value, then V_B will be set equal to the limit value.

For the positive gust loads at V_C (point C') and V_D (point D'), the load factors are found by evaluating Equation (6.2) at their flight speeds, and using equivalent gust speeds as found from Table 6.1. Since the gusts can be positive and negative, the load factors are calculated twice for V_B, V_C and V_D, which causes the gust diagram to be symmetric around a horizontal line at the load factor of one. The resulting points are connected and form the gust diagram.

The V-n diagrams are created for a number of different altitudes, weights and cruise Mach numbers. For the time being the scenarios used are those listed in Table 6.2, although more can be added. From the different gust diagrams, the maximum expected load factor can be determined, and used in the Class II weight estimation. The maximum lift coefficients are estimated using the lift curve data from the aerodynamics module at the maximum angle of attack α_{max}.

Table 6.2: V-n diagram load cases

Case	Altitude	Weight	M_C	M_D	α_{max}
1	0	$W_{sup,\ mid}$	0.4	0.5	20°
2	0	$W_{land,\ max}$	0.4	0.5	20°
3	0	OEW	0.4	0.5	20°
4	h_{sub}	$W_{sub1,\ st}$	$M_{cr,\ sub}$	$M_{cr,\ sub} \cdot 1.25$	20°
5	h_{sub}	W_{land}	$M_{cr,\ sub\ st}$	$M_{cr,\ sub} \cdot 1.25$	20°
6	h_{sub}	$W_{loit\ st}$	$M_{cr,\ sub}$	$M_{cr,\ sub} \cdot 1.25$	20°
7	h_{sup}	$W_{sup,\ st}$	$M_{cr,\ sup}$	$M_{cr,\ sup} + 0.2$	14°
8	h_{sup}	$W_{sup,\ end}$	$M_{cr,\ sup}$	$M_{cr,\ sup} + 0.2$	14°

In order to verify the V-n calculations, the results were checked by manual calculations. Additionally, an example from Niu [72] was used to check the results against a known solution. The inputs used are listed in the caption, and the resulting V-n diagram is shown in Figure 6.2.

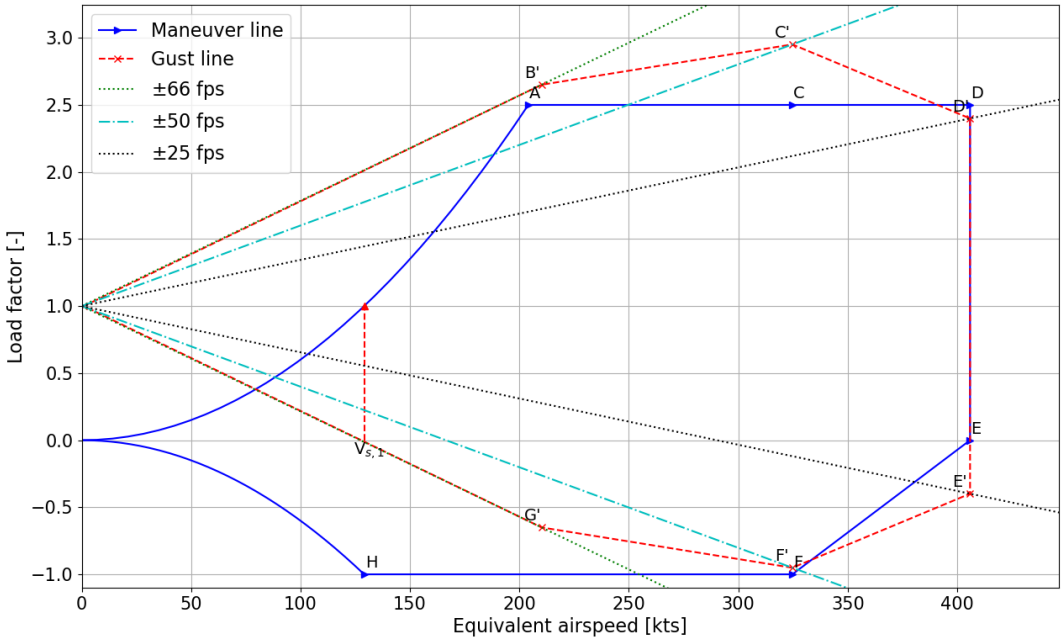

Figure 6.2: Verification V-n diagram with inputs: h = 10,000 ft ; W = 88,000 lbs ; S = 1,200 ft^2 ; b = 98 ft ; $\bar{c}$ = 13 ft ; $C_{N_{max}}$ = 1.3 ; $C_{N_{min}}$ = -1 ; C_{L_α} = 4.75 rad^{-1} (at M = 0) ; M_C = 0.592. Due to the Mach number increase, the lift curve slope value at M_C is 5.75 rad^{-1} and at M_D it is 6.75 rad^{-1} [72]

From the V-n diagram it can be seen that the positive limit load factor occurs at cruise speed for a 50 fps upwards gust, and has a value of 2.95, which would mean that the ultimate load factor is 4.43. It can also be seen that the largest negative load factor is -1 and occurs between V_H and V_F. Looking at the results in the source showed that the V-n function is indeed providing very similar results, when using the same inputs. Small deviations did occur in the order of one percent, but these could be traced back to round-off errors between the program and the reference in the atmospheric conditions and intermediate calculations.

6.2. Class II methodology

The Class II weight estimation method focuses on computing the empty and operating empty weight of aircraft. However, before the Class II weight estimation can be made, it is necessary to define the weight breakdown and determine which empirical relations are available to compute the different component weights.

The important methods that were found are those by Raymer [50], Torenbeek [34], Roskam [69], NASA's Flight Optimization System (FLOPS) [73], Kroo [65], Isikveren [74], NASA's Hypersonic Aerospace Sizing Analysis (HASA) [75], and Nicolai [17]. Several of these methods do not contain functions for all components in the breakdown. Also, to restrict the amount of functions, several sources are not used. Isikveren's method is more complex than the other options, requiring much more variables to be known or assumed, and is therefore not included. Also, HASA is aimed more at hypersonic aircraft and rockets, and is therefore not used.

As the different investigations often found different empirical relations, their estimates for a single component will vary, with some functions being better in one case, and others being better in another case. For this reason, it is advised in several aircraft design books to compute an average value from multiple methods, or to select the best method for each component, by using them on one or more aircraft for which the weight breakdown is known. Where possible, empirical relations from at least three different sources are used for each component to select the best options. To then further improve the accuracy, a correction factor will be applied to correct the function (or average) so that its weight matches that listed in the validation source.

Additionally, some component weight estimation functions could be re-calibrated with a set of aircraft to check that they are still accurate, and if not, modify them so that they better capture the trend. This was done for the Roskam landing gear equation. The aircraft that will be used for the calibration and validation are the Boeing 737-200 and Concorde. As for Concorde, no complete breakdown of the equipment group was found, the 737 will be used to determine the best functions for the components in that group. The calibration and validation of the module is treated in Section 6.3. Note that both aircraft are quite old, which could result in variations in the calculations because the construction methods and materials of aircraft have evolved since then. To correct for this, technology development factors are later introduced in Section 6.4.

Now that the approach to the weight estimation has been explained, it is possible to look at the methods that have been implemented in the program, and from which the best are selected. The aircraft empty weight is broken down into three groups, the structures, propulsion, and equipment groups. These groups are broken down into components like the wing and avionics. For each of these components several methods have been implemented in the code, and the sources used are listed in Table 6.3. As is also shown, the operating empty weight is computed by adding the operations group weight to the empty weight. The different groups and corresponding components are briefly discussed in Sections 6.2.1 to 6.2.4.

6.2.1. Structures group

The structures group of the aircraft consists of the wing, empennage (horizontal and vertical tail), fuselage, nacelles and landing gear. There is some variation possible in the definition, because for Concorde no specific weight for the nacelle was provided, so it is assumed to be part of its propulsion group weight.

Wing, empennage, fuselage and nacelle

During initial validation using Concorde data, it was found that wing weight equations for subsonic aircraft by themselves did not provide the best results. To get a better estimate, the US Air Force (USAF) fighter wing weight function from Nicolai [17] was added. The same was tried for the vertical tail, but the weights found for Concorde were even lower than those found using for example Kroo [65], so it did not make a difference because it was not a better function. To account for the higher speed, and correspondingly larger forces, a 20% penalty is introduced for the horizontal and vertical tail weights. For the fuselage weight, only transport aircraft functions were implemented. However, in the case of Concorde, to account for the moving nose structure a 5% penalty is introduced, which is removed for new aircraft. For the nacelle only transport aircraft functions are implemented.

Landing gear

For the landing gear several methods were implemented, and it was found in [76] that the function from Roskam [69] could be re-calibrated to improve its accuracy. The re-calibration was performed by applying the equation to eight aircraft including Concorde, and is shown in Figure 6.3. This resulted in a change of the function, as is shown in Equation (6.7).

$$W_{LG} = 62.61 \cdot \left(\frac{W_{TO}}{1,000}\right)^{0.84} \qquad \longrightarrow \qquad W_{LG} = 20.44 \cdot \left(\frac{W_{TO}}{1,000}\right)^{1.225} \tag{6.7}$$

Table 6.3: Class II methods tested (bold **X** indicates methods used in final Class II module)

		Group	Subgroup	Raymer [50]	Torenbeek [34]	Roskam [69]	FLOPS [73]	Nicolai [17]	Kroo [65]
Operating empty weight	Empty weight	Structures	Wing	X	**X**			**X**	X
			Horizontal tail	X	X		**X**		**X**
			Vertical tail	X	X		**X**		**X**
			Fuselage	X	X	X	**X**		
			Main gear	X	X	**X**	X		
			Nose gear	X	X	**X**	X		
			Nacelle	X	X	X	**X**		
		Propulsion	Engine						
			Engine controls & starter	X		X	**X**		
			Fuel system	X	X		**X**		
			Thrust reverser		X	X	**X**		
			Variable inlet					**X**	
			Inlet duct					**X**	
		Equipment	Flight controls	X	**X**	X	X		
			APU						
			Instruments	X	X	X	**X**		
			Hydraulics	X	X		**X**		
			Electrical	**X**	**X**	X	**X**		
			Avionics	X			**X**		
			Furnishings	X	**X**	X	X		
			Air conditioning	**X**	**X**		**X**		
			Anti-ice	**X**	**X**		**X**		
			Handling gear	**X**					
	Operations		Crew				**X**		
			Unusable fuel				**X**		
			Engine oil weight				**X**		
			Pax service weight				**X**		
			Cargo container weight				**X**		

Before calibration, the average absolute error was 34.6%, and the standard deviation 17.1%. After calibration, the average absolute error was 6.3% and standard deviation 8.7%. This shows that the re-calibration has been successful. For Concorde specifically, the original function had a 38% underestimation, while the new function results in a 12% overestimation.

6.2.2. Propulsion group

The propulsion group of the aircraft consists of the dry engine, the engine controls and starter system, fuel system, thrust reverser, and in case of a non-podded engine, the air induction system. For supersonic aircraft it is assumed that the propulsion group also includes the nacelle weight.

Engine (dry)

During validation, the dry engine weight values are simply taken from literature sources. For the Boeing 737-200 the dry engine weight of the Pratt & Whitney (PW) WJT8-15A is 3,474 lbs[1], and for Concorde's Olympus 593 it is 7,000 lbs[2]. For the Olympus engine, this also includes the afterburner and nozzle weight. The dry engine weight for the supersonic aircraft is estimated during the engine sizing routine in the final program version (Equation (4.3)).

[1] IHS Markit, *Pratt & Whitney JT8D*, https://janes.ihs.com/AeroEngines/Display/1306384 (accessed August 8 2018)

[2] Jane's, *Rolls-Royce SNECMA Olympus*, https://web.archive.org/web/20100806140324/http://www.janes.com/transport/news/jae/jae000725_1_n.shtml (accessed August 12 2018)

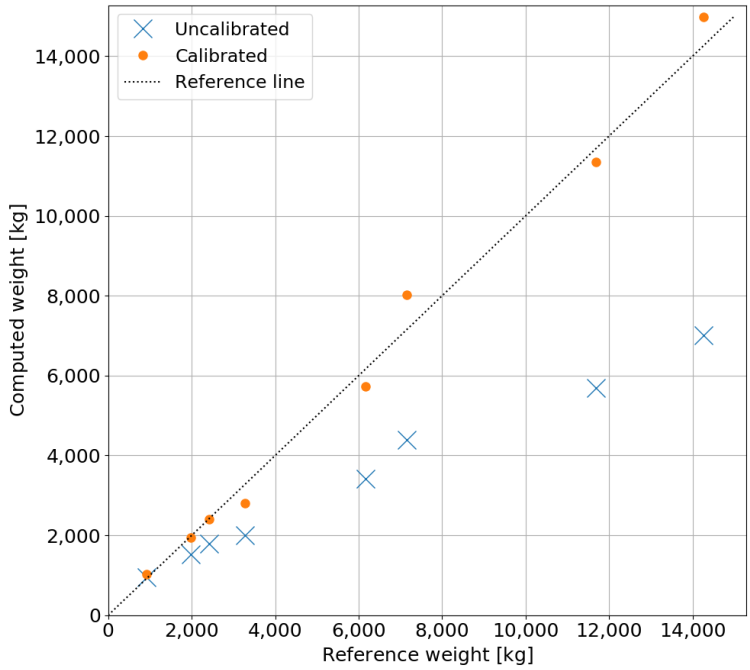

Figure 6.3: Landing gear weights before and after calibration with reference values from [76]

Propulsion system accessories

For the propulsion system accessories the majority of the equations used are those from subsonic transport aircraft because of their compatibility. An exception to this is the inlet system. For the majority of the subsonic transport aircraft the inlet weight is either not included or small, because the inlet is relatively short and can be included in the nacelle weight. For supersonic aircraft the inlet becomes more important since it has to slow down the flow to subsonic speeds with minimal losses, and can become lengthy. In case of Concorde, this internal ducting is complemented with a variable geometry inlet ramp. In order to take these components into account, equations from Nicolai [17] are used. Also, it should be noted that the propulsion installation component listed in the weight breakdown tables of Section 6.3 consists of the engine starter and engine controls.

6.2.3. Equipment group

The equipment group contains the different systems that the aircraft needs to be flown safely. It includes the flight controls, auxiliary power unit (APU), instruments avionics and electronics (IAE), hydraulics, electrical system, furnishings, and the environment control system (air conditioning and anti-ice).

Flight controls

For the flight controls, the higher speeds and potential control system requirements would result in an increase of the component weight for Concorde, compared to the base value found from the statistical relations. However, Concorde was the first aircraft to feature fly-by-wire with Power Flying Control Units (PFCU) which use electro-hydraullic servo control units to move the surfaces[3]. It is assumed that this change in system offsets the effect of the higher flight speeds, so no weight penalty is added.

APU

In order to estimate the weight of the Auxiliary Power Unit (APU) the results from [77] were used instead of relations from other literature (e.g. Roskam). There, it was found that the APU weight fraction depends strongly on the design range of the aircraft, as short-range single-aisle aircraft (e.g. Boeing 737-series and Airbus A318-A321), and long-range aircraft (e.g. Airbus A350 and A380, and Boeing 777 and 787) each formed a cluster. The data points are shown in Figure 6.4. It is assumed that the supersonic aircraft being designed fall in the long-range category.

[3] https://www.heritageconcorde.com/fly-by-wire

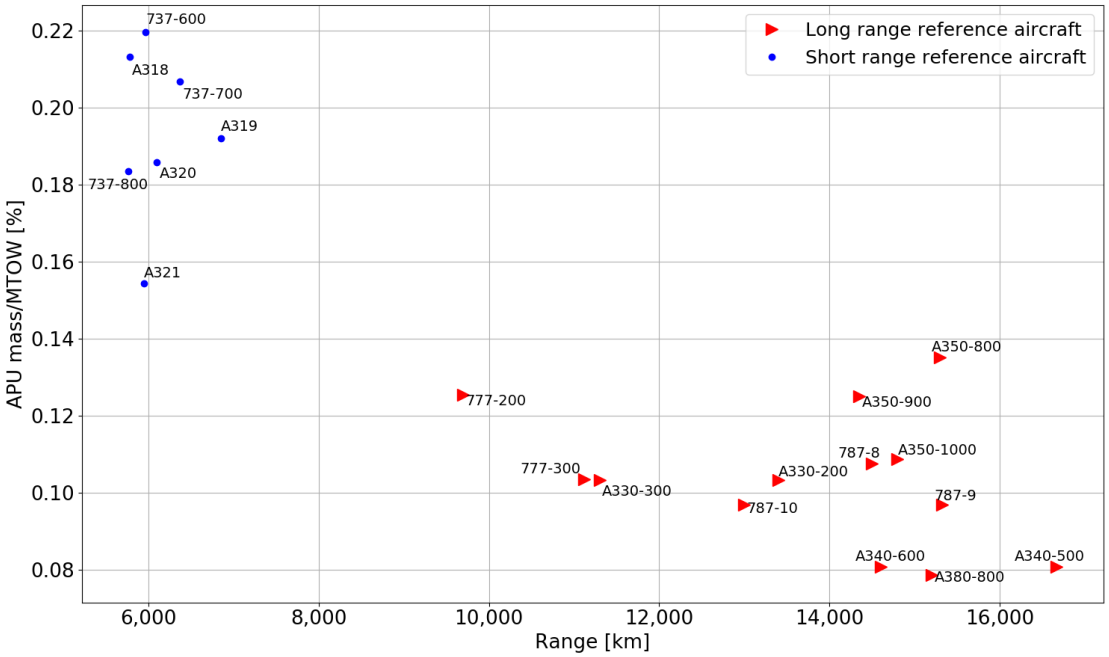

Figure 6.4: APU weight fraction graph with values from [77]

For each of the two clusters an attempt was made to create a curve fit, but the overall accuracy of the fits was not sufficient for either aircraft cluster (R^2<0.2). Instead, starting with the long-range group, it was decided to use the average value (0.104%) and add one standard deviation of 0.017% to it, to end up with a 0.120% APU weight percentage of the total aircraft takeoff weight. According to Raymer [50] the total installed APU weight is 2.2 times this value, so the following equation will be applied in the design routine:

$$W_{APU,\,lr} = 2.2 \cdot 0.120\% = 0.265\% \cdot W_{TO} \tag{6.8}$$

Similarly, for the short-range aircraft the average value was found to be 0.194%. Again one standard deviation of 0.021% was added to this, which results in the APU weight being calculated as follows:

$$W_{APU,\,sr} = 2.2 \cdot 0.214\% = 0.471\% \cdot W_{TO} \tag{6.9}$$

Instruments, Avionics and Electronics (IAE)

The instruments, avionics and electronics components are grouped together as a single entity (IAE) given their overlap. This is also done in other books such as Torenbeek [34] and Roskam [69]. For Concorde, it is assumed that there is not really a large difference in comparison to other contemporary aircraft, so no additional penalties are introduced. The base uninstalled avionics weight as used in the method by Raymer [50] is assumed to be 1,100 lbs for Concorde, which falls in the typical range of 800-1,400 lbs, and which was also assumed in [78].

Hydraulics

Concorde featured a hydraulic system with a pressure of 4,000 psi [79], which was similar to that of contemporary fighter aircraft, while subsonic transports were closer to 3,000 psi. The Boeing 787, being a more recent aircraft, uses a 5,000 psi[4] hydraulics system, which is powered by electrical pumps rather than the air-turbine driven pumps used in most aircraft. For Concorde, the hydraulic system not only powered the different flight controls, but it also had to move the nose. To account for this and the higher control forces at high speed the hydraulic weight is increased by 20%. For aircraft without movable nose, the penalty is zero.

Electrical

Concorde had an electrical system rating of 240 kVA[5] provided by four generators, one on each engine. Compared to the power rating of other passenger aircraft from the same era, 240 kVA is a high value, with the Boeing 737NG having a rating of only 180 kVA in 1997 [80]. The electrical system ratings for several modern aircraft were taken from [81]. This showed that compared to the time at which Concorde was designed, the

[4] https://www.boeing.com/commercial/aeromagazine/articles/qtr_4_07/article_02_3.html (accessed August 8 2018)
[5] https://www.heritageconcorde.com/concorde-electrical-power-supply (accessed August 12 2018)

amount of electrical power has increased even more, with for example the Boeing 787 boasting 1,000 kVA. This development is also known as that of More Electrical Aircraft (MEA) [79]. These power ratings are much larger than the values indicated by Raymer [50] (40-80 for transports, 110-160 kVA for fighters/bombers) for the sizing equation, but it is assumed that the equation can still be used for Concorde, which has a 240 kVA rating. For the newer aircraft with even higher ratings it is not certain whether the function is still representative as it scales with the rating $(K_{kva})^{0.782}$. This can result in a large increase, outside the range indicated by Raymer, and could affect accuracy. Therefore, the electrical system weight is the average of the Raymer [50], FLOPS [73] and Torenbeek [34] method, so that the sensitivity is reduced.

Environmental control system

The Environmental Control System (ECS) consists of the air conditioning and anti-icing systems. These systems are grouped together because in Torenbeek [34], the two systems are also combined in a single function. For Concorde, the cabin pressure that was maintained at cruising altitude is that at 5,500 ft[6]. This is a lower altitude than that maintained by most other subsonic aircraft which are around 7,500 ft. However, new aircraft like the Boeing 787 also feature a 6,000 ft pressure altitude in the cabin as it helps improve passenger comfort[7]. New supersonic aircraft are expected to have a similar cabin pressure altitude.

Since Concorde has more aerodynamic heating of the fuselage, and maintains a higher cabin pressure than most passenger aircraft, a 25% weight penalty is assumed for the environmental control system. Because of the aerodynamic heating the risk of ice accretion on the wing during supersonic cruise is non-existent. The anti-icing system is therefore assumed to be similar to that of contemporary subsonic aircraft so no additional penalty for the ECS is included.

6.2.4. Operations group

The operations group contains the different components which are needed for the aircraft to be operational for airlines. To reduce the complexity of this group, the only method used is that of FLOPS [73]. This decision was also made because it is the most recent method that was found. The components in this group are crew weight, weight of unusable fuel, engine oil weight, passenger services weight and the weight of cargo containers. For passenger services weight, it is necessary that the seating configuration of the cabin is known, because first class passengers should be offered better services than economy passengers. A better service will require more items and thus a larger weight.

6.3. Calibration and validation

In order to perform the calibration of the different aircraft components and groups, a large number of inputs had to be defined (145 in total). These values were found by looking at literature [82, 83], as well as aircraft related websites[8,9,10,11,12]. Should more equations be added in the future, then even more inputs might be needed. However, at the end of the calibration and validation, some equations will not be used, which reduces the number of inputs needed for the aircraft Class II analysis.

Starting with the Boeing 737-200, the Class II estimation module provided the weight values listed in Table 6.4. This table presents the component and group weights found from the reference Nicolai [17], and the average weight that is found from the different methods as well as their error. Based on the results from the different methods, the best are selected and listed with their weight and error. In most cases a single method is best, but for the empennage and environmental control system the average of all methods provides the best result. These best methods can then be used for the calibration of the module using the Concorde data.

Looking at the results for the Boeing 737-200, the structures group shows that the deviation using the best functions is only -2.2% which is good. For the propulsion group, the total weight is overestimated by 8.0%. This is largely caused by the engine weight which is overestimated by about 700 lbs, despite the fact that the engine weight was taken from Jane's, as indicated earlier. The discrepancy can be explained by the reference using a Boeing 737-200 with a different engine type. For the equipment group there is a larger variation on a component basis, but for the group overall the deviation is only +0.4%.

[6] https://www.heritageconcorde.com/concorde-pressurization-system (accessed August 12 2018)
[7] Baird, F., *Dreamliner Cabin Pressure Tech Reduces Altitude Sickness, Benefits PaxEx*, https://apex.aero/2015/12/10/turning-down-the-cabin-pressure (accessed August 22 2018)
[8] http://www.b737.org.uk/techspecsdetailed.htm (accessed August 8 2018)
[9] *Table 2 Boeing Aircraft*, https://booksite.elsevier.com/9780340741528/appendices/data-a/default.htm (accessed August 8 2018)
[10] IHS Markit, *Boeing 737-200*, https://janes.ihs.com/JAWAInServices/Display/1337315 (accessed August 8 2018)
[11] IHS Markit, *Boeing 737-300*, http://large.stanford.edu/courses/2013/ph240/eller1/docs/737.pdf (accessed August 8 2018)
[12] IHS Markit, *Pratt & Whitney JT8D*, https://janes.ihs.com/AeroEngines/Display/1306384 (accessed August 8 2018)

Table 6.4: Class II Boeing 737-200 (reference weight from [17])

Component	*Reference weight [lb]*	*Average weight [lb]*	*Error [%]*	*Best function*	*Best value [lb]*	*Error [%]*
Wing	10,613	11,255	+6.0	Kroo	10,184	-4.0
Empennage	2,718	2,660	-2.1	Average	2,660	-2.1
Hor. tail	-	-	-	-	1,576	-
Vert. tail	-	-	-	-	1,084	-
Fuselage	12,108	9,668	-20.2	FLOPS	11,999	-0.9
Nacelle	1,392	1,364	-2.0	FLOPS	1,379	-1.0
Landing gear	4,354	4,153	-4.6	Roskam	4,275	-1.8
Main	-	-	-	-	3,492	-
Nose	-	-	-	-	782	-
Structure total	**31,185**	**29,099**	**-6.7**	**-**	**30,496**	**-2.2**
Engine	6,217	6,948	+11.8	-	6,948	+11.8
Reverser	1,007	1,152	+14.4	FLOPS	1,054	+4.7
Air induction	0	0	-	-	0	-
Fuel system	575	682	+18.6	FLOPS	537	-6.6
Prop. install	378	245	-35.2	FLOPS	295	-21.9
Propulsion total	**8,177**	**9,027**	**+10.4**	**-**	**8,835**	**+8.0**
IAE	1,581	1,775	+12.3	FLOPS	1,593	+0.8
Flight controls	2,348	1,586	-32.5	Torenbeek	2,095	-10.8
Hydraulics	873	934	+7.0	FLOPS	814	-6.8
Electrical	1,066	1,674	+57.1	Raymer	1,207	+13.3
APU	836	648	-22.4		661	-20.9
Environmental control	1,416	1,452	+2.5	Average	1,394	-1.6
Furnishings	6,643	5,806	-12.6	Torenbeek	7,145	+7.6
Miscellaneous	124	35[13]	-71.8	Raymer	35[13]	-71.8
Equipment total	**14,887**	**13,911**	**-6.6**	**-**	**14,944**	**+0.4**
Empty weight	**60,210**	**53,077**	**-11.8**	**-**	**54,275**	**-9.9**

The empty weight is 9.9% lower than that of the reference despite all individual groups being much closer. This is caused by the 10% margin that is added to the sum of the structure, propulsion and equipment group by Nicolai [17]. For this additional margin no explanation is provided, so it is unclear exactly why it is done. A possible reason would be to account for future growth of the empty weight, but the 10% would be a very conservative value compared to the 2% mentioned by Raymer [50]. If the 10% factor were used, this would result in a close match to the reference empty weight.

Next, Concorde is used to calibrate the module for supersonic aircraft. The weight data were taken from [84]. This source only listed part of the components described earlier: the wing, fuselage, vertical tail and landing gear, engine & accessories, intakes, nozzle, furnishings, systems and services. As mentioned earlier, it is assumed that the nacelle is part of the propulsion group. Services is assumed to be the operations group, and furnishings and systems together are assumed to represent the equipment group.

As with the Boeing 737-200, the required inputs for the Class II calculations were taken from literature [78] and websites[14,15] where possible, and otherwise measured. Only if after all this they could not be found, an educated guess was made. Using the inputs found, the Class II results shown in Table 6.5 were computed. It shows for each component the reference weight, and the average weight found when combining all implemented methods. Based on the findings the best functions are again selected. These functions are then finally calibrated to make the resulting value match that from the reference source.

[13] handling gear equipment from Raymer [50]
[14] https://www.heritageconcorde.com (accessed August 12 2018)
[15] http://www.concordesst.com (accessed August 12 2018)

Table 6.5: Class II breakdown Concorde (reference weight from [84])

Component	*Reference weight [lb]*	*Average weight [lb]*	*Error [%]*	*Best function*	*Best value [lb]*	*Error [%]*	*Calibration factor [-]*	*Final value [lb]*
Wing	30,076	42,845	+42.5	USAF/ Torenbeek[16]	29,922	-0.5	1.005	30,076
Empennage	7,128	3,720	-47.8	Kroo	6,705	-5.9	1.063	7,128
Hor. tail	-	-	-	-	-	-	-	-
Vert. tail	7,128	3,720	-47.8	Kroo	6,705	-5.9	1.063	7,128
Fuselage	25,729	43,205	+67.9	FLOPS	24,942	-3.1	1.032	25,729
Landing gear	15,820	14,570	-7.9	Roskam	17,680	+11.8	0.895	15,820
Main	-	-	-	-	14,444	-	-	12,925
Nose	-	-	-	-	3,236	-	-	2,895
Structure total	**78,753**	**104,340**	**+32.5**	**-**	**79,249**	**+0.6**	**-**	**78,753**
Engine	29,206[17]	26,120	-10.6	Custom fit	26,120	-10.6	1.040	27,157
Nacelle	-	5,121	-	FLOPS	6,143	-	1.040	6,387
Reverser	-	4,935	-	FLOPS	5,168	-	1.040	5,373
Air induction	-	8,270	-	Nicolai	8,270	-	1.040	8,599
Fuel system	-	3,569	-	FLOPS	3,110	-	1.040	3,233
Prop. install	-	619	-	FLOPS	682	-	1.040	709
Propulsion total	**51,459**	**48,635**	**-5.5**	**-**	**49,494**	**-3.8**	**1.040**	**51,459**
IAE	-	3,119	-	FLOPS	3,180	-	1.305	4,151
Flight controls	-	4,184	-	Torenbeek	4,049	-	1.305	5,284
Hydraulics	-	2,196	-	FLOPS	2,717	-	1.305	3,546
Electrical	-	3,635	-	Raymer/ Torenbeek/ FLOPS	3,832	-	1.305	5,002
APU	-[18]	0	-	-	0	-	-	0
Environmental control	-	4,213	-	Raymer/ Torenbeek/ FLOPS	4,213	-	1.305	5,500
Miscellaneous	-	122	-	Raymer	122	-	1.305	160
Systems[19]	*23,643*	*17,469*	*-26.1*	-	*18,113*	*-23.4*	1.305	*23,643*
Furnishings	11,822	8,990	-23.9	Torenbeek	13,428	+13.6	0.880	11,822
Equipment total	**35,465**	**26,460**	**-25.4**	**-**	**31,541**	**-11.1**	**-**	**35,465**
Empty weight	**165,677**	**179,434**	**+8.2**	**-**	**160,284**	**-3.3**	**-**	**165,677**
Services	7,823	5,450	-30.3	FLOPS	5,450	-30.3	1.435	7,823
OEW	**173,500**	**184,885**	**+6.6**	**-**	**165,735**	**-4.5**	**-**	**173,500**

From the table it can be seen that if only the average values were used, the empty weight and operating empty weight found would be 8.2% and 6.6% too high, respectively. However, the structures group weight was overestimated by 32.5% while the equipment group weight was underestimated by 25.4%, showing that using the average would not be very accurate. As with the Boeing 737-200, the best functions were selected starting with the wing, for which the weighted average of the USAF fighter aircraft and Torenbeek methods is the best. The use of the USAF fighter method is a reasonable finding since Concorde's wings are much closer in resemblance to thin fighter wings, than to the thicker subsonic transport wings. The transport aircraft equation from Torenbeek somewhat corrects the USAF equation by introducing subsonic transport aircraft data. For the vertical tail, Kroo's method was the best, while FLOPS and Roskam were most accurate for the fuselage and landing gear, respectively. With these equations the structures group weight was overestimated by only 0.6%. After calibration the deviation was reduced to zero.

[16] USAF with weight 1 and Torenbeek with weight 2
[17] indicated in [84] as engines & accessories
[18] Concorde had no APU
[19] systems listing in reference source which is assumed to contain all equipment components except furnishing

For the propulsion and equipment group components the methods used were those found to best approximate the Boeing 737-200 components, with the exception being the air induction system, which is taken from Nicolai [17], and the electrical and environmental control systems which take the average of three functions. Using these equations the propulsion group weight was underestimated by 3.8%, compared to the 5.5% underestimation when the average values are used. Since the group breakdown in the reference source was not very clear, each component in the propulsion group is calibrated by the same value. Because the factor of 1.040 is small, the impact is limited.

For the equipment group, the best functions result in an 11.1% underestimation, which is a substantial improvement over the 25.4% underestimation for the average of all methods. However, the 11.1% is providing a distorted image because the furnishings weight is overestimated by 13.6%, while the other systems combined result in a 23.4% underestimation. To correct for this, the furnishings component is calibrated by 0.880, while the other equipment group components are all calibrated by a factor 1.305.

These factors ensure that the aircraft empty weight estimation now has zero deviation from the reference value. For the services (operations group), the weight is underestimated by 30.3% and then calibrated, which results in the operating empty weight being 173,500 lbs as indicated by the reference source. The larger difference is likely because the FLOPS method used is more recent, and accounts for technological developments. This shows that the Class II weight estimation module has been calibrated and is providing accurate results, meaning it can be used for new supersonic aircraft designs. Also, as fewer functions are used to compute the aircraft weight the number of required inputs has also been reduced from 145 to 72. The output values from the Class II analysis are stored in a text file as shown in Appendix D.2.

6.4. Technological developments

Now that the Class II analysis has been verified and validated, it can be used in the design program. However, the two aircraft used for the validation and calibration are old and therefore do not represent the current technologies and materials. Factors such as improved construction methods and advanced composite materials result in weight reductions, which lower the (operating) empty weight. To account for these improvements, it is possible to apply a 'technology development factor' based on recent developments. The technology development factors defined for the different aircraft components in literature are listed in Table 6.6, and are briefly motivated after this.

Table 6.6: Class II technology development factors empty weight

Source	NASA M2.4 [29]	Raymer [50]	Roskam [69]	Kroo [65]	Nicolai [17]	Isikveren [74]	Average	Applied factor
YEIS	2005	-	-	-	-	2020	-	2020
Wing	0.70	0.85	0.893	0.85	0.80	0.85	0.824	0.85
Vert. tail	0.80	0.83	0.85	0.85	0.75	0.85	0.822	0.85
Hor. tail	-	0.83	0.85	0.85	0.75	0.85	0.826	0.85
Fuselage	0.82	0.90	0.893	0.85	0.825	0.85	0.856	0.85
Nacelle	-	0.90	0.90	-	-	-	0.900	0.85
Nose gear	0.85	0.95	-	-	0.92	0.85	0.893	0.88
Main gear	0.75	0.95	-	-	0.92	0.85	0.868	0.85
Air induction	-	0.85	-	-	0.70	-	0.775	0.80
Engine	-	-	-	-	-	-	-	0.78
Reverser	-	-	-	-	-	-	-	0.88
Fuel system	-	-	-	-	-	-	-	0.90
Propulsion install	-	-	-	-	-	-	-	0.88
Flight controls	0.75	-	0.85	-	-	0.891	0.830	0.86
Hydraulics	0.03	-	-	-	-	0.891	0.460	0.60
IAE	0.70	-	-	-	-	0.891	0.795	0.86
Electrical	0.95	-	-	-	-	0.891	0.920	0.92
Furnishings	0.85	-	-	-	-	0.891	0.870	0.85
Air conditioning	0.65	-	-	-	-	0.891	0.770	0.86
Anti-icing	1.12	-	-	-	-	0.891	1.005	0.86
APU	0.81	-	-	-	-	0.891	0.850	0.96

For the wing, fuselage, and empennage structural weights, the factors are all set to 0.85. From the different sources there was some variation, although the average values are quite similar. Isikveren [74] mentions that the value of 0.85 is quite an optimistic value. For the nacelle weight two sources were available, with the average being 0.9. However, as both sources are relatively old, it is assumed that some more development has taken place, further reducing the factor to 0.85.

For the nose and main gear the technology factors deviate slightly from the average value. Given that the main gear is a larger structure and consists of two struts its weight savings potential is expected to be slightly better than for the nose gear. For this reason it has a 0.85 factor compared to the 0.88 for the nose gear. The air induction system is only listed specifically by two of the sources, with the 0.70 value being the most recent. Still, this value is seen as very optimistic so it was decided to use a value of 0.80 instead.

In order to estimate the change in engine weight, the results from a study on engine development shown in Figure 6.5 were used. It is unclear from the source whether the weight used is the dry or installed engine weight. The trend shows that the engine thrust-to-weight ratio has improved over time. Concorde's Olympus 593 engines were first run in 1966 and had a dry thrust-to-weight ratio of about 4.48. Following the curve, for 2005 the ratio improves to about 6.7 compared to 4.7 in 1966. Assuming that the thrust remains unchanged, this represents an engine weight factor of 0.701, which for 2020 service entry could be even lower. To be conservative, a weight factor of 0.78 will be applied to the engines. Note that it is assumed that the engine thrust requirements are unchanged for the new Concorde. It is likely that for a new supersonic aircraft of similar dimensions to Concorde, different engine thrust requirements apply, but these are currently unknown.

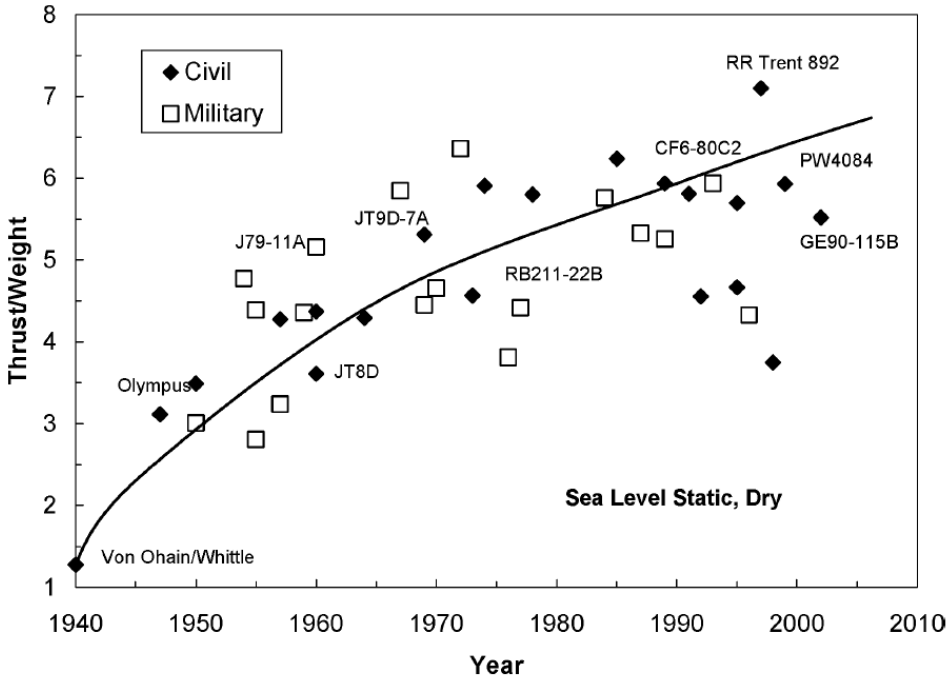

Figure 6.5: Engine dry thrust-to-weight ratio trend [40]

No clear weight savings values were found for the thrust reverser, fuel system and propulsion installation components. Based on the other categories, for the thrust reverser, a factor of 0.88 will be used, which is less than for the structures group because of the higher operating temperature for the reverser material, which is therefore expected to be slightly heavier. For the fuel system 0.90 is used as it is expected that lighter materials and changes to the fuel controls will have a smaller impact on the weight of the tanks. The propulsion installation component is assigned a factor of 0.88.

For the equipment group components two sources were available. While NASA provided single values for 2005 entry into service, Isikveren [74] provided a function which could be used to determine the weight savings with respect to the year 1975:

$$\Pi_{ATM} = e^{2.965 - 0.001525 \cdot YEIS} \tag{6.10}$$

In this equation YEIS is the year of entry into service. For a service entry in 2020, the weight savings factor is 0.891. Since Concorde was designed before 1975 an additional 3% reduction is added, so the factor will be

0.86. For the surface controls, instruments, avionics, air conditioning, and anti-icing, this value will be used, while for the remaining components other considerations led to further adjustments of the values.

The hydraulics system is expected to be 40% lighter, due to the system switching from more hydraulically powered actuators to electro-hydraulic actuators (EHA) [85]. These are smaller self-contained actuator units with their own hydraulic fluid reservoir, and allow for removing the external hydraulic source and fluid piping. Also, the nose will no longer have to be rotated, further reducing the size of the hydraulics system.

For the electrical system the average value of 0.92 will be used. The savings are less than according to Isikveren [74] because the required electrical system power has increased, while on the other hand new wiring methods and power supply are assumed to be used, which offer weight savings potential [80]. Meanwhile, for the furnishings there can be more savings with the seats and other interior materials becoming lighter through the application of new materials. For this reason the value of 0.85 from NASA is applied [29].

Lastly, for the APU weight estimation, a function is used that is based on more recent aircraft data, so that the weight savings potential is expected to be smaller. A 4% weight reduction will be implemented for the APU. In the new weight estimation of Concorde, it is assumed that an APU is integrated in the design.

It should be noted that the values selected are relatively conservative, and that some more recent technologies might have been missed and not taken into consideration. Also, for later entries into service some new technologies could be considered like the replacement of the APU with a battery or new anti-icing systems (see [85, 86]).

All factors mentioned so far pertain to the empty weight components of the aircraft. However, the operations group items have also changed since Concorde, and should be considered as shown in Table 6.7.

Table 6.7: Class II technology factors operating items

Component	Crew	Unusable fuel	Engine oil	Pax service	Cargo container
Factor	1	0.85	0.90	0.90	0.85

The crew weight is found by multiplying the number of pilots (225 lbs each) and attendants (155 lbs each) with a constant weight [73]. This means that no real changes can be made other than reducing crew count. In Concorde three flight crew members were needed, but with a modern fully digital cockpit the flight engineer is no longer required, so the flight crew count is changed from three to two.

With the development of new design techniques it is assumed that the ability to locate places where fuel will be trapped has been improved, and that they can be at least partially resolved. The weight of the unusable fuel is consequently reduced by applying a 0.85 factor. Similarly, for the engine oil, less oil is burnt by the engine which means that less oil is needed for the same period. The oil systems are also expected to be made from lighter materials, so a factor of 0.9 is used.

Looking at the passenger service weight, the weight of the galley bar equipment has been reduced by implementing lighter materials. Meanwhile, since Concorde, entertainment systems have been introduced which introduce some extra weight. Cutlery and other equipment has been changed from metal to plastic post 9-11, and passengers can indicate before the flight what food they want, so that less excess food is brought on-board. Lavatories have also become lighter. Overall, it is assumed that the passenger service weight is reduced by 10% compared to the 1970s. Lastly, for the cargo containers, lighter materials are implemented which help reduce their weight by an assumed value of 15%.

To show the impact of these technology factors, the Concorde is evaluated once again using the same inputs as before, but now with the application of the technology factors. Note that several inputs were changed; the number of pilots was decreased from three to two, the movable nose removed, hydraulic system pressure increased from 4,000 to 5,000 psi, and an APU is now included. The resulting weight breakdown is shown in Table 6.8. It shows that the updated Concorde would have a 16.9% lower empty weight, and a 16.8% lower operating empty weight than the original aircraft. This decrease is rather similar for the four groups. The absolute weight savings are largest for the structures group, because its initial weight represents the largest part of the operating empty weight. It should be noted that the weight savings factors used are somewhat conservative, so the savings could be larger.

The reduction in operating empty weight will also indirectly affect the takeoff weight of the aircraft. To determine the effect, Equation (3.2) from the Class I analysis can be used. Assuming that the aerodynamic efficiency, specific fuel consumption and other inputs used for Concorde in the Class I analysis are unchanged, the fuel fraction is also unchanged (0.52556). The payload weight is still 8,845 kg and the operating empty weight is 144,370 lbs or 65,485 kg. Since the operating empty weight from the Class I solution (79,378 kg) was

Table 6.8: Class II results for updated Concorde with technology factors included

Component	Original weight [lbs]	New weight [lbs]	Weight change [lbs]	Change [%]
Wing	30,076	25,564	-4,512	-15.0
Empennage	7,128	6,059	-1,069	-15.0
Hor. tail	-	-	-	-
Vert. tail	7,128	6,059	-1,069	-15.0
Fuselage	25,729	20,829	-4,900	-19.0
Landing gear	15,820	13,534	-2,286	-14.5
Main	12,925	11,057	-1,868	-14.5
Nose	2,895	2,477	-418	-14.4
Structure total	**78,753**	**65,986**	**-12,767**	**-16.2**
Engine	27,157	21,183	-5,974	-22.0
Nacelle	6,387	5,429	-958	-15.0
Reverser	5,373	4,728	-645	-12.0
Air induction	8,599	6,879	-1,720	-20.0
Fuel system	3,233	2,910	-323	-10.0
Propulsion install	709	624	-85	-12.0
Propulsion total	**51,459**	**41,753**	**-9,706**	**-18.9**
IAE	4,151	2,858	-1,293	-31.1
Flight controls	5,284	4,545	-739	-14.0
Hydraulics	3,546	1,968	-1,578	-44.5
Electrical	5,002	4,553	-449	-9.0
APU	0	1,038	+1,038	-
Environmental control	5,500	4,710	-790	-14.4
Miscellaneous	160	137	-23	-14.0
Systems	*23,643*	*19,830*	*-3,834*	*-16.1*
Furnishings	11,822	10,048	-1,773	-15.0
Equipment total	**35,465**	**29,858**	**-5,607**	**-15.8**
Empty weight	**165,677**	**137,597**	**-28,080**	**-16.9**
Services	7,823	6,773	-1,050	-13.4
OEW	**173,500**	**144,370**	**-29,130**	**-16.8**

0.86% higher than the reference value, the operating empty weight savings are slightly larger than shown in the table above at 13,893 kg (17.5% reduction vs 16.8% found before). The only remaining unknown is the takeoff weight, and it can be found by solving the equation numerically. The takeoff weight found is 156,669 kg, which is 29,245 kg less than the original Class I value (185,914 kg), and represents a 15.7% reduction. With the unchanged fuel fraction, the fuel weight is found to be 82,338 kg which is a saving of 15,377 kg (15.7% reduction).

6.5. Technology sensitivity

The previous section showed the effect of relatively conservative technology factors on the operating empty weight of Concorde. Because the actual technology factors can be different from those used, it is good to look at the effect that their variation can have on the operating empty weight. To try and evaluate this variation, a random number generator will be used to generate a large variation of technology factors. The method used to generate these factors is explained in Appendix D.3 and was used to generate an array of 100,000 technology factors for each weight component. These were then entered into the Class II module with the dimensions of Concorde. The resulting operating empty weight distribution is shown in Figure 6.6.

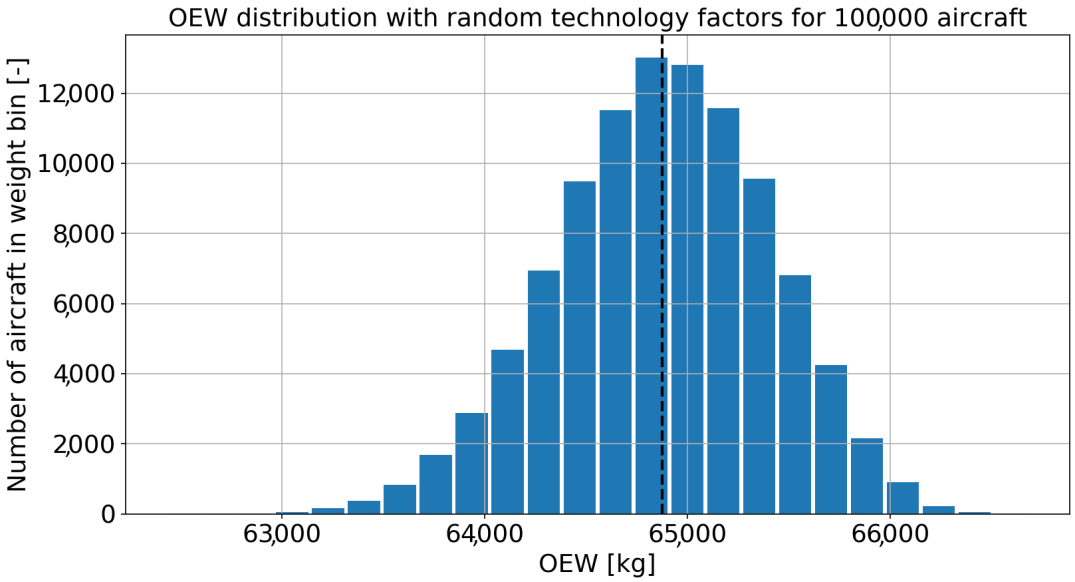

Figure 6.6: Operating empty weight distribution for 100,000 aircraft using randomized technology factors

This graph shows that there is quite some variation in the aircraft operating empty weight, but that there is a clear peak visible. As anticipated from the beta distribution that was selected for the random technology development factors, the operating empty weight distribution is skewed slightly to the right. The mean value for the weight distribution is 143,021 lbs (64,873 kg) as indicated by the vertical dashed line, and the standard deviation is 1,166 lbs (529 kg). This means that the value found in the previous section falls just inside one standard deviation from the mean value, and shows that it is not an outlier.

The minimum value found is 137,637 lbs (62,431 kg), and the maximum 147,006 lbs (66,681 kg). These represent an operating empty weight reduction of 20.7% and 15.3% compared to the original weight of 173,500 lbs (78,698 kg), respectively. Using these values it is also possible to once again estimate the maximum takeoff weight, which for the minimum operating empty weight is 150,232 kg, a 19.2% reduction compared to 185,914 kg. For the maximum operating empty weight it is 159,190 kg, which is a 14.4% reduction. This shows that there is quite some variation possible. Note that the distribution values could be tuned by the user if desired.

6.6. Class II remarks

The previous sections of this chapter have focused on the Class II setup and calibration, but for the implementation in the full design program some further modifications were made. The first is that to account for unforeseen weight growth of the components, a 5% increase is added to each component. This is more than the 2% advised by Raymer [50] to account for the reduced knowledge on supersonic aircraft, and could be increased to 15% by the user. This latter limit is slightly above the 10% margin added by Nicolai [17].

Additionally, during testing of the full program it was found that for larger aircraft the Kroo method used for the horizontal and vertical tail would return too high component weights. This is likely the combination of the increased surface area and thin airfoil used. To resolve this, the more recent FLOPS method is implemented. Since this is a recent method, the corresponding calibration and technology factors are assumed to be one. The accuracy was checked by using it on several past studies, and showed smaller deviations. Similarly, during the calibration of the Class II module using Concorde the engine weight was taken directly from literature. The corresponding technology factor was assumed to be 0.78. However, in the full program the engine weight is estimated by using a regression fit which also includes more recent engines. Consequently, a 0.78 technology factor is too optimistic, and replaced by a factor 0.92.

7
Program Validation & Supersonic designs

This chapter looks at the supersonic aircraft designs produced by the design program. Before the designs could be created, it is necessary to check whether the program is providing reliable results. Testing was performed and the findings are shown in Section 7.1. Runtime information for the program was also gathered and is summarized in Section 7.2. Next, in Section 7.3 the top-level requirements for five supersonic aircraft are defined. The resulting designs and their performance are evaluated in Section 7.4, and Section 7.5 studies the effects of design range and Mach number.

7.1. Full program testing

Having combined all of the different modules discussed in the previous chapters, the full design program was completed. Since the individual modules were all validated separately, it is expected that the full program will also produce valid results. As a first set of checks, several different designs were created by varying the inputs to find bugs and other potentially weird behavior. Any issues encountered were fixed when possible or otherwise attempts were made to explain their cause so that they could be avoided.

Having performed these checks, it was decided to attempt to produce several aircraft designs similar to those in other studies, and explain the differences. The main metric used for the comparison is the aircraft takeoff weight since many other parameters like engine performance and aerodynamic efficiency are dependent on methods used in the design studies, and those often vary from those used in the design program. A second, less important metric is the operating empty weight. Aside from design studies, designs are also produced with similar design requirements as the Concorde and Tu-144 aircraft. It should be noted that for all designs used in the comparison, there are many design variables which are unknown and these are therefore assumed in the design program. The main purpose of this comparison is not to show that the designs from the program are the same, but that they are in the same range, and to try to explain major differences.

To achieve this, 11 designs were produced and the results are displayed in Figures 7.1 and 7.2, with the weights listed in Table 7.1. The main design parameters and top level requirements used for the aircraft can be found in Appendix E.1.

Table 7.1: Full program validation aircraft weight comparison

Aircraft	$\mathbf{W_{OEW,ref}}$ **[kg]**	$\mathbf{W_{OEW,calc}}$ **[kg]**	**Delta [%]**	$\mathbf{W_{TO,ref}}$ $[kg]$	$\mathbf{W_{TO,calc}}$ **[kg]**	**Delta [%]**
1. Concorde	79,264	75,793	-4.38	185,066	186,723	+0.90
2. Concorde new	*79,264*	*51,257*	*-35.3*	*185,066*	*126,075*	*-31.9*
3. Tu-144	99,199	90,427	-8.84	206,794	213,095	+3.05
4. Tu-144 new	*99,199*	*59,236*	*-40.3*	*206,794*	*145,134*	*-29.8*
5. Boom SST	*34,464*	*47,036*	*+36.5*	*77,100*	*118,888*	*+54.2*
6. Boom SST mod	34,464	33,335	-3.27	77,100	82,226	+6.65
7. Aerion AS2[1]	26,218	22,105	-15.7	54,884	55,699	+1.49
8. HELESA	19,577	18,697	-4.50	43,100	46,009	+6.75
9. Cranfield SSBJ	21,000	19,269	-8.24	44,900	48,918	+8.95
10. NLR M1.6	136,000	136,786	+0.58	340,000	355,184	+4.47
11. N+1 overwater	62,489	60,704	-2.86	140,160	149,074	+6.36
Absolute average			**6.05**[2] (*10.20*[3])			**4.82**[2] (*10.77*[3])

[1] design has a 5% too small fuel volume available in current version, but this deficit is deemed small enough to ignore given that some additional volume remains available

[2] not including new Concorde and Tu-144 or regular Boom SST aircraft

[3] not including new Concorde and Tu-144, but including regular Boom SST (aircraft 5) instead of modified Boom SST (aircraft 6)

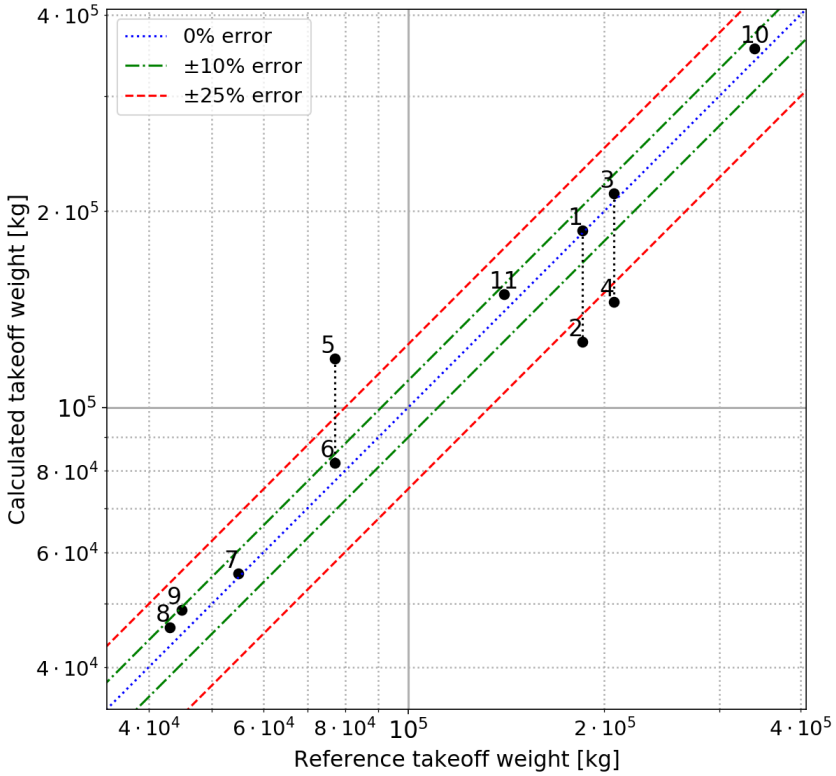

Figure 7.1: Supersonic design program takeoff weight comparison to other studies for 11 designs

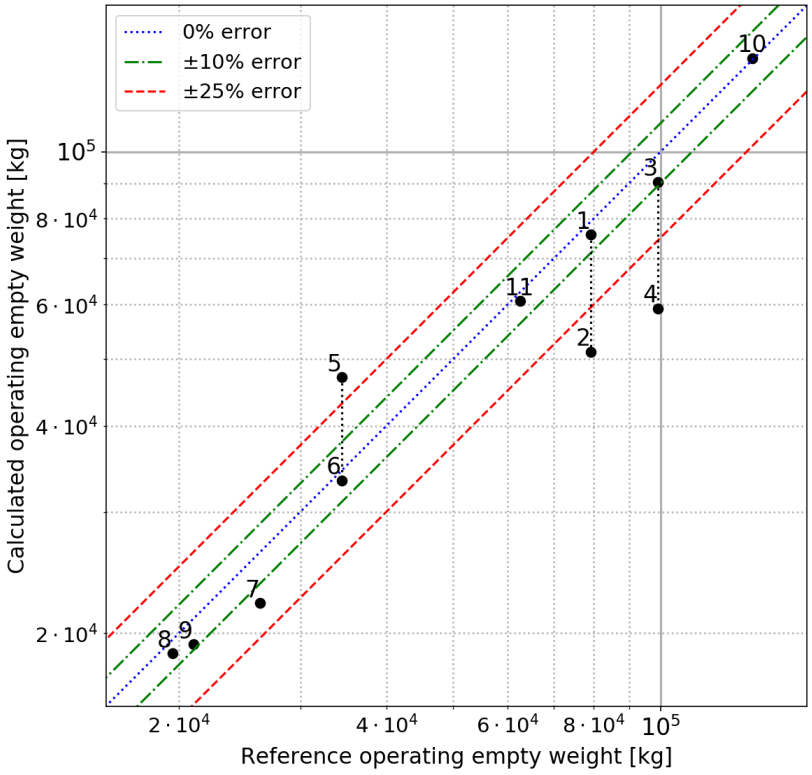

Figure 7.2: Supersonic design program operating empty weight comparison to other studies for 11 designs

Looking at the results, it can be seen that the prediction of the aircraft takeoff and operating empty weight has a good accuracy. For both parameters, the absolute deviation is less than 7%, when excluding the new Concorde, new Tu-144 and unmodified Boom SST aircraft. However, there is a discrepancy since the takeoff weight is often overestimated, whereas the operating empty weight is mostly underestimated. The aircraft for which this is most visible are the SSBJs (aircraft 7, 8 and 9) for which the operating empty weight is underestimated by 9.5%, and takeoff weight overestimated by 5.7%. As a result, the operating empty weight fraction of the aircraft are also underestimated. For the larger aircraft these differences are smaller.

The main reason found for this behavior is that the Class II module has been calibrated using Concorde, while also using the best empirical relations for that aircraft. While these work well for larger aircraft (>50 pax), for smaller business jets it might be that different component estimation methods are better, providing a lower deviation. To partially remedy this, the Class II component weight growth factor, which is used to account for unforeseen component weight growth, has been increased from 5 to 10 or even 15%. Additionally, changes were made to the Class II calibration before the above final results were produced as briefly described in Section 6.6. It is also found for the business jets that the distribution of the operating empty weight is not entirely accurate with the engines sometimes weighing more than the wings. Still, the full operating empty weight value is seen as sufficiently accurate, so this discrepancy in the weight distribution is ignored. The cause of this discrepancy is likely also the calibration of the Class II module.

Another relatively large operating empty weight outlier is the Tu-144, for which the program underestimated the value by 8.84%. As was shown during the Class I validation, the main reason for this is that Tu-144 has a higher operating empty weight fraction than most other SSTs since it used different (heavier) materials. To also show the effect of new technologies, new versions of the Concorde and Tu-144 were created with reduced takeoff and landing distances, lower stall speeds, technology factors included, and low bypass ratio turbofans. The result was an average takeoff weight reduction of 30.9%. For Concorde, this is more than the 17.5% found in Section 6.4 because the impact of the operating empty weight savings increases through the snowball effect. Also, the engines are more efficient and lighter which results in a lower takeoff weight, and consequently lower operating empty weight. For the new Tu-144 the operating empty weight reduction seems larger, but this is because the reference value is taken from literature and not the design program.

A final important remark is about the Boom SST aircraft, which for its design mission operates at Mach 2.2. With the method used to select the leading edge sweep angles to achieve the highest subsonic leading edge fraction, this results in excessive sweep angles, and consequently an unrealistic design. In addition, the aerodynamic performance is worse and the operating empty weight increases, making the aircraft too heavy (+54.2%). For this reason, it was decided to slightly modify the design mission, reducing the Mach number to 2, and changing some other parameters like increasing the aspect ratio to better match that of Concorde. This is reasonable since the Boom SST is seen as a scaled version of Concorde with a similar wing shape. With these modifications, the aircraft more closely matched the reference aircraft weight. This also shows that the current program does not work adequately for Mach numbers above 2.05-2.1.

The findings show that the design program has a good accuracy given the level of fidelity provided, although many assumptions are used to generate the designs. This concludes the testing of the supersonic aircraft design program. More information about the results produced by the program such as its sensitivity and other attributes is provided in [7].

7.2. Program runtime information

Now that it has been shown that the program has a good accuracy, it is also interesting to briefly discuss some attributes of the program itself like the runtime and number of iterations required to converge to a design. The results found are listed in Table 7.2.

Table 7.2: Design program runtime information based on 50 aircraft design runs

Parameter	Value	Unit
Maximum number of iterations	**15**	-
Average number of iterations	**9.68**	-
Average iteration time	**6.05**	s
Average ParaPy & PDF time	**29.5**	s
Average total runtime	**87.9**	s

The data used to calculate the attributes was compiled from the 11 aircraft used previously to test the program, and an additional 39 designs produced using the requirements detailed in the next section for a number of design ranges to assess the design sensitivity. The convergence criterion used was that the takeoff weight had to be stable within 0.1% for two successive iterations. The system was run on a Windows 7 laptop with an i7-3630QM 2.40 GHz processor, and 8 GB RAM. Note that the computer is almost six years old and that for the newer computers, the runtimes are expected to be at least 20% lower.

The table shows that the maximum number of iterations performed is 15, which is half of the current program iteration limit (30). It should be noted that during these runs the option to show the takeoff weight convergence was disabled, because it would increase the average iteration time by about 115% (to ≈ 13.0 seconds). This is largely caused by the five second pause included in the program for each iteration to allow the user to properly see the weight convergence graph. Still, the full runtime is limited to at most several minutes, so the program could be used to analyze a large number of designs in a relatively short period.

7.3. SST design requirements

When considering the design requirements for a 'new' aircraft type, it is important to consider a variety of designs, particularly in terms of payload and range. As this requires a small investigation, only a summary is shown here. More details can be found in Appendix E.2. The resulting design requirements are summarized in Table 7.3.

To cover a larger range of aircraft sizes, five passenger capacities were selected: 18, 50, 100, 170 and 250. The first can be seen as a SSBJ, and the others as SSTs, with the 50 and 100 passenger variants featuring a business class configuration. The 170 and 250 passenger SSTs will use a seating configuration similar to subsonic long-range aircraft. The largest two aircraft are unlikely to be built during the first generation of supersonic aircraft. The load factors are selected as explained in Appendix F.6. For the ranges, the first (4,200 NM) offers good Transatlantic performance and the third (5,000 NM) offers good Transpacific performance. The median value of 4,600 NM provides good Transatlantic and decent Transpacific coverage, although some city pairs will require an intermediate refueling stop. The supersonic Mach number is set to 1.6 based on a study of other SSTs and SSBJs. Subsonic flight is to be performed at Mach 0.95 to still have a small speed benefit over subsonic aircraft.

Table 7.3: Requirements for supersonic aircraft designs

Category		SSBJ	SST	SST	SST	SST
Aircraft		*SSBJ*	*SST50*	*SST100*	*SST170*	*SST250*
$n_{pax,max}$	[-]	18	50	100	170	250
Range	[NM]	4,200/4,600/5,000				
Load factor	[-]	0.70	0.70	0.80	0.85	0.85
M_{sup}	[-]	1.6				
M_{sub}	[-]	0.95				
s_{TO}	[m]	1,900-2,000	2,400	2,800	3,000	3,200
s_{land}	[m]	1,300	1,800	2,100	2,300	2,500
h_{sup}	[km]	15-17				
h_{sub}	[km]	10-12				
W/S	[N/m^2]	4,000-4,400	4,000-4,400	4,200-4,600	4,200-4,600	4,200-4,600
ETOPS	[-]	180				
Sonic boom intensity	[PLdB]	70-90				
Airport noise	[-]	Stage 5				
EI(NO_x)	[g/kg]	5-15				
EI(H_2O)	[g/kg]	1,400				

For the definition of the takeoff and landing distance requirements a study was performed on airports and a set of reference aircraft. This showed a clear distinction between the SSBJ, which has relatively short takeoff and landing distances, although they are higher than that of subsonic business aircraft. For the SSTs, the distances increase as the payload increases. The 3,200 m for the biggest SST is loosely based on the lowest maximum runway length found for 34 major airports (see Table E.4). These distances are defined for sea-level altitude with standard day temperatures. In the future, other scenarios like hot days could be considered which can be encountered in regions like the Middle East.

The cruising altitudes are set to a range which can be refined during the design process, and was selected by looking at the aircraft used in the Class I module validation, as well as other surveys in literature [5]. The wing loading range is used to determine what the expected stall speeds of the aircraft are at takeoff weight under sea-level conditions, and is based on data from other aircraft designs. The ETOPS 180 rating was selected by looking at the key city pairs affected such as the ability to fly to Hawaii, which would not be possible with an ETOPS 120 rating. Most new aircraft can get ratings of ETOPS 180 and higher even before being operated commercially as was the case for the Airbus A350 XWB, which was certified for ETOPS 370 at entry into service (EIS)[4]. For SSTs on the other hand, it might not be as straightforward since they are a "new" category of aircraft, but given the modern design programs and flight testing, they are likely certifiable for ETOPS 180 at EIS so it should not be an issue.

For the environmental requirements, the values are based on the goals set in other supersonic design projects. However, they are not part of the main design routine, and are only evaluated for the final set of designs, so they do not steer the design process. Additionally, the values might be modified by the user to study the sensitivity of the environmental impact to specific design inputs. For example, with climate impact the emission index of NO_x can be made lower or higher than it actually is according to the modules to show under which conditions the performance would be best.

Starting with the sonic boom intensity requirement, the range currently defined is rather large and based on other studies. This is because at the time of writing, the noise module is not yet in production, and consequently, the sonic boom requirements are unknown. Further information on the final sonic boom requirements can be found in [7]. In terms of the airport noise, it is expected that the new supersonic aircraft have to meet the same Stage 5 requirements as subsonic aircraft. As shown in Appendix E.2.6, there is the possibility to use Stage 4 regulations for SSBJ aircraft if the application is done before 2020. However, this is bad for the market potential of the aircraft as it might not be allowed to operate from specific airports if they ban non-Stage 5 aircraft. The emission index values for NO_x and H_2O are taken from [4, 33]. Note that under normal circumstances the combustion of jet fuel will always meet the 1,400 g/kg requirement for water vapor.

7.4. SST designs

Using the supersonic aircraft design program and applying the requirements specified in the previous section, five aircraft designs were produced. It was found that for all scenarios, the 5,000 NM mission was feasible. However, for the SSBJ the maximum amount of fuel could not fit inside the aircraft, which was in part due to the high fuel fraction (over 60%). Instead of making larger modifications to the aircraft design, it was decided to use a 4,600 NM design range instead. This range is similar to that used in most other SSBJ design studies. For the SST50 and SST100 the fuel fractions at 5,000 NM were also over 60% and the fuel efficiency decreased strongly compared to the 4,600 NM design. Therefore, for these aircraft the design range is also 4,600 NM. Compared to the Boom SST (SST50) and particularly Concorde (SST100), this still represents an improvement in operating range. For the larger SST170 and SST250 the design range of 5,000 NM is used.

The design payload values are determined by multiplying the average passenger weight with the number of passengers. The average passenger weight for the smaller SSTs is assumed to be slightly lower than for the larger SSTs since business passengers are less likely to bring additional luggage than the average economy passenger. For the SSBJ the average weight (including luggage) is 98 kg, for SST50/100 it is 100 kg and for the SST170/250 it is 102 kg. The aircraft Mach numbers are the same as those defined in the requirements.

For the cruise altitude, it is assumed that the two smallest supersonic aircraft fly slightly lower at 15.5 km, and the larger SSTs at 16 km altitude. The latter is also used for the NLR Mach 1.6 airliner with 250 passengers [31]. All aircraft have an outbound subsonic cruise altitude of 10.2 km, and inbound altitude of 11.5 km. The increase in altitude is introduced to account for the fuel burn of the aircraft during supersonic cruise.

The wing aspect ratios are increased from 2.1 for the SSBJ to 2.5 for the SST170/250 aircraft. This increase was introduced because for the smaller business jets, the aspect ratios are often in the range 2-2.2, while for the large NLR Mach 1.6 airliner the aspect ratio is 2.8 [31]. An investigation into the effect of aspect ratio on performance will be included in the sensitivity study in [7]. The number of engines is set to four for all aircraft except the SSBJ. The reason for this is that for the SST50, it was found that four engines would result in a lighter aircraft design than two engines. The overall pressure ratio of the engines is assumed to be 35 for all aircraft, and for the SSBJ it is assumed that the engines feature a slightly lower bypass ratio of 2.5, compared to the 3.0 used for the larger aircraft.

[4] *EASA certifies A350 XWB for up to 370 minute ETOPS*, https://www.airbus.com/newsroom/press-releases/en/2014/10/easa-certifies-a350-xwb-for-up-to-370-minute-etops.html, October 2014 (accessed April 30 2019)

Using these inputs the main results found for the five aircraft are shown in the lower half of Table 7.4.

Table 7.4: Main supersonic aircraft design inputs and results

Parameter	Unit	Aircraft				
		SSBJ	SST50	SST100	SST170	SST250
$W_{PL,des}$	kg	1,235	3,500	8,000	14,739	21,675
Range	NM	4,600	4,600	4,600	5,000	5,000
M_{sup}	-	1.6	1.6	1.6	1.6	1.6
M_{sub}	-	0.95	0.95	0.95	0.95	0.95
s_{TO}	m	1,900	2,400	2,800	3,000	3,200
s_{land}	m	1,300	1,800	2,100	2,300	2,500
h_{sup}	km	15.5	15.5	16	16	16
h_{sub}	km	10.2/11.5[5]				
AR_W	-	2.1	2.2	2.2	2.5	2.5
n_{eng}	-	2	4	4	4	4
OPR	-	35	35	35	35	35
BPR	-	2.5	3.0	3.0	3.0	3.0
W_{TO}	kg	51,887	77,335	136,189	218,987	332,722
W_{OEW}	kg	20,099	30,166	52,494	83,050	129,042
W_{OEW}/W_{TO}	-	0.387	0.390	0.385	0.379	0.388
$W_{f,des}$	kg	30,525	43,669	75,695	121,198	182,004
$W_{f,des}/W_{TO}$	-	0.589	0.565	0.556	0.553	0.547
$W_{f,max}$	kg	31,525	45,922	80,254	129,152	194,037
$W_{PL,des}/W_{TO}$	-	0.024	0.045	0.059	0.067	0.065
Fuel eff design	pax.km/kg	3.62	7.40	9.79	11.84	11.61
W/S	N/m^2	4,289	4,281	4,281	4,409	4,409
T/W	-	0.445	0.311	0.289	0.275	0.278
T_{eng}	kN	113.3	59.0	96.5	148.6	226.7

Starting with the SSBJ, its takeoff weight of 51,887 kg falls roughly in between the Cranfield SSBJ and HELESA, and the Aerion AS2 designs (see Table 7.1). This is expected because its range also falls in between those used in the design studies mentioned. Similarly, the takeoff weight for the SST50 is close to that of the Boom SST, which has a slightly lower design range and higher Mach number. The SST100 is 8% heavier than the 'new' Concorde aircraft, while having a 1,050 NM greater range, lower speed, and about 10% less payload. This is the result of the SST100 having a higher bypass ratio engine, and lower Mach number. The SST250 is about 8,000 kg lighter than the NLR Mach 1.6 airliner and has 500 NM lower range. This difference is partially the result of the NLR design having a slightly higher aspect ratio and better supersonic lift-to-drag ratio. The SST170 falls in between the SST100 and SST250. All in all, the takeoff weight results are as was expected based on the other supersonic design studies.

The operating empty weights are not unrealistic and result in an average operating empty-to-takeoff weight ratio of 0.386, which is slightly lower than what most reference studies found. It should be noted that for the SSBJ the weight growth factor was set to 10% instead of the 5% normally used. This correction was done to partially account for the Class II not being calibrated for small business jets, as was found during program testing. The results also show that fuel accounts for more than half of the takeoff weight with an average design range fuel weight fraction of 0.562, where the smaller aircraft have even higher fuel fractions. Consequently, the payload fraction is also smaller, on average 0.052 but smaller for the business jet aircraft because of their higher fuel fractions. Overall, the values fall in the range found in Table 3.3 during the Class I analysis. Compared to subsonic aircraft these payload fractions are low, often one half to one fourth that of equivalent subsonic aircraft (see Table B.3 for SST170/250). Note that the Boeing 737 aircraft do not make for a good comparison because their design range is much smaller.

Looking at the fuel efficiency values, which indicate how much fuel is needed to transport a passenger one kilometer, the performance is better for the larger aircraft than for the business jet. This is because for the larger aircraft the payload fraction increases, while the fuel fraction decreases. As expected, the efficiency

[5] outbound subsonic cruise altitude/inbound subsonic cruise altitude

is larger for the harmonic range than for the design range, because the amount of passengers increases much more than the decrease in mission range and fuel. A small comparison is made to similar subsonic aircraft like the Boeing 787-8 for a range of 5,000 NM with a payload of 19,622 kg, which offers a fuel efficiency of 42.2 pax.km/kg according to Piano-X. Compared to the 11.61 pax.km/kg for the design mission of the SST250 this is about 3.6 times better. Similarly, for the SSBJ, the fuel efficiency of 3.62 pax.km/kg at 4,600 NM is about 2.46 times worse than that of a Gulfstream G550 with 12 passengers (≈8.89 pax.km/kg).

The wing loading values for the aircraft designs all fall within the bounds defined by the top-level requirements. The engine thrust is higher for the SSBJ than for the SST50 and SST100. This is the result of the higher thrust loading for the two-engine configuration, and because the takeoff thrust has to be provided by just two engines. The engines of the SST50 in particular are quite weak, but still more powerful than most subsonic business jet engines.

These aircraft designs will also be used for the climate performance study in Chapter 9. In the following subsections more results for the five aircraft designs are discussed, starting with the payload-range performance.

7.4.1. Payload-range performance

In the Class I analysis, the main design point does not show the full picture because aircraft can be operated at higher or lower loads, which can reduce or increase the mission range. The method used to analyze this was explained in Section 3.5, and was applied to the five supersonic aircraft designs described earlier. The payload-range diagrams found are combined into Figure 7.3, with values listed in Table 7.5.

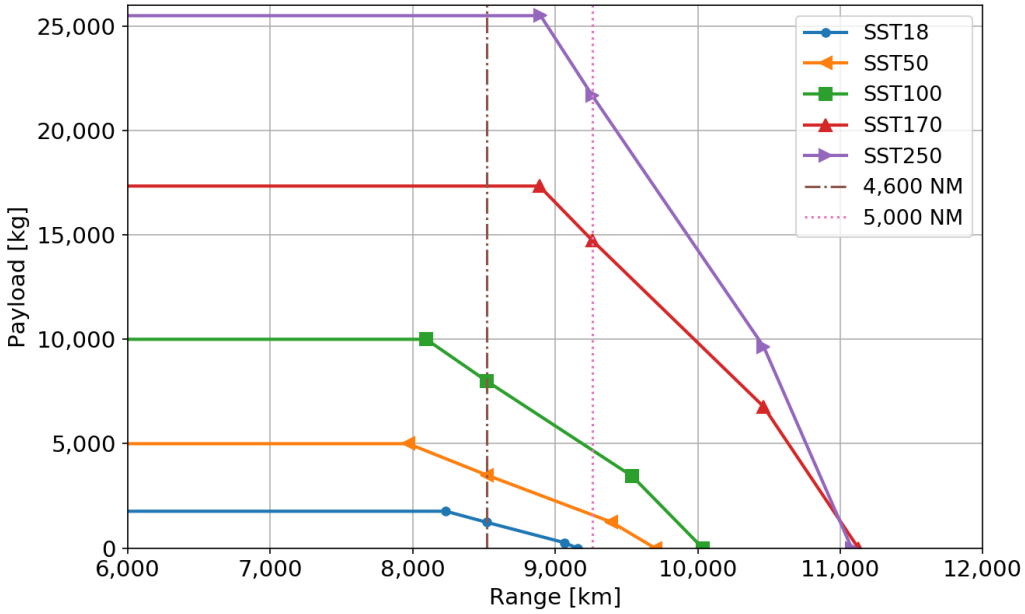

Figure 7.3: Payload-range diagram for the five supersonic aircraft designs

Table 7.5: Supersonic aircraft designs payload-range data

Parameter	Unit	Aircraft				
		SSBJ	SST50	SST100	SST170	SST250
$W_{PL,harm}$	kg	1,764 (+42.9%)	5,000 (+42.9%)	10,000 (+25%)	17,340 (+17.6%)	25,500 (+17.6%)
R_{harm}	NM	4,446 (-3.3%)	4,303 (-6.5%)	4,371 (-5.0%)	4,799 (-4.0%)	4,804 (-3.9%)
$W_{PL,des}$	kg	1,235	3,500	8,000	14,739	21,675
R_{des}	NM	4,600	4,600	4,600	5,000	5,000
$W_{PL,C}$	kg	263 (-78.7%)	1,247 (-64.4%)	3,441 (-57.0%)	6,785 (-54.0%)	9,642 (-55.5%)
R_C	NM	4,894 (+6.4%)	5,072 (+10.3%)	5,152 (+12.0%)	5,648 (+13.0%)	5,650 (+13.0%)
R_{ferry}	NM	4,943 (+7.5%)	5,238 (+13.9%)	5,418 (+17.8%)	6,008 (+20.2%)	5,983 (19.7%)
Fuel eff design	pax.km/kg	3.62	7.40	9.79	11.84	11.61
Fuel eff harm	pax.km/kg	5.36 (+48.1%)	10.33 (+39.6%)	12.02 (+22.8%)	13.77 (+16.3%)	13.50 (+16.3%)

Looking at the graph it can be seen that each curve includes four visible points which from left to right (increasing range) represent the harmonic range, design range, range at maximum fuel (C), and ferry range. It can clearly be seen that the two largest SSTs have the largest design range, and that the ferry range for SST170 is slightly larger than for the SST250. This is the result of the slightly better fuel efficiency of the smaller SST170 compared to the SST250, which is also shown in the table. Especially for the SSBJ the range increase for the ferry range is small at 7.5%. This is largely the result of the SSBJ having a smaller maximum fuel ratio of 1.05, compared to the 1.089 used for the other SSTs. This change was made to ensure that the maximum fuel quantity could be stored in the fuel tanks.

As was also found in Table 3.6 during the Class I analysis, for the smaller SSBJ aircraft the relative increase in range at points C and the ferry range (D) is smaller than for the larger aircraft. This is related to the lower payload fraction of SSBJs, which means that a similar change in payload has a larger relative impact on the overall payload weight than for the SST170 or SST250.

Looking at the fuel efficiency values for the design and harmonic mission it can be seen that the harmonic mission has better performance. This can be expected because the payload increase is greater than the nominal (excluding reserves) mission fuel decrease. It is also found that for the smaller aircraft the relative improvement in fuel efficiency is substantially higher. In part, this is due to the lower design point load factor, which means that the relative improvement in payload is also larger for the harmonic mission. Furthermore, given that the fuel fraction method is used, combined with the higher fuel fraction for the smaller aircraft, a reduction in range will result in a larger reduction of the fuel fraction for the harmonic range.

7.4.2. Aerodynamic performance

Aside from the payload-range performance, it is interesting to briefly discuss the aerodynamic performance of the supersonic aircraft. The main results for the five designs are summarized in Table 7.6.

Table 7.6: Main supersonic aircraft aerodynamic performance

Parameter	Unit	Aircraft				
		SSBJ	SST50	SST100	SST170	SST250
$L/D_{sup,max}$	-	8.09	8.65	9.14	9.85	10.04
L/D_{cont}	-	11.97	12.75	13.10	14.27	14.59
L/D_{div}	-	11.85	12.65	13.01	14.18	14.51
L/D_{loit}	-	11.86	12.20	12.24	13.45	13.50
L/D_{final}	-	13.09	13.60	13.77	15.11	15.62
Flaps TE	-	Fowler/Fowler	Fowler/Fowler	Fowler/Fowler	Fowler/Fowler	Fowler/Fowler
Flaps LE	-	-	-	-	-	-
$C_{L,max,TO}$	-	1.15	1.09	1.14	1.22	1.23
$C_{L,max,land}$	-	1.25	1.17	1.23	1.32	1.34

Starting the with the main aerodynamic parameter, the supersonic maximum lift-to-drag ratio, the larger aircraft have higher values. In part, this can be explained by their higher wing aspect ratio, which together with the wave drag method used, results in a lower volume wave drag contribution and better overall L/D. This change with aspect ratio was also found in the supersonic drag method source [31]. Also, for the higher aspect ratio wing a slightly larger subsonic leading edge fraction can be achieved, which also results in a small drag reduction. Additionally, for the aircraft designs no real optimization has been used, which means that the L/D-ratios found likely have room for improvement by further modifying design parameters. Looking at the supersonic L/D-ratios found for reference studies listed in Table 3.1, the values are realistic.

Looking at the L/D-ratios for the subsonic reserve segments the larger aircraft again have the best performance. This is largely because of the higher aspect ratio which reduces the lift-induced drag. Compared to the subsonic L/D-ratios of other studies in Table 3.1, the values are quite high although some studies like the NASA M2.4, and 1080-874 also feature subsonic cruise lift-to-drag ratios of 13.2 to 17.6. Still, compared to subsonic aircraft which can achieve lift-to-drag ratios of 20 and higher, the supersonic aircraft offer a worse subsonic performance. Note also that the loiter L/D is often worse than the contingency and diversion L/D. This is the result of the lower speed, and increased operating lift coefficient, meaning that the lift-induced drag contribution becomes more important. Similarly, for the final reserve, the lower altitude and higher air density allow for a lower lift coefficient than the loiter phase. Consequently, the L/D-ratios are better.

The second key item of the aerodynamics module was the low-speed maximum lift performance. For all five aircraft, it was decided to make use of fowler flaps at the trailing edge so that the amount of complexity

and weight is limited. There are still options to further improve performance by using double slotted flaps, but it was found to not result in improvements to the overall design. To further limit complexity no leading edge high-lift systems are included, because their lift contribution is small as was shown in Section 5.2.3. It could be that more detailed aerodynamic analysis shows that leading edge devices are beneficial, especially in combination with trailing edge devices, as was found in [44]. However, the level of detail achieved in the current study does not allow for evaluating this. Note also that compared to subsonic aircraft which can easily reach values of 2-3 [13, 60], the maximum lift coefficient values of the SSTs are low.

For the five designs, the maximum lift coefficients at takeoff and landing are all quite closely grouped with the maximum difference being less than 0.2. The two largest aircraft have the highest $C_{L,max}$ values largely because of their higher aspect ratio. This allows for a slightly larger part of the wing to be flapped, increasing the potential lift increase. Additionally, for a higher aspect ratio the Polhamus method returns a higher clean wing lift coefficient. The drop in maximum lift between the SSBJ and SST50 can be explained by the larger number of engines. Since the region behind the engines is not flapped, a smaller part of the wing is affected by the trailing edge devices, which reduces the lift increment.

7.4.3. Propulsion system

A second key system for the Class I analysis is the propulsion system, for which the specific fuel consumption (SFC) values are estimated. Some of the engine performance parameters are summarized in Table 7.7.

Table 7.7: Main supersonic aircraft propulsion system performance

Parameter	Unit	Aircraft				
		SSBJ	SST50	SST100	SST170	SST250
BPR	-	2.5	3.0	3.0	3.0	3.0
$T_{eng,TO}$	kN	113.3	59.0	96.5	148.6	226.7
$\dot{m}_{f,TO}$	kg/s	1.815	0.878	1.436	2.211	3.373
$\dot{m}_{f,TO}/T_{eng,TO}$	kg/(s.kN)	0.0160	0.0149	0.0149	0.0149	0.0149
SFC_{sup}	lb/(lbf.hr)	1.001	1.002	1.011	1.005	1.002
SFC_{cont}	lb/(lbf.hr)	0.787	0.784	0.790	0.786	0.784
SFC_{div}	lb/(lbf.hr)	0.787	0.782	0.788	0.784	0.782
SFC_{loit}	lb/(lbf.hr)	0.864	0.860	0.867	0.862	0.861
SFC_{final}	lb/(lbf.hr)	0.879	0.876	0.882	0.878	0.876
Fuel tank margin	m^3	+0.1	+2.0	+15.5	+44.7	+132.5

As was already mentioned earlier, the engines for the SST50 and SST100 are less powerful than for the SSBJ because of their lower thrust loading and the thrust being produced by four engines. This is also reflected in the engine takeoff fuel flows, which are greater for the more powerful engines. When dividing the takeoff fuel flow by the engine thrust an interesting finding is made, namely that the ratio is the same for the four SSTs. This is because in the current method used for the takeoff engine sizing, the takeoff fuel flow is linearly dependent on the required takeoff thrust. The dependency is the same for the four aircraft, because engine parameters like bypass ratio, OPR and the engine component efficiency values are the same. This finding will also be used during discussion of the LTO cycle results in Section 9.1. The reason the SSBJ engine deviates is that it has a lower bypass ratio.

The second key contribution of the propulsion system is the determination of the specific fuel consumption values for the segments of the Class I mission. Looking at the SFC values, it can be seen that all engines have a similar performance with deviations of no more than a few percent. The reason the contingency and diversion SFCs are very similar for the aircraft, is that the engine parameters and flight conditions (speed, altitude) are the same. The only parameter which varies is the required thrust, and therefore engine air flow, but this variation is not very large and only has a small impact on the overall performance. Since the subsonic SFC values are similar, the supersonic values are similar as well because they are simply the subsonic SFCs scaled by a factor 1.24. The same also holds for the loiter and final reserve SFC values which are scaled values of the diversion segment SFC.

When comparing the specific fuel consumption values to other studies in Table 3.1, the results fall in the expected range, and are not excessively high or low. More information about the engine design routine and validation of the model through test cases can be found in [7].

7.5. SST design sensitivity

While the previous section elaborated on the five supersonic aircraft designs, it is also interesting to briefly look at the sensitivity of the designs to several top-level requirement. Two important requirements are the design range and the supersonic cruise Mach number, which are discussed in Sections 7.5.1 and 7.5.2, respectively. Additionally, for the SST50 the decision was made to use a four-engine configuration and not a two-engine configuration. In Section 7.5.3 this decision is supported with several design program results. Note that this discussion will be limited and that further sensitivity analyses for the full design program can be found in [7].

7.5.1. Effect of design range

The design range used for the aircraft has a large impact on the fuel fraction method applied in the Class I module. A larger range will, if all other performance parameters (e.g. L/D, SFC) remain unchanged, result in an increase of the mission fuel fraction through the Breguet range equation. This larger fuel fraction will in turn result in an increase of the aircraft takeoff weight. To show the effect of the range on the supersonic aircraft designs, the design range was varied from 3,000 NM to 5,400 NM for the five aircraft designs, and the result is visualized in Figure 7.4.

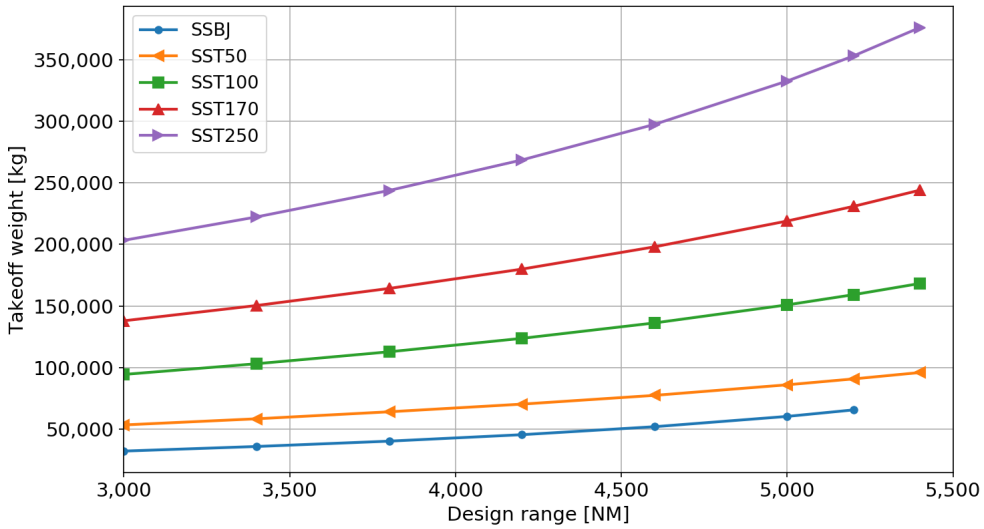

Figure 7.4: SST takeoff weight as function of design range

Looking at the graph, it can be seen that for all aircraft, the takeoff weight increases with a higher design range. Note that for the SSBJ the design range of 5,400 NM was not feasible because the fuel fraction became so large that the payload fraction became negative. This will become more clear a little later. Additionally, the curves all seem to follow an exponential trend, and the resulting fits are listed in Table 7.8.

Table 7.8: Exponential fits for takeoff weight as function of range R with absolute weight in second column and weight ratio in third column

Aircraft	Regular weight (Figure 7.4)	Normalized weight (Figure 7.5)	R^2
SSBJ	$W_{TO} = 11,908 \cdot e^{0.000323 \cdot R}$	$W_{TO,R}/W_{TO,3000NM} = 0.3712 \cdot e^{0.000323 \cdot R}$	0.9957
SST50	$W_{TO} = 25,400 \cdot e^{0.000244 \cdot R}$	$W_{TO,R}/W_{TO,3000NM} = 0.4763 \cdot e^{0.000244 \cdot R}$	0.9957
SSST100	$W_{TO} = 45,411 \cdot e^{0.000241 \cdot R}$	$W_{TO,R}/W_{TO,3000NM} = 0.4813 \cdot e^{0.000241 \cdot R}$	0.9957
SST170	$W_{TO} = 66,993 \cdot e^{0.000237 \cdot R}$	$W_{TO,R}/W_{TO,3000NM} = 0.4857 \cdot e^{0.000237 \cdot R}$	0.9957
SST250	$W_{TO} = 93,017 \cdot e^{0.000323 \cdot R}$	$W_{TO,R}/W_{TO,3000NM} = 0.4575 \cdot e^{0.000256 \cdot R}$	0.9957

These show that the weight indeed increases exponentially, which is expected since the Breguet range equation used in the Class I analysis also varies exponentially with range. However, the graph is just showing the absolute weight change, making it difficult to compare the different aircraft designs. For this reason, in Figure 7.5 the takeoff weight for all design ranges is divided by the takeoff weight at a design range of 3,000 NM.

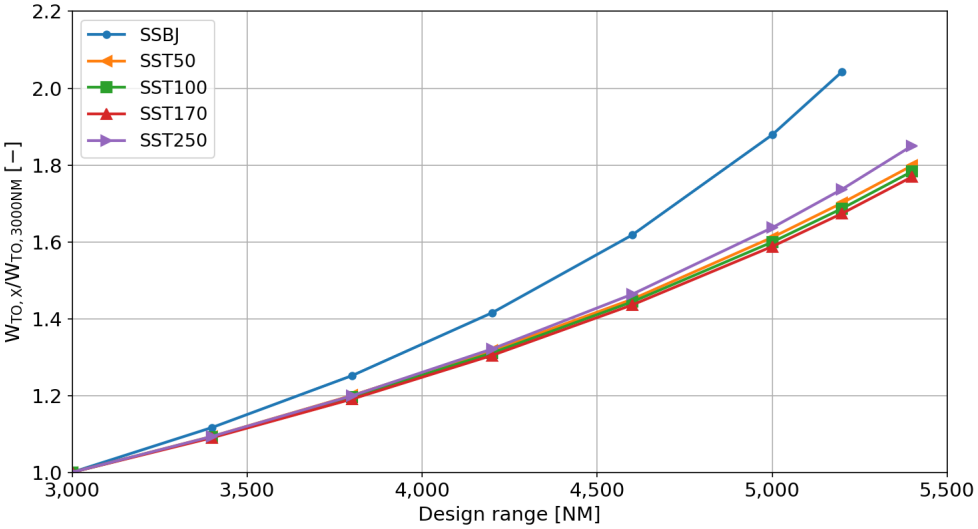

Figure 7.5: Normalized SST takeoff weight change as function of design range

With this set of graphs and the curve fits, it is clear that the SSBJ design is by far the most sensitive aircraft design to changes in design range. This can be explained in part by the lower supersonic L/D-ratio found earlier in Section 7.4.2, which means that an increase in range has a larger impact on the fuel fraction of the Breguet range equation. To visualize this, the fuel mission fuel fractions are plotted in Figure 7.6. Of the other four designs, the SST250 shows the largest relative increase in takeoff weight, although the difference is small compared to the remaining three designs. In particular for the lower design ranges of less than 4,600 NM, the four SSTs all have a similar takeoff weight increase.

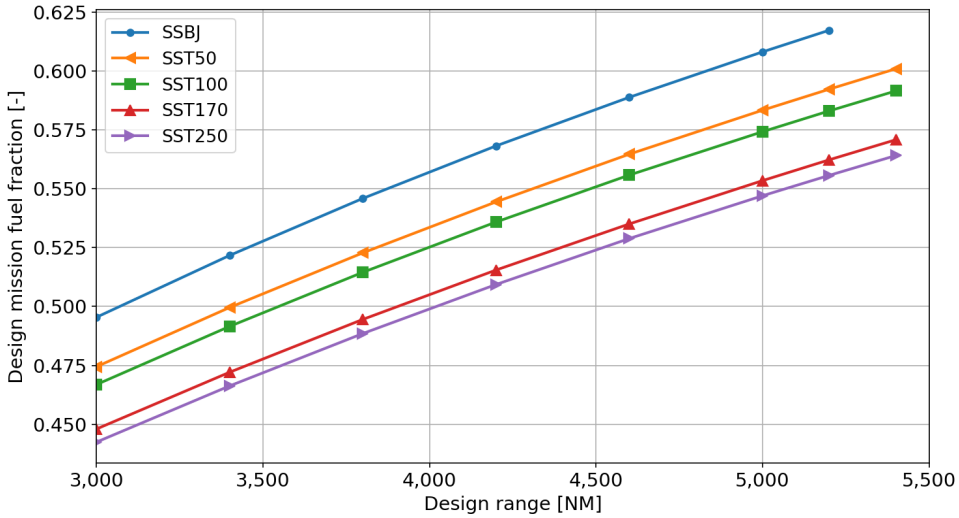

Figure 7.6: Design fuel fraction as function of design range

The fuel fraction graph shows that the larger aircraft have a lower fuel fraction for the same design mission. Again, this is primarily related to the better supersonic L/D-ratio, given that the specific fuel consumption values are similar for the different aircraft. Note also that the graphs are all slowly leveling out, which is because the relative increase in range and therefore the change in the supersonic segment fuel fraction decreases as the design range is increased further. Note also that for the SSBJ the fuel fraction for 5,200 NM is over 0.61, which with an operating empty weight fraction of about 0.37-0.38 leaves only a small payload fraction. For 5,400 NM there would be no payload fraction remaining, making the mission impossible. Additionally, the low payload fraction shows why the takeoff weight is increasing more rapidly for the SSBJ.

7.5.2. Effect of Mach number

Like the design range, the supersonic Mach number also has a large effect on the overall aircraft design. To investigate the effect of the Mach number, the mission definitions for the five supersonic aircraft designs

(Table 7.4) were used, but modifications were made to several inputs. First of all, the Mach number was varied from 1.4 to 2.0 in steps of 0.2. Second, the supersonic cruise altitudes were reduced by 750 meter for Mach 1.4, and increased by 750 meter and 1,500 meters for Mach 1.8 and 2.0, respectively. Third, the engine overall pressure ratios which could be achieved were altered because the change in Mach number also affects the total temperature in the inlet. The OPR will then have to be reduced for increasing Mach number to ensure that the total temperature behind the compressor is not too high. More information about this is provided in [7]. To account for this, the engine OPR is 40 for Mach 1.4, 27.5 for Mach 1.8 and 20 for Mach 2.0. The last modification is that for Mach 2.0, the subsonic leading edge fraction is not maximized but set to 0.8. This ensures that the leading edge sweep angles are less excessive and therefore more realistic.

The change in takeoff weight for a change in Mach number using the modified inputs described above, was then normalized by dividing it by the weight corresponding to the reference situation at Mach 1.6. The result is shown in Figure 7.7 for the five aircraft designs.

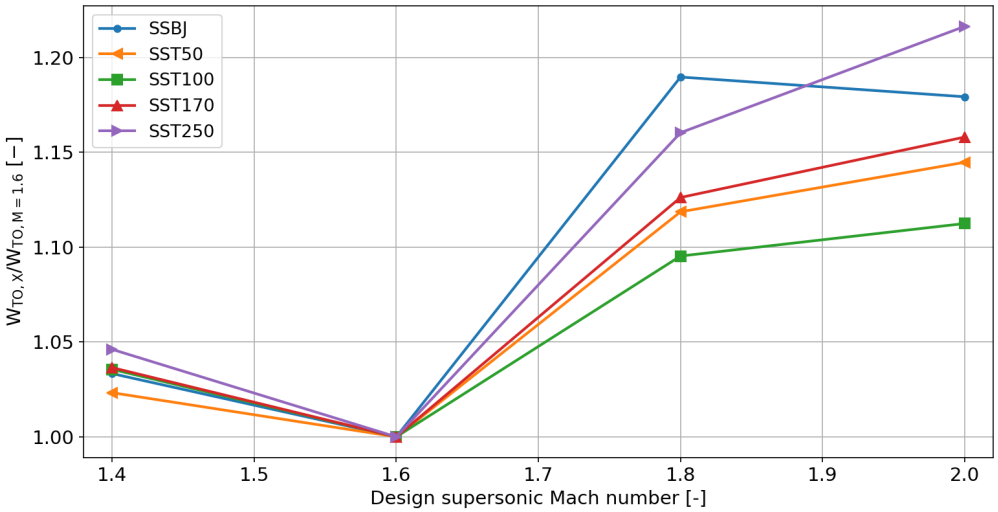

Figure 7.7: Normalized SST takeoff weight change as function of supersonic Mach number

Looking at the graph, it can be seen that the takeoff weight for Mach 1.4 is about 2.5 to 5% larger than that at Mach 1.6. Meanwhile, for an increase in Mach number to 1.8 and 2.0, the takeoff weight also increases, but by a much larger amount. From Mach 1.8 to 2.0 all aircraft weights increase, except for the SSBJ. To try to explain the takeoff weight changes, the fuel fraction for the design missions were calculated and plotted against the Mach number as shown in Figure 7.8.

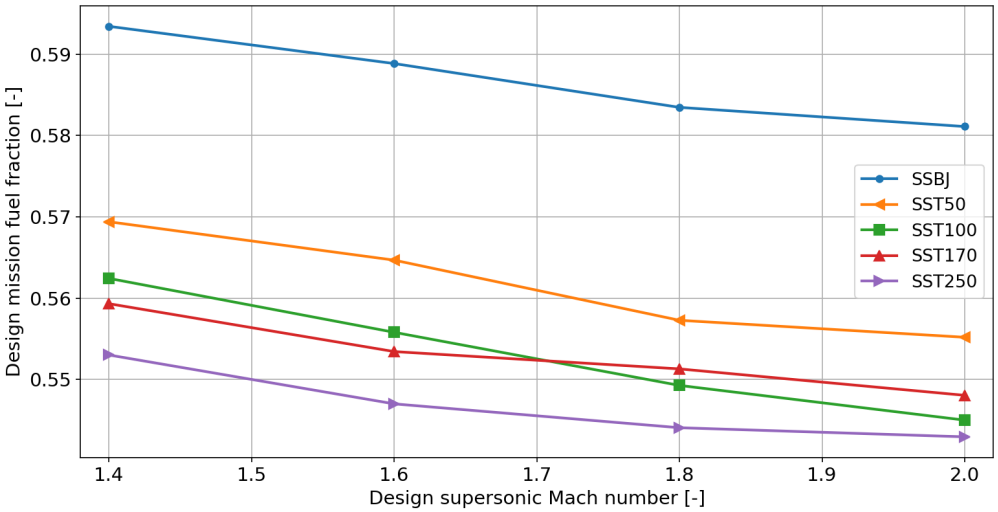

Figure 7.8: Design fuel fraction as function of supersonic Mach number

The graph shows that for an increase in Mach number, the fuel fraction decreases for all aircraft designs, which seems to contradict the increase in takeoff weight found previously for Mach 1.8 and 2.0, but does explain the increase in weight found for Mach 1.4. The reason for the takeoff weight increase for Mach 1.8 and 2.0 is that the operating empty weight increases more strongly. This is because the wing shape and weight changes, and also because the weight of several OEW components increase with the (maximum) Mach number (see Appendix D.1). A visualization of this is produced in Figure 7.9 where the operating empty weight fraction, and design fuel fraction are summed. The graph shows clearly that there is a minimum at Mach 1.6, and because of the way the Class I method calculates the takeoff weight (Equation (3.2)), the weight is the lowest at that speed. The remaining fraction represents the payload fraction, and it can be seen that for the SSBJ it is always the lowest.

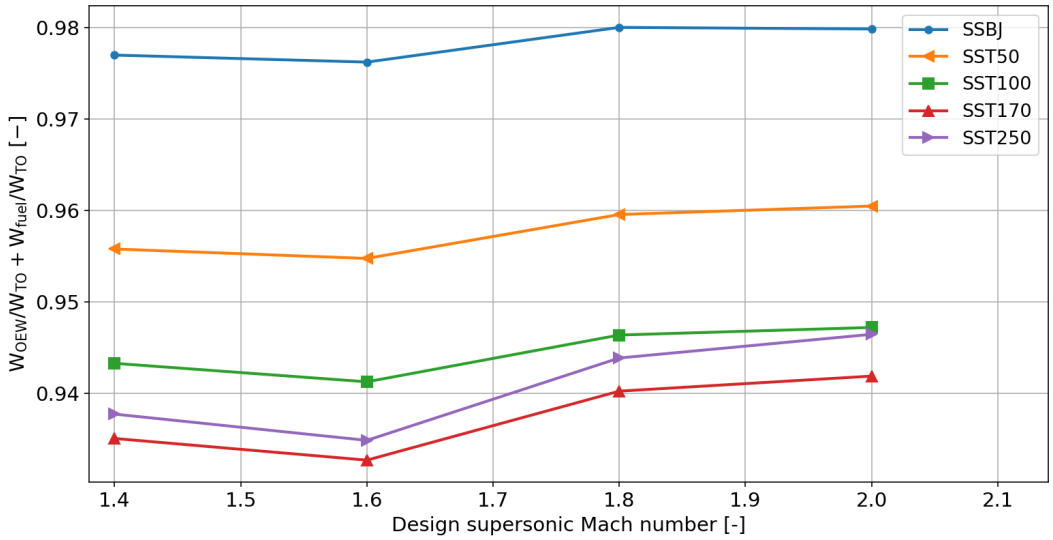

Figure 7.9: Sum of operating empty and fuel fractions as function of supersonic Mach number

As a last step it is interesting to show why the mission fuel fraction decreases. Several performance parameters which are used in the Breguet equations for the SST100 and SST250 aircraft are listed in Table 7.9. Note that only the SST100 and SST250 are included, but that the behavior of the other three aircraft is very similar.

Table 7.9: Breguet equation information for SST100 and SST250 as function of Mach number

Parameter	Unit	Aircraft							
		SST100				SST250			
Mach	-	1.4	1.6	1.8	2.0	1.4	1.6	1.8	2.0
L/D_{sup}	-	8.543	7.912	7.551	7.348	9.403	8.699	8.193	7.882
SFC_{sup}	1/hr	0.989	1.011	1.047	1.096	0.980	1.002	1.038	1.088
V_{sup}	m/s	413.1	472.1	531.1	590.1	413.1	472.1	531.1	590.1
R_{sup}	km	7,917	7,785	7,654	7,523	8,672	8,541	8,410	8,278
Breguet fraction	-	0.540	0.557	0.574	0.590	0.545	0.561	0.573	0.584
Change	*%*	*-3.05*	-	*+3.07*	*+5.88*	*-2.85*	-	*+2.18*	*+4.01*
L/D_{cont}	-	13.04	13.10	13.46	13.87	14.52	14.59	14.95	15.37
SFC_{cont}	1/hr	0.771	0.790	0.821	0.863	0.765	0.784	0.815	0.857
V_{cont}	m/s	280.3	280.3	280.3	280.3	280.3	280.3	280.3	280.3
R_{cont}	km	514.7	514.7	514.7	514.7	514.7	514.7	514.7	514.7
Breguet fraction	-	0.9703	0.9697	0.9694	0.9688	0.9735	0.9730	0.9726	0.9720
Change	*%*	*+0.06*	-	*-0.04*	*-0.10*	*+0.05*	-	*-0.04*	*-0.10*

Starting with the middle block of the table, which represents the supersonic cruise segment, it can be seen for both aircraft that the L/D-ratio decreases with increasing Mach number, and that the specific fuel consumption increases. However, the cruise speed also increases and because of the method used to estimate the climb and descent distance (see Appendix B.1), a higher Mach number means that there is a larger climb

and descent distance. Consequently, the supersonic cruise distance decreases. When these factors are combined into the Breguet range equation the result is that the fuel fraction increases with Mach number. If all other segments remain the same this would cause a decrease of the mission fuel fraction, and would lead to a reduction in the takeoff weight. It shows that the speed benefit from higher Mach numbers outweighs the reduction in aerodynamic efficiency and increase of the specific fuel consumption.

For the subsonic reserve segments the same is done with the contingency L/D-ratio and specific fuel consumption. Note that the L/D-ratio improves with Mach because with the larger takeoff weight, and therefore larger wing area, the aircraft will operate at a lower lift coefficient during the subsonic cruise. Consequently, the lift induced drag is less, and L/D improves. The contingency speed (Mach 0.95) and distance are the same for all scenarios. By then using the Breguet range equation again, it can be seen that the relative change of the fuel fraction is at most 0.1%, which is a much less than the change found for the supersonic cruise segment. However, for the subsonic segments the higher Mach numbers will result in a slightly lower fuel fraction, which means that more fuel would be burnt if the segment starting weight is unchanged.

For the other subsonic reserve segments, similar changes are found. All in all, the effect of the improved supersonic fuel fraction outweighs the small reduction of the subsonic segment fuel fractions, which explains why for higher supersonic Mach numbers the overall mission fuel fraction is smaller. Note that beyond Mach 2-2.1 no designs were produced because it was found during the program validation that the design program does not work properly beyond that range.

7.5.3. Two vs Four engine SST50

As was indicated in Section 7.4, during the selection of the inputs for the SST50 aircraft, the four-engine configuration was chosen over the two-engine configuration because it resulted in a design with a lower takeoff weight. However, it is still interesting to show what the impact is of the change in engine count. For this reason, Figure 7.10 shows the takeoff weight variation of the two designs against design range.

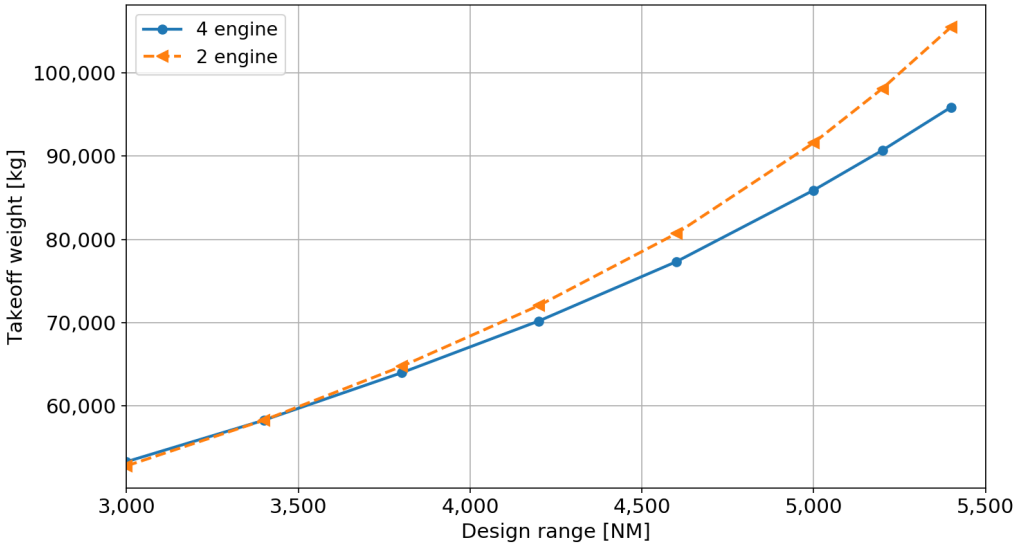

Figure 7.10: SST50 takeoff weight as function of design range for two- and four-engine configuration

The figure clearly shows that for low design ranges of up to about 4,200 NM, the difference between a two- and four-engine configuration is quite small, with the takeoff weight deviating by at most a few percent. For a design range of 3,000 NM the four-engine configuration is slightly better with a 0.9% lower takeoff weight. For larger ranges, the four-engine configuration is superior. This can also be seen in the two exponential fits listed below, where it should be noted that the four-engine configuration fit is the same as that listed in Table 7.8.

Table 7.10: Exponential fits for takeoff weight as function of supersonic Mach number for two- and four-engine configuration SST50

SST50 configuration	Takeoff weight	R^2
2-engine configuration	$W_{TO} = 21,933 \cdot e^{0.000287 \cdot R}$	0.9967
4-engine configuration	$W_{TO} = 25,400 \cdot e^{0.000244 \cdot R}$	0.9988

Looking at the exponential fits, the exponential growth for the two-engine configuration is larger, which confirms that it is more sensitive to an increase in design range. In order to better explain the takeoff weight trend several design parameters were selected and extracted for both designs at four design ranges. These are shown in Table 7.11 with the data for the four-engine configuration printed in italic. Note that the delta (Δ) values are in percent (%).

Table 7.11: Main supersonic aircraft performance comparison for two- and four-engine SST50 (note Δ in %)

Range		3,000 NM			3,800 NM			4,600 NM			5,400 NM		
Attribute	Unit	2eng	4eng	Δ	2eng	4eng	Δ	2eng	4eng	Δ	2eng	4eng	Δ
MTOW	kg	52,822	*53,322*	+0.9	64,757	*63,993*	-1.2	80,715	*77,335*	-4.2	105,521	*95,897*	-9.1
OEW	kg	24,535	*24,526*	0.0	27,796	*27,039*	-2.7	32,181	*30,166*	-6.3	39,389	*34,771*	-11.7
FF	-	0.469	*0.474*	+1.1	0.517	*0.523*	+1.2	0.558	*0.565*	+1.3	0.594	*0.601*	+1.2
L/D_{sup}	-	8.092	*8.236*	+1.8	8.391	*8.516*	+1.5	8.666	*8.773*	+1.2	8.940	*9.023*	+0.9
L/D_{cont}	-	11.99	*12.33*	+2.8	12.24	*12.59*	+2.9	12.39	*12.75*	+2.9	12.47	*12.86*	+3.1
SFC_{sup}	lb/(lbf.hr)	0.983	*1.022*	+4.0	0.973	*1.011*	+3.9	0.965	*1.002*	+3.8	0.959	*0.995*	+3.8
SFC_{cont}	lb/(lbf.hr)	0.780	*0.807*	+3.5	0.769	*0.794*	+3.3	0.761	*0.784*	+3.0	0.755	*0.775*	+2.6
T/W	-	0.427	*0.311*	-27.2	0.433	*0.311*	-28.2	0.438	*0.311*	-29.0	0.442	*0.311*	-29.6
$T_{eng,TO}$	kN	110.5	*40.7*	-63.2	137.4	*48.8*	-64.5	173.3	*59.0*	-66.0	228.9	*73.3*	-68.0
W_{eng}	kg	2,137	*1,006*	-52.9	2,573	*1,138*	-55.8	3,155	*1,303*	-58.7	4,055	*1,534*	-62.2
$W_{engines}$	kg	4,275	*4,026*	-5.8	5,147	*4,553*	-11.5	6,310	*5,212*	-17.4	8,110	*6,134*	-24.4

Looking at the first rows of the table shows that the takeoff weight for the four-engine configuration is 0.9% larger for 3,000 NM and 9.1% lower for 5,400 NM. Similarly, it can be seen that the operating empty weight is also lower for the four-engine configuration as the design range is increased. Since the change in operating empty weight is greater than the change in takeoff weight, the two-engine configuration has a higher operating empty weight ratio. Looking at the fuel fraction FF, the four-engine configuration has a fraction which on average is about 1.2% higher. This fuel fraction difference explains why for 3,000 NM the two-engine configuration is lighter than the four-engine configuration given that their operating empty weights are almost the same. However, for the larger design ranges, the increased operating empty weight (ratio) of the two-engine configuration has a larger effect than its lower fuel fraction, which is why its takeoff weight increases compared to the four-engine configuration.

The difference in the fuel fractions is investigated by extracting the supersonic and subsonic contingency L/D-ratios and specific fuel consumption values. This shows that for the two-engine configuration, the specific fuel consumption is about 3-4% lower, and the lift-to-drag ratios about 1-3% higher. The values for the other subsonic segments show similar differences, and are not included in the table. Given that the segment fuel fractions are calculated by using the Breguet equations, the higher specific fuel consumption and lower L/D-ratio partially cancel each other out. However, the difference in SFC is larger, which results in the mission fuel fraction being lower for the two-engine configuration.

For the difference in operating empty weight, the main focus is on the engine weight. Because of the use of two engines, the thrust loading is higher, which means that the total thrust is also higher. Additionally, for the four-engine configuration, the smaller total thrust is divided by four engines, while for the two-engine configuration, a larger thrust is distributed over two engines. As a result of this, the thrust of an engine in the four-engine configuration is about 65% lower on average. Since the dry engine weight is estimated by using a fit against engine thrust (Equation (4.3)), the weight of an engine for the four-engine configuration is between 53 and 62% lower. However, the four-engine configuration also features twice as many engines, which partially offsets this weight reduction. Still, the total engine dry weight for the four-engine configuration is 5.8% (at 3,000 NM) to 24.4% (at 5,400 NM) lower than for the two-engine configuration. For 5,400 NM this difference represents about 2,000 kg which is substantial. For the two-engine configuration this increase in weight introduces a further takeoff weight increase through the snowball effect. Additionally, some other component weights in the Class II analysis will also increase when the engine weight and thrust increase. Together, this results in the found operating empty weight increase of the two-engine configuration compared to the four-engine configuration.

This concludes the discussion of the performance and sensitivity of the expected supersonic aircraft designs which were created by using the validated aircraft design program. The results generated will also be used for the climate analyses in Chapter 9, and to make recommendations for future expansions as discussed in Chapter 11.

8 Emissions and Climate Effects

This chapter focuses on the methodology to evaluate some of the potential climate effects of new supersonic transport aircraft, in particular the designs shown in the previous chapter. To this end, Section 8.1 defines the regulatory system currently in place for aircraft emissions, as well as the methods used to check the compliance to the regulations. It will also describe the method applied to estimate the global temperature change, for which currently no regulations exist. Having discussed the methods, the second step is to define the scenarios which will be used to evaluate the performance of the supersonic aircraft. This is done in Section 8.2, and then used in the following chapter to evaluate the performance of the aircraft designs. It should be noted that only a small part of the aircraft related climate effects are studied in this report.

8.1. Emissions regulations and methodology

The main emissions regulations for aviation can be split into two groups, the first is that for the landing and takeoff (LTO) cycle and the second is that for CO_2. The regulations and methods used to evaluate the performance are discussed in Sections 8.1.1 and 8.1.2, respectively. For the global impact no regulations exist at this time, and the method used is explained in Section 8.1.3.

8.1.1. LTO cycle

The current LTO emissions regulations for supersonic aircraft engines can be found in chapter 3 of Volume II of ICAO Annex 16 [87]. They have to be applied to all engines designed for supersonic speed which were manufactured after the 17th of February 1982, and it defines regulatory limits for the following species:

- Smoke (number)
- Carbon monoxide (CO)
- Unburned hydrocarbons (UHC or HC)
- Nitrogen oxides (NO_x)

These species are the same as those used for subsonic aircraft, although the regulatory emission levels are different. The maximum emission levels set for supersonic aircraft have been unchanged since the 1980s and are likely no longer representative, especially with the larger focus on the climate impact of aviation. Some more information about these species can be found in Appendix F.2.

The LTO cycle definition for supersonic aircraft is different from that of subsonic aircraft as can be seen in Table 8.1. The cycle is used to approximate the operations of an aircraft below 3,000 ft [88].

Table 8.1: LTO cycle definition for super- and subsonic aircraft [87]

	Supersonic		Subsonic	
Operating mode	Thrust setting [% T_{TO}]	Time [min]	Thrust setting [% T_{TO}]	Time [min]
Take-off	100[1]	1.2	100	0.7
Climb	65[1]	2.0	85	2.2
Descent	15[1]	1.2	-	-
Approach	34[1]	2.3	30	4.0
Taxi/ground idle	5.8[2]	26.0	7	26.0

[1] with afterburner engaged if available
[2] without afterburner

The comparison shows that the thrust settings and segment times vary considerably. Additionally, the supersonic LTO cycle features a descent phase which is not included in the subsonic definition. The difference can be due to changes in the definition of the LTO cycle between the 1980s and now, so it could be that the supersonic LTO cycle should simply be updated. Alternatively, it might also be due to the different climb and descent performance of past supersonic aircraft that the engine settings and segments are dissimilar.

In [89] an LTO cycle for a Boeing 767 is modeled and compared to the reference data in terms of time, fuel burn and emissions (both index and absolute mass values). From that comparison it was found that for climbout, the actual time spent is about half of that in the LTO definition (1.25 min vs 2.2 min), while the emission indices were similar. Consequently, the actual emissions would be about half of that found when using the standard LTO definition. For the approach segment the time was found to be very similar (3.95 min vs 4.0 min), but the fuel burn and emission indices varied significantly, resulting in higher total emissions for that phase. The cause of this difference is the descent phase, which in the subsonic LTO cycle definition is partially included in the approach phase. During that phase, the aircraft operates at flight idle conditions, which is the least efficient operating mode, and explains the increased emission index values [89]. This provides an additional reason explaining the difference between the sub- and supersonic LTO cycle, where the latter still includes a descent phase at just 15% of takeoff thrust (i.e. flight idle).

It should also be noted that the supersonic LTO cycle has nearly the same duration as the subsonic cycle (0.2 minute shorter). This is because the taxi speeds and distances for both types are likely the same, and even though the supersonic aircraft will fly slightly faster during takeoff and approach, the takeoff run is longer, increasing the segment duration. Because in all literature about the (supersonic) emission evaluation, the subsonic LTO cycle is used, it will also form the basis in the following analyses. However, it will be interesting to look at the difference between the two cycles for some aircraft designs.

The regulations for the emission species are listed in Table 8.2, where the values all represent the ratio D_p/F_{oo} which is the characteristic mass of the emitted species 'p' (in grams) during the LTO cycle, divided by the takeoff thrust (in kN). Note that the smoke number is unitless (see Appendix F.2.6 for definition). Additionally, for the supersonic values the thrust F^* used is that with afterburners engaged (only if present). Note also that π_{oo} is the engine overall pressure ratio at takeoff.

Table 8.2: LTO regulations for subsonic engines produced after January 1 2014 and for supersonic engines [87]

	Subsonic			Supersonic
SN	lower of $83.6 \cdot F_{oo}^{-0.274}$ or 50			lower of $83.6 \cdot \left(F_{oo}^{*}\right)^{-0.274}$ or 50
HC	19.6			$140 \cdot 0.92^{\pi_{oo}}$
CO	118			$4550 \cdot \pi_{oo}^{-1.03}$
NO_x	$\pi_{oo} \leq 30$	$F_{oo} > 89.0kN$	$7.88 + 1.408 \cdot \pi_{oo}$	$36 + 2.42 \cdot \pi_{oo}$
		$26.7 < F_{oo} \leq 89.0kN$	$40.052 + 1.5681 \cdot \pi_{oo} - 0.3615 \cdot F_{oo} + -0.0018 \cdot \pi_{oo} \cdot F_{oo}$	
	$30 < \pi_{oo} < 104.7$	$F_{oo} > 89.0kN$	$-9.88 + 2.0 \cdot \pi_{oo}$	
		$26.7 < F_{oo} \leq 89.0kN$	$41.9435 + 1.505 \cdot \pi_{oo} + -0.5823 \cdot F_{oo} + 0.005562 \cdot \pi_{oo} \cdot F_{oo}$	
	$\pi_{oo} \geq 104.7$	$32 + 1.6 \cdot \pi_{oo}$		

To show the difference between the two sets of regulations, several engines were selected and their regulatory limits calculated using both the sub- and supersonic definitions. One engine is the Olympus 593 which represents the SSTs. The second is the CFM56-7B27 which is used on Boeing 737-aircraft, and its engine series forms the basis for the GE Affinity engine of the Aerion AS2. The third engine is the Honeywell HTF7700L as it was recently certified and is used by business jets. The values found are listed in Table 8.3.

The values in the table show that the smoke number difference is zero, as expected because the rules are the same. In terms of hydrocarbons there is a difference with the supersonic limit being more stringent for the non-SST engines. This has to do with the dependency of the supersonic HC regulations on the engine overall pressure ratio. Because the SST-engines on which the rules were based featured relatively low overall pressure ratios, especially compared to current engines, the rules are likely outdated. For the newer engines with higher OPR this results in relatively low HC-emission allowances.

Table 8.3: Comparison of engine LTO cycle regulatory limits when using the sub- and supersonic rules

Engine	Olympus 593			CFM56-7B27			HTF7700L (AS907-2-1S)[3]		
	OPR=15.5; F=139.4 kN			OPR=32.7; F=80 kN			OPR=28.2; F=33.36		
Species	Sub	Sup	Delta	Sub	Sup	Delta	Sub	Sup	Delta
SN	21.61	21.61	0%	25.16	25.16	0%	31.98	31.98	0%
HC	19.6	38.4	+96.1%	19.6	9.16	-53.3%	19.6	13.3	-32.0%
CO	118	270.4	+129.1%	118	125.3	+6.2%	118	146.0	+23.7%
NO_x	29.7	73.5	+147.5%	59.1	115.1	+94.7%	70.5	104.2	+47.8%

Looking at the carbon monoxide and nitrogen oxide limits, the supersonic limits are often much less stringent than the subsonic ones. This shows that the rules for supersonic engines are not in line with the performance that is expected from new subsonic aircraft, and substantiates the statement that the supersonic emission regulations should be updated. However, this can only be done once the supersonic engines reach a sufficient level of maturity, which is only expected to happen in the coming years. As it is likely that the rules will at least be the same as those for subsonic engines those will primarily be applied in the current analysis.

Now that the LTO cycle and regulations are defined, the last step is to show how the total emitted species masses for a full LTO cycle are calculated. For this, the following equation is used:

$$M_X = \sum_{segments} EI(X) \cdot \dot{m}_f \cdot \Delta t \tag{8.1}$$

where EI (X) is the emission index value for a specific segment as determined using one of the methods described in Appendix F.5. Also, the fuel flow $\dot{m}_f$ in kg/s for each segment has to be determined. Δt is the time in seconds spent in each segment (engine mode). The resulting masses are expressed in grams, but they cannot yet be used for the regulatory limit evaluation, because an additional correction has to be applied. The correction factor depends on the number of individual engines used in the certification test (of the same type). The larger this number, the more reliable the results and smaller the correction factor. The factors are shown in Figure 8.1 and the total masses are divided by them, after which the corrected mass is called the characteristic mass. Note that the factor also varies depending on the species type.

Number of engines tested (i)	CO	HC	NO_x	SN
1	0.814 7	0.649 3	0.862 7	0.776 9
2	0.877 7	0.768 5	0.909 4	0.852 7
3	0.924 6	0.857 2	0.944 1	0.909 1
4	0.934 7	0.876 4	0.951 6	0.921 3
5	0.941 6	0.889 4	0.956 7	0.929 6
6	0.946 7	0.899 0	0.960 5	0.935 8
7	0.950 6	0.906 5	0.963 4	0.940 5
8	0.953 8	0.912 6	0.965 8	0.944 4
9	0.956 5	0.917 6	0.967 7	0.947 6
10	0.958 7	0.921 8	0.969 4	0.950 2
more than 10	$\frac{1-0.130\,59}{\sqrt{i}}$	$\frac{1-0.247\,24}{\sqrt{i}}$	$\frac{1-0.096\,78}{\sqrt{i}}$	$\frac{1-0.157\,36}{\sqrt{i}}$

Figure 8.1: LTO cycle smoke number and gaseous emissions correction factors as function of number of engines tested [87]

These characteristic masses are then divided by the engine takeoff thrust, and compared to the regulatory limits to check whether the engine is sufficiently 'clean'. In order to verify the method several engines in the Emissions Databank were selected and analyzed to determine whether the values found matched those in the Databank[4]. The comparisons are shown in Appendix F.3. It was found that the method is correct since only very small deviations were found (order <0.5%), which are likely caused by round-off errors.

[3] https://janes.ihs.com/AeroEngines/Display/jae_0721-jae_ (accessed January 17 2019)

[4] ICAO Aircraft Engine Emissions Databank, https://www.easa.europa.eu/easa-and-you/environment/icao-aircraft-engine-emissions-databank (accessed January 30 2019)

Note that for the smoke number a different method is used for the measurements (see Appendix F.2.6), and that even though for most engines in the Emissions Databank, the smoke numbers for each LTO segment is listed, they are not used for the regulations. Instead, the maximum measured value is used, which in most cases is greater than the value found for any of the four LTO segments. As with the total emission quantities, this maximum smoke number is corrected to a characteristic value by a factor which depends on the number of engines tested. This value is then checked against the regulatory limit value.

8.1.2. CO_2 certification

A new set of environmental regulations for CO_2 has recently been finalized by the Committee on Aviation Environmental Protection (CAEP) and is being published by ICAO in Annex 16 Volume III [90]. It applies to subsonic aircraft with a maximum takeoff mass greater than 5,700 kg with type certification on or after 1 January 2020, although there is an exception for aircraft with MTOM under 60,000 kg and less than 20 passengers. For these aircraft the date of application is the first of January 2023. The metric used is the average of 1/SAR (specific air range) measured for three takeoff weights, and is corrected using the Reference Geometric Factor (RGF):

$$\text{CO}_2 \text{ emissions evaluation metric} = \frac{(1/\text{SAR})_{\text{avg}}}{\text{RGF}^{0.24}} \tag{8.2}$$

The specific air range is a common metric in the aviation industry used to measure cruise fuel burn and is often measured in units of km traveled per kg of fuel. The inverted value is selected so that a reduction in the CO_2 intensity would be reflected by a reduction of the metric score [91]. It is to be measured as follows [90]:

$$SAR = \frac{TAS}{W_f} \tag{8.3}$$

where TAS is the true airspeed in km/hr and W_f the total aircraft fuel flow in kg/hr. The three reference weights for which SAR needs to be calculated (or measured) are the following (note MTOM in kg):

- High gross weight: W = 92% of MTOM
- Mid gross weight: simple average of high and low gross weights
- Low gross weight: W = $(0.45 \cdot MTOM) + \left(0.63 \cdot MTOM^{0.924}\right)$

For new aircraft the SAR values have to be determined either by using full-scale flight tests, or by using a performance model approved by the certifying authority [90]. In the current situation no mention is made of supersonic aircraft but it is likely that they need to adhere to the same rules. The method used to evaluate the supersonic SAR is explained and tested in Appendix F.4.2.

The RGF correction was added because the SAR only uses cruise fuel consumption and is sensitive to the operating conditions (e.g. altitude). Consequently, certain aircraft types (business jets and long-range aircraft) would have disproportionately good scores compared to other aircraft operating at lower altitudes or those designed for larger payloads [91]. The RGF is defined as shown in Figure 8.2 and approximates the length of the pressurized fuselage section (excluding cockpit) times its maximum width. It is non-dimensionalized by dividing it by 1 m^2:

$$RGF \approx \frac{L_{cabin} \cdot w_{max,cabin}}{1m^2} \tag{8.4}$$

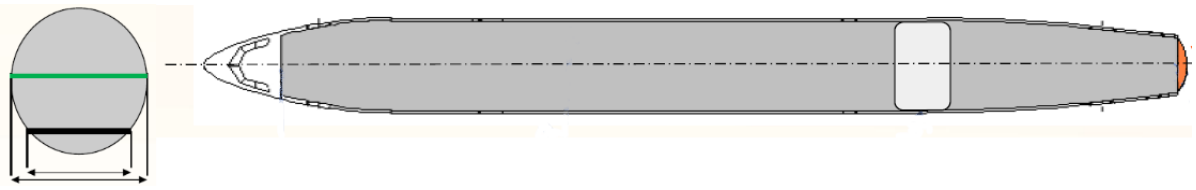

Figure 8.2: Example of RGF maximum width (green) and area between cockpit door and rear bulkhead taken from [5]

[5] Dickson, N. *Progress on the development of the ICAO CO_2 Standard*, https://www.icao.int/Meetings/Green/Documents/day%201pdf/session%203/3-Dickson.pdf (accessed January 22 2019)

Note that the width is not the width of the floor but the maximum width of the fuselage outer mold line (OML). Given that the fuselage used in the design program is a cylinder the width is similar to the diameter. Since the fuselage design module also places some of the galleys and lavatories in the tail section, the RGF uses a cabin length which is slightly longer than the cyclindrical section. The exponent 0.24 used for the RGF was developed by empirical comparisons between current business jets, turboprops, and turbofan aircraft [91]. The RGF values found by the program were tested with the results as described in Appendix F.4.1.

The resulting CO_2 evaluation metric is then representative for the performance of the aircraft and should be checked against the regulatory limit, which depends on takeoff weight. These regulatory limits are:

$$\text{For MTOM} \leq 60{,}000\text{ kg}: \quad 10^{\left[-2.73780+\left(0.681310\cdot\log_{10}(\text{MTOM})\right)+\left(-0.0277861\cdot\log_{10}(\text{MTOM})^2\right)\right]} \tag{8.5}$$

$$\text{For } 60{,}000 < \text{MTOM} \leq 70{,}395\text{ kg}: \quad 0.764 \tag{8.6}$$

$$\text{For MTOM} > 70{,}395\text{ kg}: \quad 10^{\left[-1.412742+\left(-0.020517\cdot\log_{10}(\text{MTOM})\right)+\left(0.0593831\cdot\log_{10}(\text{MTOM})^2\right)\right]} \tag{8.7}$$

The values are also visualized in Figure 8.3 as a function of the aircraft takeoff weight and clearly shows the kink at takeoff weights of 60,000 and 70,395 kg.

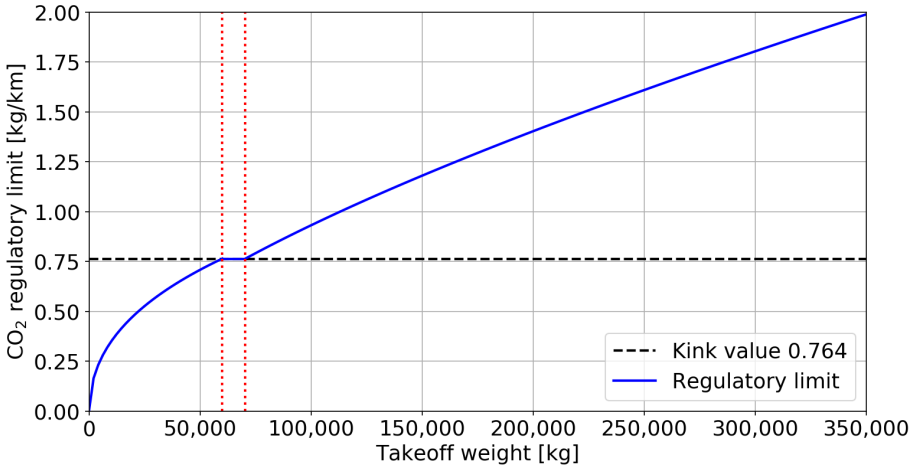

Figure 8.3: CO_2 regulatory limit variation with takeoff weight

If it is found that the aircraft CO_2 metric value is above the limit, then it does not meet the requirements. It should be noted that there are some issues with the new regulations which are listed in [91]. These include its failure to measure non-cruise fuel burn, which means that attempts to reduce fuel burn during taxiing, climb or descent are not included in the metric. Also, in most normal operations aircraft cannot operate at their optimum altitude consistently, which means that the points used for the SAR calculation are not entirely representative. Additionally, lightweight materials and new aircraft configurations (e.g. blended-wing-body) are not taken into account in the rules, but these can be adjusted in the future.

It should be noted that non-compliance to the regulations will result in the aircraft not being certified by the certifying body (e.g. EASA in Europe) in their jurisdiction area [92]. This can result in production of the aircraft being delayed or in the worst case it may no longer be financially viable. More information about the CO_2 certification process and testing of the regulations on several subsonic aircraft is provided in Appendix F.4. In a test performed on an aircraft similar to the Boom SST, the resulting exceedance of the regulatory limits (+63.2%) was found to be close to the most likely scenario (+67%) listed in [93]. This showed that the method is providing decent results although more supersonic test cases would be recommended when they become available in the future.

8.1.3. Global emission impact

For the global climate impact of supersonic aircraft there are various options, such as the use of large climate models, the linear AirClim model or less complex climate functions. As the first requires large computational effort and was complex, it was not selected. Similarly, the AirClim model which is described in Appendix F.7 is not used as it requires a detailed 3D emission distribution for the aircraft fleet, indicating where aircraft fly and what is emitted at each location. This is too complex given the limited resources available. The choice was therefore made to use the simpler climate functions described in [94]. These allow for determining the

global near surface temperature change caused by water vapor, ozone, methane and carbon dioxide for a fleet of aircraft, while only requiring information about the total fuel consumption, nitrogen oxide emission index, and cruise altitude. The model utilizes the results of the SCENIC analysis found using the AirClim model (see Appendix F.7), and some of the functions are normalized by using the SCENIC fleet reference values ($FC^{SCENIC} = 6.77 \cdot 10^{11}$ kg ; $EI(NO_x) = 10.84$ g/kg) [94].

$$\Delta T^{H_2O}(p_{cr}, FC) = \left[-626 \cdot \log_{10}(p_{cr}) + 1449\right] \cdot \frac{FC}{FC^{SCENIC}} \tag{8.8}$$

$$\Delta T^{O_3}(p_{cr}, FC, EI(NO_x)) = \left[-53.4492836 + \sqrt{68730.2188 \cdot \log_{10}(p_{cr}) - 11675.68}\right] \cdot \frac{FC \cdot EI(NO_x)}{FC^{SCENIC} \cdot EI\left(NO_x^{SCENIC}\right)} \tag{8.9}$$

$$\Delta T^{CH_4}(p_{cr}, FC, EI(NO_x)) = \left[-109.328255 \cdot \log_{10}(p_{cr}) \cdot \log_{10}(p_{cr}) + 462.227 \cdot \log_{10}(p_{cr}) - 504.7347\right] \cdot \frac{FC \cdot EI(NO_x)}{FC^{SCENIC} \cdot EI\left(NO_x^{SCENIC}\right)} \tag{8.10}$$

$$\Delta T^{CO_2}(FC) = 1.65 \cdot 10^{-10} \cdot FC \tag{8.11}$$

The total mean surface temperature change for 2050 is then found by adding the four contributions. It was found that the results are reasonably accurate and can be used for preliminary design of high flying supersonic aircraft [94]. From personal communications with one of the authors, it was concluded that the method could also be applied to subsonic aircraft. This means that it is possible to compare sub- and supersonic aircraft fleets in terms of their climate impacts. Note that in [94] the recommendation is given that higher-order climate-chemistry models should be used for several pre-optimized aircraft configurations. A similar procedure and results have been described in [95] with inclusion of a few more factors, but it was not created specifically for supersonic aircraft.

The temperature change functions were implemented in the design program, and to show that they have been implemented correctly a sensitivity analysis in [94] was used for comparison of the results. This comparison is shown in Figure 8.4.

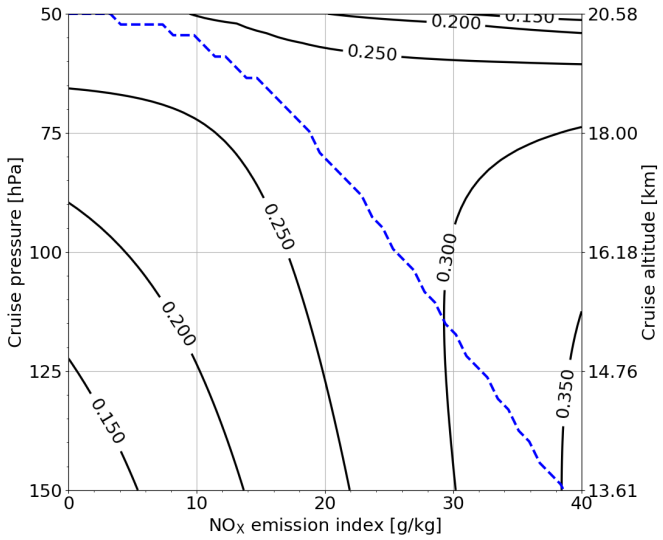

(a) Temperature change contour from program

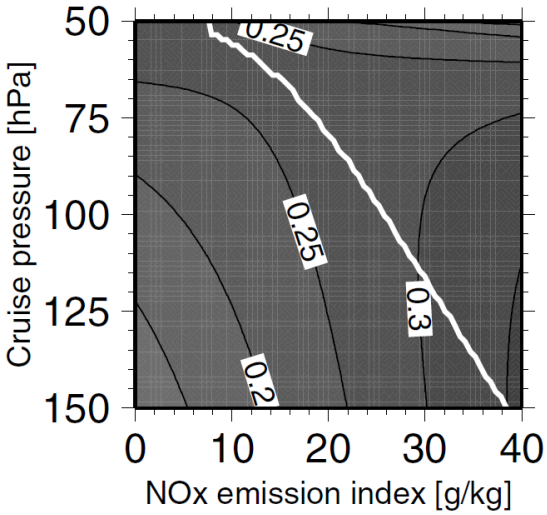

(b) Temperature change contour from reference [94]

Figure 8.4: Global near surface temperature change in mK contours for fuel consumption of 400 ktons showing sensitivity to cruise pressure and NO_x emission index. Blue dashed line (left) and white line (right) indicate turnaround point where increasing cruise altitude will result in lower total temperature change in exchange for ozone depletion.

Looking at the different contour lines, it can be seen that they match nicely, meaning that the temperature change equations are implemented properly. Additionally, the blue dashed (left) and white line (right) also match closely. They represent the altitude where the total temperature change is largest, and is also indi-

cated in Figure 8.5. By determining this maximum for each emission index (0-40 g/kg) and combining the corresponding pressure altitudes, the blue line is created. Only for emission indices of less than 7 g/kg there is some difference between the values found by the module and in the reference. This is likely the result of being close to the 50 hPa limit, but no definitive reason could be found. The accuracy shown indicates that the module is verified. Furthermore, since the climate functions have been validated in [94], it also means that the program provides valid results under the same assumptions/considerations as those used to create the functions.

These limitations and important considerations/assumptions are the following:

- The effects of contrails and contrail cirrus clouds on the temperature change are not included.
- The following distribution of the fleet over the world is assumed in terms of its operations and emission: 40% of emissions between 30°N-60°N and 20% for the other three regions (see Appendix F.7 for region definitions).
- The NO_x emission index used is the average value achieved during the (supersonic) cruise phase.
- The total fuel consumption (FC) is the total (supersonic) cruise fuel consumed by the entire fleet in 2050. It does not include the fuel burnt during the transonic acceleration, climb or descent.
- As indicated earlier, the minimum ambient pressure that can be used for the different equations is 50 hPa (≈20.58 km), as above that altitude, the methane function no longer works. Similarly, for the lower altitudes, it is assumed best to stay above 150 hPa (≈13.61 km) which is used as the lower limit in the sensitivity study in [94]. During the study of subsonic aircraft it was found that this lower limit is violated by most subsonic aircraft so it was decided to set a lower limit at 200 hPa (≈ 11.8 km) instead. This is deemed acceptable because the total temperature change curve shows a nearly linear variation from 200 to 150 hPa, but this should be kept in mind when looking at the results.
- The first aircraft enter service in 2015. This assumption is important because it is in the past. However, because the goal of the investigation is to compare similar sub- and supersonic fleets it is ignored in the current evaluation. For more detailed studies in the future, the scenarios should be such that the supersonic aircraft go into service in the period 2020-2025.

Now that the module is shown to be valid (within limitations), it is possible to look at the variations for each of the emitted species with altitude. To show the effect of altitude, the emissions data from the SCENIC model (emission index and fuel consumption) are used, which results in Figure 8.5.

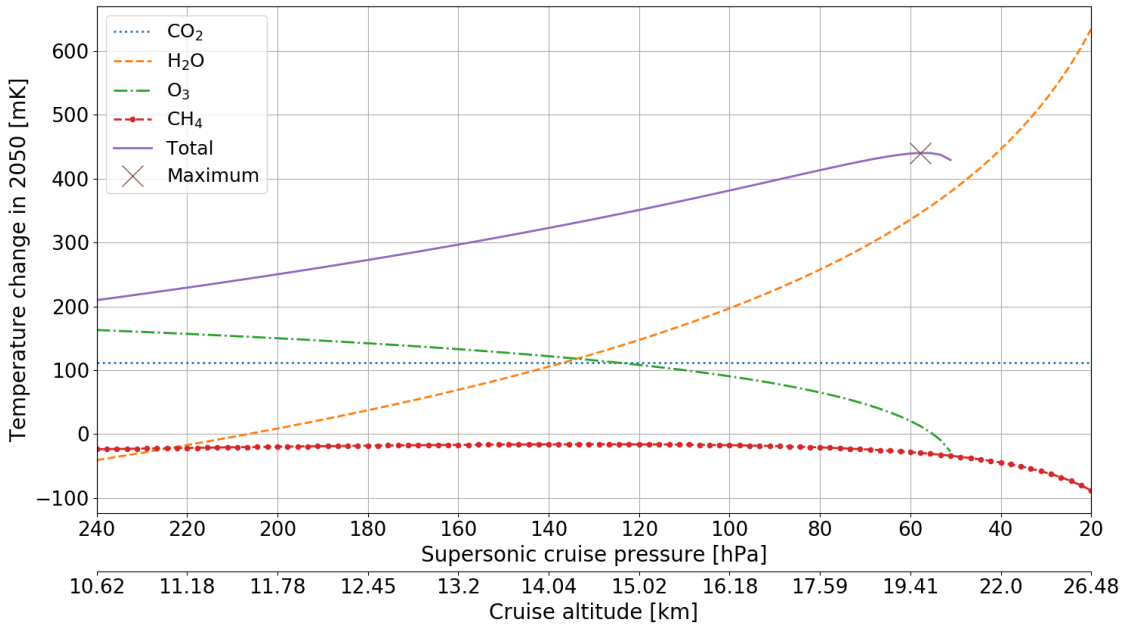

Figure 8.5: Temperature change per emitted species as function of cruise altitude using SCENIC inputs (note that cruise altitude axis is not linear)

The figure shows a number of things, the first is that the contribution of carbon dioxide is constant which also follows from the equation used. This is connected to the behavior of the species as it has a long lifetime of multiple decades (rule of thumb that roughly 50% is removed after 50 years). Consequently, it is well-mixed in the atmosphere over time, meaning that the location of the emission is less important. Second, the impact of water emissions increases drastically as altitude is increased (and pressure reduced). From past studies it was found that water vapor emissions are much more important for higher cruise altitudes because of the increased lifetime in the more stable lower stratosphere.

Methane contribution is negative as its breakdown of ozone is resulting in a net negative radiative forcing. As altitude increases, the temperature change becomes more negative which could be related to the increase in ozone concentration at higher altitudes in the lower stratosphere. This can improve the ozone destruction and consequently the cooling effect. Looking at the ozone contribution shows that the function works up to a pressure altitude of roughly 50 hPa, which was explained in the limitations/assumptions earlier, and that the contribution decreases with altitude.

As a last item the sensitivity of the temperature change estimation method to the three variables in the functions are discussed. First of all, the fuel consumption appears in all four equations as a multiplier, which means that the full system is linearly dependent on it. A doubling of the fuel consumption will also double the temperature change if the cruise altitude and NO_x emission index remain the same. The effect of altitude was shown in Figure 8.5 for the SCENIC inputs and explained earlier. This leaves the emission index value as the last factor. Since it affects only the ozone and methane contributions to the temperature change, it is not a fully linear dependency. In Figure 9.12 it is shown that for a higher emission index value of 18 g/kg, the total temperature curve flattens out more, because the contribution of ozone in particular, becomes much larger at low altitudes. The water vapor and CO_2 contributions do not change, and although the methane contribution becomes a bit more negative, it is small relative to the ozone contribution. A similar graph was also created with an NO_x emission index value of 5 and is shown below in Figure 8.6.

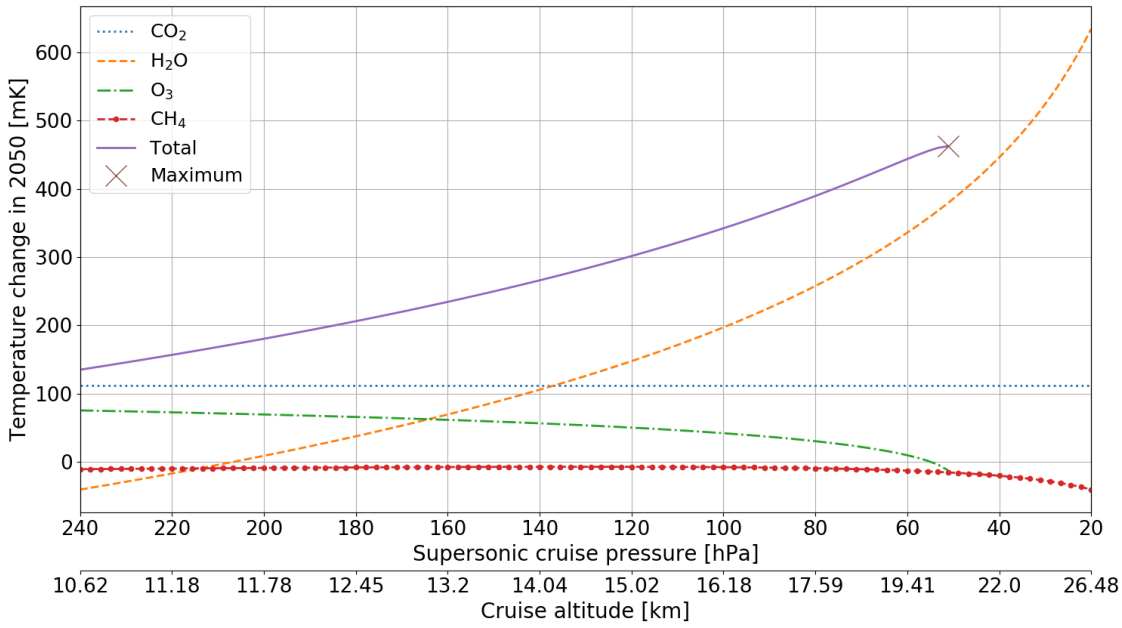

Figure 8.6: TTemperature change per emitted species as function of cruise altitude for SCENIC fuel consumption but with 5 g/kg NO_x emission index (note that cruise altitude axis is not linear)

It shows that compared to the 10 and 18 g/kg NO_x emission index scenario the ozone contribution is smallest, and that the curve is a bit more steep because increase in the contribution from water vapor is not compensated for by the decrease of the ozone temperature change contribution. More sensitivity analyses could be performed, but given the relatively low fidelity level of the method, it is decided that this will not really add much more useful information.

8.2. Scenarios

The last step remaining before the climate evaluation can be performed is to define the different scenarios to be analyzed. As shown in the methodology, several performance parameters have to be defined (and assumed) to evaluate the LTO and CO_2 regulations, as well as global climate impact.

8.2.1. LTO scenarios

For the LTO cycle analysis the values needed are the emission indices and smoke number values for the LTO segments, as well as fuel flow corresponding to those points. As was indicated in Section 4.2, the current engine off-design method does not allow for calculating the engine cycle parameters at low-thrust settings (i.e. approach and idle settings). This restricts the use of direct emission index estimation methods. Instead, the necessary values are estimated by making use of the method in Appendix F.5.4. Note however, that for the supersonic definition, the emission index values for the segments are different from those estimated using the fits. In that case the fuel flow methods are used to find the emission index values for the supersonic LTO segments.

To get an idea for the effect of the different options, the LTO cycle analysis will use all four engine series (CFM56, LEAP, CF6, GenX) as reference, together with the sub- and supersonic LTO cycle definition, and the sub- and supersonic LTO regulatory limits. Based on the findings made from looking at the engine database and other literature, it is expected that the CO, HC and SN limits will be met without many issues. The primary problem will likely be NO_x, but this will be investigated in Section 9.1.

8.2.2. CO_2 certification scenarios

For the CO_2 certification there is no real option to select scenarios given that the engine model does not allow for including the effects of changing mission parameters like cruise altitude, which makes sensitivity studies less accurate. In fact, the regulations themselves already include three scenarios, being the different takeoff weights.

Instead of scenarios, it will be interesting to look at the effect of several top-level requirements such as the design range and payload to see how it affects the margin by which the regulations are met or exceeded. This is particularly interesting since early results during the research and findings in [93] seem to indicate that supersonic aircraft are unable to meet the regulations by quite a margin (>50%). If that is found for all aircraft then it might be that the regulations have to be altered for supersonic aircraft.

8.2.3. Global emissions scenarios

As indicated in the global impact method, there are three key variables that can be adjusted, the fuel consumption, EI(NO_x) and cruise altitude. The cruise altitude used is that which is defined in the top-level requirements. The fuel consumption is the fuel burnt during the supersonic cruise phase which is calculated by the Class I analysis, and is dependent on the design top-level requirements and its performance. For the emission index estimation several methods were considered as explained in Appendix F.5. However, since the engine model does not allow for estimating the values of the internal temperatures and pressures, direct emission index estimation methods cannot be applied. Additionally, tests with the fuel flow methods showed that the emission indices found were too high due to a too high corrected fuel flow during cruise. The main reason for this high corrected fuel flow is the combination of the higher cruise altitude, and the supersonic Mach number. As a last option, it is possible to instead make assumptions for the emission index values.

It is decided to use three scenarios for the NO_x emission index, 5 g/kg (optimistic), 10 g/kg (realistic) and 18 g/kg (pessimistic). The pessimistic performance is selected such that it is similar to Concorde which had an index value of roughly 17-20 g/kg during supersonic cruise [96, 97]. From measurements of Concorde jet plumes a higher average emission index of 23.3 g/kg was found, but this measurement had a ±20% uncertainty [98], allowing for the 18 g/kg to fall within just over one deviation. The 10 g/kg is similar to the values found for the reference scenario of the global climate impact method, which was 10.84 g/kg for SCENIC [94, 99]. Additionally, it falls in the 9-11 g/kg estimate by MTU in [97] for future engines (15-20 years wrt 1993). The optimistic scenario of 5 g/kg is based on past studies and was found to be a theoretically possible value [100]. Additionally, in the SCENIC project a fleet with a Lean Premixed Prevaporized (LPP) combustor featured an emission index of 4.6 g/kg [99].

Aside from the supersonic scenarios, it is also interesting to include one or more subsonic aircraft scenarios such that it is possible to compare them. The subsonic aircraft data was produced by making use of

Piano-X[6]. For several aircraft a number of missions were selected in the range 3,500 NM to about 5,000 NM and then analyzed by using block mission analyses. From the results, the cruise emission index was then estimated by dividing the total cruise NO_x weight by the cruise fuel weight.

The subsonic aircraft cruise altitude was first determined by taking the median of the flight levels calculated by Piano-X for several missions. For most subsonic aircraft (excluding business jets), the median cruise altitude is less than 39,000 ft ($p_{cr} \approx 197$ hPa), which is quite far from the lower limit of 150 hPa recommended for the climate functions. Consequently, the results for these aircraft might not be as reliable as those for the Boeing 787-8, which has a higher cruise altitude of over 41,000 ft, and subsonic business jets. However, looking at an alternate tool (Master Emissions Calculator 2016[7]) which provides the most observed cruise flight level, the cruise altitudes are somewhat higher than those found by Piano-X. For example, for the Boeing 767-300 at 4,500 NM Piano-X gives an average cruise altitude of roughly 37,000 ft, while the other tool indicates that 40,000 ft is the most frequently observed cruise altitude. This difference can be because in real-life, the aircraft will be forced to operate at slightly higher altitudes due to traffic restrictions. Meanwhile, for some aircraft like the Boeing 787-8, the difference is only a couple hundred feet.

In the end, it was decided to increase the flight levels for several subsonic aircraft by several thousand feet to be more in line with the most frequently observed cruise altitudes. Similarly, for the subsonic business jets, the altitudes are reduced by several thousand feet as they are seen as too high values of about 48,000 ft, compared to the 44,000 ft common cruise altitude from the Master Emissions Calculator. The fuel consumption per flight is assumed to be equal to the cruise fuel quantity as calculated by Piano-X. As these values are averages, it can be that there is some error introduced, but for current study it is seen as acceptable given that many studies also use Piano-X as source for aircraft emission data.

The subsonic reference aircraft that have been included in the database so far for each of the categories are the following:

- *Business jets:* Gulfstream G550, Gulfstream G650 and Dassault Falcon 7X
- *Small subsonic transports (up to 150 pax):* Airbus A319neo and Airbus Corporate Jet, Boeing 737BJ
- *Medium subsonic transports (150-350 pax):* Boeing 787-8, 767-300ER/300ERW, 767-400, and Airbus A330-200, A340-642 and A350-800XWB
- *Large subsonic transports (350+ pax):* Airbus A380-800 and Boeing 777-300ER

It should be noted that in particular for the small subsonic transport category, no real reference aircraft exist which are capable of performing missions of over 3,500-4,000 NM unless the payload is reduced substantially. For the Airbus A319neo the maximum range with 95 passengers was about 4,200 NM and with 85 passengers it was 4,500 NM. These types of flights are unlikely to be operated in real life because the aircraft is not designed for such a mission, but would instead be replaced by the larger Airbus A330 or Boeing 787. Similarly, the Boeing 737BJ and Airbus Corporate Jet are modified versions of existing narrow-body aircraft and the results found for those aircraft are therefore not expected to be very reliable. In the design program, the user can select up to two aircraft to which the supersonic aircraft will be compared.

Based on the fleet definition explained in Appendix F.6, the subsonic fleets are set up such that they have nearly the same RPK as the supersonic fleet, making the comparison more realistic. This concludes the definition of the climate scenarios for the evaluation of the supersonic aircraft designs.

[6] http://www.lissys.demon.co.uk/PianoX.html (accessed April 10 2019)

[7] EEA, *1.A.3.a Aviation - Annex 5 - Master emission calculator 2016*, www.eea.europa.eu (accessed March 16 2019)

9 Results & Discussion

This chapter will show and discuss the main results found during the climate analyses as described in the previous chapter. The aircraft used for generating the results have already been described and discussed in Chapter 7. This chapter is split into three main areas, the LTO cycle, CO_2 certification and global climate impact. These are discussed in Sections 9.1 to 9.3. Some additional notes are presented in Section 9.4.

9.1. LTO cycle

Within the LTO cycle several scenarios were investigated by making use of four reference engine series to estimate the emission index values, as well as using the sub- and supersonic LTO cycle definition and regulatory limits. To visualize the effects of these variations the LTO cycle was analyzed using the four engine series, and the two LTO cycle definitions for the five supersonic aircraft designs. Using corrections the characteristic masses were then calculated and with the engine takeoff thrust, these were checked against both the sub- and supersonic regulatory limits. The results for NO_x emissions are shown in Figure 9.1 for the sub- (left) and supersonic (right) regulations.

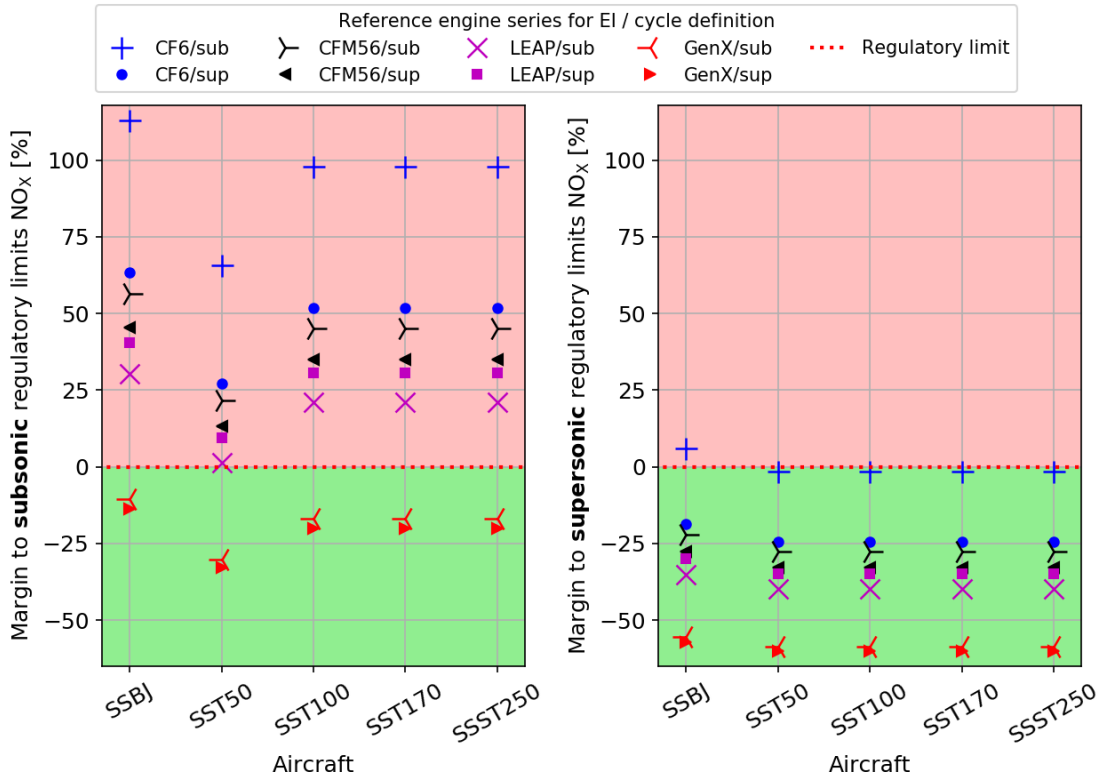

Figure 9.1: Supersonic aircraft LTO cycle NO_x margins to sub- (left) and supersonic (right) regulatory limits for four reference engine series and the sub- and supersonic LTO cycle definitions

Looking at the NO_x graphs, the first thing that can be seen is that there is a difference between the margins found for the sub- and supersonic LTO cycle definitions, regardless of which regulation set is used. This difference can be explained by the lower thrust levels for the supersonic LTO cycle during climbout and ap-

proach/descent (see Table 8.1). Because a fuel flow method is used for the estimation of the emission index values corresponding to these segments, which have a lower fuel flow than for subsonic LTO thrust settings, the corresponding NO_x emission index values will also be lower. Overall, this causes the total NO_x emission mass to be lower, and consequently reduces the margin value. Note that for the CO and HC analyses, the emission indices will be higher for the supersonic cycle than for the subsonic cycle because at the lower thrust levels associated with the supersonic LTO segments, the CO and HC emission index values are higher. As a result, the overall CO and HC mass is often higher for the supersonic LTO cycle. This can be seen in Figures 9.2 and 9.3 for most engines, although the differences are much smaller than for NO_x. The differences are smaller because the relative contribution of the non-idle segments for CO and HC is much smaller than the long idle segment contribution, because the emission index values and segment times are substantially lower.

The NO_x graph also shows that the subsonic regulations are much more stringent than the supersonic regulations. With the supersonic regulations, even the older reference engines meet the regulations, while only the aircraft using the GenX engine series as reference for the emission index values can meet the subsonic NO_x regulations. This shows that it is possible for new supersonic aircraft engines to meet the subsonic CAEP8 NO_x regulations, but also that the supersonic NO_x regulations are outdated.

Looking at the four largest aircraft, it can be seen that the margins to the regulatory limits are the same for NO_x, CO and HC. The one exception is the subsonic regulatory NO_x limit for the SST50, which is because it is subject to a less stringent regulatory limit as a result of its engine thrust being less than 89 kN (see Table 8.2). The reason for the aircraft having the same LTO regulatory margins is that their engine thrust and takeoff fuel flow are linearly dependent as was shown in Table 7.7 with each engine using 0.0149 kg/s of additional fuel per kN of thrust. This is the result of them having the same engine components and efficiencies. Because the emission index values are estimated using four fits which only depend on engine OPR, those remain the same for each aircraft in both the sub- and supersonic LTO cycle. Consequently, the total emitted species mass is scaled by the same amount as the engine thrust. As a result of this the ratio of the emitted species mass for the LTO cycle, and the engine thrust is the same for the four aircraft. This term is used as the LTO cycle metric, and because the regulatory limits are the same for the three largest SSTs, their margins are also the same.

An analysis similar to that for NO_x was also performed for CO and the results are shown in Figure 9.2.

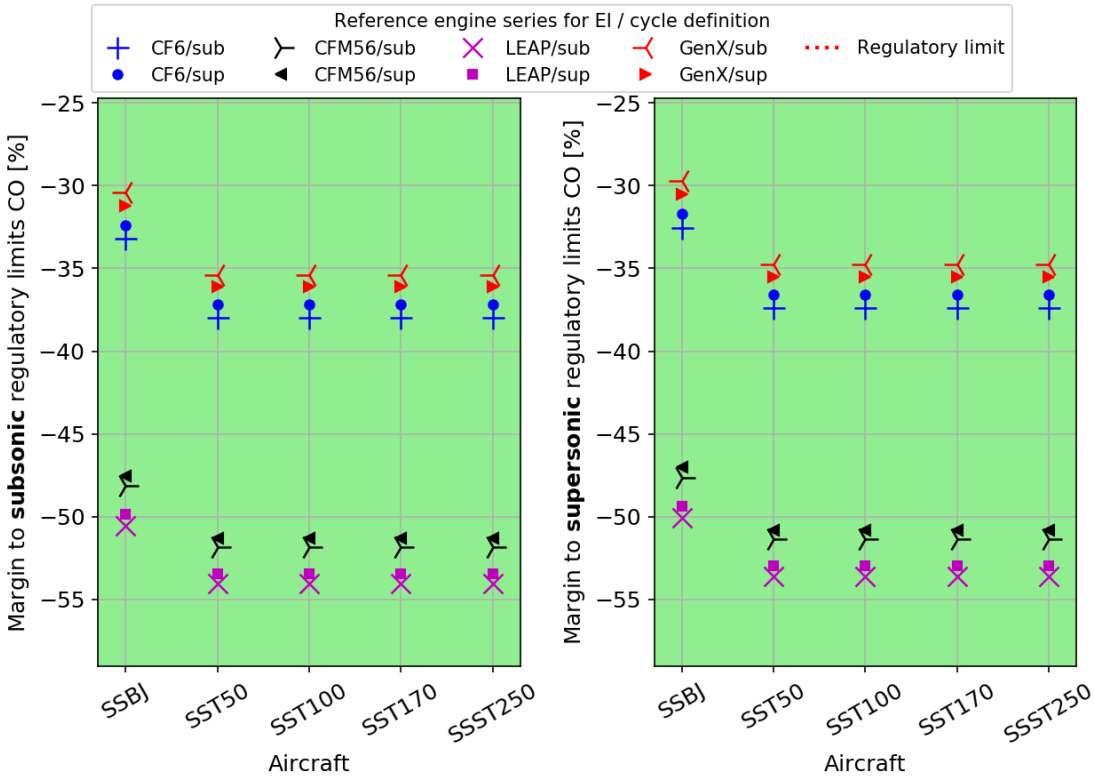

Figure 9.2: Supersonic aircraft LTO cycle CO margins to sub- (left) and supersonic (right) regulatory limits for four reference engine series and the sub- and supersonic LTO cycle definitions

The figure shows that there is again a difference between the margins for the sub- and supersonic LTO definition, but that the difference is smaller as was explained earlier. It can also be seen that regardless of the reference engine, cycle definition, and regulations selected, the CO limits are met without issues. It also shows that for the situations considered, the difference between the sub- and supersonic regulations is very small. It can be that for different engine OPR values, the differences are larger, but this is not investigated. Also note that the margins for the four largest aircraft are again the same.

Next, the hydrocarbon (HC) regulations for the LTO cycle were checked with the results in Figure 9.3.

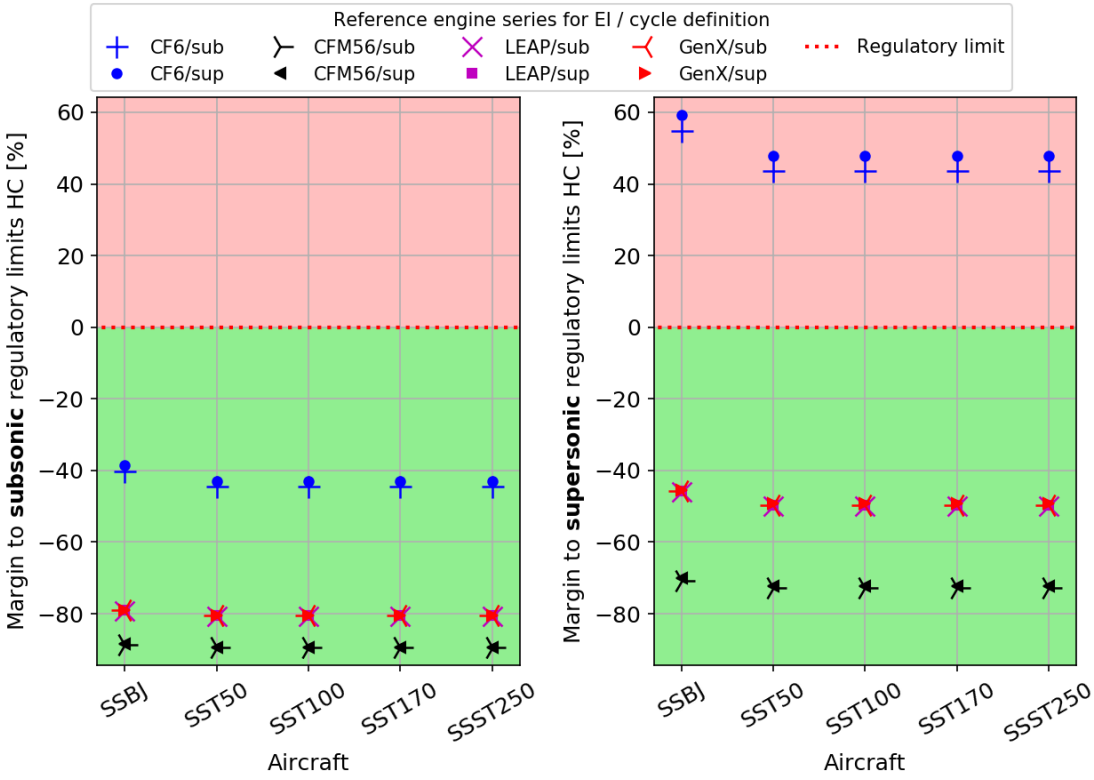

Figure 9.3: Supersonic aircraft LTO cycle HC margins to sub- and supersonic regulatory limits for four reference engine series and sub- and supersonic LTO cycle definitions

As with the NO_x and CO graphs, there is a small difference between the sub- and supersonic cycle LTO HC masses and margins. In terms of absolute HC mass, the engine based on CF6 emission index values produces at least three times as much HC as the GenX, LEAP and CFM56 engine series. Consequently, the performance of the CF6 engine is significantly worse, as indicated by its smaller margins for the subsonic regulations, and even its exceedance of the supersonic regulatory limits. The other engines are capable of meeting the regulations by a substantial margin.

Additionally, it can be seen that there is a large difference between the sub- and supersonic regulatory limits. This has to do with the subsonic limit being a constant value of 19.6 g/kN, while the supersonic limit varies with the engine OPR (see Table 8.2). Because that function is based on past experience with supersonic engines, which featured relatively low OPR values in the range 15-20, it is questionable whether the same rule should be applied to engines with an OPR of 35. It will likely be better to simply use the subsonic regulations because they are the same for all aircraft regardless of their engine design.

Now, the last species to check is the smoke number. Since the sub- and supersonic regulations are the same, only one graph is shown in Figure 9.4. It shows that there is no difference between the results found for the sub- and supersonic LTO cycle definitions. This is because the maximum smoke number is used, and that value is the same regardless of the cycle definition. In the reference engine fits, it was found that for the engine series considered, the maximum smoke number value was constant. The only variable then is the regulatory limit which becomes more stringent with increasing engine thrust. This explains why the margins to the regulatory limit are smallest for the SST250, and largest for the SST50, which features the least powerful engines.

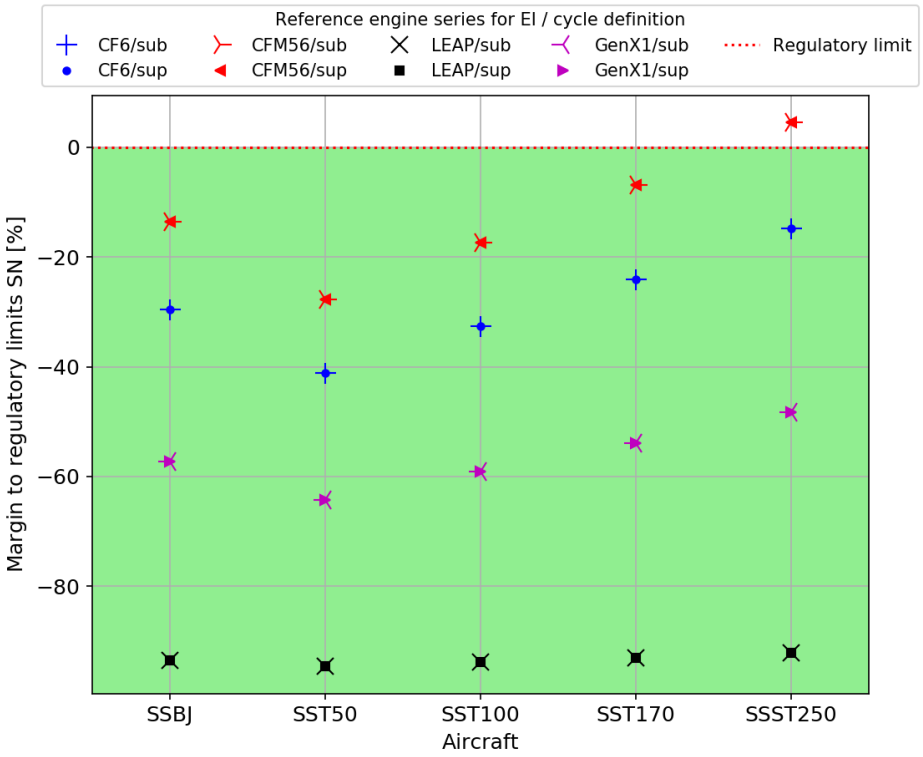

Figure 9.4: Supersonic aircraft LTO cycle SN margins to regulatory limits for four reference engine series and sub- and supersonic LTO cycle definitions

All in all, the above results for the LTO cycle showed that the new supersonic aircraft will likely be capable of meeting the subsonic regulations for HC, CO and the smoke number. The NO_x regulations on the other hand, are more difficult to meet although it was found that for an engine emission performance similar to the GenX engine series, the limits can be met. Given that the supersonic engine OPR falls in the range of OPR for the GenX series engines its results are expected to be the most reliable. However, no definitive statements can be made about the NO_x LTO performance until new SST engines are tested and certified.

On the regulations side, it has been shown that the supersonic regulations are outdated, and that they should either be replaced with the subsonic regulations, or updated to reflect improvements in engine design. Again, this can only be done properly once SST engine development has reached a sufficient level of maturity.

9.2. CO_2 certification

The second set of regulations that have to be adhered to are the new CO_2 regulations. Using the five supersonic aircraft designs, their performances were analyzed and the results found for their design missions are summarized in Table 9.1.

Table 9.1: Supersonic aircraft CO_2 certification data

Parameter	Unit	Aircraft				
		SSBJ	SST50	SST100	SST170	SST250
SAR_{high}	km/kg	0.3443	0.2457	0.1431	0.0968	0.0648
SAR_{mid}	km/kg	0.3688	0.2638	0.1542	0.1048	0.0703
SAR_{low}	km/kg	0.3973	0.2850	0.1674	0.1141	0.0768
$(1/SAR)_{avg}$	kg/km	2.7111	3.7897	6.4820	9.5448	14.226
RGF	-	24.4	46.9	88.3	129.9	188.3
Metric value	kg/km	1.260	1.505	2.212	2.968	4.047
Regulatory limit	kg/km	0.719	0.805	1.115	1.484	1.926
Margin	**%**	**+75.2**	**+86.9**	**+98.4**	**+100.1**	**+110.1**

The table shows that all five aircraft are not capable of meeting the regulations, with the margins ranging from +75.2% to +110.1%. This would mean that the supersonic aircraft cannot be officially certified by the

aviation authorities under the current regulations. To allow for a comparison to subsonic aircraft, Figure 9.5 was produced which displays the margins to the CO_2 regulations against the maximum number of passengers the aircraft can transport.

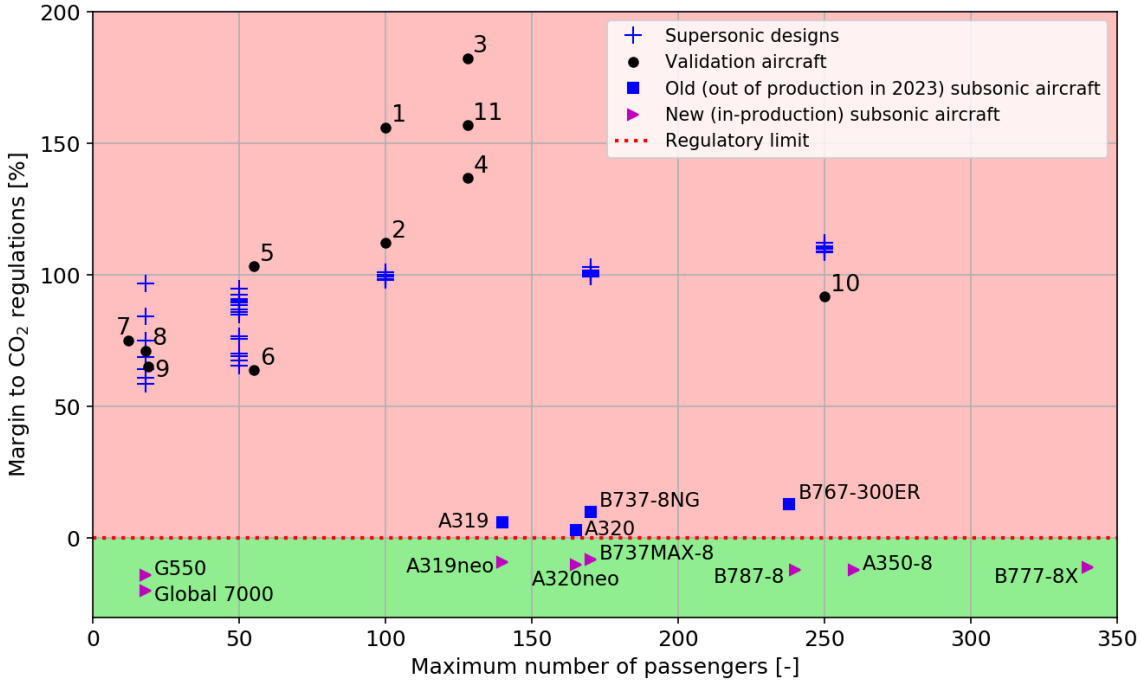

Figure 9.5: Margins to CO_2 regulations for supersonic aircraft and several subsonic aircraft (from [92])

The graph shows that the supersonic designs highlighted by the blue "+" are all exceeding the regulatory margins by at least 58%. Note that there are more markers than the five aircraft listed in the table above, because the supersonic aircraft designs for different design ranges are also included. This shows that the variation for the smaller SSBJ and SST50 is much larger than for the SST100/170/250 aircraft where the points are bunched together. For the SST50 there are more points visible in the graph because both the two- and four-engine configuration aircraft design are included.

The aircraft used for the validation of the design program are also included with the numbers corresponding to those in Table 7.1. The SSBJs (7, 8 and 9) all fall within the range found for the SSBJ designs at Mach 1.6. The old Tu-144 (3), old Concorde (1), and the N+1 aircraft (11) each have a much larger exceedance of at least +150%. This has to do with the designs not having the best performance during cruise and for Concorde and Tu-144 it is also because the engines were turbojets with lower efficiency, and they did not include technology factors to reduce the operating empty weight. When new engines and weight reductions are added (aircraft 2 and 4), the margins are reduced by over 40%. For the Boom SST, the change from Mach 2.2 (5) to Mach 2 (6), and corresponding improvement of performance is also reflected by the decrease of the CO_2 margin. Lastly, the NLR Mach 1.6 aircraft has a smaller margin than the SST250 aircraft, which is primarily because it used a supersonic SFC scaling factor of 1.16 instead of the 1.24 used by the SST250 aircraft. Without this change, the NLR aircraft would be closer to the SST250 cluster.

All this shows that the supersonic aircraft will not be capable of meeting the new CO_2 regulations by quite a margin. The smaller aircraft feature a slightly lower margin, but the exceedance will still be over 50%. When a number of subsonic aircraft are included in the graph, the disparity between the two groups of aircraft becomes more clear. Two subsonic sets of aircraft are included, one representing subsonic aircraft which will likely cease production in the near future (year 2023), and a second representing aircraft which will still be in production beyond 2023. The data used for the plots was taken from [92], and shows that the new (in-production) subsonic aircraft can all meet the CO_2 regulations. The older (out of production in 2023) subsonic aircraft do not meet the regulations, but only have small margins. More importantly, because they were already certified years ago they do not have to meet the regulations unless they are modified.

The main reason for the strong contrast between the sub- and supersonic aircraft in terms of CO_2 margins is the result of the SSTs having much lower specific air range values than their subsonic counterparts. An example of this is the SST250 which has a $(1/SAR)_{avg}$ value of 14.23 kg/km, which is about 2.9 times higher

than that of the Boeing 787-8 (4.90 kg/km) found in Table F.5. This is the result of the lower aerodynamic efficiency and greater specific fuel consumption of the SST during cruise, which outweigh the flight speed differential.

In conclusion, it has been shown that the supersonic aircraft cannot be expected to meet the new CO_2 regulations, even if their performance is improved significantly. A solution would be to exempt SSTs, or to give them their own CO_2 regulations. However, this presents a problem because it is questionable whether it is acceptable to produce much more CO_2 to reduce flight time in the current environment. In the near future, new supersonic aircraft will show more clearly what is possible, but it is better to anticipate and make a decision before their introduction.

9.2.1. CO_2 margin sensitivity to design range

Using the aircraft data from the range sensitivity study in Section 7.5.1, it is also possible determine how the CO_2 regulatory margins are affected by a change in the aircraft design range. To visualize the effect of design range Figure 9.6 was created.

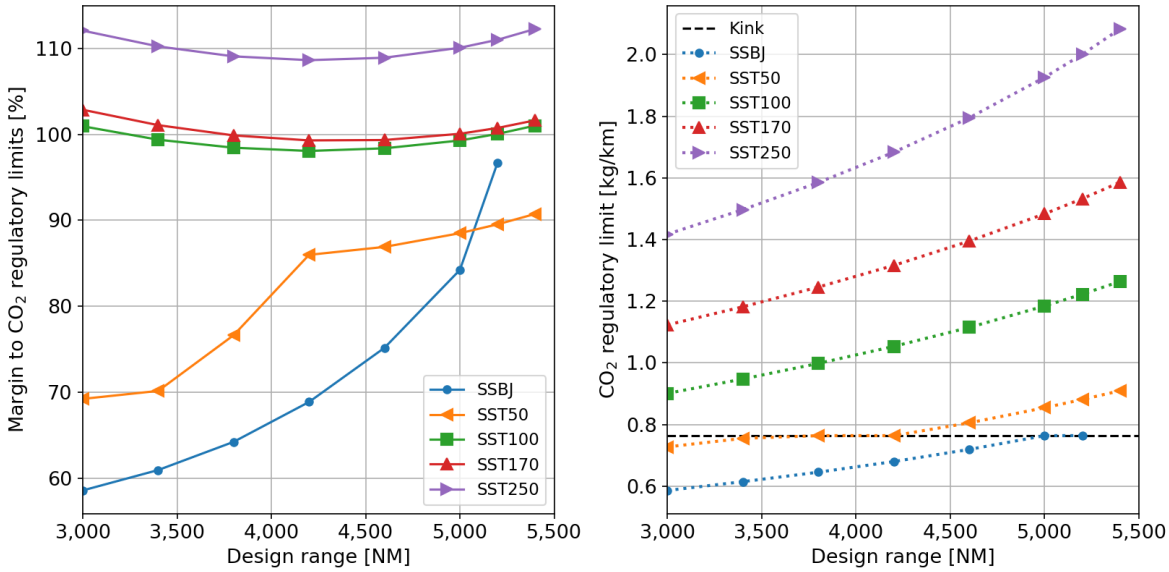

Figure 9.6: Margins to CO_2 regulations (left) and CO_2 regulatory limits (right) for supersonic aircraft as function of design range

The figure shows that for the SSBJ and SST50, the margins to the regulatory limit increases continuously. However, there is a discrepancy for the SST50 at the 3,800 and 4,200 NM ranges where the slope is much higher, before nearly leveling off from 4,200 to 4,600 NM. Additionally, for the SSBJ there is a large change in margin from 5,000 to 5,200 NM. These behaviors are the result of the regulatory limit definition (see Equations (8.5) to (8.7) and Figure 8.3), which features kinks at takeoff weights of 60,000 and 70,395 kg. This can be seen in the right graph where the black dashed line represents the constant regulatory limit at the kink. For the SST50 the lines overlap between 4,200 and 4,600 NM, and for the SSBJ that happens between 5,000 and 5,200 NM. This indicates that the regulatory limit remains the same there. Meanwhile, the CO_2 metric value increases between those ranges, so the relative increase in the margin is larger, as seen in the left graph. Beyond 4,600 NM the SST50 regulatory limit increases again, reducing the relative increase in CO_2 margin.

For the larger SST100, SST170 and SST250 on the other hand, the left graph indicates that there initially is a reduction of the margin to the regulations, with a minimum at about 4,200 NM, followed by an increase. Looking at the right graph, the regulatory limits are not affected by the kink because their takeoff weights are greater than 70,395 kg, meaning that a different reason has to be found. Having studied the CO_2 metric values for the SSTs, it was found that they always increased with range, because the specific air range (SAR) values worsened while the RGF remained the same. This means that the only possible reason that remains is that the regulatory limit initially increases more quickly in relative terms, than the CO_2 metric value. To try to show this the following value was plotted against design range for the three largest SSTs:

$$\text{relative } CO_2 \text{ margin change ratio}_i = \frac{\frac{CO_2\text{metric}_{i+1} - CO_2\text{metric}_i}{CO_2\text{metric}_i}}{\frac{CO_2\text{limit}_{i+1} - CO_2\text{limit}_i}{CO_2\text{limit}_i}} \tag{9.1}$$

where for range i, the relative change in the CO_2 margin is the ratio of the relative change in the CO_2 metric, and the relative change in the CO_2 regulatory limit. When this ratio is less than one, the CO_2 metric increases slower than the regulatory limit, which would be visible as a decrease in the margin to the regulatory limit. When the ratio is greater than one, the metric value increases faster than the regulatory limit, and the margin becomes larger. When plotting this factor for the three largest SSTs, the result in Figure 9.7 is found.

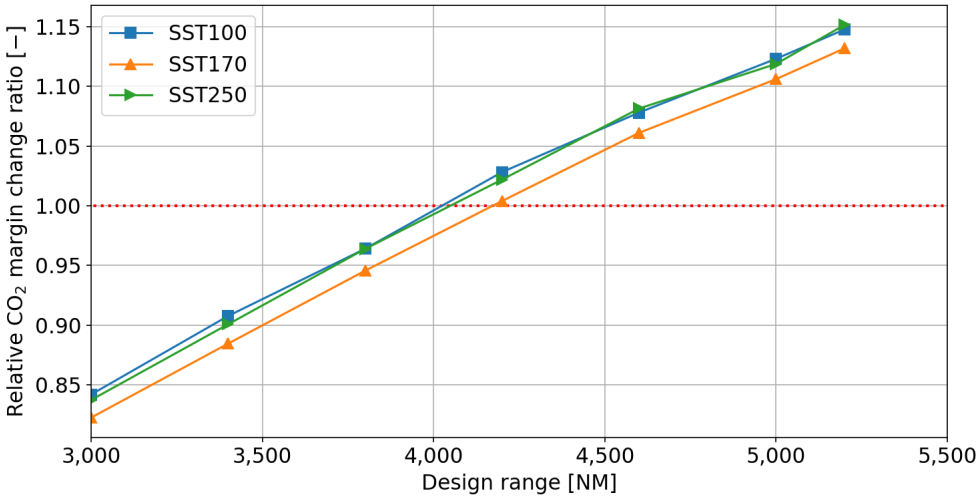

Figure 9.7: Relative CO_2 margin change ratio as function of design range for SST100, SST170 and SST250

The graph shows that for the SST100, SST170 and SST250 it is indeed true that the relative change of the regulatory limit is greater than the metric change for ranges below 4,200 NM. The opposite is true for higher ranges, which supports the findings made that there is a local optimum of the CO_2 margin to the regulatory limits. Note that the exact minimum values have not been determined, but are expected to be located between design ranges of 4,000 and 4,600 NM.

9.2.2. CO_2 margin sensitivity to Mach number

As with the variation in supersonic aircraft design range, the supersonic Mach number was also varied for the five design missions. The Mach number ranges from 1.4 to 2.0 in steps of 0.2, where the value at Mach 1.6 is that of the supersonic designs in Table 9.1. The resulting plot showing the margin to the regulations is shown in Figure 9.8, and some corresponding data is listed in Table 9.2.

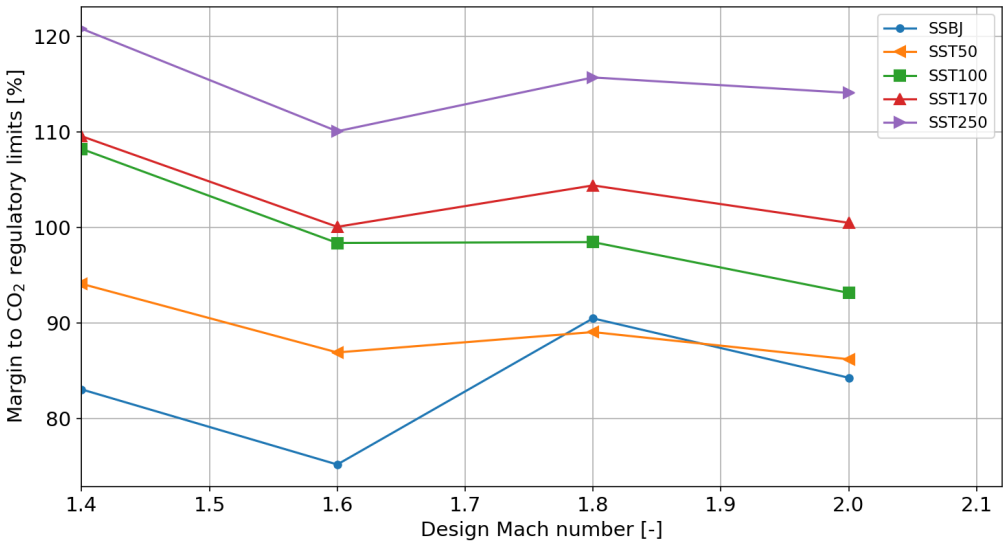

Figure 9.8: SST CO_2 metric margin to regulatory as function of supersonic Mach number

Table 9.2: Supersonic aircraft CO_2 data with varying Mach number

Aircraft	Parameter	Unit	M=1.4	M=1.6	M=1.8	M=2.0
SSBJ	1/SAR	kg/km	2.872	2.711	3.131	3.029
	CO_2 metric	kg/km	1.335	1.260	1.455	1.408
	Reg. limit	kg/km	0.729	0.719	0.764	0.764
	Margin	**%**	**+83.0**	**+75.2**	**+90.5**	**+84.3**
SST50	1/SAR	kg/km	3.989	3.790	4.083	4.074
	CO_2 metric	kg/km	1.584	1.505	1.622	1.618
	Reg. limit	kg/km	0.816	0.805	0.858	0.869
	Margin	**%**	**+94.1**	**+86.9**	**+89.0**	**+86.2**
SST100	1/SAR	kg/km	6.946	6.482	6.844	6.722
	CO_2 metric	kg/km	2.370	2.212	2.335	2.294
	Reg. limit	kg/km	1.138	1.115	1.177	1.188
	Margin	**%**	**+108.2**	**+98.4**	**+98.5**	**+93.1**
SST170	1/SAR	kg/km	10.22	9.545	10.49	10.47
	CO_2 metric	kg/km	3.178	2.968	3.263	3.256
	Reg. limit	kg/km	1.517	1.484	1.596	1.624
	Margin	**%**	**+109.6**	**+100.1**	**+104.4**	**+100.5**
SST250	1/SAR	kg/km	15.39	14.23	16.07	16.44
	CO_2 metric	kg/km	4.378	4.047	4.570	4.676
	Reg. limit	kg/km	1.983	1.926	2.119	2.184
	Margin	**%**	**+120.8**	**+110.1**	**+115.7**	**+114.1**

It can be seen that for Mach 1.4 the margin to the regulatory limits is always about 7-11% higher than at Mach 1.6. This is the result of worse SAR values, which increase the CO_2 metric value more relative to the increase in regulatory limits caused by the small increase in takeoff weight (see Figure 7.7 for this increase).

From Mach 1.6 to Mach 1.8, the margins increase for most aircraft, although the change is only a few percent, with the exceptions being the SSBJ, which has an increase of almost 15%, and the SST100 with a change of less than one percent. For each of the aircraft the SAR values become worse, but the regulatory limit change varies. In case of the SSBJ the limit for Mach 1.8 and Mach 2.0 is equal to the value of 0.764 at the kink (see Figure 8.3). This explains why the change from Mach 1.6 to Mach 1.8 is much larger compared to the other aircraft. For the other SSTs, the regulatory limit increases, although in case of the SST100 the relative change is larger, which is why the margin remains almost the same from Mach 1.6 to 1.8.

Next, from Mach 1.8 to Mach 2.0 all aircraft show a decrease in the margin value. This is the result of the SAR values improving slightly, and the regulatory limit increasing due to the larger takeoff weight. In case of the SST50 and SST100 the margin at Mach 2.0 is slightly smaller than at Mach 1.6. However, the difference is only several percent, and the performance found by the program for Mach 2.0 may not be entirely representative. Overall, the choice to design for Mach 1.6 is thus seen as a good decision, although a more detailed study would be beneficial.

9.2.3. CO_2 metric prediction fits

In the search for subsonic reference aircraft CO_2 metric data a web page of Piano-X[1] was found, where charts were shown with the ICAO CO_2 metric value plotted against the maximum takeoff weight and the span loading, and linear fits were introduced (see Appendix F.8). If such fits could be produced for supersonic aircraft these could be used by others to get an indication of the expected CO_2 metric value early in the SST design process. To see whether such fits were also possible for the supersonic aircraft, two similar plots were created as shown in Figures 9.9 and 9.10 with one or two types of best fits applied.

Looking at both figures, the quality of the fits is good for the 62 supersonic designs (47+15) used. Note that the validation aircraft are shown in the graphs but not used in the fit generation because they are not all seen as representative (e.g. Concorde and Tu-144 are too old). With these fits, it is possible to get a first rough estimate of the CO_2 metric value for a supersonic aircraft by using either the takeoff weight or span loading. Still, it should be noted that the fit primarily uses 47 supersonic aircraft designs operating at Mach 1.6, and five each at Mach 1.4, 1.8 and 2.0. For this reason, it could be that at different Mach numbers, the resulting fit

[1] http://www.lissys.demon.co.uk/co2metricdata-update1.html (accessed May 2 2019)

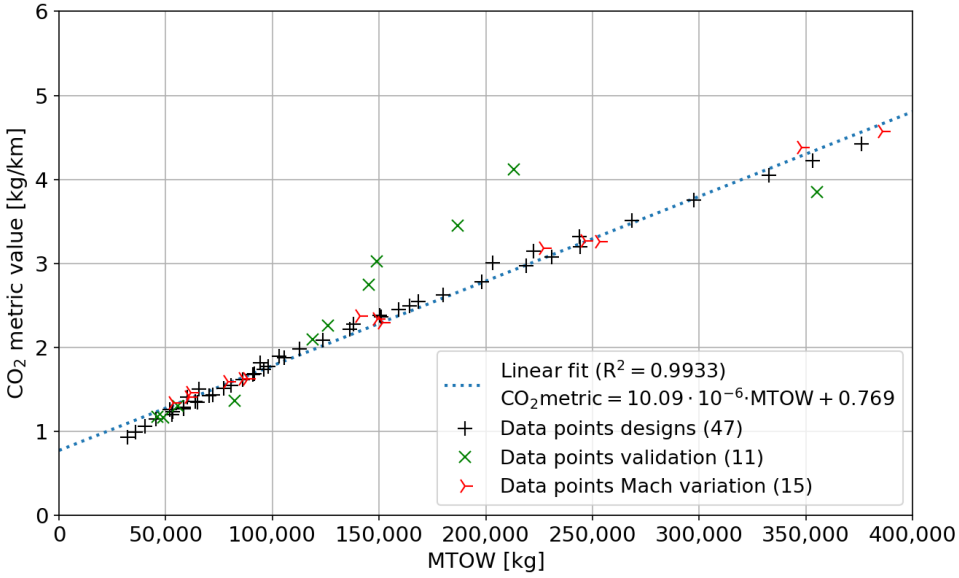

Figure 9.9: SST CO_2 metric value against maximum takeoff weight

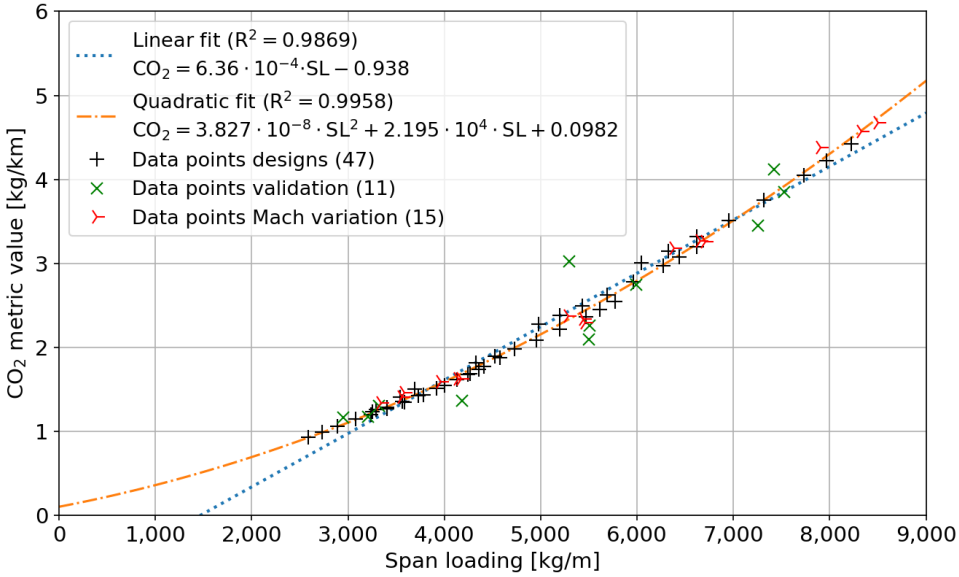

Figure 9.10: SST CO_2 metric value against span loading

will be somewhat different. Also, for different design choices like the use of lower or higher aspect ratio wings, and different engine types, the CO_2 metric might not behave like the fit. To check whether this is true, further testing and more advanced analyses are needed. For now however, the following fit is found as function of takeoff weight:

$$CO_2 \text{ metric [kg/km]} = 10.09 \cdot 10^{-6} \cdot \text{MTOW} + 0.769 \tag{9.2}$$

And for the CO_2 metric as function of span loading (SL in kg/m) the following two were found:

$$CO_2 \text{ metric [kg/km]} = 6.36 \cdot 10^{-4} \cdot \text{SL} - 0.938 \tag{9.3}$$

$$CO_2 \text{ metric [kg/km]} = 3.827 \cdot 10^{-8} \cdot \text{SL}^2 + 2.195 \cdot 10^{-4} \cdot \text{SL} + 0.0982 \tag{9.4}$$

where both fits have a good accuracy, although the quadratic fit seems to match better with the data distribution when looking at the graph. It should be noted because the design program used to generate the data is of low-fidelity, it is expected that there could be a deviation of up to ±15%.

9.3. Global climate impact

The third climate related analysis is that for the global climate impact. The five aircraft designs were analyzed and using the scenarios defined in Figure 9.11, the global temperature changes for the year 2050 were determined. The left plot shows the absolute temperature increase for the three supersonic scenarios, and two subsonic fleets, each set up to offer the same RPK (see Appendix F.6). The right plot shows the temperature increase when normalized with respect to the subsonic scenario with the lowest temperature change.

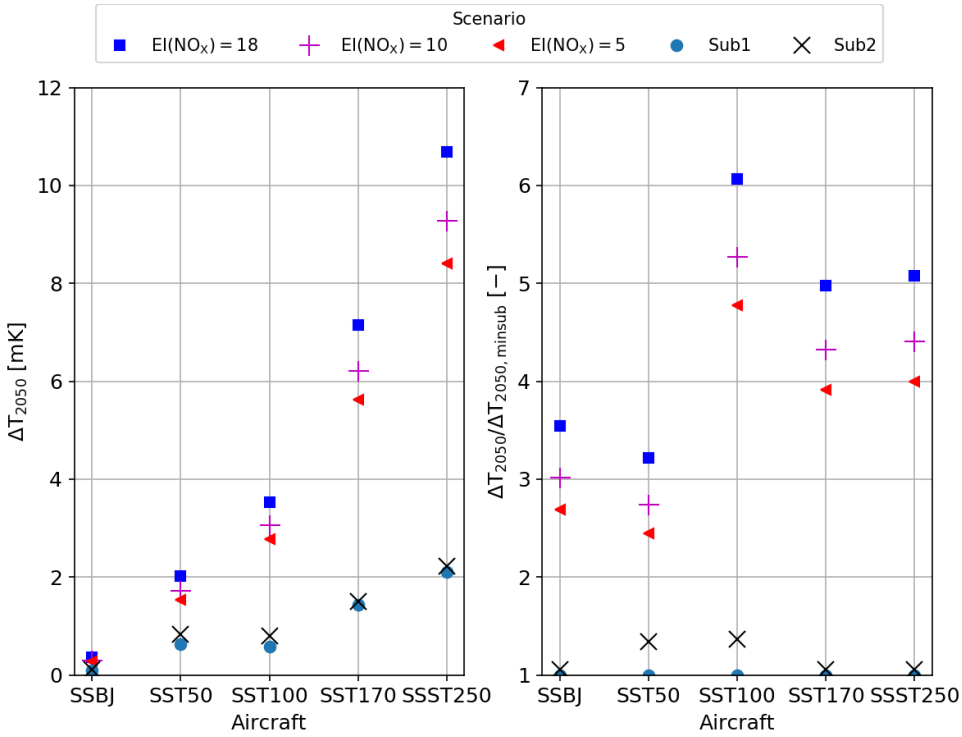

Figure 9.11: Absolute aircraft fleet induced temperature increase in 2050 (left) and normalized temperature change with respect to the subsonic fleet with the lowest impact (right)

The graphs show that the climate impact of the supersonic fleets is larger than that of the subsonic fleets. For the SSBJ in the best case scenario (EI(NO_x=5)), the temperature change is 2.7 times that of an equivalent subsonic fleet of Gulfstream G550 aircraft. In the pessimistic scenario (EI(NO_x=18)) this ratio increases to 3.54. Compared to the findings in [100], where for the HISAC fleet, the radiative forcing (RF) of a supersonic fleet was found to be 3±0.4 times as large as that of a subsonic counterpart, this is a reasonable finding.

For the larger aircraft the absolute temperature increase becomes larger as could be expected given the increase in fuel consumption. For the SST50 and SST100 subsonic reference scenarios, the Boeing 737BJ and Airbus Corporate Jet (SST50), and Airbus A319neo and Boeing 787-8 (SST100) were used. However, the first two aircraft are not seen as very representative, because the first two are usually sized to transport a payload of at most 10-25 passengers with a luxurious interior. Therefore, it is also questionable whether the subsonic reference results found using Piano-X are representative. Similarly, for the SST100 the Airbus A319neo cannot fly the 4,600 NM mission used to size the SST100. For this reason, it uses a lower range, which means that more aircraft are needed to provide the same number of RPKs. On the other hand, the Boeing 787-8 is much larger than the SST100, which again makes it an unrealistic comparison. As a result of this, the SST100 has a climate impact between 4.8 and 6.1 times that of the subsonic fleet of Boeing 787-8s.

The two largest supersonic aircraft are compared to the Boeing 787-8 and Airbus A350-800XWB, and show that the supersonic fleets produce a global temperature change between 3.9 and 5.1 times that of an equivalent subsonic fleet. This finding again falls in between the value RF increase found for the HISAC SSBJs (3±0.4), and the value of roughly six found for the SCENIC SST fleet in [100]. The values also show that the effect of replacing a subsonic fleet of business jets by SSBJs is smaller than the effect of changing a fleet of large subsonic aircraft by large SSTs.

The main reason for this is that the difference in cruise altitude between a sub- and supersonic business jet is smaller than that between a larger sub- and supersonic passenger aircraft. Because of the way that the

global temperature change is affected by the cruise altitude pressure (see Figure 8.5), an increased cruise altitude differential will increase the relative change. In terms of cruise NO_x emission index the subsonic business jets feature average values of about 7.3-8.5 g/kg, while the larger aircraft like the Airbus A350-800XWB, and Boeing 767-300ERW and 787-8 produce about 10.5-13.5 gram of NO_x per kilogram of fuel as estimated using data from Piano-X. For the SSBJ, SST170 and SST250 the supersonic and subsonic fleet data are shown in Tables 9.3 and 9.4, respectively. For more information about the fleet setup see Appendix F.6.

Table 9.3: Supersonic fleet definition for SSBJ, SST170 and SST250

Parameter	Unit	SSBJ			SST170			SST250		
Fleet size	-	250			250			250		
$n_{pax,flight}$	-	12			144			212		
$n_{flights,ac}$	-	100			500			500		
RPK	10^{10} pax.km	0.2556			16.668			24.539		
FC_{2050}	10^8 kg	5.771			113.2			169.3		
h_{cr}	m	15,500			16,000			16,000		
$EI(NO_x)$	g/kg	5	10	18	5	10	18	5	10	18
ΔT_{2050}	mK	0.272	0.305	0.358	5.62	6.21	7.15	8.41	9.29	10.69

Table 9.4: Subsonic fleet definition for SSBJ (G550, G650), SST170 and SST250 from left to right

Parameter	Unit	G550	G650	B787-8	A350-8	B787-8	A350-8
Fleet size	-	301	301	210	195	308	288
$n_{pax,flight}$	-	12	12	206	221	206	221
$n_{flights,ac}$	-	83	83	417	417	417	417
RPK	10^{10} pax.km	0.2554	0.2554	16.705	16.641	24.500	24.577
FC_{2050}	10^8 kg	2.478	2.551	35.18	35.57	51.60	52.53
h_{cr}	m	13,659	13,797	12,619	12,924	12,619	12,924
$EI(NO_x)$	g/kg	7.38	7.69	10.67	10.79	10.67	10.79
ΔT_{2050}	mK	0.101	0.107	1.44	1.51	2.11	2.23

The tables show that for the SSBJ the subsonic fleet is 20% larger than the supersonic fleet, which is because of the 20% higher productivity assumed for the supersonic aircraft. For the SST170, the equivalent subsonic fleet is smaller because the capacity of the A350-800XWB and Boeing 787-8 is larger than 170 passengers, which compensates for their lower productivity. For the SST250 this is not the case, with the subsonic fleet having more aircraft. Looking at the cruise altitudes for the subsonic aircraft it can be seen that the G550 and G650 operate at somewhat higher cruise altitudes than the Boeing 787-8 and Airbus A350-800XWB, which shows that the altitude differential between the sub- and supersonic fleets is larger for the SSTs than for the SSBJ.

It should be noted however, that the fleet setup used to produce the results is not very detailed, and that it could for example be that the supersonic aircraft have an even higher productivity than the 20% gain assumed here, when compared to subsonic aircraft. However, the only factors which affect the temperature change are the fuel consumption, cruise altitude and NO_x emission index. To come up with an equivalent fleet the subsonic RPK has to be close to the supersonic RPK, which means that the total fleet fuel consumption, emission index and cruise altitude are independent of the fleet size. Consequently, the results found earlier could for example be used to show that a single SST250 will produce between 4 and 5.1 times the temperature increase of a Boeing 787-8 when it operates an equivalent number of RPKs.

Having discussed the performance of the five supersonic aircraft designs, two additional smaller subsections will look at the effects of design range and Mach number on the global temperature change. These are discussed in Sections 9.3.1 and 9.3.2, respectively.

9.3.1. Effect of range

Having shown that the temperature change of the supersonic fleets at their design range is roughly 3 (SSBJ) to 4.5 (SST250) that of an equivalent subsonic fleet for the most likely emission index scenario, it is also possible to determine what effect the aircraft design range is. To this end, the designs were all analyzed for design ranges from 3,000 to 5,400 NM. The resulting temperature changes for the most likely scenario

(EI(NO_x)=10) were then divided by the design mission value (i.e. 4,600 NM for SSBJ, SST50/100 and 5,000 NM for SST170/250). Additionally, for each design range the ratios of the temperature change from a super- and subsonic fleet for that range were also determined for all three scenarios. Note however that for ranges below 3,800 NM no subsonic reference data was available so those cells are left empty. The results from this analysis are listed in Table 9.5.

Table 9.5: Global temperature change variation with supersonic aircraft design range

Aircraft	Variable	Unit	Range [NM]						
			3,000	3,400	3,800	4,200	4,600	5,000	5,400
SSBJ	FC_{2050}	10^8 kg	2.622	3.230	3.928	4.759	5.771	7.058	-
	$\Delta T_{ml,2050}/\Delta T_{ml,2050,ref}$	-	0.454	0.560	0.681	0.825	1	1.223	-
	$\Delta T_{pes,2050}/\Delta T_{2050,sub}$	-	-	-	2.98	3.23	3.54	3.95	-
	$\Delta T_{ml,2050}/\Delta T_{2050,sub}$	-	-	-	2.54	2.75	3.02	3.36	-
	$\Delta T_{opt,2050}/\Delta T_{2050,sub}$	-	-	-	2.26	2.45	2.69	3.00	-
SST50	FC_{2050}	10^8 kg	16.33	19.74	23.54	27.74	32.49	38.07	44.55
	$\Delta T_{ml,2050}/\Delta T_{ml,2050,ref}$	-	0.503	0.608	0.725	0.854	1	1.172	1.371
	$\Delta T_{pes,2050}/\Delta T_{2050,sub}$		-	-	2.92	3.05	3.22	3.41	3.70
	$\Delta T_{ml,2050}/\Delta T_{2050,sub}$	-	-	-	2.48	2.60	2.74	2.90	3.15
	$\Delta T_{opt,2050}/\Delta T_{2050,sub}$	-	-	-	2.21	2.32	2.45	2.59	2.81
SST100	FC_{2050}	10^8 kg	28.10	33.96	40.44	47.68	55.89	65.38	76.44
	$\Delta T_{ml,2050}/\Delta T_{ml,2050,ref}$	-	0.503	0.608	0.724	0.853	1	1.169	1.368
	$\Delta T_{pes,2050}/\Delta T_{2050,sub}$	-	-	-	5.44	5.73	6.07	6.49	6.99
	$\Delta T_{ml,2050}/\Delta T_{2050,sub}$	-	-	-	4.73	4.98	5.27	5.64	6.08
	$\Delta T_{opt,2050}/\Delta T_{2050,sub}$	-	-	-	4.28	4.51	4.77	5.10	5.50
SST170	FC_{2050}	10^8 kg	48.63	58.76	69.97	82.52	96.80	113.2	132.6
	$\Delta T_{ml,2050}/\Delta T_{ml,2050,ref}$	-	0.423	0.519	0.618	0.729	0.855	1	1.171
	$\Delta T_{pes,2050}/\Delta T_{2050,sub}$		-	-	4.17	4.39	4.65	4.98	5.37
	$\Delta T_{ml,2050}/\Delta T_{2050,sub}$	-	-	-	3.62	3.82	4.04	4.32	4.67
	$\Delta T_{opt,2050}/\Delta T_{2050,sub}$	-	-	-	3.28	3.46	3.66	3.92	4.23
SST250	FC_{2050}	10^8 kg	70.32	85.31	102.1	121.1	143.1	169.3	201.2
	$\Delta T_{ml,2050}/\Delta T_{ml,2050,ref}$	-	0.415	0.504	0.603	0.716	0.845	1	1.188
	$\Delta T_{pes,2050}/\Delta T_{2050,sub}$	-	-	-	4.15	4.40	4.69	5.08	5.56
	$\Delta T_{ml,2050}/\Delta T_{2050,sub}$	-	-	-	3.61	3.82	4.08	4.41	4.88
	$\Delta T_{opt,2050}/\Delta T_{2050,sub}$	-	-	-	3.26	3.46	3.69	3.99	4.37

The table shows that for a reduction in range, the total fleet fuel consumption decreases, and that it increases for larger ranges. Because the climate functions used for the global temperature change estimation are linearly dependent on the fuel consumption, the temperature ratio in the second row for each aircraft is equal to the ratio of the fuel consumption at range X divided by that at the design point (where the ratio is 1). For example, for the SST170 at 3,400 NM the fuel consumption is 0.519 times that at the design mission of 5,000 NM. Consequently, the temperature change at 3,400 NM will be 0.519 times that for the same scenario at 5,000 NM.

The three other rows show the ratio of the supersonic fleet temperature change compared to the best equivalent subsonic fleet. For the SSBJ in the pessimistic scenario (EI(NO_x)=18) at 3,800 NM, the supersonic fleet would produce about 2.98 times as much temperature increase as an equivalent subsonic fleet (in terms of RPK). Overall, the values show that for a lower range, the ratio decreases. This is largely the result of the supersonic aircraft experiencing a larger decrease in fuel than the subsonic aircraft, because the SSTs have higher fuel fractions. Since the cruise altitude and emission index differential between sub- and supersonic fleets remains virtually the same for all scenarios, these do not have a large effect on the changes. However, the results do show that the climate impact is quite sensitive to the design range.

9.3.2. Effect of Mach number

Using the designs described in Section 7.5.2, it is also possible to analyze the effect of the supersonic Mach number on the SST fleet global temperature change. The same methodology is applied as that described earlier for the altitude variation study, and the results found are shown in Table 9.6.

Table 9.6: Global temperature change variation with SST design Mach number

Mach	Variable	Unit	1.4	1.6	1.8	2.0
SSBJ	FC_{2050}	10^8 kg	6.213	5.771	6.567	6.243
	$\Delta T_{ml,2050}/\Delta T_{ml,2050,ref}$	-	1.01	1	1.20	1.20
	$\Delta T_{pes,2050}/\Delta T_{2050,sub}$	-	3.70	3.54	4.14	4.00
	$\Delta T_{ml,2050}/\Delta T_{2050,sub}$	-	3.05	3.02	3.63	3.62
	$\Delta T_{opt,2050}/\Delta T_{2050,sub}$	-	2.65	2.69	3.31	3.38
SST50	FC_{2050}	10^8 kg	34.74	32.49	34.46	33.79
	$\Delta T_{ml,2050}/\Delta T_{ml,2050,ref}$	-	1.01	1	1.12	1.15
	$\Delta T_{pes,2050}/\Delta T_{2050,sub}$		3.34	3.22	3.50	3.50
	$\Delta T_{ml,2050}/\Delta T_{2050,sub}$	-	2.76	2.74	3.07	3.16
	$\Delta T_{opt,2050}/\Delta T_{2050,sub}$	-	2.39	2.45	2.81	2.96
SST100	FC_{2050}	10^8 kg	60.87	55.89	58.07	56.05
	$\Delta T_{ml,2050}/\Delta T_{ml,2050,ref}$	-	1.03	1	1.09	1.10
	$\Delta T_{pes,2050}/\Delta T_{2050,sub}$	-	6.43	6.07	6.44	6.29
	$\Delta T_{ml,2050}/\Delta T_{2050,sub}$	-	5.54	5.27	5.76	5.81
	$\Delta T_{opt,2050}/\Delta T_{2050,sub}$	-	4.79	4.77	5.34	5.51
SST170	FC_{2050}	10^8 kg	123.0	113.2	122.6	120.4
	$\Delta T_{ml,2050}/\Delta T_{ml,2050,ref}$	-	1.03	1	1.14	1.17
	$\Delta T_{pes,2050}/\Delta T_{2050,sub}$		5.26	4.98	5.50	5.48
	$\Delta T_{ml,2050}/\Delta T_{2050,sub}$	-	4.44	4.32	4.93	5.06
	$\Delta T_{opt,2050}/\Delta T_{2050,sub}$	-	3.92	3.92	4.57	4.79
SST250	FC_{2050}	10^8 kg	185.9	169.3	188.4	189.7
	$\Delta T_{ml,2050}/\Delta T_{ml,2050,ref}$	-	1.04	1	1.17	1.23
	$\Delta T_{pes,2050}/\Delta T_{2050,sub}$	-	5.42	5.08	5.77	5.88
	$\Delta T_{ml,2050}/\Delta T_{2050,sub}$	-	4.57	4.41	5.16	5.43
	$\Delta T_{opt,2050}/\Delta T_{2050,sub}$	-	4.04	3.99	4.78	5.15

The table shows that for all five aircraft, the fleet fuel consumption at Mach 1.4, 1.8 and 2.0 is greater than that at Mach 1.6. Also, from Mach 1.8 to Mach 2.0 the fuel consumption decreases for all aircraft except the SST250, although the change is relatively small. This is the result of the lower mission fuel fraction, and limited increase in takeoff weight as shown in Figures 7.7 and 7.8.

At Mach 1.4, the fleet fuel consumption is greater, but depending on the scenario, the temperature change of the supersonic fleet is either slightly lower or higher than the Mach 1.6 reference fleet. The pessimistic and most likely scenarios at Mach 1.4 are always worse than at Mach 1.6, but the optimistic scenario is slightly better for the SSBJ and SST50. This is the result of those aircraft operating 500 meter lower than the SST100/170/250 aircraft at Mach 1.4. This reduces the climate impact through the altitude dependence of the climate functions, and somewhat overcompensates for the increased fleet fuel consumption.

When comparing the ratios for Mach 1.8 to those for Mach 1.6 it is found that the climate impact at Mach 1.8 is always greater than at 1.6. This has to do with the combination of the increased cruise altitude, and the increased fuel consumption, which together increase the temperature change. For Mach 2.0, the impact will be greater than at Mach 1.8 in all optimistic scenarios, and several of the most likely scenarios. However, for all but the SST250 aircraft, the temperature ratio decreases in the pessimistic scenario. This means that flying 750 meters higher and 0.2 Mach faster results in the supersonic fleet having a slightly smaller impact than the equivalent supersonic fleet at Mach 1.8. The cause of this is a combination of the decrease in fleet fuel consumption, but also the decrease of the sensitivity of the climate functions due to the greater NO_x emission index value. This greater emission index value means that the relative importance of methane (CH_4) and especially ozone (O_3) increase, which flattens the total climate change function, when compared to the curve in Figure 8.5. To visualize this, a similar graph is created in Figure 9.12 with the same inputs except that the NO_x emission index now is 18 g/kg instead of 10.84 g/kg.

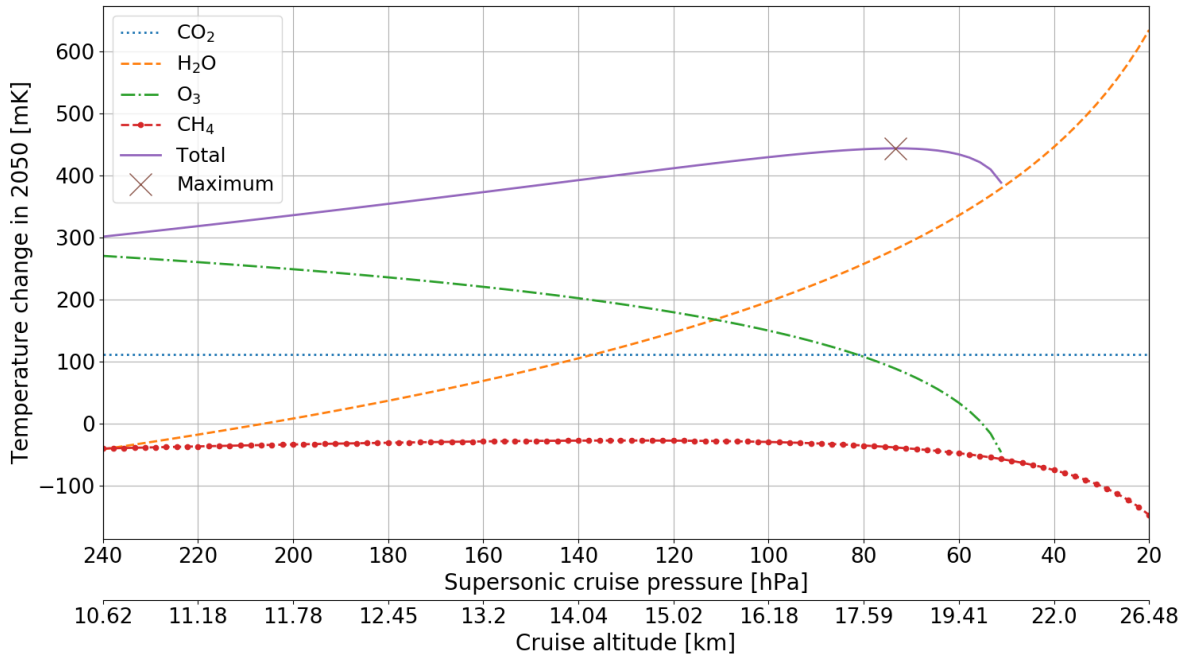

Figure 9.12: Temperature change per emitted species as function of cruise altitude for SCENIC fuel consumption but with 18 g/kg NO_x emission index (note that cruise altitude axis is not linear)

Looking at the curve, the carbon dioxide and water vapor induced temperature changes are the same as in Figure 8.5, but the contribution of ozone has become larger for low altitudes. Also, the effect of methane is slightly more negative. Because with increasing cruise altitude, the absolute temperature change contribution of ozone decreases more quickly, it compensates more strongly for the increasing water vapor contribution, resulting in the total temperature change curve being less steep. The end result of this is that the fleet fuel consumption reduction from Mach 1.8 to Mach 2.0 overcompensates for the effect of the 750 meter increase in cruise altitude. For this reason, the pessimistic scenarios can have a slightly lower temperature change at Mach 2.0 than at Mach 1.8.

While this seems to indicate that it might be better to fly higher and with higher emission indices to partially negate the added fuel consumption compared to the Mach 1.6 designs, emitting NO_x at these altitudes is highly undesirable because of the ozone layer breakdown. This item is briefly touched upon in the final section below. All in all, the above Mach sensitivity analysis shows that operating at Mach 1.6 is the best option for the designs studied. Note that if other choices were made it could be that the findings are different, and that the level of accuracy is limited because climate functions were used instead of climate models.

9.4. Additional notes

In the above sections, the results related to the climate analyses performed using the supersonic aircraft designs have been shown and discussed. However, certain items which are also important have not been studied either due to a lack of resources or because the regulations are not yet available. These are each briefly discussed here:

- Given the higher cruise altitude associated with supersonic transportation, when compared to the majority of the subsonic aircraft, the SSTs will operate closer to or inside the ozone layer. As a result, their NO_x emissions will have a larger effect and can cause additional breakdown of the ozone layer. In [101] it is stated that above altitudes of 18 to 20 kilometer (depending on kinetic data used in climate model), the emission of NO_x will usually result in net ozone destruction. It is also shown that with increasing NO_x emission index from 5 to 15, the amount of ozone column depletion increases from 1.0% to 2.5-3.0%, although this depends on the model used [101]. Additionally, the SCENIC study has found that replacing part of a subsonic fleet by SSTs will result in an additional ozone loss of 1 to 16 Tg [99].

- In the climate analyses, three areas have been investigated, the LTO cycle regulations, new CO_2 regulations, and global temperature change. While the LTO cycle can be a useful means to determine the impact of aviation related emissions on the local air quality near airports, it does not say much about the air quality far from the airports. Emissions with a relatively long lifetime which are produced by aircraft during its entire flight (i.e. also including cruise) can also affect the air quality far away after spreading within the atmosphere. In [102] it was estimated that about 8,000 premature mortalities per year can be attributed to aircraft cruise emissions. These impacts have not been considered in the current study. It should be noted though, that because SSTs will likely only represent a small fraction of the future global aviation fleet, their contribution to air quality will be smaller, but should not be ignored.

- During the recent CAEP11 meeting in February 2019 several items such as the CO_2 certification, the implementation of a new methodology for nvPM (non-volatile particulate matter), and the definition of emission standards for supersonic aircraft have been discussed[2]. However, the decisions made, and updates to the regulations or new amendments are not yet publicly available or unfinished, and could therefore not be implemented. With regards to the nvPM regulations, a new method has been published specifically to predict the black carbon (BC) mass and BC number emissions at the engine exit plane, which is referred to as the Smoke Correlation for Particle Emissions–CAEP11 (SCOPE11) [103] method. It is an improvement over earlier methods discussed in [104, 105], and can be used for both the LTO cycle and global emissions.

- In the climate functions used for the global temperature change estimation, the contributions of contrails were ignored. However, some studies have been performed on this topic, such as [106] which discusses the formation of contrails. Supersonic aircraft will more often fly in higher in dryer regions of the atmosphere, where the probability of forming a contrail are smaller [107]. It was also shown in the same study that by replacing a subsonic fleet with supersonic aircraft, the contrail occurrence shifts from the mid to the lower latitudes, and that the resulting change in climate impact is nearly negligible. The same was also found in [99] for the SCENIC fleet. These findings supports the decision to ignore contrail contributions when comparing the sub- and supersonic fleets through the temperature change functions. Note that the radiative forcing effects of contrail induced cirrus clouds are currently not well understood [3], and that no definitive statement can be made here about their contribution or importance.

It should be noted that there are also other issues which have not been investigated or mentioned above. This concludes the climate analysis results discussion.

[2] https://www.icao.int/environmental-protection/Pages/CAEP11.aspx (accessed May 22 2019)

10 Conclusion

This thesis has discussed the study of the performance of new supersonic aircraft both in terms of weight, aerodynamics and propulsion, and in terms of environmental impact. It was produced at the request of the International Civil Aviation Organization (ICAO), to attempt to bridge the gap between past supersonic aircraft like Concorde, and new ones planned for production in the coming decade like the Aerion AS2. Because of the size of the investigation, it is performed by two students, with the second thesis [7] focusing more on aircraft noise, and the design program sensitivity.

The goal of this master thesis is twofold, the first goal is the development of a low-fidelity design program to support the conceptual design of new supersonic transport aircraft. Using a set of top-level requirements, this program has to be capable of generating aircraft designs and provide information about their performance. These findings can then be used for the second goal, to investigate the climate impact of supersonic aircraft and use the findings to evaluate the current environmental regulations defined by ICAO.

Starting with the individual design program modules, the following findings were made:

- **Class I**: During the validation of the Class I module it was found that the takeoff weight was predicted to within 5.6%, while the operating empty weight was predicted to within 9.9%. The larger OEW deviation was largely caused by the use of a logarithmic fit to estimate the operating empty weight as a function of takeoff weight, which did not account for design choices and technological improvements. Implementation of the Class II module largely resolved this issue.

- **Wing loading, engine and aircraft design**: These modules have been tested, and validated, but no specific values are currently available. More information about their validation can be found in [7].

- **Aerodynamics**: The aerodynamics module uses relatively simple relations, primarily because of the lack of resources. Application of the module on two aircraft designs during supersonic cruise showed that it predicts L/D with at most ±5% difference. Subsonic L/D-values are also predicted and found to return good values. For low-speed performance the Polhamus method was found to be best, and combined with a simple HLD sizing function it is used to estimate the maximum lift coefficients.

- **Class II**: The Class II module estimates the weights of four groups, the structures, propulsion, equipment and operational items groups. For this, empirical relations from multiple sources are used, and the module was calibrated using Concorde. The prediction capability of the structures and propulsion groups is good, with errors of less than ±4%, but the equipment (-11.1%) and especially operating items group (-30.3%) showed larger deviations. Calibration reduced these errors to zero. Additionally, technology factors were included to account for changes in design and construction methods, which reduced the operating empty weight of an unmodified Concorde by 16.8%.

By combining these modules in Python the supersonic aircraft design program was created, and additional modules were introduced to for example produce PDFs and link to the KBE program ParaPy. Some object-oriented programming was used to enable future expansions and replacement of existing modules.

Validation of the full supersonic aircraft design program showed that the takeoff weight is predicted to within 4.8% on average when using inputs from six supersonic design studies, as well as the Concorde and Tu-144. Operating empty weight prediction is within 6.1% on average. The operating empty weight prediction for the three SSBJs is less reliable with an average underestimation of almost 9.5%, which shows that the Class II module should ideally be modified for business jets in an attempt to reduce this error. However, given the level of fidelity expected from the program, the results are seen as accurate enough to continue with the design of supersonic aircraft. Additionally, the program produced has a runtime of at most several minutes per design, such that various designs can be analyzed in a short period of time. This concludes the first goal.

Using the program five aircraft were created to cover the expected range of passenger capacities, with an SSBJ of 18 passengers, and SSTs of 50, 100, 170 and 250 passengers. Their design range is 4,600 (SSBJ, SST50/100) or 5,000 (SST170/250) NM to offer full Atlantic and at least partial Pacific coverage. Overland supersonic flight is not considered feasible in the near future given the need for sonic boom regulation updates, so most flights will be overwater at Mach 1.6. The resulting aircraft design takeoff weights fall within the ranges expected based on past design studies, and show that supersonic aircraft have payload fractions less than half that of similar subsonic aircraft. They are also heavier, and require substantially more fuel to transport a payload over the same distance, with the fuel efficiency of the SSBJ being about 2.5 times lower than that of a Gulfstream G550, and that of the SST250 being about 3.6 times lower than that of a Boeing 787-8.

For the second research goal, three climate analyses were set up, the LTO cycle emissions estimation, CO_2 certification, and a global temperature change estimation. Using the five designs, and a set of reference engines for the emission index estimation, it was found that the supersonic aircraft can be expected to meet the LTO regulations for CO, HC and SN. The regulations for NO_x can be met when the emissions performance is similar to that of GenX engines, but will likely be the critical factor. To completely check this, more advanced models would be needed, and new supersonic engine development has to be mature enough. Additionally, when using a subsonic LTO cycle definition, the margins will be slightly different from those for the supersonic definition, because the emission index values associated with the segments change. For NO_x, the supersonic cycle has a lower total mass, while for CO and HC it depends on the engine series used. In terms of the regulatory limits, the supersonic ones have to be updated once sufficient information is available about new supersonic engines, or replaced with the current (or slightly modified) subsonic regulations.

The results from the second environmental analysis for CO_2 certification show that the supersonic aircraft are incapable of meeting the regulations. Of the five designs the SSBJ is best though it still exceeds the regulatory limit by 75.2%. The SST250 has the largest margin as it exceeds regulations by 110%. Compared to in-production subsonic aircraft which can meet the regulations by 5-20%, this shows that the regulations in their current form should not be applied to supersonic aircraft. This is largely because the specific air range values achieved by the supersonic designs are much worse than for subsonic aircraft, as was also found when comparing the aircraft fuel efficiency values. Additionally, the reference geometric factor is smaller for the SST170/250 aircraft compared to long-range subsonic aircraft, because of the narrower cabin used to reduce wave drag.

To enable estimation of the CO_2 metric value of supersonic aircraft, good fits were produced with the takeoff weight and span loading on the x-axis using 62 supersonic aircraft designs. While these functions are not entirely accurate with an expected accuracy of $\pm$15%, they can be used in early design to get an idea of the aircraft performance. Sensitivity studies show that the exceedance of the regulations varies with design range and Mach number although the specific behavior found depends on the aircraft size, and situation.

The third environmental analysis for the global temperature change showed that the impact of a supersonic fleet is about 2.7 to 6.1 times that of an equivalent subsonic fleet in terms of RPK. For the supersonic business jet design the relative temperature increase is smallest (2.7-3.5) because of the smaller altitude differential between the sub- and supersonic fleets. The comparisons of the SST50 (2.45-3.2) and SST100 (4.75-6.1) to subsonic fleets are mainly disregarded since the subsonic reference fleets are not seen as representative. This is because no subsonic aircraft exist which are designed for at least 4,600 NM while transporting 50 to 100 passengers. The larger SST170 and SST250 produce four to five times the temperature increase produced by fleet of Boeing 787-8s. The ratio is larger than for the SSBJ because of the greater difference in cruise altitude between the sub- and supersonic aircraft, as well as the larger SST fleet fuel consumption. To further improve the quality of the comparison of the sub- and supersonic fleets, a more detailed climate analysis is required using a climate model with a detailed fleet setup and flight network.

All in all, there are still a large number of important environment-related questions which are not (fully) answered, and in some cases this can only be done once new supersonic aircraft are produced and flight-tested. Also, further investigations of the LTO NO_x, and CO_2 regulations will help in supporting future supersonic transportation in a more sustainable manner. However, it is also questionable whether the reduction in travel time offered by supersonic flight is worth the larger potential temperature increase in the long term. This is a question which has to be answered in the coming years given the increased attention to the climate impact of aviation worldwide, and the expected continued growth of air travel in the coming decades.

11 Recommendations

The purpose of the research in this report was to look into the design of new supersonic transport aircraft, and use their performance to evaluate their climate impact using several regulations and global temperature change functions. The main result was a low-fidelity design program capable of generating conceptual supersonic aircraft designs, combined with a climate module and in the near future a noise module (see [7] for the latter). However, the amount of resources available were limited and the topic is broad. During the work many methods and potential extensions for the program were encountered which could therefore not be implemented. To this end, the most important recommendations are discussed in this chapter, which could be used as starting point for further research. As the thesis had two goals, design and performance of supersonic aircraft, and their climate impact, the recommendations are split into those two categories.

Starting with the aircraft design and performance, several recommendations are made:

- Add new features to design modules or improve the existing ones:
  - Introduce an aircraft stability analysis to more accurately predict the behavior of the aircraft, and better size the tail surfaces. This will also include the determination of the center of gravity and its shift during the entire mission. Given that the aerodynamic center shifts during transonic acceleration this can be an interesting topic, and one could also look at the use of aircraft fuel tanks to trim the aircraft. Additionally, for ground maneuvers, the landing gear can be sized and positioned on the aircraft.
  - Implement Class II.V methods such as EMWET [108] for improved component weight estimation. This program has primarily been validated using subsonic aircraft designs so it is necessary to check that the program also provides valid results for thinner wings. This could potentially also be a separate thesis, and may require the use of FEM program to validate the results.
  - Improve the aerodynamics module so that it returns more reliable results, and becomes sensitive to a larger number of aircraft design inputs and dimensional parameters. A detailed list of the different opportunities can be found in Appendix C.8.
  - Improve the engine model so that it can be used for the supersonic off-design calculation of the internal characteristics (e.g. pressure, temperature). These can then be used for cruise emission index calculation through direct estimation methods, and allow for better prediction of the cruise specific fuel consumption for the Class I weight estimation. Additionally, it will be an interesting option to add more engine configurations like the ones discussed in [109, 110]. A possible solution to implement the features mentioned would be to link the aircraft design program to the GasTurb [111] or GSP [112] engine design programs.
  - Add a cost estimation module for the aircraft conceptual design. This will allow for predicting early in the design process what the direct and indirect operating costs will be, but also the expected sales price and sales numbers required to break-even and start making a profit. This can then be used to determine together with market analyses whether there is enough sales potential to warrant funding of the full aircraft development. A past MSc thesis research has been performed in this area for the Initiator by Zijp [113] and could be used as a basis for supersonic aircraft, with modifications to account for differences in components and operating regimes.
  - Introduce the ParaFuse program created at TU Delft [114] which uses ParaPy to size the fuselage interior. While the existing version could be used, it might be necessary to make adjustments to enable the area ruling of the aircraft, which is needed to reduce the amount of supersonic wave

drag. Additionally, the seating configuration in supersonic aircraft could be slightly different depending on the mission, and it should also be checked that the current version of ParaFuse can be used for the smaller business jet aircraft.

- Use different aircraft configurations than the double delta studied in the current report. This includes options like the variable sweep wing, but also a different type of empennage structure and positioning like the canard or three-surface configuration. A more exotic option, the oblique flying wing is discussed in a bit more detail in Appendix H.

- Implement an aircraft design optimization routine in the design program. This will allow the user to create designs which are optimized for a specific objective while subjected to a set of constraints, other than the current method which does not use constraints to steer the design process. Optimization can also enable the creation of designs with minimal climate, airport noise or sonic boom impacts and improve the understanding of what is possible in supersonic aircraft design.

- Introduce a detailed flight profile analysis to get a more accurate flight trajectory including a fuel burn breakdown and the flight levels being operated at. This will help improve the accuracy of the aircraft design and can offer a better understanding of its performance in various flight phases.

Based on the findings made during the climate impact analysis several recommendations are made, of which the first is by far the most important to consider for future supersonic transportation.

- The evaluation of the CO_2 certification regulations has shown that the supersonic aircraft will likely substantially exceed the regulatory limits. These differences can not be overcome through technological developments in the near future so it is important that a decision is made about this. The rules could be modified for supersonic aircraft or they could be exempted entirely. However, given the increased importance of climate impacts, and the much (2.7-6.1 times) larger temperature increase found for a supersonic fleet compared to equivalent subsonic fleets, it is difficult to say whether that would be a good decision. In an era where countries look to reduce their climate impact as stated in the Paris Agreement, it will also be difficult to explain to the public why less efficient aircraft with substantially larger climate effects are allowed to be flown. This is the most important question and has to be answered as soon as possible, so that it can be decided whether civil supersonic transportation should even be allowed.

- As shown in the evaluation of the LTO cycle, the new supersonic aircraft will be capable of meeting the CO, HC and SN subsonic regulations without any problems. The subsonic NO_x regulations represent an issue however, as the aircraft can only meet the regulations if their performance is similar to that of a GenX engine. While it is likely that this is possible, it should still be checked that it is indeed feasible using a detailed engine and emissions model. Additionally, the supersonic LTO regulations, in particular for HC and NO_x are outdated and should ideally be replaced by the current CAEP 8 subsonic regulations, to ensure that there is no disparity between the aircraft types.

- The current global climate impact analysis uses temperature change functions produced for business jets based on results from the AirClim model (see Appendix F.7 for more information). These results are sufficient to get a first estimate of the climate impact, but for future investigations it is better to make use of the AirClim model directly. This will require several things. The first is an improved study of the market to determine what the fleet size would be and what the network looks like. Additionally, a detailed mission breakdown is needed for each city pair to determine the 3D distribution of the emissions for the entire fleet. By making this part of the design routine it is possible to study the impact of changing the flight network, cruise altitude and cruise speed at a global scale.

- Once the engine model is capable of analyzing the engine cycle parameters for supersonic and low thrust (e.g. approach, idle) off-design conditions, try to apply different direct emission index estimation methods. It will be particularly interesting to look at engine certification data for the new GE Affinity engine of the Aerion AS2, because it will be one of the first new SST reference engines. The findings could be used to calibrate existing direct emission index estimation methods, or to produce new functions for SSTs. The findings of this engine study can then be used in the global climate impact analysis to better estimate the emitted species for the full network, as well as for the LTO cycle analysis.

This concludes the recommendations for future research related to the current thesis. Note that some more recommendations specific to noise and aircraft design can be found in [7].

Bibliography

[1] Airbus. Global Market Forecast 2017/2036. http://www.airbus.com/aircraft/market/global-market-forecast.html, 2017. Accessed March 6 2018.

[2] United Nations. Paris Agreement. https://unfccc.int/process-and-meetings/the-paris-agreement/the-paris-agreement, 2015. Accessed February 27 2019.

[3] D.S. Lee, D.W. Fahey, P.M. Forster, P.J. Newton, R.C.N. Wit, L.L. Lim, B. Owen, and R. Sausen. Aviation and global climate change in the 21st century. *Atmosperic Environment*, 43(22):3520–3537, 2009.

[4] Y. Sun and H. Smith. Review and prospect of supersonic business jet design. *Progress in Aerospace Sciences*, 90:12–38, December 2016.

[5] D.J. Maglieri. Compilation and Review of Supersonic Business Jet Studies from 1963 through 1995. Contractor Report NASA/CR–2011-217144, NASA, May 2011.

[6] B. Liebhardt and K. Lütjens. An Analysis of the Market Environment for Supersonic Business Jets. In *Deutscher Luft- und Raumfahrtkongress 2011*, January 2011.

[7] J.I. Nijsse. Assessing Supersonic Aircraft Design Sensitivity and Noise Effects. Msc thesis, TU Delft, 2019. Thesis title subject to change. To be published via repository.tudelft.nl in Q4 2019.

[8] M.P. den Boer. Assessing the Impact and Acceptability of Future Supersonic Aircraft. Literature study, TU Delft, July 2018. Study in preparation for this thesis report.

[9] M.H. Sadraey. *Aircraft Design: A Systems Engineering Approach*. John Wiley & Sons Inc., 2012.

[10] G. La Rocca. *Knowledge Based Engineering Techniques to Support Aircraft Design and Optimization*. PhD thesis, TU Delft, April 2011.

[11] R.J.M. Elmendorp. Synthesis of Novel Aircraft Concepts for Future Air Travel. Master's thesis, TU Delft, January 2014.

[12] R.J.M. Elmendorp, R. Vos, and G. La Rocca. A Conceptual Design and Analysis Method for Conventional and Unconventional Airplanes. In *29th Congress of the International Council of the Aeronautical Sciences*. ICAS, September 2014.

[13] J. Roskam. *Part I: Preliminary Sizing of Airplanes*. Airplane Design series. Roskam Aviation and Engineering Corporation, First edition, 1986.

[14] Z. Berdowski, F.N. van den Broek-Serlé, J.T. Jetten, Y. Kawabata, J.T. Schoemaker, and R. Versteegh. Survey on standard weights of passengers and baggage. Published by NEA, May 2009.

[15] F.J. Hale. *Introduction to Aircraft Performance, Selection, and Design*. John Wiley and Sons, First edition, 1984.

[16] G.J.J. Ruijgrok. *Elements of airplane performance*. Delft Academic Press, Second edition, 2009.

[17] L.M. Nicolai and G.E. Carichner. *Fundamentals of Aircraft and Airship Design*, volume Volume I - Aircraft Design of *AIAA Education Series*. AIAA, 2010.

[18] ICAO. Annex 6 Operation of Aircraft: Part I International Commercial Air Transport — Aeroplanes, July 2010. Ninth edition.

[19] E. Torenbeek. *Advanced Aircraft Design: Conceptual Design, Analysis and Optimization of Subsonic Civil Airplanes*. Aerospace Series. John Wiley & Sons, First edition, June 2013.

[20] ICAO. Aircraft Operations - Volume I Flight Procedures, October 2016.

[21] S. Candel. Concorde and the Future of Supersonic Transport. *Journal of Propulsion and Power*, 20(1):59–68, January 2004.

[22] D. Collard. Concorde Airframe Design and Development. In *The Jean J. Ginoux Lecture*. Von Karman Institude for Fluid Dynamics, November 2000.

[23] R. Agosta, D. Bilbija, M. Deutsch, D. Gallant, D. Rose, G. Shreve, D. Smario, and B. Suffredini. The Edge Supersonic Transport. Design Report NASA-CR-192074, California Polytechnic State University, 1992.

[24] R.J. Mack. A Supersonic Business-Jet Concept Designed for Low Sonic Boom. Technical Memorandum TM-2003-212435, NASA, October 2003.

[25] D. Bray, N. Lawson, and S. Harding. Supersonic Business Jet Aircraft Design. In *ICAS 2002 congress*, 2002.

[26] D. Silberhorn and D. Schaupp. Conceptual Design and Analysis of a High-Efficient Low-Emission Supersonic Aircraft HELESA. Stuttgart University, January 2017. Accessed April 12 2018.

[27] R.D. Fitzsimmons. The advanced supersonic transport: what it is and how it compares. *Acta Astronautica*, 4:131–143, 1977.
[28] H.T. Baber and E.E. Swanson. Advanced Supersonic Technology Concept AST-100 Characteristics developed in a Baseline-Update Study. Technical Report NASA/TM X-72815, NASA, January 1976.
[29] J.W. Fenbert, L.P. Ozoroski, K.A. Geiselhart, E.W. Shields, and M.O. McElroy. Concept Development of a Mach 2.4 High-Speed Civil Transport. Technical Report NASA/TP-1999-209694, NASA, December 1999.
[30] G.T. Haglund and S.S. Ogg. Two HSCT Mach 1.7 Low Sonic Boom Designs. In *High-Speed Research: Sonic Boom, volume 2*, pages 65–87, February 1992.
[31] E. Torenbeek, E. Jesse, and M. Laban. Conceptual Design and Analysis of a Mach 1.6 Airliner. In *10th AIAA/ISSMO Multidisciplinary Analysis and Optimization Conference*. AIAA, August 2004. Part of information taken from non-published document.
[32] M.S. Mathieu, A.M. Marin, K.J. Stephenson, J.E. Beard, E. Castillo, C.W. Weaver, D. Teni, and T.T. Takahashi. Preliminary Design of a N+1 Overwater Supersonic Commercial Transport Aircraft. In *AIAA SciTech Forum*. AIAA, January 2017.
[33] J. Morgenstern, N. Norstrud, M. Stelmack, and C. Skoch. Final Report for the Advanced Concept Studies for Supersonic Commercial Transports Entering Service in the 2030 to 2035 Period, N+3 Supersonic Program. Contractor Report NASA/CR-2010-216796, NASA, August 2010.
[34] E. Torenbeek. *Synthesis of Subsonic Airplane Design*. Delft University Press, 1982.
[35] T. Lukaczyk et al. SUAVE: An Open-Source Environment for Multi-Fidelity Conceptual Vehicle Design. In *16th AIAA Multidisciplinary Analysis and Optimization Conference*. AIAA, June 2015.
[36] EASA. Certification Specifications and Acceptable Means of Compliance for Large Aeroplanes CS-25. https://www.easa.europa.eu/regulations, March 2018. Amendment 21. Accessed April 27 2018.
[37] D. Howe. *Aircraft Conceptual Design Synthesis*. Professional Engineering Publishing Limited, First edition, 2000.
[38] J.D. Mattingly, W.H. Heiser, and D.T. Pratt. *Aircraft Engine Design*. AIAA Education Series. AIAA, Second edition, 2002.
[39] P.M. Sforza. *Theory of Aerospace Propulsion*. Elsevier Aerospace Engineering Series. Elsevier Science & Technology, First edition, 2011.
[40] D.R. Ballal and J. Zelina. Progress in Aeroengine Technology (1939-2003). *Journal of Aircraft*, 41(1):43–50, January 2004.
[41] F.S. Mirza-Baig and H.I.H. Saravanamuttoo. Off-Design Performance Prediction of Turbofans using Gasdynamics. In *International Gas Turbine and Aeroengine Congress and Exposition*. American Society of Mechanical Engineers, June 1991.
[42] J. Roskam. *Part II: Preliminary Configuration Design and Integration of the Propulsion System*. Airplane Design series. Roskam Aviation and Engineering Corporation, First edition, 1986.
[43] D. Lednicer. The Incomplete Guide to Airfoil Usage. https://m-selig.ae.illinois.edu/ads/aircraft.html. Accessed September 10 2018.
[44] Z. Lei. Flow Simulation of a Supersonic Transport Configuration at Low-Speed and High-Lift Conditions. *Journal of Aircraft*, 45(5):1514–1521, September 2008.
[45] D.L. Allison, C.C. Morris, J.A. Schetz, R.K. Kapania, and L.T. Watson. Reevaluating conceptual design fidelity: An efficient supersonic air vehicle design case. *Proceedings of the Institution of Mechanical Engineers, Part G: Journal of Aerospace Engineering*, 230(3):581–598, March 2016.
[46] H.W. Carlson and M.J. Mann. Survey and Analysis of Research on Supersonic Drag-Due-to-Lift Minimization With Recommendations for Wing Design. Technical Report NASA TP-3202, NASA, 1992.
[47] C.L. Ladson and C.W. Brooks. Development of a Computer Program to Obtain Ordinates for NACA 6- and 6A-series Airfoils. Technical Report NASA TM X-3069, NASA, September 1974.
[48] L.K. Loftin. Theoretical and Experimental Data for a number of NACA 6A-series Airfoil Sections. Technical Report RM L6J01, NACA, December 1946.
[49] D.E. Hoak and R.D. Finck. USAF Stability and Control DATCOM Volume 2. Technical report, USAF, April 1978.
[50] D.P. Raymer. *Aircraft Design: A Conceptual Approach*. AIAA Education Series. AIAA, Second edition, 1992.
[51] J.E. Williams and S.R. Vukelich. The USAF Stability and Control Digital DATCOM Volume I Users Manual. Technical Report TR-79-3032 VOL1, USAF, April 1979.
[52] R.M. Snow and E.A. Bonney. Aerodynamic Characteristics of Wings at Supersonic Speeds. Bumblebee series no. 55, Johns Hopkins University, March 1947.

[53] F.E. McLean and D.E. Fuller. Effects of Thickness on Supersonic Performance of a Wing-Body Configuration Employing a Warped Highly Swept Arrow Wing. Technical Note TN D-3034, NASA, October 1965.
[54] C.S. Leyman. A Review of the Technical Development of Concorde. *Progress in Aerospace Sciences*, 23:185–238, 1986.
[55] E.C. Polhamus. Charts for Predicting the Subsonic Vortex-Lift Characteristics of Arrow, Delta and Diamond Wings. Technical Report TN D-6243, NASA, April 1971.
[56] S. Corda, M.T. Stephenson, F.W. Burcham, and R.E. Curry. Dynamic Ground Effects Flight Test of an F-15 Aircraft. Technical Report TM-4604, NASA, September 1994.
[57] R. Blockley and W. Shyy. *Encyclopedia of Aerospace Engineering*. John Wiley & Sons, First edition, December 2010.
[58] I. Gursul, Z. Wang, and E. Vardaki. Review of flow control mechanisms of leading-edge vortices. *Progress in Aerospace Sciences*, 43(7-8):246–270, October 2007.
[59] J.E. Lamar and J.F. Campbell. Vortex flaps- advanced control devices for supercruise fighters. *Aerospace America*, pages 95–99, January 1984.
[60] E. Obert. *Aerodynamic Design of Transport Aircraft*. IOS Press, First edition, 2009.
[61] P. Sturdza. Extensive Supersonic Natural Laminar Flow on the Aerion Business Jet. In *45th AIAA Aerospace Sciences Meeting and Exhibit*. AIAA, January 2007.
[62] M.N.D. Scholz. Estimating the Oswald Factor from Basic Aircraft Geometrical Parameters. In *Deutscher Luft- und Raumfahrtkongress 2012*. DLR, 2012.
[63] R.S. Feagin and W.D. Morrison. Delta Method, an Empirical Drag Buildup Technique. Technical Report NASA CR-151971, Lockheed California, December 1978.
[64] R.S. Shevell. *Fundamentals of Flight*. Prentice Hall, Second edition, 1989.
[65] I Kroo and R. Shevell. *Aircraft Design: Synthesis and Analysis*. Desktop Aeronautics, January 2001. Digital version 0.99.
[66] H.W. Carlson, M.O. McElroy, W.B. Lessard, and L.A. McCullers. Improved Method for Prediction of Attainable Wing Leading-Edge Thrust. Technical Paper TP-3557, NASA, April 1996.
[67] H.W. Carlson and M.J. Mann. Survey and Analysis of Research on Supersonic Drag-Due-to-Lift Minimization With Recommendations for Wing Design. Technical Paper TP-3202, NASA, September 1992.
[68] B. Demarest, K. Anders, J. Manchec, E. Yang, D. Overgaard, and M. Kalkwarf. MM-122 High Speed Civil Transport. Technical report, California Polytechnic State University, June 1992. Published by NASA as NASA-CR-192011.
[69] J. Roskam. *Part V: Component Weight Estimation*. Airplane Design series. Roskam Aviation and Engineering Corporation, First edition, 1986.
[70] S. Özgen. AE 452 Aeronautical Engineering Design II: Air Loads. http://www.ae.metu.edu.tr/~ae452/lecture2_air_loads.pdf, February 2017. Accessed July 14 2018.
[71] M. Neubauer and G. Günther. Aircraft Loads. In *RTO AVT Lecture Series on Aging Aircraft Fleets: Structural and Other Subsystem Aspects*, November 2000.
[72] M.C. Niu. *Airframe Structural Design*. Conmilit Press Ltd., Eighth edition, January 1988.
[73] D.P. Wells, B.L. Horvath, and L.A. McCullers. The Flight Optimization System Weights Estimation Method. Technical Report NASA/TM-2017-219627/Volume I, NASA, June 2017.
[74] A.T. Isikveren. *Quasi-Analytical Modelling and Optimisation Techniques for Transport Aircraft Design*. PhD thesis, Royal Institute of Technology (KTH) Stockholm, May 2002.
[75] G.J. Harloff and B.M. Berkowitz. HASA-Hypersonic Aerospace Sizing Analysis for the Preliminary Design of Aerospace Vehicles. Contractor Report NASA-CR-182226, NASA, November 1988.
[76] A.S. Walker. *Development of a Conceptual Flight Vehicle Design Weight Estimation Method Library and Documentation*. Master's thesis, University of Texas, May 2014.
[77] D. Scholz. An Optional APU for Passenger Aircraft. In *5th CAES Air & Space Conference*, 2015.
[78] E. Reshotko, G. Garbinsky, J. Fellenstein, P. Struk, M. Taillon, G. Warzynski, J. Hooper, M. Ryan, B. Taggart, and M. Botting. Tesseract Supersonic Business Transport. Design Report NASA-CR-192072, Western Reserve University, 1992.
[79] R.I. Jones. The more electric aircraft–assessing the benefits. *Proceedings of the Institution of Mechanical Engineers, Part G: Journal of Aerospace Engineering*, 216(5):259–269, May 2002.
[80] B.H. Nya, J. Brombach, and D. Schulz. Benefits of Higher Voltage Levels in Aircraft Electrical Power Systems. In *2012 Electrical Systems for Aircraft, Railway and Ship Propulsion*. IEEE, October 2012.

[81] R. Abdel-Fadil, A. Eid, and M. Abdel-Salam. Electrical Distribution Power Systems of Modern Civil Aircraft. In *2nd International Conference on Energy Systems and Technologies*, February 2013.

[82] Boeing Commercial Airplanes. 737 Airplane Characteristics for Airport Planning. http://www.boeing.com/assets/pdf/commercial/airports/acaps/737.pdf, September 2013. Accessed August 9 2018.

[83] M. Sharpe and R. Shaw. *Boeing 737-100 and 200*. MBI Publishing Company, 2001.

[84] H. Mizuno, S. Hagiwara, T. Hanai, and H. Takami. Feasibility Study on the Second Generation SST. In *AIAA Aircraft Design Systems and Operations Meeting*. AIAA, September 1991.

[85] B. Sarlioglu and C.T. Morris. More Electric Aircraft: Review, Challenges, and Opportunities for Commercial Transport Aircraft. *IEEE Transactions on Transportation Electrification*, 1(1):54–64, May 2015.

[86] S.V. Venna, Y. Lin, and G. Botura. Piezoelectric Transducer Actuated Leading Edge De-Icing with Simultaneous Shear and Impulse Forces. *Journal of Aircraft*, 44(2):509–515, March 2007.

[87] ICAO. Environmental Protection Volume II: Aircraft Engine Emissions. Technical Report Annex 16, ICAO, July 2008. Including amendment 8.

[88] M. Winther and K. Rypdal et al. EMEP/EEA air pollutant emission inventory guidebook 2016 - Update July 2017. Technical report, EEA, July 2017.

[89] S.A. Shakariyants. *Generic Methods for Aero-Engine Exhaust Emission Prediction*. Phd thesis, TU Delft, September 2008.

[90] ICAO. Environmental Protection Volume III: CO2 Certification Requirement. Technical report, ICAO, March 2017. Document used is not original ICAO document but converted version of https://www.easa.europa.eu/document-library/notices-of-proposed-amendment/npa-2017-01. It can be assumed that this text is very similar (if not identical) to the final version of the 1st edition. Accessed June 6 2018.

[91] The International Council on Clean Transportation. International Civil Aviation Organization's CO2 certification requirement for new aircraft. https://www.theicct.org/sites/default/files/publications/ICCTupdate_ICAO_CO2cert_aug2013a.pdf, August 2013. Accessed January 16 2019.

[92] International Council on Clean Transportation. International Civil Aviation Organization's CO2 Standard for New Aircraft, January 2017. Accessed January 16 2019 via https://www.theicct.org/publications/international-civil-aviation-organization-co2-standard-new-aircraft.

[93] A. Kharina, T. MacDonald, and D. Rutherford. Environmental performance of emerging supersonic transport aircraft. Working paper 2018-12, The International Council on Clean Transportation, July 2018. Accessed January 16 2019 via https://www.theicct.org/publications/environmental-performance-emerging-commercial-supersonic-aircraft.

[94] V. Grewe, A. Stenke, M. Plohr, and V.D. Korovkin. Climate functions for the use in multi-disciplinary optimisation in the pre-design of supersonic business jet. *The Aeronautical Journal*, 114(1154):259–269, April 2010.

[95] A. Dopelheuer and M. Lecht. Influence of engine performance on emission characteristics. In *RTO AVT Symposium on Gas Turbine Engine Combustion, Emissions and Alternative Fuels*. RTO, October 1998.

[96] S.L. Baughcum, T.G. Tritz, S.C. Henderson, and D.C. Pickett. Scheduled Civil Aircraft Emission Inventories for 1992: Database Development and Analysis. Contractor Report CR-4700, NASA, April 1996.

[97] M.J. Prather, H.L. Wesoky, R.C. Miake-Lye, A.R. Douglass, R.P. Turco, D.J. Wuebbles, M.K.W. Ko, and A.L. Schmeltekopf. The Atmospheric Effects of Stratospheric Aircraft: A First Program Report. Reference Publicration RP-1272, NASA, January 1992.

[98] D.W. Fahey et al. Emission Measurements of the Concorde Supersonic Aircraft in the Lower Stratosphere. *Science*, 270(5233):70–74, October 1995.

[99] V. Grewe et al. Climate impact of supersonic air traffic: an approach to optimize a potential future supersonic fleet–results from the EU-project SCENIC. *Atmospheric Chemistry and Physics*, 7(19):5129–5145, October 2007.

[100] V. Grewe et al. Estimates of the climate impact of future small-scale supersonic transport aircraft–results from the HISAC EU-project. *The Aeronautical Journal*, 114(1153):199–206, March 2010.

[101] D.S. Lee et al. Transport impacts on atmosphere and climate: Aviation. *Atmospheric Environment*, 44(37):4678–4734, 2010.

[102] S.R.H. Barrett, R.E. Britter, and I.A. Waitz. Global Mortality Attributable to Aircraft Cruise Emissions. *Environmental Science & Technology*, 44(19):7736–7742, September 2010.

[103] A. Agarwal, R.L. Speth, T.M. Fritz, S.D. Jacob, T. Rindlisbacher, R. Iovinelli, B. Owen, R.C. Miake-Lye, J.S. Sabnis, and S.R.H. Barrett. SCOPE11 Method for Estimating Aircraft Black Carbon Mass and Particle Number Emissions. *Environmental Science & Technology*, 53(3):1364–1373, January 2019.

[104] M.E.J. Stettler, J.J. Swanson, S.R.H. Barrett, and Boies A.M. Updated Correlation Between Aircraft Smoke Number and Black Carbon Concentration. *Aerosol Science and Technology*, 47(11):1205–1214, 2013.

[105] R.L. Wayson, G.G. Fleming, and R. Iovinelli. Methodology to Estimate Particulate Matter Emissions from Certified Commercial Aircraft Engines. *Journal of the Air & Waste Management Association*, 59(1):91–100, January 2009.

[106] U. Schumann. On conditions for contrail formation from aircraft exhausts. *Meteorologische Zeitschrift*, 5:4–23, February 1996.

[107] C. Fichter, S. Marquart, R. Sausen, and D.S. Lee. The impact of cruise altitude on contrails and related radiative forcing. *Meteorologische Zeitschrift*, 14(4):563–572, August 2005.

[108] A. Elham, G. La Rocca, and M.J.L. van Tooren. An Advanced Quasi-Analytical Weight Estimation Method for Airplane Lifting Surfaces. In *71st International Conference on Mass Properties*. Society of Allied Weight Engineers, May 2012.

[109] J.J. Berton, W.J. Haller, P.F. Senick, S.M. Jones, and J.A. Seidel. A Comparative Propulsion System Analysis for the High-Speed Civil Transport. Technical Memorandum NASA/TM—2005-213414, NASA, February 2005.

[110] J. Whurr. Propulsion system concepts and technology requirements for quiet supersonic transports. *International Journal of Aeroacoustics*, 3(3):259–270, 2004.

[111] GasTurb GmbH. *GasTurb 13: Design and Off-Design Performance of Gas Turbines*. GasTurb GmbH, 2018. Accessed January 16 2019 via http://www.gasturb.de/.

[112] W.P.J. Visser, O. Kogenhop, and M. Oostveen. A Generic Approach for Gas Turbine Adaptive Modeling. *Journal of Engineering for Gas Turbines and Power*, 128(1):13–19, January 2006.

[113] S.O.L. Zijp. Development of a Life Cycle Cost Model for Conventional and Unconventional Aircraft. Master's thesis, TU Delft, June 2014. Accessed October 14 2018 via repository.tudelft.nl.

[114] R.L.A. de Jonge. Development of a Knowledge- Based Engineering Application to Support Conceptual Fuselage Sizing and Cabin Configuration. Master's thesis, TU Delft, January 2017. Accessed March 17 2019 via repository.tudelft.nl.

[115] A.W. Robins, S.M. Dollyhigh, F.L. Beissner, K.A. Geiselhart, G.L. Martin, E.W. Shields, E.E. Swanson, P.G. Coen, and S.J. Morris. Concept Development of a Mach 3.0 High-Speed Civil Transport. Technical Memorandum TM-4058, NASA, 1988.

[116] C.S. Domack, S.M. Dollyhigh, F.L. Beissner, K.A. Geiselhart, M.E. McGraw, E.W. Shields, and E.E. Swanson. Concept Development of a Mach 4 High-Speed Civil Transport. Technical Memorandum TM-4223, NASA, 1990.

[117] V.R. Mascitti. A Preliminary Study of the Performance and Characteristics of a Supersonic Executive Aircraft. Technical Memorandum TM-74055, NASA, September 1977.

[118] M. Wintzer, P. Sturdza, and I. Kroo. Conceptual Design of Conventional and Oblique Wing Configurations for Small Supersonic Aircraft. In *44th AIAA Aerospace Sciences Meeting and Exhibit*. AIAA, January 2006.

[119] D.E. Fetterman. Preliminary Sizing and Performance of Aircraft. Technical Memorandum TM-86357, NASA, July 1985.

[120] R.J. Mack. A Rapid Empirical Method for Estimating the Gross Takeoff Weight of a High Speed Civil Transport. Technical Memorandum NASA/TM-1999-209535, NASA, December 1999.

[121] NASA. High-Speed Research — The Tu-144LL: A Supersonic Flying Laboratory. https://www.nasa.gov/centers/langley/pdf/70817main_FS-1996-09-18-LaRC.pdf, 1996. Accessed June 26 2018.

[122] J.F. Dugan. Preliminary Study of Supersonic-Transport Configuration with low values of Sonic Boom. Technical Memorandum NASA/TM X-2746, Lewis Research Center, March 1973.

[123] J. Morgenstern et al. Advanced Concept Studies for Supersonic Commercial Transports Entering Service in the 2018-2020 Period Phase 2. Contractor Report NASA/CR-2015-218719, NASA, July 2015.

[124] D.C. Aronstein and K.L. Schueler. Two Supersonic Business Aircraft Conceptual Designs, With and Without Sonic Boom Constraint. *Journal of Aircraft*, 42(3):775–786, May 2005.

[125] Y. Sun and H. Smith. Supersonic Business Jet Conceptual Design in a Multidisciplinary Design Analysis Optimization Environment. In *AIAA SciTech Forum*. AIAA, January 2018.

[126] Boeing. 777-200LR/-300ER/-Freighter Airplane Characteristics for Airport Planning. http://www.boeing.com/assets/pdf/commercial/airports/acaps/777_2lr3er.pdf, October 2001. Revision-E May 2015. Accessed October 11 2018.

[127] Boeing. 777-200/300 Airplane Characteristics for Airport Planning. http://wpage.unina.it/fabrnico/DIDATTICA/PGV/Specifiche_Esercitazioni/B777/Manuale%20777_23.pdf, February 1992. Revision October 2004. Accessed October 11 2018.
[128] Airbus. A330 Aircraft Characteristics Airport and Maintenance Planning. https://www.airbus.com/content/dam/corporate-topics/publications/backgrounders/techdata/aircraft_characteristics/Airbus-Commercial-Aircraft-AC-A330.pdf, January 1993. Revision July 2018. Accessed October 11 2018.
[129] Airbus. A321 Aircraft Characteristics Airport and Maintenance Planning. https://www.airbus.com/aircraft/support-services/airport-operations-and-technical-data/aircraft-characteristics.html, September 1992. Revision Feb 01/18. Accessed October 29 2018.
[130] Boeing. 787 Airplane Characteristics for Airport Planning. https://www.boeing.com/commercial/airports/plan_manuals.page, April 2006. Revision M March 2018. Accessed October 29 2018.
[131] É. Roux. *Avions civils à réaction : plan 3 vues et données caractéristiques*. Elodie Roux, May 2007.
[132] J.E. Williams and S.R. Vukelich. The USAF Stability and Control Digital DATCOM Volume II Implementation of Datcom Methods. Technical Report TR-79-3032 VOL2, USAF, April 1979.
[133] J.E. Williams and S.R. Vukelich. The USAF Stability and Control Digital DATCOM Volume III Users Manual. Technical Report TR-79-3032 VOL3, USAF, April 1979.
[134] E.C. Polhamus. A Concept of the Vortex Lift of Sharp-Edge Delta Wings based on a Leading-Edge-Suction Analogy. Technical Note TN D-3767, NASA, December 1966.
[135] E.C. Polhamus. Application of the Leading-Edge-Suction Analogy of Vortex Lift to the Drag Due to Lift of Sharp-edge Delta Wings. Technical Note TN D-4739, NASA, August 1968.
[136] J.E. Lamar. Extension of Leading-Edge-Suction Analogy to Wings with Separated Flow around the Side Edges at Subsonic Speeds. Technical Report TR R-428, NASA, October 1974.
[137] S. Lee. An Analytical Representation of Delta Wing Aerodynamics. In *4th AIAA Theoretical Fluid Mechanics Meeting*. AIAA, June 2005.
[138] J. Winchester. *Jet Fighters: Inside & Out*. The Rosen Publishing Group, December 2011.
[139] ESDU. External wave drag at zero incidence in inviscid flow of simple ducted forebodies and truncated afterbodies. Data Item Bodies S.02.03.02, 1981.
[140] D. Küchemann. *The Aerodynamic Design of Aircraft*. AIAA, First edition, 2012. Original book published in 1978.
[141] R.M. Wood. Supersonic Aerodynamics of Delta Wings. Technical Paper TP-2771, NASA, March 1988.
[142] E.J. Jumper. Wave Drag Prediction Using a Simplified Supersonic Area Rule. *Journal of Aircraft*, 20(10):893–895, October 1983.
[143] R.T. Jones. Properties of low-aspect-ratio pointed wings at speeds below and above the speed of sound. Technical Report TR-835, NACA, January 1946.
[144] G.R. Saaris, E.N. Tinoco, J.L. Lee, and P.E. Rubbert. *A5021 User's Manual PAN AIR Technology Program for Solving Problems of Potential Flow about Arbitrary Configuration*. Boeing, February 1992.
[145] W.H. Mason and B.S. Rosen. The COREL and W12SC3 Computer Programs for Supersonic Wing Design and Analysis. Contractor Report CR-3676, NASA, December 1983.
[146] R.V. Harris. An Analysis and Correlation of Aircraft Wave Drag. Technical Memorandum TM X-947, NASA, March 1964.
[147] W.J. Fredericks, K.R. Antcliff, G. Costa, N. Deshpande, M.D. Moore, E.A. San Miguel, and A.N. Snyder. Aircraft Conceptual Design Using Vehicle Sketch Pad. In *48th AIAA Aerospace Sciences Meeting Including the New Horizons Forum and Aerospace Exposition*. AIAA, January 2010.
[148] M.J. Waddington. Development of an Interactive Wave Drag Capability for the OpenVSP Parametric Geometry Tool. Master's thesis, California Polytechnic State University, July 2015.
[149] F. Palacios, M.R. Colonno, A.C. Aranake, A. Campos, S.R. Copeland, T.D. Economon, A.K. Lonkar, T.W. Lukaczyk, T.W.R. Taylor, and J.J. Alonso. Stanford University Unstructured (SU2): An open-source integrated computational environment for multi-physics simulation and design. In *51st AIAA Aerospace Sciences Meeting including the New Horizons Forum and Aerospace Exposition*. AIAA, January 2013.
[150] Z. Lei. Flow Simulation of a Supersonic Transport Configuration at Low-Speed and High-Lft Conditions. *Journal of Aircraft*, 45(5):1514–1521, September 2008.
[151] B. Singh. A Medium-Fidelity Method for Rapid Maximum Lift Estimation. Master's thesis, TU Delft, January 2017. Available via repository.tudelft.nl. Accessed May 30 2018.
[152] J. Vargas. Development of a Wave Drag Prediction Tool for the Conceptual Design Phase. Master's thesis, TU Delft, July 2015. Available through repository.tudelft.nl. Accessed October 10 2018.

[153] B. Chudoba, G. Coleman, A. Oza, and P.A. Czysz. What price supersonic speed? A design autonomy of supersonic transportation - Part 1. *The Aeronautical Journal*, 112(1129):141–151, March 2008.
[154] B. Chudoba, A. Oza, K. Roberts, B. Mixon, B. Mixon, G. Coleman, and P.A. Czysz. What Price Supersonic Speed? -An Applied Market Research Case Study - Part 2. In *45th AIAA Aerospace Sciences Meeting and Exhibit*. AIAA, 2007.
[155] B. Liebhardt, K. Lütjens, and V. Gollnick. Estimation of the Market Potential for Supersonic Airliners via Analysis of the Global Premium Ticket Market. In *Aviation Technology, Integration, and Operations (ATIO) Conference 2011*. AIAA, September 2011.
[156] P.A. Henne. Case for Small Supersonic Civil Aircraft. *Journal of Aircraft*, 42(3):765–774, May 2005.
[157] B. Sweetman. Skunk Works plans worldwide network of Thunderbirds-style supersonic jets. http://archive.li/UktFb#selection-479.0-479.73, July 2006. Accessed March 7 2018.
[158] S. Horinouchi. Conceptual Design of a Low Boom SSBJ. In *43rd AIAA Aerospace Sciences Meeting and Exhibit*. AIAA, January 2005.
[159] G. Müller et al. *Handbook of Engineering Acoustics*. Springer, First edition, 2013.
[160] B.M. Sullivan, J. Klos, R.D. Buehrle, D.A. McCurdy, and E.A. Haering. Human Response to Low-Intensity Sonic Booms Heard Indoors and Outdoors. Technical Memorandum NASA/TM-2010-216685, NASA, April 2010.
[161] K.D. Kryter, P.J. Johnson, and J.R. Young. Psychological Experiments on Sonic Booms Conducted at Edwards Air Force Base. Final Report AD689844, Stanford Research Institute, August 1968.
[162] P.N. Borsky. Community Reactions to Sonic Booms in the Oklahoma City Area. Report AD625332, National Opinion Research Center, October 1965.
[163] J.D. Leatherwood, B.M. Sullivan, K.P. Shepherd, D.A. McCurdy, and S.A. Brown. Summary of recent NASA studies of human response to sonic booms. *The Journal of the Acoustical Society of America*, 111(1):586–598, 2002.
[164] D.J. Maglieri, P.J. Bobbitt, K.J. Plotkin, K.P. Shepherd, P.G. Coen, and D.M. Richwine. Sonic Boom: Six Decades of Research. Technical Report NASA/SP-2014-622, NASA, 2014.
[165] N. Dickson. ICAO Noise Standards. https://www.icao.int/Meetings/Green/Documents/day%201pdf/session%202/2-Dickson.pdf, May 2013. Accessed March 24 2018.
[166] J.J. Berton, S.M. Jones, J.A. Seidel, and D.L. Huff. Noise predictions for a supersonic business jet using advanced take-off procedures. *The Aeronautical Journal*, pages 1–16, 2018.
[167] Federal Aviation Administration. Stage 5 Airplane Noise Standards. https://www.federalregister.gov/documents/2017/10/04/2017-21092/stage-5-airplane-noise-standards, October 2017.
[168] National Research Council. *Commercial Supersonic Technology The Way Ahead*. National Academies Press, 2001.
[169] K. Saha. *The Earth's Atmosphere: It's Physics and Dynamics*. Springer, First edition, 2008.
[170] NASA, NOAA, and USAF. U.S. Standard Atmosphere 1976. Technical Report NASA-TM-X-74335, NOAA-S/T-76-1562, NASA, NOAA and USAF, October 1976.
[171] R. Sausen and U. Schumann. Estimates of the Climate Response to Aircraft CO_2 and NOx Emissions Scenarios. *Climatic Change*, 44(1):27–58, January 2000.
[172] K. Dahlmann, C. Fichter, V. Grewe, B. Kärcher, R. Sausen, U. Schumann, A. Koch, and V. Gollnick. Climate impact evaluation as part of aircraft pre-design. In *9th AIAA Aviation Technology, Integration, and Operations Conference (ATIO)*. AIAA, September 2009.
[173] H. Akimoto. *Atmospheric Reaction Chemistry*. Springer, First edition, 2016.
[174] J.C. McConnell and J.J. Jin. Stratospheric ozone chemistry. *Atmosphere-Ocean*, 46(1):69–92, 2008.
[175] M. Dutta, K. Patten, and D. Wuebbles. Parametric Analyses of Potential Effects on Stratospheric and Tropospheric Ozone Chemistry by a Fleet of Supersonic Business Jets Projected in a 2020 Atmosphere. Contractor Report 2004-213306, NASA, October 2004.
[176] L.J. Wilcox, K.P. Shine, and B.J. Hoskins. Radiative forcing due to aviation water vapour emissions. *Atmospheric Environment*, 63:1–13, 2012.
[177] A. Kugele, F. Jelinek, and R. Gaffal. Aircraft Particulate Matter Emission Estimation through all Phases of Flight. Report EEC/SEE/2005/0014, EUROCONTROL, 2005.
[178] M. Masiol and R.M. Harrison. Aircraft engine exhaust emissions and other airport-related contributions to ambient air pollution: A review. *Atmospheric Environment*, 95:409–455, October 2014.
[179] B.E. Anderson et al. Experiment to Characterize Aircraft Volatile Aerosol and Trace-Species Emissions (EXCAVATE). Technical Memorandum NASA/TM-2005-213783, NASA, August 2005.

[180] Embraer. Embraer 190 Airport Planning Manual. https://www.embraercommercialaviation.com/commercial-jets/e190/, August 2005. Revision 14 May 25 2018. Accessed May 5 2019.

[181] Airbus. A319 Aircraft Characteristics Airport and Maintenance Planning. https://www.airbus.com/aircraft/support-services/airport-operations-and-technical-data/aircraft-characteristics.html, July 1995. Revision Feb 01/19. Accessed May 5 2019.

[182] Airbus. A320 Aircraft Characteristics Airport and Maintenance Planning. https://www.airbus.com/aircraft/support-services/airport-operations-and-technical-data/aircraft-characteristics.html, September 1985. Revision Feb 01/19. Accessed May 5 2019.

[183] Airbus. A350 Aircraft Characteristics Airport and Maintenance Planning. https://www.airbus.com/aircraft/support-services/airport-operations-and-technical-data/aircraft-characteristics.html, November 2016. Revision Jun 01/18. Accessed January 31 2019.

[184] Airbus. A340-500/-600 Aircraft Characteristics Airport and Maintenance Planning. https://www.airbus.com/aircraft/support-services/airport-operations-and-technical-data/aircraft-characteristics.html, April 2001. Revision Jul 01/18. Accessed January 14 2019.

[185] N. Chandrasekaran and A. Guha. Study of Prediction Methods for NOx Emission from Turbofan Engines. *Journal of Propulsion and Power*, 28(1):170–180, January 2012.

[186] N.E. Antoine and I.M. Kroo. Framework for Aircraft Conceptual Design and Environmental Performance Studies. *AIAA Journal*, 43(10):2100–2109, October 2005.

[187] R.P. Henderson, J.R.R.A. Martins, and R.E. Perez. Aircraft Conceptual Design for Optimal Environmental Performance. *The Aeronautical Journal*, 116(1175):1–22, January 2012.

[188] M. Schaefer and S. Bartosch. Overview on fuel flow correlation methods for the calculation of NOx, CO and HC emissions and their implementation into aircraft performance software. Internal Communication IB-325-11-13, Deutsches Zentrum für Luft- und Raumfahrt (DLR), July 2013. Accessed February 13 2019 via https://www.researchgate.net/publication/271210746_Overview_on_fuel_flow_correlation_methods_for_the_calculation_of_NOx_CO_and_HC_emissions_and_their_implementation_into_aircraft_performance_software.

[189] D.L. Allaire. A Physics-Based Emissions Model for Aircraft Gas Turbine Combustors. Master's thesis, Massachusetts Institute of Technology, May 2006.

[190] M.G. Turner, A. Norris, and J.P. Veres. High-Fidelity Three-Dimensional Simulation of the GE90. In *33rd AIAA Fluid Dynamics Conference and Exhibit*. AIAA, June 2003.

[191] D.L. Daggett. Water Misting and Injection of Commercial Aircraft Engines to Reduce Airport NOx. Contractor Report 2004-212957, NASA, March 2004.

[192] M.V. Morales and C.A. Hall. Modeling Performance and Emissions from Aircraft for the Aviation Integrated Modelling Project. *Journal of Aircraft*, 47(3):812–819, May 2010.

[193] K.G. Kyprianidis, D. Nalianda, and E. Dahlquist. A NOx Emissions Correlation for Modern RQL Combustors. *Enery Procedia*, 75:2323–2330, August 2015.

[194] N.K. Rizk and H.C. Mongia. Semianalytical Correlations for NOx, CO, and UHC Emissions. In *International Gas Turbine and Aeroengine Congress and Exposition*. ASME, June 1992.

[195] F. Jelinek, S. Carlier, and J. Smith. The Advanced Emission Model (AEM3) - Validation Report. Report EEC/SEE/2004/004, EUROCONTROL, 2004. Appendices A, B and C.

[196] B. Kim et al. SAGE System for assessing Aviation's Global Emissions Technical Manual. Report FAA-EE-2005-01, FAA, September 2005.

[197] S. Herndon, E. Wood, J. Franklin, R. Miake-Lye, W.B. Knighton, M. Babb, A. Nakahara, T. Reynolds, and H. Balakrishnan. Measurement of Gaseous HAP Emissions from Idling Aircraft as a Function of Engine and Ambient Conditions. ACRP Report 63, National Academies of Sciences, Engineering, and Medicine, 2012.

[198] F. Deideweg, A. Döpelheuer, and M. Lecht. Methods to Assess Aircraft Engine Emissions in Flight. In *ICAS 1996 Proceedings*. AIAA, September 1996.

[199] B. Graver and D. Rutherford. Transatlantic Airline Fuel Efficiency Ranking, 2017. White paper, The International Council on Clean Transportation, September 2018.

[200] B. Graver and D. Rutherford. Transpacific Airline Fuel Efficiency Ranking, 2016. White paper, The International Council on Clean Transportation, January 2018.

[201] H. Bofinger and J. Strand. Calculating the Carbon Footprint from Different Classes of Air Travel. Policy Research Working Paper 6471, The World Bank Development Research Group, May 2013.

[202] G. Pitari et al. Radiative forcing from particle emissions by future supersonic aircraft. *Atmos. Chem. Phys.*, 8(14):4069–4084, 2008.

[203] V. Grewe and A. Stenke. AirClim: an efficient tool for climate evaluation of aircraft technology. *Atmospheric Chemistry and Physics*, 8:4621–4639, 2008.

[204] R. Hein, M. Dameris, C. Schnadt, C. Land, and V. Grewe et al. Results of an interactively coupled atmospheric chemistry general circulation model: Comparison with observations. *Annales Geophysicae*, 19(4):435–457, 2001.

[205] R.T. Jones. The oblique wing-aircraft design for transonic and low supersonic speeds. *Acta Astronautica*, 4:99–109, 1977.

[206] A.J.M. Van der Velden and I. Kroo. The Aerodynamic Design of the Oblique Flying Wing Supersonic Transport. Contractor Report NASA/CR-177552, NASA, June 1990.

[207] T. Galloway, P. Gelhausen, M. Moore, and M. Waters. Oblique Wing Supersonic Transport Concepts. In *AIAA Aircraft Design Systems Meeting*. AIAA, August 1992.

[208] M. Waters, M. Ardema, C. Roberts, and I. Kroo. Structural and Aerodynamic Considerations for an Oblique All-Wing Aircraft. In *AIAA Aircraft Design Systems Meeting*. AIAA, August 1992.

[209] P. Li, R. Seebass, and H. Sobieczky. The Sonic Boom of an Oblique Flying Wing SST. In *1st Joint aeroacoustics conference*. Deutsche Gesellschaft fur Luft- und Raumfahrt, 1995.

[210] G. Zha, H. Im, and D. Espinal. Toward Zero Sonic Boom and High Efficiency Supersonic Flight, Part I: A Novel Concept of Supersonic Bi-Directional Flying Wing. In *48th AIAA Aerospace Sciences Meeting Including the New Horizons Forum and Aerospace Exposition*. AIAA, January 2010.

A
Program support

This appendix is created to give a future user additional information about the program. This is done by looking at the installation, setup and inputs, work flow, outputs and the division of the work on the program. It should be noted that the level of detail is limited and that further understanding requires studying the full program.

A.1. User guide

This section aims to provide the user with some more information about the program, such as installation setup, and required packages.

A.1.1. Program information

The program is written in Python 2.7. This means that it is not directly compatible with the newer Python 3, which uses a slightly different syntax. The choice to use 2.7 was made because some packages used are not yet functional for Python 3. For the inputs of the program, Excel sheets are used since they allow for a good overview and conditional formatting to provide some feedback to the user on their inputs. For future users, it might be better to switch to csv files instead, because of their better compatibility. If the user wants to modify the inputs it is recommended that Microsoft Excel is installed although there is also the option to use other programs such as Google Spreadsheets and LibreOffice. These allow the user to open .xlsx files, alter them, and then save the modified version as a .xlsx file, which should be compatible with the design program. The main output of the program is a pdf document which can be opened using programs like Adobe Acrobat Reader or even a web browser.

A.1.2. Installation

The design program is currently not an executable and should instead be run by the user through an integrated development environment (IDE). Some examples of IDEs which are free to download are PyCharm[1], Spyder[2] and PyDev[3]. After installing an IDE, the folder (or zip-file) containing the design program should be downloaded and stored on the computer. Within the main folder there is a file called *run_master.py*. Using the IDE in the storage location, this file should be opened. This file is used to run the design program.

When installing a Python IDE a large number of additional packages are usually also included. The full design program will require a few packages which might not be among those 'standard' packages. These are listed below along with a short description of what they are used for:

- numpy/scipy: Numerical packages for Python which allows the user to apply operations such as interpolation, but also optimization routines if needed.
- matplotlib: Package which provides Python with many options for the visualization of data originating from the different modules. It is used to produce all graphs shown in the outputs.
- warnings: Package which allows for Python to print warning messages in the console so that the user can be informed of known issues which could affect the results.
- openpyxl: A package allowing for Python to interact with Excel sheets. These are used to provide the different inputs required by the program so that it can be run successfully.

[1] https://www.jetbrains.com/pycharm/ (accessed December 28 2018)
[2] https://www.spyder-ide.org/ (accessed December 28 2018)
[3] http://www.pydev.org/ (accessed December 28 2018)

- sympy: A package for scientific computations in Python which offers the ability to solve, or rewrite (complex) equations. It is used by the Class I module to directly solve equations for the aircraft takeoff weight value.
- reportlab: A package for Python which can be used to automatically generate pdf documents. It is used in the output writer to produce the pdf showing the performance and other attributes of the final aircraft design.

To try to prevent the user from having to install those packages themselves, a small routine has been added which will check the presence of the various packages and prompt a message if one or more are missing. The user can then decide whether the packages should be installed automatically or choose to install them manually. While this method has been tested, it is still prone to errors, and also requires that 'pip' is installed, which is a package manager for Python.

A.1.3. ParaPy

ParaPy is another package for Python but is mentioned separately because it is different from the other packages discussed previously, as it is not open-source. Instead, it is a package which requires a license in order to be installed and executed. Through contacts at the faculty of Aerospace Engineering, it is possible for TU Delft students to get a license if proper reasoning is provided. ParaPy also forms the basis for the KBE Master course, so some experience was already gained.

ParaPy is an object-oriented KBE package which can be used to link analyses to a 3D geometry creation tool. The 3D geometry can also be used to calculate different attributes of the components from which it is built such as the fuselage volume, or the exposed area of a wing. The program has been created by ParaPy[4], a start-up company which originated from a TU Delft project, and is being used by companies like Fokker. Note that the aircraft program has been built in such a way that it can also be run without having ParaPy available. In that case some features such as the Raymer volume drag calculations, and the production of images of the aircraft design will not be executed and not be included in the output. Also, in the current program version a patch is used to improve the accuracy of the area distribution calculation, but this patch is not yet available to other users of ParaPy. In the near future, it is likely that this is resolved for a new version of ParaPy. Note also that ParaPy is a program under constant development and that it might be that future updates break the current methodology, requiring additional changes to be made to ensure that the design program continues to function.

A.1.4. Important dictionary remark

For the transfer of data between the different design modules, the program uses dictionaries as described in the main text. While the dictionary is a nice way of storing data because values are assigned to a known key, allowing for them to be extracted where needed, it also has a trait that has to be kept in mind. When a dictionary is assigned to a different variable (i.e. copied) within a module so that it can be used, as shown below using a simple example in a Python console, the new dictionary (copy) and the main dictionary (original) both refer to the same object:

```
>>> a = dict()
>>> a["test"] = 10.
>>> copy = a
>>> a["test"]
10.0
>>> copy["test"]
10.0
>>> copy["test"] = 0.
>>> a["test"]
0.0
>>> copy["test"]
0.0
```

This means that any changes made to the "copy" dictionary entry "test" also apply to the main dictionary "a" which is unintentional and could result in issues if for example, weights in SI units are overwritten with Imperial values. To overcome this issue, the 'deepcopy' function is used from the copy-package. It allows for a new variable to be a copy of the main dictionary without them being linked, meaning that changes to the copy do not affect the main dictionary, as is shown below.

[4] www.parapy.nl (accessed January 2 2019)

```
>>> a = dict()
>>> a["test"] = 10.
>>> import copy
>>> copy = copy.deepcopy(a)
>>> a["test"]
10.0
>>> copy["test"]
10.0
>>> copy["test"] = 0.
>>> copy["test"]
0.0
>>> a["test"]
10.0
```

This time, changing the value corresponding to the "test" key does not result in a change of the value corresponding to that key in 'a', solving the problem.

A.2. Inputs

The program utilizes a number of different input files, either for defining the settings of the system, or for accessing data used for statistical regression in specific module functions. These input files are either Excel sheets or text files (with .txt or .dat extension).

The main input file is the "all_inputs.xlsx" file. It is an Excel sheet containing several tabs, each of which has a large number (20+) inputs that can be altered by the user. The tabs are the following:

- The first tab is the most important as it contains the main inputs for the run, and provides the requirements for the aircraft design to be produced by the program. This includes (but is not limited to) the following items:
  - Aircraft name (used for storage)
  - Design point range and payload
  - Subsonic range (if any)
  - Use of technology factors
  - Segment altitudes (sub- and supersonic)
  - Cruise speed (sub- and supersonic)
  - Performance requirements (e.g. takeoff/-landing distance and clean sea-level stall speed)
  - Wing aspect ratio
  - Type of HLDs
  - Climate setup such as subsonic reference aircraft and LTO definition

  Each item is defined in a row of the excel sheet with the following entries:
  - Entry which is a kind of abbreviation of the definition used to assign the key name used for the dictionary, e.g. "n_pax" for number of passengers.
  - The unit of the entered parameter value.
  - The value which should be used, and which can be altered by the user.
  - A column with a conditional formatting, which is green when the user-provided input is in the allowed range. Note that these are indicative and that selecting a value outside of the range will often not result in the program returning an error. An exception to this is a check for negative values which in some cases are not allowed (e.g. number of pilots cannot be negative).
  - A description of the input parameter to clarify what it represents such that the user understands what it is used for.
  - Two columns with the lower and upper limits of the input, which are used for the conditional formatting. These limits are defined by the user, and could be adjusted if they are deemed too conservative.
- The secondary inputs tab contains inputs which are often of lesser importance and which are usually kept constant. They define the settings for the iterator such as the iteration limit and convergence criterion, but also engine parameters like overall pressure ratio and component efficiency. It is also used to define the locations where the outputs from the program have to be stored, and where the ParaPy

patch is located. The layout of the setup tab is similar to that of the first, with the values, conditional formatting, and descriptions, although the order of the columns differs a little. The number of inputs (+100) is large but the majority of the variables will only have to be changed on rare occasions.

- The technology factor tab contains the technology factors for each of the components used in the Class II weight breakdown as found in several literature sources. Based on these values, a column is filled with values that are used in case of non-random technology factors. The tab also contains the lower and upper limits for the technology factors which are used when random technology factors are selected in the setup tab to define the random factor distribution. The technology factor values can be changed by the user.
- The LTO engine tab contains data for the LTO cycle of a custom engine that can be modified by the user. If the option is selected to use the custom engine instead of a reference engine from the Engine databank, then the values from this tab will be used for the climate LTO cycle analysis.

It is possible for future users to introduce new tabs, or expand/alter existing ones. In that case, in the inputs reader program it will be necessary to alter the range of the Excel sheet that should be read such that the variables contained are all extracted.

A.3. Module flowcharts

In this section, flowcharts for the different design modules are included to show more of the steps being performed in the modules, and their order. Still, the level of detail is limited because the charts would otherwise become too complex and large. For additional information on the steps and methods go to the chapters where the methods are detailed, or study the code. Note that a noise module chart is not included because it was not available at the time of writing.

Class I

For the Class I there are two main routines, the first routine uses the initial inputs and the second uses the outputs of modules from a previous iteration. The method applied is the fuel fraction method as explained in Chapter 3. After the takeoff weight is found some more performance parameters are determined for subsequent modules, and then passed on to the wing loading module.

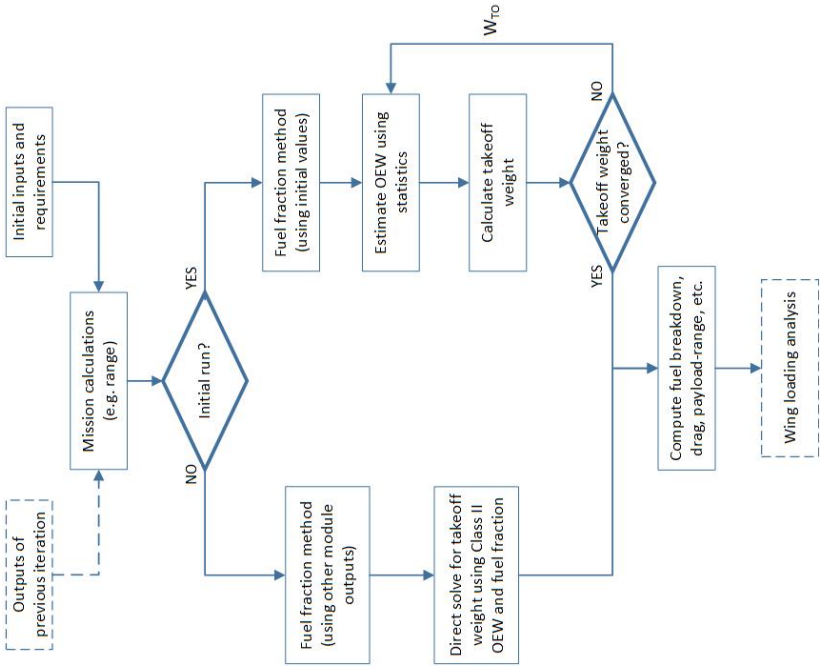

Figure A.1: Class I module flow chart

Wing loading

In the wing loading module the first step is to setup the flight and atmospheric conditions for the different constraints such as the sub- and supersonic cruise. Following this the constraints (e.g. takeoff distance and

climb gradients) are analyzed. The resulting lines are then combined into a single wing loading diagram and used to find the feasible region, and consequently select the design point. Then, using the thrust and wing loading together with the known takeoff weight, the wing area and takeoff thrust are estimated.

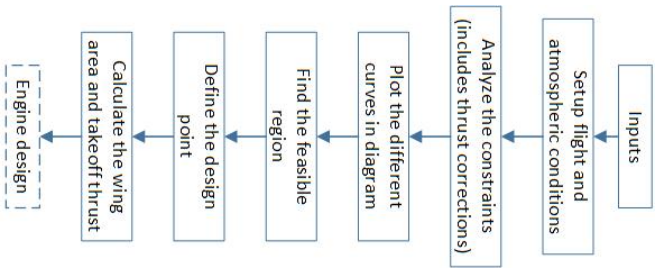

Figure A.2: Wing loading module flow chart

Engine design

For the engine design module, the first step is to extract the efficiency of the engine components as defined in the secondary inputs tab. Following this, the optimization routine is executed for the design point to size the engine in terms of performance. Following this, other engine attributes like its dimensions and mass are calculated. From the Class I mission, the off-design conditions are known and used with the engine parameters found to estimate off-design engine performance. All results are then combined into a single dictionary for the engine, and passed on to subsequent modules.

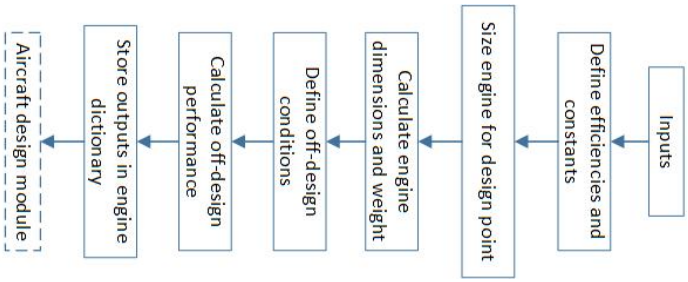

Figure A.3: Engine design module flow chart

Aircraft design

The aircraft design routine consists of the creation of the different components that make up the aircraft design. It starts with the fuselage and wing. Following this, the output of the engine module is combined with other dimensions to position the engines. After this the horizontal and vertical tail are added. During the last steps some miscellaneous dimensions are calculated (e.g. electrical routing distance), aircraft drawings are produced, and all component dimensions are combined into a single dimension dictionary, which is passed on to the aerodynamics module.

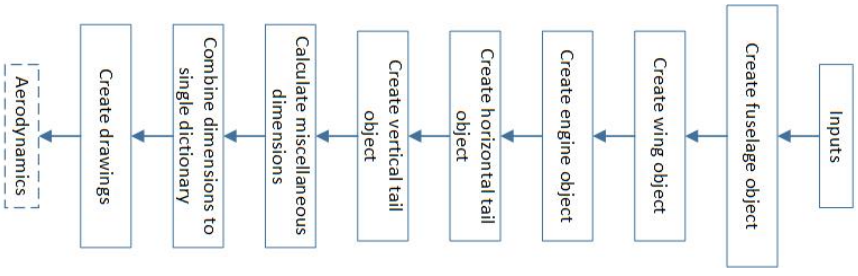

Figure A.4: Aircraft design module flow chart

Aerodynamics

The aerodynamics module starts with setting up the flight and atmospheric conditions, and other preparations (e.g. C_L-calculation). Following this the low-speed performance (including HLD sizing), subsonic and supersonic drag analyses are executed. The results are used for creating L/D-curves and calculating the mid-segment L/D values. Then, as a last step values are calculated which will be needed for the gust analysis in

the Class II module. Following this, outside the aerodynamics module the maximum lift coefficients found are compared to those used in wing loading. If they are too low, the values are reduced and wing loading is run again. Otherwise, the Class II module is called.

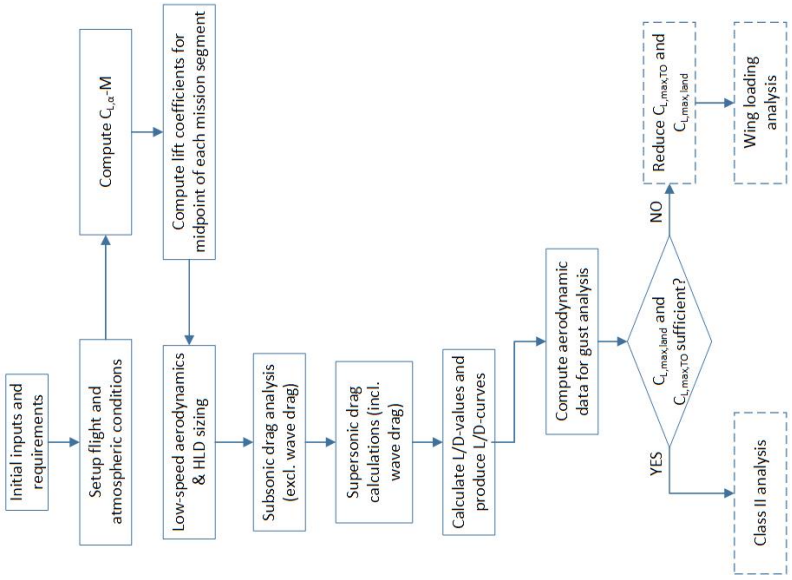

Figure A.5: Aerodynamics module flow chart

Class II

For the Class II module the first step is to perform the calculations needed to produce V-n diagrams, and determine the maximum load factors. After this, using the aircraft data (dimensions, fuel weight, etc.) the four weight groups are each analyzed, starting with structures, followed by propulsion, equipment, and operating items. Combining the groups, the (operating) empty weight is calculated. The calculations for the groups can include technology factors if selected by the user and depending on whether random factors are used, a different output is provided. For random technology factors an operating empty weight distribution is returned and for non-random factors a single breakdown file is returned.

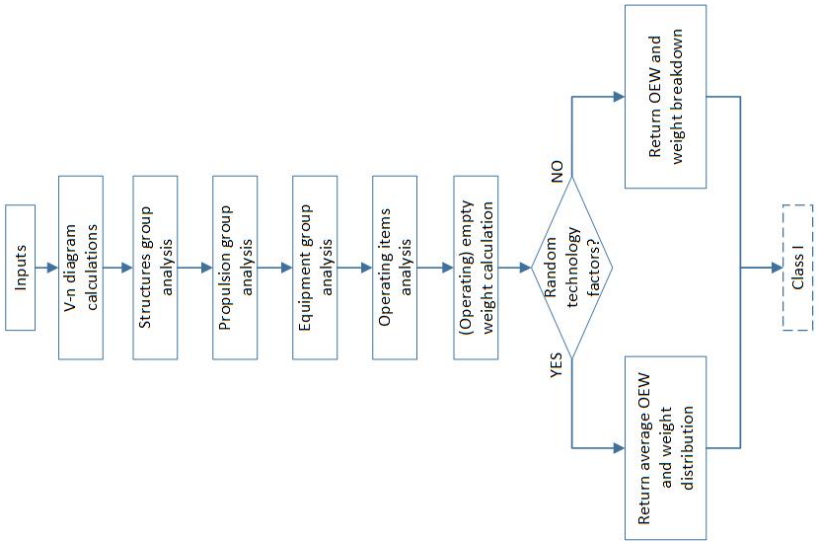

Figure A.6: Class II module flow chart

Climate

The climate module starts with extracting the correct reference engine LTO data, either from the LTO tab of the input Excel sheet, or from the engine databank. After this the data for the reference subsonic aircraft is loaded, and the fleets are set up, and used for the global climate analysis. Next, using the reference engine

LTO data, and modified fuel flow, the LTO cycle is analyzed and compared to the regulations. The last step then is to run the CO_2 certification analysis using the specific air range values found for the aircraft. All results are combined in a climate dictionary and passed on to the PDF writer.

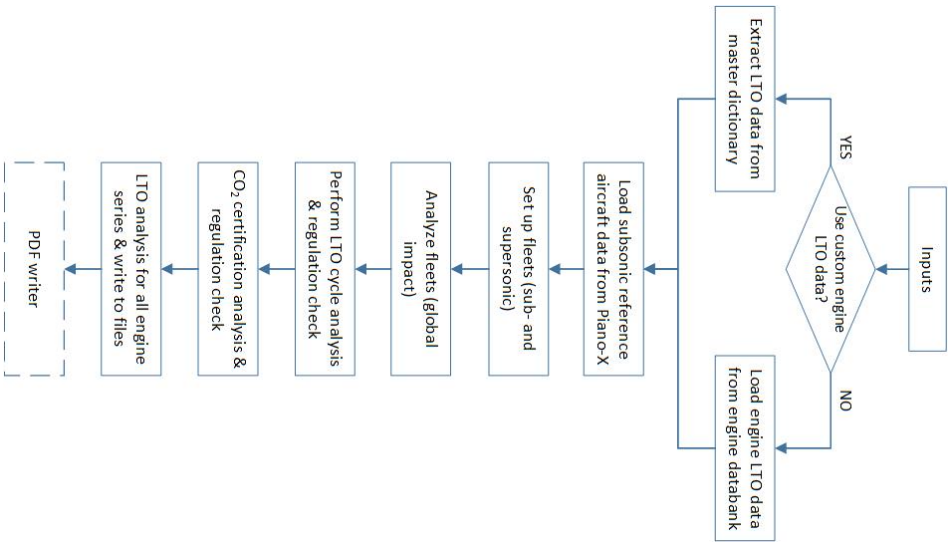

Figure A.7: Climate module flow chart

A.4. Outputs

The design program will provide the user with a set of outputs, which can be used to evaluate the aircraft design. As this output can be a bit unclear, a brief description is given here. The program currently returns two key outputs, the first is the final version of the aircraft master dictionary. This dictionary can be used to create additional output files that can give the option to more easily compare different designs, and in the future to steer an optimization routine.

The main output however, which also provides a clear overview of the resulting design, is a PDF document created by using the reportlab package for Python. An eight page example output PDF is shown in Appendix G. In the current version it contains seven or more pages with the content depending on the settings and available Python packages. The location where these PDFs are stored is defined by the user in the input file through a path. At this location, a folder is created if it does not already exist. Within this folder, an empty folder is produced for each design with the name provided in the main input tab, which contains the different output files such as plots and Class II weight breakdown alongside the PDF. The pages of the PDF contain the following information:

1. Main run information (e.g. runtime), main requirements (e.g. payload, cruise Mach numbers) and a set of images showing the resulting aircraft design created by ParaPy. If ParaPy is not available no images are included.

2. Payload range performance page showing a payload-range diagram as well as the key weights and ranges of the aircraft design at each of the points along the curve.

3. Aircraft design characteristics showing the wing loading diagram with the design space bound by the constraints, and the design point values for wing and thrust loading. From these values the other characteristics of the aircraft design are derived and listed in four tables; for the fuselage, main wing, horizontal tail and vertical tail.

4. Aerodynamics page showing the drag polars and operating points for the different flight segments of the Class I weight analysis mission. Key information about the supersonic cruise and the L/D-ratios for each segment are shown in tables. The type of high-lift devices is also listed. To conclude, an area distribution curve is shown as generated by ParaPy with a supporting text listing the maximum value and how many slices were used.

5. Engine page showing the different design characteristics of the engine in two tables. The table on the left contains information about the engine at the design point and some performance values like bypass

ratio and dry mass. The second table on the right lists the fuel flows and specific fuel consumption for each of the mission segments. Below these tables, there is a table for the fuel tank volumes and an engine cycle graph at the takeoff conditions.

6. Operating empty weight breakdown page showing the relative component weight contributions in a pie chart, and the absolute weight values in a table. With random technology factors selected, this page will instead show the random weight distribution with the selected value highlighted by a vertical dashed line.

7. Climate (or environmental) impact page is an optional page which is only included if the user sets a switch to True. This page will show the results for the three environmental analyses considered, the LTO cycle, CO_2 certification and the global climate impact values. Each is contained in a separate table.

8. Noise page is an optional page which will be added in the near future and will be detailed in [7]. It is expected to show estimations of the airport noise production and sonic boom strength for the aircraft design produced.

9. The last page might be of lesser interest to the user, as it shows the convergence of the aircraft takeoff weight, which is used by the iterator to check for convergence. It is mainly of interest to those looking to make changes such that they can better trace the impact of changes on the behavior of the design program.

The user is free to add more pages or make changes, but it should be noted that the reportlab package does not have the clearest documentation. Using the existing code in combination with the reportlab user guide, however, it should be possible to generate the desired reports. Additionally, to ensure the inputs used for the aircraft are available for future reference, a copy of the Excel input file is also included in the results folder.

A.5. Work division

Since the project was worked on by two students, it is important to identify the contributions made by each member. To this end, Table A.1 indicates the relative contributions for each of the major modules or steps taken during the thesis research, expressed as a percentage. Note that this does not include work on the literature study and project plan as those are part of other courses within the Masters curriculum. Also note that these values subject to change because and that an updated table can be found in [7].

Table A.1: Project task division (up to mid-May 2019)

Module/step	M. den Boer	J. Nijsse	Remarks
Requirements definition	80%	20%	
Class I	100%		
Wing loading	20%	80%	
Engine design		100%	
Aircraft design	20%	80%	
Aerodynamics	100%		
Gust analysis & Class II	100%		
ParaPy integration	100%		i.e. the use of ParaPy for area distributions (aerodynamics) and image generation
Output writer	100%		
Overall program	80%	20%	i.e. creating the master program, overall structure, and linking all modules
Support programs	100%		e.g. input reader, package check, iterator part, atmosphere
Climate impact	100%		
Noise & sonic boom		100%	To be added to program in near future (see [7])

B
Class I support

B.1. Climb and descent distances

For the Class I mission analysis it is necessary to have an estimate of the distance that is covered by the aircraft during the climb and descent phase. This distance can then be subtracted from the total mission range to find the remaining cruise range. Due to the lack of data on Concorde and Tu-144 flight climb profiles, the decision was made to look for values that were used in past SST design projects, which are listed in Table B.1.

Table B.1: SST design climb and descent distances

Aircraft	M_{cr} [-]	h_{cr} [m]	R_{climb} [km]	$R_{descent}$ [km]	Source
NASA 2.4M	2.4	19,500	833	594	[29]
NASA 3M	3	19,812	345	657	[115]
NASA 4M	4	24,690	381	745	[116]
SSXJET	2.2	18,250	746	370	[117]
SSXJET I	2.2	17,970	700	370	[117]
SSXJET II	2.2	18,471	700	370	[117]
SSXJET III	2.2	18,897	700	370	[117]
PASS optimized	1.6	13,106	556	-	[118]
NASA SST	2.62	-	874	506	[119]

The NASA Mach 3 and 4 designs were excluded from the analysis because they represented outliers in terms of climb distances, but also because their Mach numbers are much higher than that for which aircraft will be designed in this project (up to Mach 2-2.2). To get a fit, the climb distance was plotted against the Mach number as shown in Figure B.1.

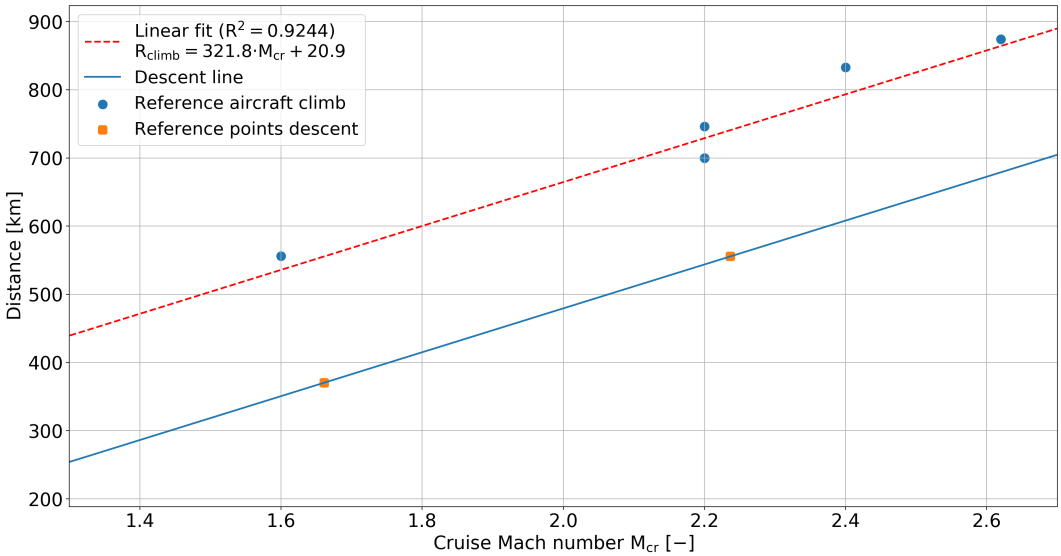

Figure B.1: Climb and descent distance fit

The curve fit can then be used to determine the climb distance based on the cruise Mach number. In [120] it is stated that for climbing, 300 to 400 nautical miles are covered, which corresponds to Mach numbers of 1.66 and 2.24, respectively, according to the curve fit. These seem like reasonable values based on what was found during the literature study. For the descent distance no real trend could be distinguished. In [120] it was indicated that descent distances of 200 to 300 nautical miles could be assumed for low boom SSTs. These distances were then coupled to the Mach numbers that corresponded to the climb distances also indicated in that source (i.e. Mach 1.66 and 200 NM descent; Mach 2.24 and 300 NM descent). A curve was then fit through these two points to find the descent distance for all Mach numbers, and was found to be (in nautical miles) for the cruise Mach number:

$$R_{descent} = 173.61 \cdot (M_{cr} - 1.661) + 200 \tag{B.1}$$

B.2. Operating Empty weight data

The data in the table below was compiled for the operating empty weight regression fit used in the Class I analysis.

Table B.2: Takeoff and operating empty weight for reference supersonic aircraft

Aircraft	Type	Year	Takeoff weight [kg]	OEW [kg]	Source
Concorde	SST	1960s	185,066	78,700	[1,2][21]
Tu-144	SST	1960s	206,974	99,199	[3] [13, 121]
Boeing 969-512BA	SST	-	154,309	77,399[4]	[13]
Boeing 959-512BB	SST	-	340,194	170,634[4]	[13]
SM-SST	SST	-	25,492	12,002[4]	[13]
GD-F111A	Fighter	1960s	41,504	22,623[4]	[13]
GD-B58A	Fighter	1960s	72,575	27,624[4]	[13]
Edge Supersonic Transport	SST	1992	377,389	147,186[4]	[23]
NASA low boom business jet	SSBJ	2003	45,103	18,999[5]	[24]
Cranfield SSBJ	SSBJ	2002	44,900	21,000	[25]
HELESA	SSBJ	2017	43,100	19,577	[26]
Low boom SST concept	SST	1973	56,699	24,210	[122]
AST	SST	1976	325,679	149,448	[27, 28]
NASA 2.4M SST	SST	1999	276,889	90,332	[29]
1080-874	SST	1989	302,482	120,255	[30]
1080-910	SST	1992	373,597	164,321	[30]
1080-911	SST	1992	352,328	152,773	[30]
NASA Mach 3 SST	SST	1988	322,050	123,822	[115]
Mach 1.6 airliner	SST	2004	340,000	136,000	[31]
SSXJET	SSBJ	1977	35,720	16,321	[117]
SSXJET I	SSBJ	1977	34,927	15,756	[117]
SSXJET II	SSBJ	1977	33,566	15,436	[117]
SSXJET III	SSBJ	1977	36,081	18,094	[117]
N+1 overwater	SST	2017	140,160	62,489	[32]
NASA N+3	SST	2010	129,266	58,766	[33]
NASA N+2	SST	2015	145,226	64,232	[123]
HSCT8-A	SST	-	690,000	267,750[4]	[120]
Boom constrained a/c	SSBJ	2005	119,200	49,200	[124]
Non-boom constrained a/c	SSBJ	2005	101,400	42,200	[124]
E5 SSBJ	SSBJ	2018	100,209	40,274	[125]

[1] http://www.concordesst.com (accessed April 24 2018)
[2] IHS Markit, *Concorde*, https://janes.ihs.com/JAWAInServices/Display/1336723 (accessed April 24 2018)
[3] http://www.tu144sst.com/index.html (accessed April 24 2018)
[4] Values scaled by factor 1.05
[5] Empty weight plus crew weight

B.3. Payload weight fraction data

For the payload weight fraction, a small database was created with the values and the sources listed in the table below.

Table B.3: Payload weight fractions for seven subsonic aircraft

Aircraft	Takeoff weight [kg]	Payload [kg]	Ratio [-]	Source
737-900	74,389	19,831	0.267	[82]
737-800[6]	79,061	21,319	0.270	[82]
777-200LR	347,814	63,956	0.184	[126]
777-300ER	352,441	69,853	0.198	[126]
777-200 (GE eng)	242,630	55,670	0.229	[127]
A330-300	242,000	45,600	0.188	[128]
A330-200	242,000	49,400	0.204	[128]

B.4. Maximum fuel capacity estimation

For the maximum fuel capacity estimation used for payload-range calculations, a dataset had to be created to estimate the average maximum fuel to harmonic range fuel ratio. Ten subsonic aircraft are included to represent the long-range wide-body, and larger single-aisle aircraft (A321, 737), while Concorde and Tu-144 represent the supersonic aircraft. The average ratio found was 1.242 with a standard deviation of 0.152. Since the Concorde and Tu-144 are both on the low side compared to the average, it was decided to use the average value minus one standard deviation, which is 1.089. This means that the maximum fuel capacity is 8.9% greater than the harmonic mission fuel.

Table B.4: Maximum fuel ratio table

Aircraft	Harmonic range [NM]	MTOW [kg]	MZF [kg]	Harmonic fuel [kg]	Max fuel [kg]	Ratio	Source
777-300ER	5,650	352,000	237,683	114,318	145,540	1.273	[126]
777-200LR[7]	7,600	347,000	209,106	137,894	145,541	1.055	[126]
777-200LR[8]	7,600	347,000	209,106	137,894	162,636	1.179	[126]
777-200[9]	3,280	254,000	190,500	63,500	94,240	1.484	[127]
737-900[10]	2,000	79,000	62,732	16,268	20,894	1.284	[82]
737-700[10]	2,170	70,100	55,202	14,898	20,894	1.402	[82]
737-600[10]	1,980	70,000	51,710	18,290	20,894	1.142	[82]
A330-300[11]	3,680	233,000	175,000	58,000	72,400	1.248	[128]
A321neo	2,550	93,500	75,600	17,900	21,266	1.188	[129]
787-8	5,450	228,000	161,025	66,975	101,323	1.513	[130]
Concorde	unknown	185,066	92,080	92,986[12]	95,680	1.029	[13,14][21, 131]
Tu-144	2,878	206,974	114,198[12]	92,776	101,968	1.099	[15] [13, 121]
Average [-]						**1.242**	
St. dev [-]						*0.152*	
Selected value [-]						**1.089**	

[6] winglet configuration
[7] configuration with no auxiliary fuel tanks
[8] configuration with 3 auxiliary fuel tanks
[9] baseline aircraft
[10] CFM56-7B series engine
[11] TRENT 700 series engine
[12] assumed equal to difference between MTOW and MZF
[13] http://www.concordesst.com (accessed April 24 2018)
[14] IHS Markit, *Concorde*, https://janes.ihs.com/JAWAInServices/Display/1336723 (accessed April 24 2018)
[15] http://www.tu144sst.com/index.html (accessed April 24 2018)

C
Aerodynamics support

C.1. Digital DATCOM input file

The digital DATCOM program requires an input file that defines the geometry and flight conditions before it can be executed. An example file is shown below, and its contents are briefly explained here to clarify the workings. This is done to allow the reader to understand some more of the input file before having to go through the elaborate digital DATCOM manuals [51, 132, 133]. Before starting, it should be noted that the digital DATCOM program is written in Fortran, but that it can be converted to an executable through "gfortran"[1] or similar methods. Additionally, an open-source executable file was found[2].

```
 $FLTCON  NMACH=4.0, MACH=1.4, 1.6, 1.8, 2.02, LOOP=1.0,
   NALT=4.0, ALT=13500.0, 15000.0, 15500.0, 18300.0,
   HYPERS=.FALSE.,
   NALPHA=6.0, ALSCHD=-2.0, 0.0, 2.0, 4.0, 8.0, 12.0,
   STMACH=0.85, TSMACH=1.2$
 $OPTINS SREF=358.25, CBARR=18.41, BLREF=25.6$
 $SYNTHS XW=0.0, ZW=0.0, ALIW=0.0, XCG=0.0$
 $WGPLNF CHRDR=30.1, CHRDTP=2.83, SSPN=12.8, SSPNE=12.8,
   CHSTAT=0.0, SAVSI=71.5,
   TWISTA=0.0, DHDADI=0.0,
   CHRDBP=12.89, SSPNOP=7.04,
   SAVSO=55.0, DHDADO=0.0,
   TYPE=2.0$
NACA-W-6-64A103
DIM M
CASEID ------- TEST CASE ------
SAVE
DUMP
```

The first item of interest is the use of "$" which encloses a card containing a specific set of information. For the digital DATCOM to be run at least four cards need to be defined, the flight conditions (FLTCON), reference characteristics (OPTINS), some aircraft and wing characteristics (SYNTHS), and the wing planform definition (WGPLNF).

The flight conditions card indicates at how many and at which Mach numbers the aircraft geometry should be analyzed. Based on the type of loop selected, these Mach numbers are either analyzed at a single altitude or at multiple altitudes (which should then have the same amount as the amount of Mach numbers). A boolean indicator is used to show that no hypersonic methods should be applied. For each combination of Mach number and altitude, the angles of attack at which the different coefficients need to be computed should also be defined. Furthermore, it is possible to change the Mach number at which the transonic regime is entered (STMACH) and the transitional Mach number where the aircraft goes from the trans- to supersonic (TSMACH) regime. By default, the transonic regime extends from Mach 0.6 to Mach 1.4 [51].

The reference characteristics (OPTINS) define the reference area, reference chord (usually mean aerodynamic chord) and reference span. These are used by the program to correct the different coefficients found. If these inputs are not provided to the program, it will compute them from the vehicle geometrical inputs.

[1] https://gcc.gnu.org/fortran/ (accessed April 2 2019)
[2] http://www.pdas.com/datcom.html (accessed April 2 2019)

The aircraft and wing characteristics (SYNTHS) are more advanced features of the program and allow for defining the aircraft center of gravity position, but also the incidence angle of the wing. The center of gravity position will be used for stability analysis, but this requires additional information like the aircraft weight distribution and relative wing position. For future usage, it might be interesting to look into the stability prediction capability of the digital DATCOM.

The final set of inputs are the wing planform parameters (WGPLNF). These include values such as the root, kink and tip chord, as well as a sweep angle for both wing sections. This sweep angle can be defined at any chordwise location, but this location does have to be provided to the program and should be the chordwise location for each section sweep angle. Additional parameters are the twist and wing dihedral angles. In case a body is included in the design, part of the wing will not be exposed to the airflow. For this purpose, a semi-span value is also provided for the exposed wing section. In the current situation, where the wing is analyzed by itself, the exposed area is the same as the total reference area.

Aside from the entries discussed, it is possible to add more parameters to each card as well as extra components such as a body and empennage which works in a way that is similar to the wing planform definition. The different parameters and components are further detailed in the user manual [51]. Care should be taken in the input file to ensure that the proper values are used and that they are provided as floats. For example, early in the design process, a wrong value for the outer section span was provided (twice as high as it should have been), which caused the lift curves to become less steep. Additionally, there is a limit on the number of columns the digital DATCOM can handle so if a large number of angles of attack, altitudes or Mach numbers need to be analyzed, they should be written out over two or more rows.

Below the cards, there is also the entry for the type of airfoil that is to be used by the digital DATCOM in the aerodynamic analysis. It is possible to use several NACA series designations for which the digital DATCOM will automatically compute the shape and performance characteristics. In that line, the first item indicates that it is a NACA series airfoil, the second term 'W' indicates that it is the airfoil used by the wing, and can be changed to H for the horizontal tail, and V for the vertical tail. The number following this indicates the NACA airfoil series selected by the user (e.g. 4 for 4-series or 6 for 6-series). Following this, the description of the airfoil shape is provided (e.g. 0012 for symmetric 12% t/c 4-series airfoil). The exact definition is described in the manual [51].

Following the aircraft definition a number of additional commands are provided. The first, "DIM M" indicates that all dimensional entries provided are in SI units. Using 'DIM FT' will instruct the digital DATCOM to use Imperial units instead. After this, an ID is provided for the case, after which the data is saved and dumped. For each geometry that is provided by the previous aircraft design components, an input file is generated, and run automatically. Afterwards, the results are extracted from the output file.

C.2. Equivalent wing characteristics

For the conceptual drag curve calculations as used in [31], it is necessary that the (compound) wing be transformed into a single equivalent delta or arrow wing. While this method is not very complex, it is still beneficial to show it here so that it is better understood. In the case of the double delta wing investigated in this report, each wing consists of two trapezoidal elements with their own area. For the inner trapezoid, part of the wing is in the fuselage so that part should be excluded, i.e. the equivalent wing represents the exposed double delta wing. Through simple geometrical rules and by removing the fuselage enclosed sections, the area of the trapezoids is computed. Using these areas and the leading and trailing edge sweep angle of each trapezoid, the equivalent leading and trailing edge sweep angles of the equivalent wing are calculated using Equation (C.1), where the trailing edge angle is computed by changing the leading edge angles to those at the trailing edge. A sketch of the equivalent wing parameters is shown in Figure C.1.

$$\cos\Lambda_{LE,\,eq} = \frac{cos\Lambda_{LE,\,inb}\cdot S_{exp,\,inb} + \cos\Lambda_{LE,\,outb}\cdot S_{exp,\,outb}}{S_{exp,\,inb} + S_{exp,\,outb}} \tag{C.1}$$

Based on the equivalent sweep angles found, and by using the span and area of the exposed wing (reference wing and span minus parts contained in fuselage), the equivalent root and tip chords are computed by using Equations (C.2) and (C.3), respectively.

$$c_{r,\,eq} = \frac{S_{exp}}{b_{exp}} + \frac{b_{exp}}{4}\cdot\left(\frac{1}{\cos\Lambda_{LE,\,eq}} - \frac{1}{\cos\Lambda_{TE,\,eq}}\right) \tag{C.2}$$

$$c_{t,\,eq} = \frac{S_{exp}}{b_{exp}} - \frac{b_{exp}}{4}\cdot\left(\frac{1}{\cos\Lambda_{LE,\,eq}} - \frac{1}{\cos\Lambda_{TE,\,eq}}\right) \tag{C.3}$$

Additional values that are needed are the wing box ratio and area ratio. For this, a box is created which encloses the wing, and has a lengthwise value of 'l', and a spanwise length equal to half the effective semi-span. The box ratio equals s/l, and area ratio r_s equals $S_{exp}/(s \cdot l)$. In most situations, the wing or empennage component will have an area ratio that is close to 0.7, and this value is assumed to apply to the horizontal and vertical tail. A sketch depicting the equivalent wing and area ratio is shown in Figure C.1.

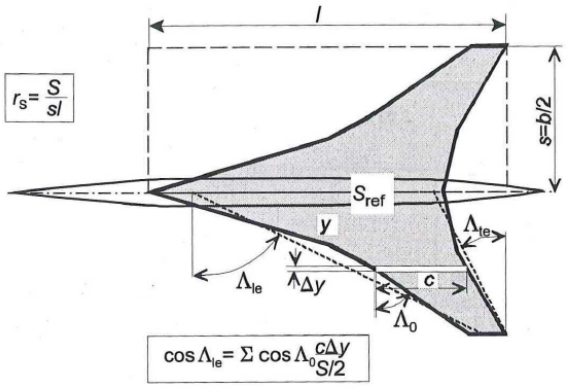

Figure C.1: Equivalent wing and area ratio definition sketch [31]

C.3. Low-speed lift model methods

For the low speed aerodynamics, it was found in Section 5.2.2 that the simple DATCOM method used to compute the lift curve slope for the linear lift region was insufficient for angles of attack greater than 5-10 degrees. For this reason, several alternative methods were considered, which will be explained here, along with the reasoning for choosing the best method.

From a brief literature search for (semi-)empirical methods, several alternative methods were found which could be used to estimate delta wing lift characteristics, and are listed below. Note that only a brief explanation is provided for each method, and that for further information, the sources cited should be studied.

- Polhamus method for predicting vortex-lift characteristics of arrow, delta and diamond wings [55].

  It has been shown in [134, 135] that the lift of sharp-edge delta wings over a large range of angles of attack can be obtained by combining the potential-flow lift and the vortex lift as predicted by the leading edge suction analogy [55], which results in the following equation:

  $$C_L = K_p \cdot \sin\alpha \cdot \cos^2\alpha + K_v \cdot \sin^2\alpha \cdot \cos\alpha \tag{C.4}$$

  Here, the first term represents the potential-flow contribution and the latter represents the vortex-related contribution. The values of the constants K_p and K_v can be estimated for the wing planform by making use of Figures C.2a and C.2c, respectively. Note that the value of the sweep angles with the apostrophe (') indicates that they are corrected for compressibility by dividing by β. Also, for the vortex contribution, an additional Mach correction is implemented through the estimation of f_M as shown in Figure C.2b.

- Lamar extension of Polhamus method [136].

  This method is similar to that of Polhamus [55], but introduces a modified vortex lift term which accounts for the effect of the leading edge vortex moving downstream over a wing with a finite tip chord [136].

  $$C_L = K_p \cdot \sin\alpha \cdot \cos^2\alpha + \left(K_{v,LE} + K_{v,se}\right) \cdot \sin^2\alpha \cdot \cos\alpha = K_p \cdot \sin\alpha \cdot \cos^2\alpha + K_{v,tot} \cdot \sin^2\alpha \cdot \cos\alpha \tag{C.5}$$

  The vortex term is now split up into two constants, one for the leading edge (LE) and one for the side edge (se). Both terms combined are listed as $K_{v,tot}$. Using a set of calculations the two contributions can be estimated, but for the total constant value ($K_{v,tot}$) several graphs are also available such as Figure C.3, depending on the wing shape. Because these graphs are relatively limited, it is more difficult to apply this method than the Polhamus method.

- Lee delta wing aerodynamics method [137].

  For this method it is assumed that there are only two aerodynamic force components, the linear and nonlinear forces, which combine into a single lift force as follows from Equation (C.6).

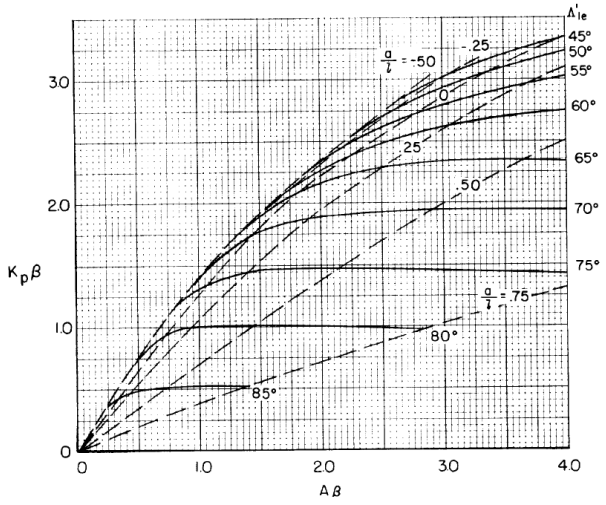

(a) Polhamus chart for determining K_p [55]

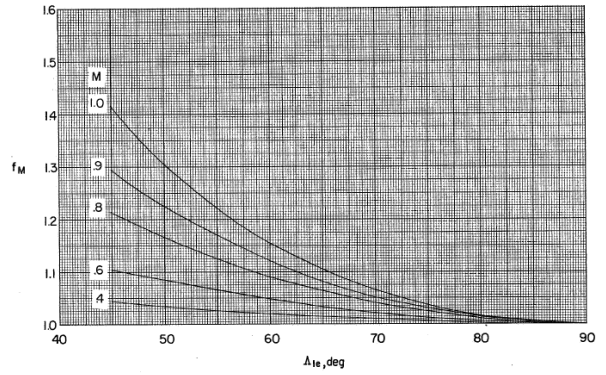

(b) Compressibility correction for K_v [55]

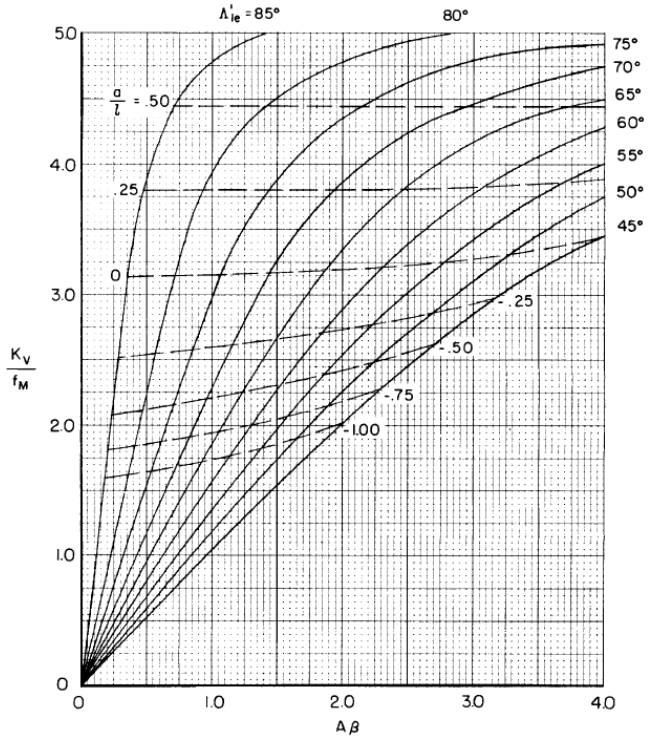

(c) Polhamus chart for determining K_v [55]

Figure C.2: Polhamus method charts [55]

$$C_L = C_{NL\alpha} \cdot \sin\alpha \cdot \cos\alpha + C_{NN} \cdot \sin^2\alpha \cdot \cos\alpha \tag{C.6}$$

This is similar to the Polhamus method described earlier, which also used two lifting contributions. For the determination of the linear component, a complex integral could be solved, but to reduce the amount of complexity, an approximated solution is also provided. The full integral was implemented in both SymPy[3] and Wolfram Mathematica[4] to numerically solve the integral, but in both cases seemed to return values which deviated by nearly a factor two from those in the reference source [137]. No causes were found for this deviation. For this reason, the approximation in Equation (C.7) is used instead. Equation (C.8) is used to estimate the non-linear lift component [137].

$$C_{NL\alpha} = \frac{7}{9} \cdot \pi \cdot A \cdot \tan\theta \tag{C.7}$$

$$C_{NN} = \frac{2}{1+A} \tag{C.8}$$

In this equation, the angle θ is equal to half the leading edge sweep angle. It should be noted that in [137] only aspect ratios up to 2.31 were shown, but it is assumed that the method can be extended up to aspect ratios of at least three.

All four methods were combined into a program to compute the low-speed lift curves for both the NLR aircraft [31] and Concorde [54], and the results are shown in Figures C.4 and C.5, respectively. Because the lines for the Polhamus and Lamar method are very similar, the values in the curves are also listed in Tables C.1 and C.2.

[3] https://www.sympy.org/en/index.html (accessed September 22 2018)
[4] http://www.wolfram.com/mathematica/ (accessed September 22 2018)

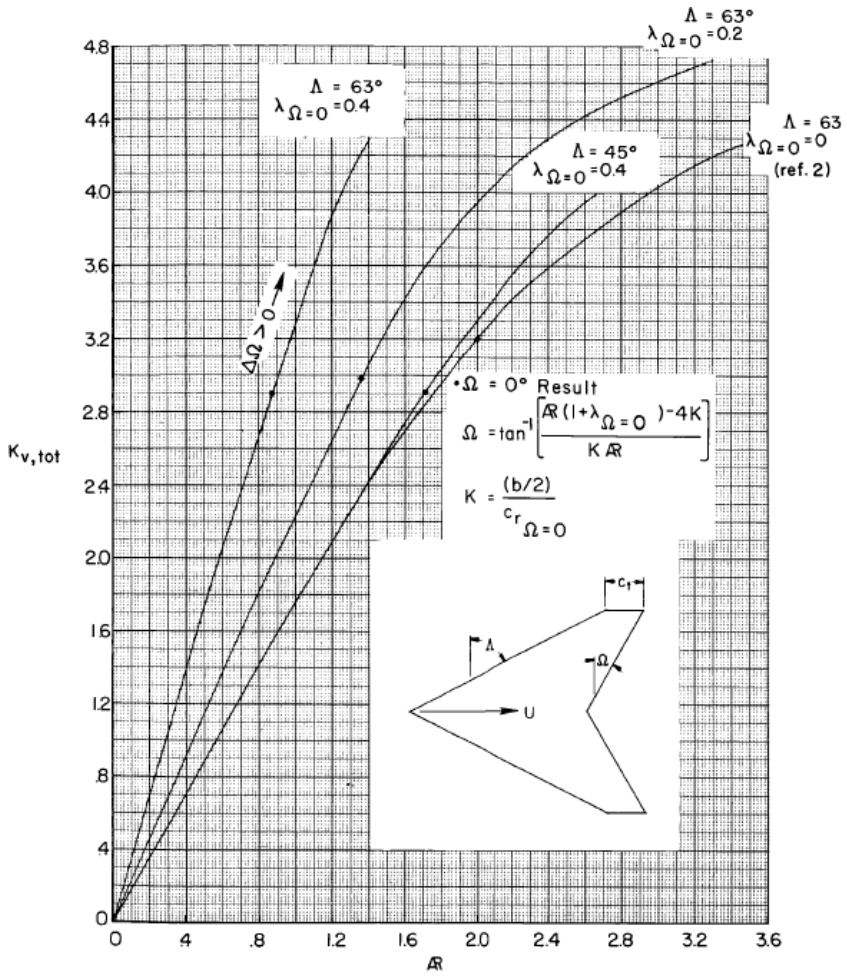

Figure C.3: Wing total vortex constant $K_{v,tot}$ prediction graph [136]

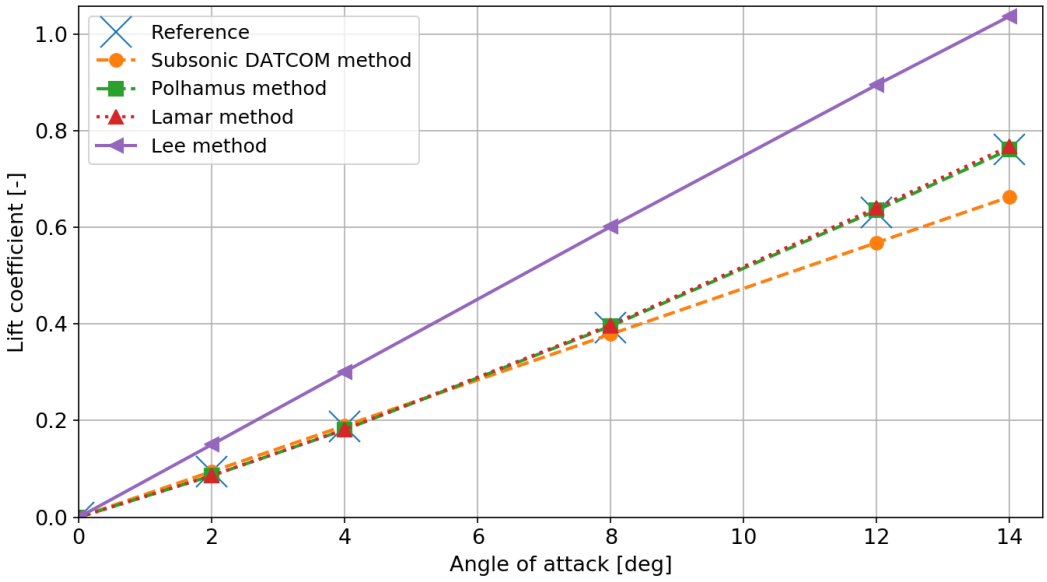

Figure C.4: NLR aircraft low-speed lift prediction comparison with reference values [31]

Table C.1: Low-speed lift coefficient method comparison NLR aircraft [31]

Angle of attack [deg]	Method for lift coefficient estimation				
	Reference	DATCOM	Polhamus	Lamar	Lee
0	0.0	0.0	0.0	0.0	0.0
2	0.094	0.094	0.086	0.086	0.150
4	0.187	0.189	0.181	0.182	0.301
8	0.392	0.378	0.395	0.398	0.601
12	0.631	0.567	0.635	0.640	0.894
14	0.761	0.661	0.761	0.768	1.037
Average absolute deviation	-	**4.74%**	**2.19%**	**2.50%**	**42.0%**

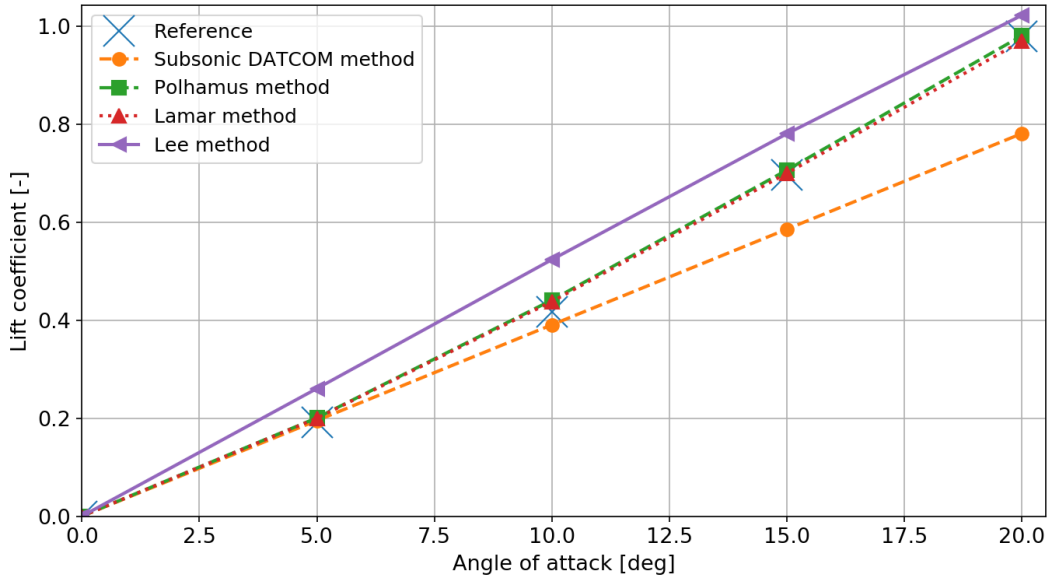

Figure C.5: Concorde low-speed lift prediction comparison with reference values [54]

Table C.2: Low-speed lift coefficient method comparison Concorde [54]

Angle of attack [deg]	Method for lift coefficient estimation				
	Reference	DATCOM	Polhamus	Lamar	Lee
0	0.0	0.0	0.0	0.0	0.0
5	0.192	0.195	0.201	0.200	0.261
10	0.417	0.391	0.441	0.438	0.524
15	0.696	0.586	0.706	0.700	0.781
20	0.979	0.781	0.981	0.970	1.02
Average absolute deviation	-	**8.82%**	**2.40%**	**2.15%**	**15.6%**

Looking at the results, it can be seen that there is quite some variation in the accuracy of the different methods. The delta method by Lee [137] gives a large overestimation of the lift coefficient for both aircraft. The Polhamus and Lamar method both perform better than the subsonic DATCOM method and have very small differences between them. This shows that for the low-speed lift prediction, one of the two methods would be preferable over the DATCOM method. Given the clearer reference graphs available for the Polhamus method, it was selected for the low-speed performance analysis of the delta wings. The graphs were transformed into a set of arrays which through interpolation will return the approximate values from the graphs making automated design possible, rather than having to read each graph for every iteration.

C.4. High Lift Device sizing

For the high lift device (HLD) sizing and selection several steps have to be performed. First, the requirement for the HLD system has to be calculated by subtracting the clean wing lift coefficient that can be achieved in the respective configuration from the required maximum lift coefficient for takeoff and landing. For takeoff, the 40% ground effect correction is included. It is also necessary to add some extra correction factors.

The first is a coupling correction factor (termed CCF here) which is 1.1 for a short-coupled aircraft and 1.05 for a long-coupled aircraft, and accounts for the tail (download) or canard (upload) lift contribution. An aircraft is short-coupled if $l_h/\overline{c} < 3.0$ and long-coupled if $l_h/\overline{c} > 5$ [42]. In between, linear interpolation is applied, but given their large mean aerodynamic chord, it is expected that most SSTs are short-coupled. On top of this, an additional trim penalty of 1.05 is included [42]. Also, some flap types will increase the wing surface area to S'_w, which will slightly increase the base lift coefficient. The required lift increment from the HLD system is then found by the following equations:

$$\Delta C_{L_{TO}} = 1.05 \cdot CCF \cdot \left(C_{L_{max,TO,req}} - C_{L_{max,ground,10^\circ}} \cdot \frac{S'_w}{S_w} \right) \tag{C.9}$$

$$\Delta C_{L_{land}} = 1.05 \cdot CCF \cdot \left(C_{L_{max,land,req}} - C_{L_{max,clean,12^\circ}} \cdot \frac{S'_w}{S_w} \right) \tag{C.10}$$

These increments have to be provided by the sum of the different HLDs as in Equation (C.11):

$$\Delta C_L = \sum \Delta C_{l,max} \cdot \frac{S_{flapped}}{S_{ref}} \cdot \cos \Lambda_{HL} \tag{C.11}$$

The first variable ($\Delta C_{l,max}$) is the approximate 2D lift increment that can be provided by the HLD, and depends on the flap type. Given that the low-speed performance of delta wings is relatively poor, there likely is a need for complex devices, which is why single slotted, fowler and double slotted flaps are included in the design routine. Triple slotted flaps are too complex, and heavy, and are therefore excluded. Double slotted flaps are also relatively complex but they have been used on the Panavia Tornado fighter [138], so it was decided to still include them.

For flaps that extend the local wing chord, the graph in Figure C.6 is used to determine the extension Δc. Multiplying it with the known flap chord and adding it to the local chord, the value c' is found which can be divided by the local chord to find c'/c. These ratios can then be multiplied with the values in Figure C.7 to find $\Delta C_{l,max}$ for the flap system.

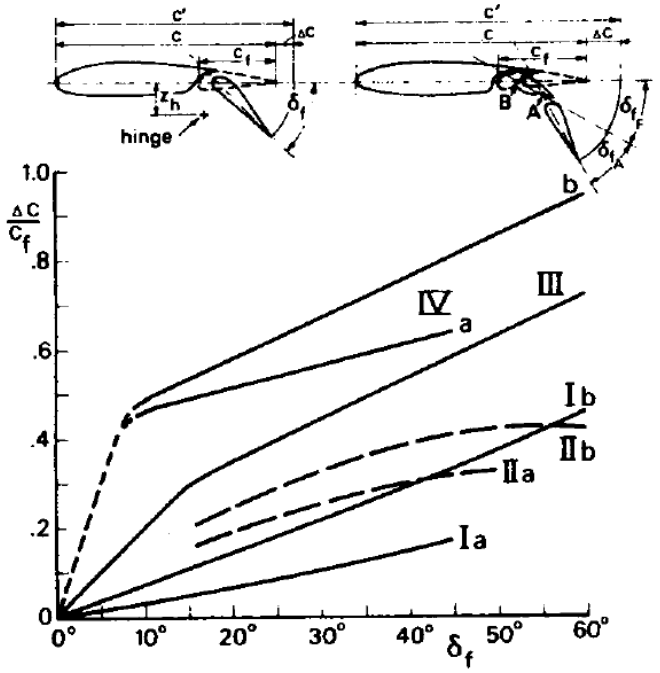

Figure C.6: Chord extension ratios as a function of deflection angle (III=double slotted, IVa=single slot fowler) [34]

Table 12.2 Approximate lift contributions of high-lift devices

High-lift device	$\Delta C_{t_{max}}$
Flaps	
Plain and split	0.9
Slotted	1.3
Fowler	1.3 c′/c
Double slotted	1.6 c′/c
Triple slotted	1.9 c′/c
Leading edge devices	
Fixed slot	0.2
Leading edge flap	0.3
Kruger flap	0.3
Slat	0.4 c′/c

Figure C.7: Approximate lift contributions of high-lift devices [50]

These chord extensions can then be used to estimate the extended wing area S'_w. Then, for the flapped areas it is important to realize that with the double delta wing, it is possible that the aircraft has two different trailing edge sweep angles, so for each part a separate calculation has to be performed. Also, to ensure that the aircraft has some form of roll control ailerons have to be present. These can be combined with flaps as so-called 'flaperons' as is the case for the Panavia Tornado [138]. These should be present both on the inner wing section (high speeds) and outer section (lower speeds), such that the risk of aileron reversal is reduced.

The dimensions of the high-lift devices are difficult to properly estimate, so in the current analysis it is assumed that the inboard flap will have a constant chord equal to about 25-30% of the kink chord. For the outboard part, it is decided to use a constant chord fraction of 25-30%. These values can be changed by the program user. The trailing edge flaps will start at about 0.1 meter from the fuselage and can extend up to 85% of the span. The leading edge system can span from close to the wing root, to 80% of the span and has a constant chord and hinge line which is approximately parallel to the leading edge. On the outer span sections the added benefit of HLDs is limited because the structural complexity increases due to the reduced local chord. In order to not interfere with the engine exhaust, which would require more expensive heat-resistant materials, the regions near the engine are not covered by trailing edge high-lift devices.

The sizing program will compute for the inboard and outboard section separately the lift increments for each of the three trailing edge flap types. Then, depending on the user inputs, the program will either use a specific HLD configuration or cycle over the options starting with the least complex (single slotted) flap inboard and outboard. If the required increment is not provided, the inboard flap type is then changed to fowler and ultimately double slotted. After this, full fowler, inboard double slotted and outboard fowler, and fully double slotted configurations are investigated until the requirement is met. As a last step, leading edge HLDs can also be added, but this is a user-defined option, because they will provide only a small lift increase at the expense of a flight control weight increase.

Regardless of whether the lift increments provided are sufficient, the program will return the maximum lift coefficient for the landing and takeoff conditions, so that the wing loading analysis can be performed with the updated values. This means that if the constraint is not attainable, a lower value will have to be used to ensure that the design is feasible. This is further detailed in the wing loading chapter of [7].

C.5. Delta method

In order to estimate the drag divergence Mach number of the SST, the Delta method has been used from [63]. First, the two-dimensional drag divergence Mach number is determined from Figure C.8 using the effective thickness. For supersonic aircraft this thickness is about 3-4%, which for a design lift coefficient of about 0.1-0.2 will result in a 2D drag divergence Mach number in the range 0.81-0.84.

This 2D value then has to be corrected for the sweep and aspect ratio to convert it to a 3D value for the wing. For most SSTs the aircraft quarter-chord sweep angle will be at least 50°, but likely closer to 60°. This means that a sweep correction of 0.12-0.14 should be added (Figure C.9). For the aspect ratio (Figure C.10) which will be in the range 1.6-3, a correction of 0.04-0.07 is added. This results in a wing drag divergence Mach number that is close to one, and this value will be used for the high subsonic compressibility calculations.

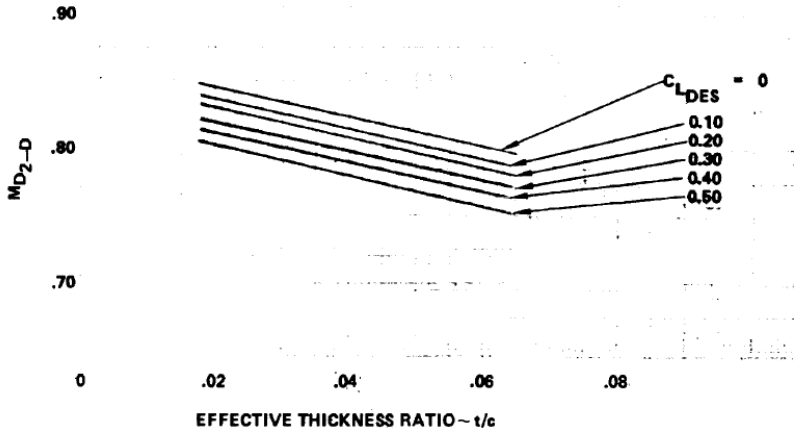

Figure C.8: Two-dimensional drag divergence Mach number for supersonic airfoil sections [63] (note that the graph y-axis has been cropped to shrink the size of the figure)

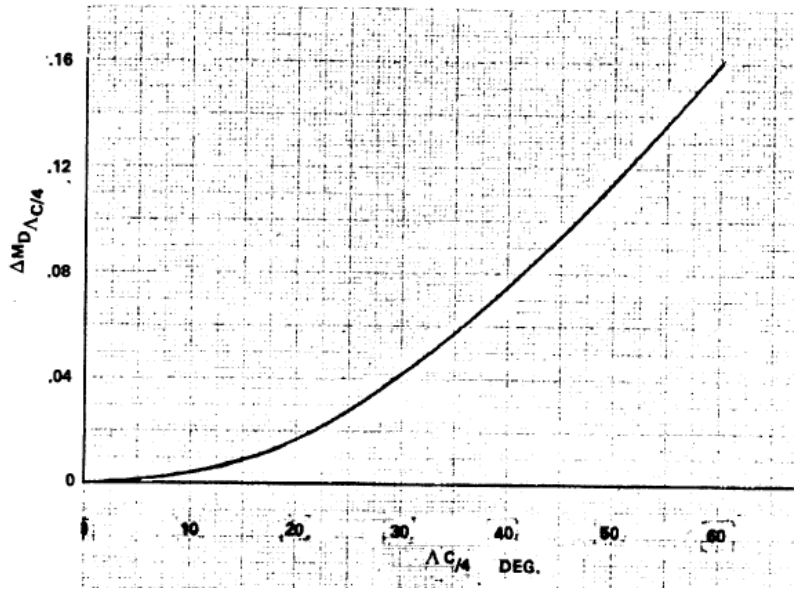

Figure C.9: Sweep angle correction for drag divergence Mach number [63]

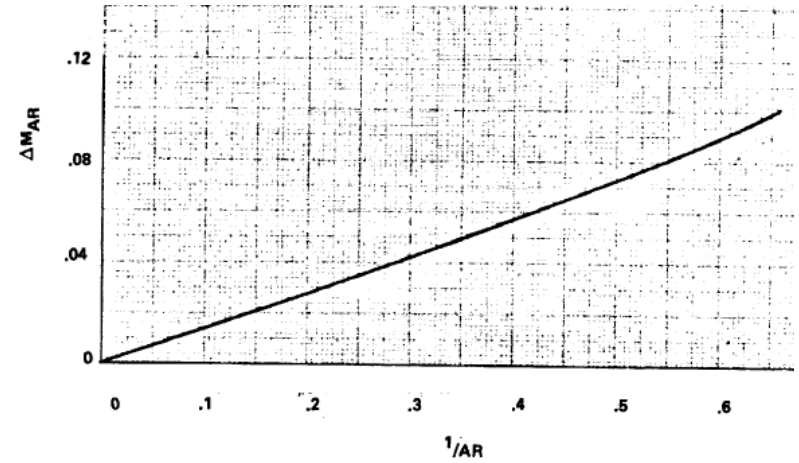

Figure C.10: Aspect ratio correction for drag divergence Mach number [63]

C.6. NLR supersonic drag model

This section will go into the method used to compute the drag coefficient for the aircraft design in the supersonic regime with some more detail. First, Appendix C.6.1 discusses the volume wave drag. Appendix C.6.2 then goes into the lift-induced wave drag, and Appendix C.6.3 shows how the components are combined to get to the full drag curve.

C.6.1. Supersonic zero-lift drag

As mentioned in the main text the supersonic volume wave drag is estimated as the sum of the contribution of four components, the fuselage, main wing and horizontal and vertical tail. Starting with the fuselage, it is approximated as two Kármán ogives, one for the forebody and one for the aftbody. The cylindrical section in between the two ogives is ignored. For each ogive the base drag coefficient can be computed by making use of the following equation:

$$C_D = \left(\frac{D_n}{l_n}\right)^2 \tag{C.12}$$

where D_n is the diameter of the cylindrical section, and l_n the length of the ogive. However, this value is only applicable at Mach one. For higher Mach numbers, the drag decreases and to correct for this, the values from the graph shown in Figure C.11 are used.

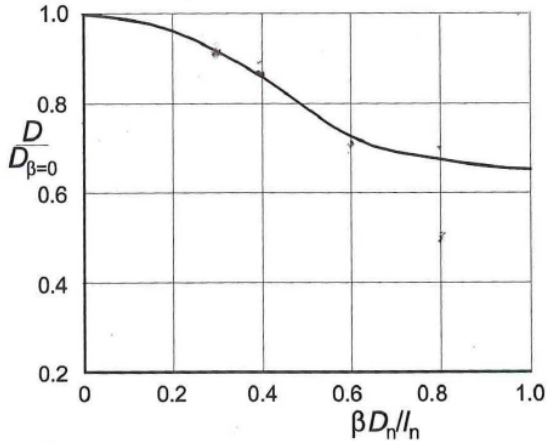

Figure C.11: Karman ogive wave drag due to volume corrected for compressibility [31, 139]

For each Mach number, the value of the compressibility factor β ($=\sqrt{M^2-1}$) can be used in combination with the diameter and length to estimate the ratio of the drag at that Mach number over that at Mach one. Then, to get the drag coefficient at that Mach number this ratio is multiplied with Equation (C.12). There is also some interference between the forebody and aftbody. To account for this, the aftbody has an additional 2% increase of its drag coefficient [31]. The coefficient found is then multiplied by the frontal area of the fuselage, which is the same as the cross-sectional area of the cylindrical section, to get its drag contribution.

For the wings, the wave drag at transonic speeds can be computed using Equation (C.13) [140] if they feature an optimal longitudinal and lateral thickness distribution [31].

$$C_{D_{WV}} S = K_{SH} \cdot \frac{128}{\pi} \cdot \frac{volume^2}{length^4} \tag{C.13}$$

For this equation, the part behind the factor K_{SH} represents the drag of a Sears-Haack body, which is achieved if K_{SH} is one. For delta wings many computational results have been published for which the drag coefficient based on the planform area can be written as follows [31].

$$C_{D_{WV}} = K_{SH} \cdot \frac{128}{\pi} \cdot \left(\frac{\cot \Lambda_{LE} \cdot volume}{S^{3/2}}\right)^2 \tag{C.14}$$

Note in this equation that the cotangent of the leading edge sweep angle is the same as the box parameter s/l for delta wings (see Figure C.12a). Using this parameter as an ordinate, the data from [140] was used to create Figure C.12b for the delta wing volume wave drag [31].

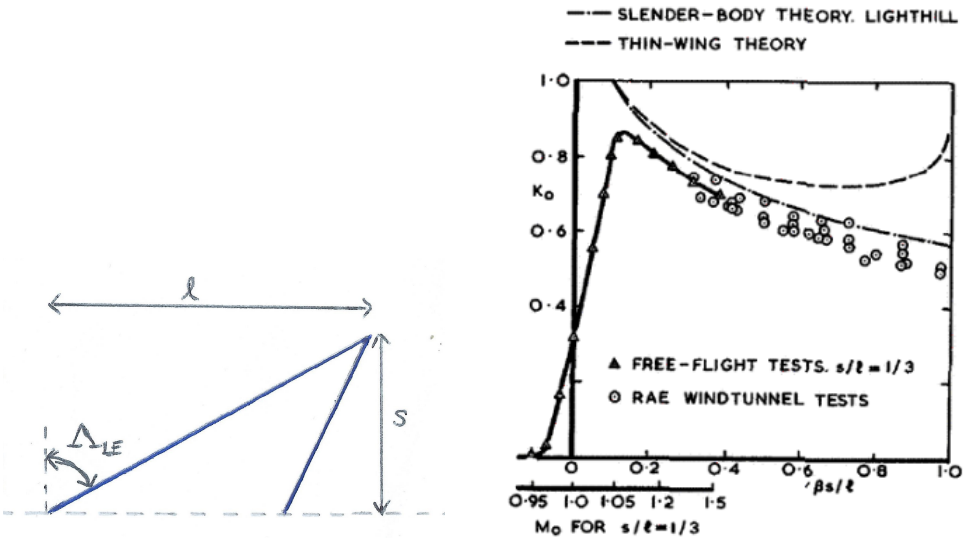

(a) Delta wing definition and box parameter

(b) Delta wing wave drag due to volume [140]

Figure C.12: Delta wing definition and volume wave drag

The following equation is said to approximate the slender-body theory presented in [141] very well according to [31]:

$$K_{SH} = 1.18 \cdot \frac{1 + 0.6 \cdot \beta \cdot \cot \Lambda_{LE}}{1 + 2.4 \cdot \beta \cdot \cot \Lambda_{LE}} \tag{C.15}$$

The wave drag coefficient for delta wings is frequently generalized by the following equation [31]:

$$C_{D_{WV}} = K_{WV} \cdot A \cdot \left(\frac{t}{c}\right)^2 = \left(\frac{r_s}{3}\right)^2 \cdot \frac{128}{\pi} \cdot K_{SH} \cdot A \cdot \left(\frac{t}{c}\right)^2 \tag{C.16}$$

where the following relationship between K_{WV} and K_{SH} is used:

$$K_{WV} = \left(\frac{r_s}{3}\right)^2 \cdot \frac{128}{\pi} \cdot K_{SH} \tag{C.17}$$

In this equation the value r_s is the area ratio and is defined as shown in Figure C.1. For most wings the value of the area ratio is about 0.7. Filling in that value shows that the value of K_{WV} is approximately 2.22 times K_{SH}. In [31], the area ratio for the horizontal and vertical tail is assumed to be roughly 0.7. Given that in this design the horizontal tail and vertical tail will largely be sized using statistics, this value is also assumed for the tail sections in the current aerodynamics module. For the main wing, which has a much larger drag contribution compared to the tail sections, this is not deemed good enough. Therefore, for each design the area ratio of the full wing is calculated and used.

The aspect ratio used in the drag coefficient equation is known from the design, and t/c represents the effective wing thickness which can be computed for each wing section by using Equation (C.18) [64].

$$\left(\frac{\bar{t}}{c}\right)_{eff} = \frac{\int_0^{b/2} \left(\frac{t}{c}\right) \cdot c\,dy}{\int_0^{b/2} c\,dy} = \frac{\int_0^{b/2} t\,dy}{\frac{b}{2} \cdot \left[\frac{c_{root}+c_{tip}}{2}\right]} = \frac{t_{root}+t_{tip}}{c_{root}+c_{tip}} \tag{C.18}$$

Where t represents the thickness of the wing at the root and tip, which can be computed by multiplying the t/c-ratio with the local chord length. The full wing thickness ratio is then determined by averaging the weighted thickness ratios, where each ratio is weighted with the area that it represents. For the horizontal and vertical tail the effective thickness is assumed to be 3% (0.03). In the current code the wing thickness ratio is a user-input because most past studies do not include airfoil thicknesses, but just the average thickness ratio.

Because no accurate generalized results have been published for cranked arrows and delta-like wings with curved leading edges, the method will use an equivalent delta wing with the mean leading edge sweep angle and area as the reference wing [31]. The drag coefficient found for each component is multiplied with its exposed area. After this, all of the contributions are known in terms of C_D times their own effective areas. To get the drag coefficient for the full aircraft it is then necessary to divide the sum of these contributions by the wing reference area.

From comparison between this method explained above and an additional analysis using the simplified supersonic area rule method by Jumper [142], it was found that the area ruled value was 70% of that found by the semi-empirical method explained. For this reason, a correction of 0.85 is added to the value found, such that it is closer to the real value [31].

C.6.2. Supersonic lift induced wave drag

For lift induced supersonic drag, the main focus is on the method described in [31] for cambered and twisted wings with a subsonic leading edge. In the optimal scenario the twist and leading edge camber should be applied such that the incoming airflow direction is close to that of the nose camberline [66]. This should be achieved close to the design lift conditions at cruise flight and can allow for achieving good suction performance.

For slender wings featuring leading edge suction along the entire span, the theoretical lower limit for drag due to lift was derived as follows [143]:

$$D_L = \frac{\left(\frac{L}{b}\right)^2}{\pi \cdot q} + \beta^2 \cdot \frac{\left(\frac{L}{l}\right)^2}{2 \cdot \pi \cdot q} \tag{C.19}$$

The first term is the vortex induced drag and can be rewritten as follows:

$$D_i = \frac{L^2}{\pi \cdot q \cdot b^2} \quad \longrightarrow \quad \frac{D_i}{q \cdot S} = \frac{\frac{L^2}{q \cdot S}}{\pi \cdot q \cdot b^2} \cdot \frac{\frac{1}{S}}{\frac{1}{S}} \tag{C.20}$$

$$C_{D_{VL}} = \frac{\frac{L^2}{q^2 \cdot S^2}}{\pi \cdot \frac{b^2}{S}} = \frac{C_L^2}{\pi \cdot A} \tag{C.21}$$

This latter equation is the vortex-induced drag assuming that the wing loading is elliptical. The second term of Equation (C.19) represents the minimum wave drag due to lift in case of an elliptic streamwise lift distribution along the lifting length l [31]. This term can also be rewritten and non-dimensionalized as follows:

$$D_{WL} = \beta^2 \cdot \frac{\left(\frac{L}{l}\right)^2}{2 \cdot \pi \cdot q} \quad \longrightarrow \quad \frac{D_{WL}}{q \cdot S} = \frac{\frac{L^2}{q \cdot S}}{2 \cdot \pi \cdot q} \cdot \left(\frac{\beta}{l}\right)^2 \cdot \frac{b^2}{b^2} \cdot \frac{\frac{1}{S}}{\frac{1}{S}} = \frac{\frac{L^2}{(q \cdot S)^2}}{2 \cdot \pi \cdot \frac{b^2}{S}} \cdot \left(\frac{\beta \cdot b}{l}\right)^2 \tag{C.22}$$

$$C_{D_{WL}} = \frac{C_L^2}{2 \cdot \pi \cdot A} \cdot \left(\frac{\beta \cdot b}{l}\right)^2 \tag{C.23}$$

Equation (C.19) was found to match quite well with the linear theory for cambered delta wings (see Figure C.13). Based on that, the lower limit of drag due to lift on twisted and cambered wings was proposed to be like shown in Figure C.14b for delta-like and arrow wings [31].

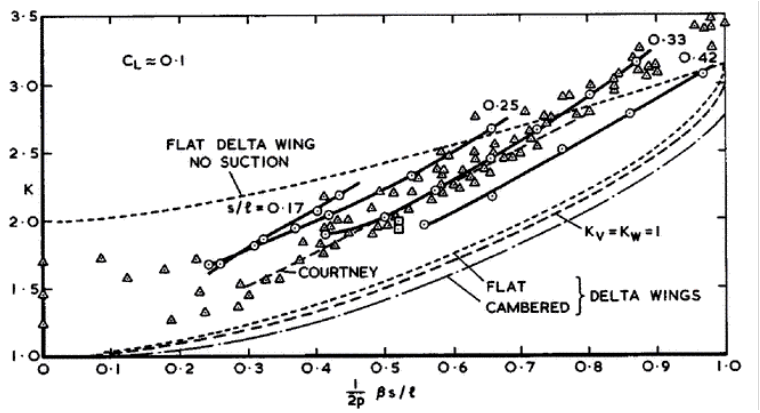

Figure C.13: Empirical method factor for selecting the optimum design lift coefficient [67]

As previously defined, the box and area ratio r_s of the wing can be calculated. Expressed as box and area ratios the minimum drag due to lift will be [31]:

$$C_{D_L} = \frac{r_s \cdot \beta \cdot C_L^2}{4 \cdot \pi} \cdot \left[\left(\beta \cdot \frac{s}{l}\right)^{-1} + 2 \cdot \beta \cdot \frac{s}{l}\right] \tag{C.24}$$

These findings are summarized in Figures C.14a and C.14b and they can be used in order to predict the drag.

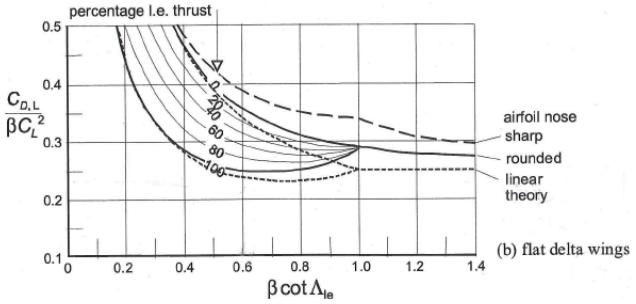

(a) Drag due to lift for flat delta wings [31]

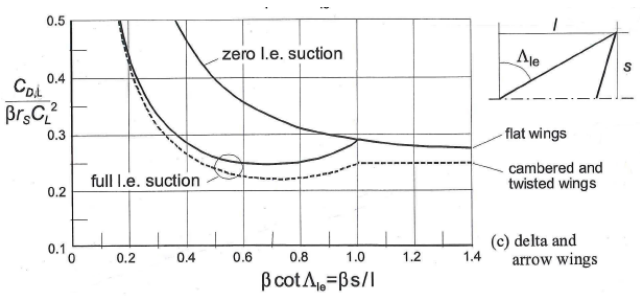

(b) Drag due to lift for delta and arrow wings [31]

Figure C.14: Supersonic drag due to lift curves [31]

C.6.3. Supersonic total drag

Now that the two main supersonic drag components have been defined, excluding friction drag which was described in Section 5.3.1, it is possible to look into the full drag curve prediction. For supersonic flow, the suction parameter is defined as follows [31]:

$$\overline{\sigma} = \frac{C_L \cdot \tan\alpha - C_{D_L}}{C_L \cdot \tan\alpha - \left(C_{D_{VL}} + C_{D_{WL}}\right)} \qquad \text{with} \qquad \mathrm{C_{D_L}} = \mathrm{C_D} - \mathrm{C_{D_0}} \tag{C.25}$$

In this case the lift and drag coefficients that apply are:

$$C_L = K_p \cdot \sin\alpha \cdot \cos\alpha^2 + \left(1-\overline{\sigma}\right) \cdot K_v \cdot \cos\alpha \cdot \sin\alpha^2 \qquad \text{and} \qquad \mathrm{C_D} = \mathrm{C_{D_0}} + \left(1-\overline{\sigma}\right) \cdot \mathrm{C_L} \cdot \tan\alpha + \overline{\sigma} \cdot \mathrm{K_d} \cdot \mathrm{C_L^2} \tag{C.26}$$

with the following definitions:

$$K_p = C_{L_\alpha} \qquad K_v = K_p \cdot \frac{1 - K_p \cdot K_d}{\cos\Lambda_{LE}} \qquad K_d = \frac{d\left(C_{D_{VL}} + C_{D_{WL}}\right)}{d\left(C_L\right)^2} \tag{C.27}$$

At small angles of attack the lift coefficient function can be rewritten to:

$$C_L = C_{L_\alpha} \cdot \alpha + \left(1-\overline{\sigma}\right) \cdot K_v \cdot \alpha^2 \tag{C.28}$$

Then, by substitution of Equation (C.24) the drag coefficient can be rewritten to the following function:

$$C_D = C_{D_0} + \left(1-\overline{\sigma}\right) \cdot \frac{C_L^2}{C_{L_\alpha}} + \overline{\sigma} \cdot (1+\delta) \cdot \frac{r_s \cdot \beta \cdot C_L^2}{4 \cdot \pi} \cdot \left[\left(\beta \cdot \frac{s}{l}\right)^{-1} + 2 \cdot \beta \cdot \frac{s}{l}\right] \tag{C.29}$$

In this drag function, the zero-lift drag coefficient is the summation of the friction drag coefficient and volume wave drag coefficient, and δ is assumed to be 0.1 [31]. Now that this drag curve is known, the last step is to indicate how it should be used to compute the drag curve.

In order to allow for the most accurate prediction of lift and drag, the suction parameter $\overline{\sigma}$ has to be known. The value of this parameter, however, is quite complex as it depends on multiple factors such as the Mach and Reynolds number. For the conceptual design stage it is assumed that the wing geometry is designed such that the best performance is reached for the design lift coefficient $C_{L,des}$. For the prediction of the suction parameter as well as additional detailed information the reader is referred to [66, 67]. The method described in those sources is rather elaborate so for now a simplified procedure will be followed:

1. Determine the design lift coefficient for the aircraft by making use of the graph in Figure C.15. This will return a value for K_D depending on the Mach number, which can then be used to calculate the design lift coefficient using the cruise lift coefficient:

$$C_{L,des} = K_D \cdot C_{L,cr} \tag{C.30}$$

2. Make an assumption about the value of the suction parameter at that design lift coefficient. In this method, it is assumed that the parameter is equal to the fraction of the wing that features a subsonic leading edge. Note that the part of the wing located inside the fuselage does not contribute to the subsonic leading edge span, so the maximum value for $\overline{\sigma}$ is about 0.9-0.92 at the design lift coefficient. This seems to agree with a graph from [50] which could be used to estimate the suction parameter.

3. By making use of Equation (C.29) the design drag coefficient can be computed which is achieved at the design lift coefficient.

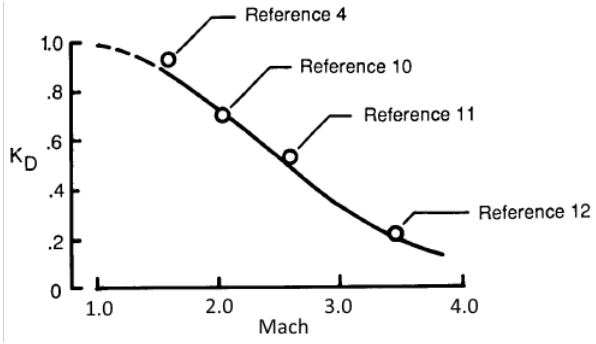

Figure C.15: Empirical method factor for selecting the optimum design lift coefficient [67]

4. Now the drag polar can be created by combining two sections, with the design lift coefficient being the boundary.

$$C_L \leq C_{L_{des}} \qquad C_D = C_{D_{des}} + (1+\delta) \cdot \frac{r_s \cdot \beta}{4 \cdot \pi} \cdot \left[\left(\beta \cdot \frac{s}{l} \right)^{-1} + 2 \cdot \beta \cdot \frac{s}{l} \right] \cdot \left(C_L^2 - C_{L_{des}}^2 \right) \tag{C.31}$$

$$C_L > C_{L_{des}} \qquad C_D = C_{D_{des}} + \frac{\left(C_L^2 - C_{L_{des}}^2 \right)}{C_{L_\alpha}} \tag{C.32}$$

By making use of this method, the L/D curve can be created, and the design L/D ratio computed. This ratio at the design lift coefficient is assumed to represent the maximum achievable value for the aircraft. During cruise, the aircraft will not operate at this aerodynamic efficiency, but it will operate at 0.866 times this maximum value. To improve the method described it is for example possible to make use of the supersonic area rule to determine the wave drag coefficient as is discussed in Appendix C.8.

C.7. Cross-sectional area distribution analysis

For the Raymer supersonic drag method, the area distribution of the aircraft design needs to be known in order to generate a comparable Sears-Haack body. While for the fuselage by itself this is not very difficult, the area distribution for the wing and empennage sections is less straightforward. Some research was performed to find empirical methods to determine their area contributions, but no satisfying options were found. To this end, a different solution was sought by making use of the 3D aircraft model in the KBE software ParaPy[5].

Using the inputs defined at the start of the design (e.g. aspect ratio, sweep angles) and outputs of the wing loading curve, the aircraft geometrical characteristics were computed as explained in Chapter 4. This data could then be used together with ParaPy to create a simple 3D aircraft model composed of the fuselage, main wing and empennage. It should be noted that for the drag calculations, the maximum cross-sectional area is the only factor of interest, and is expected to be located somewhere in the region where the main wing intersects the fuselage. An example aircraft model is shown in Figure C.16.

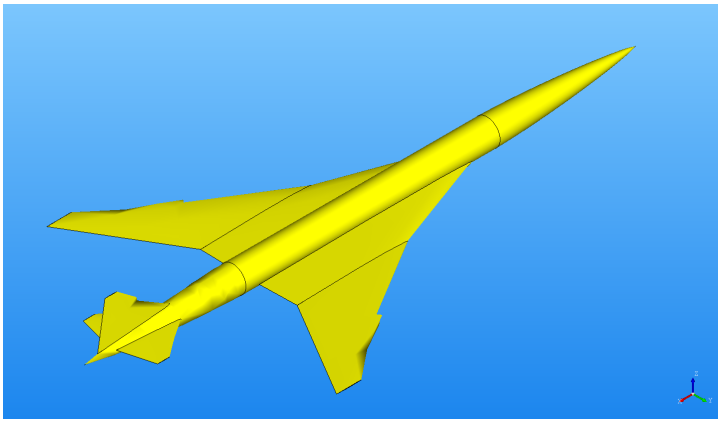

Figure C.16: Example supersonic aircraft model in ParaPy based on NLR report [31]

[5] https://www.parapy.nl/ (accessed May 7 2019)

By using ParaPy the different components can be transformed into a single solid. This solid can then be intersected by thin planes to find the common areas. Such a set of rectangles is depicted in Figure C.17.

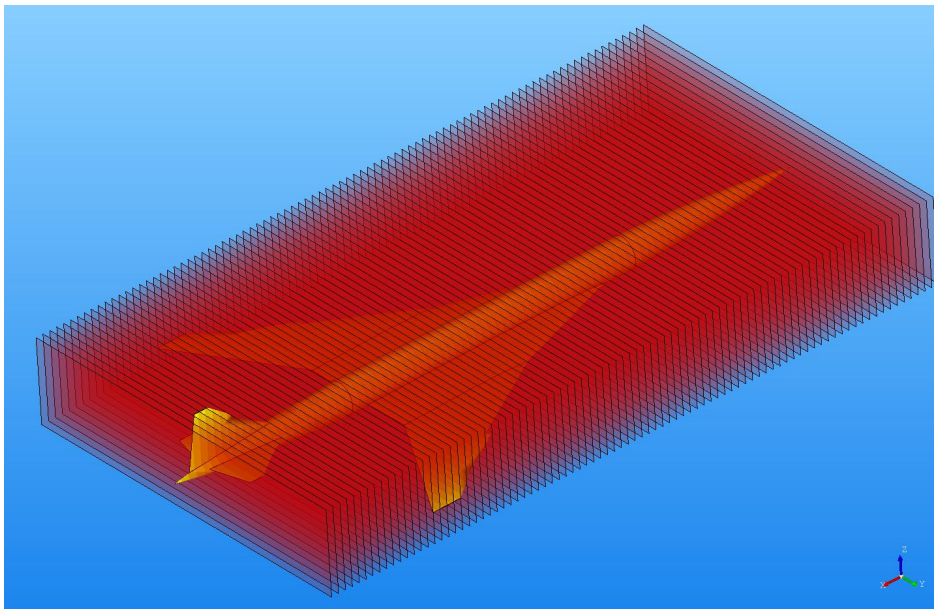

Figure C.17: Aircraft slicing example in ParaPy

The resulting intersecting area is visualized in Figure C.18 showing the common area for each slicing position.

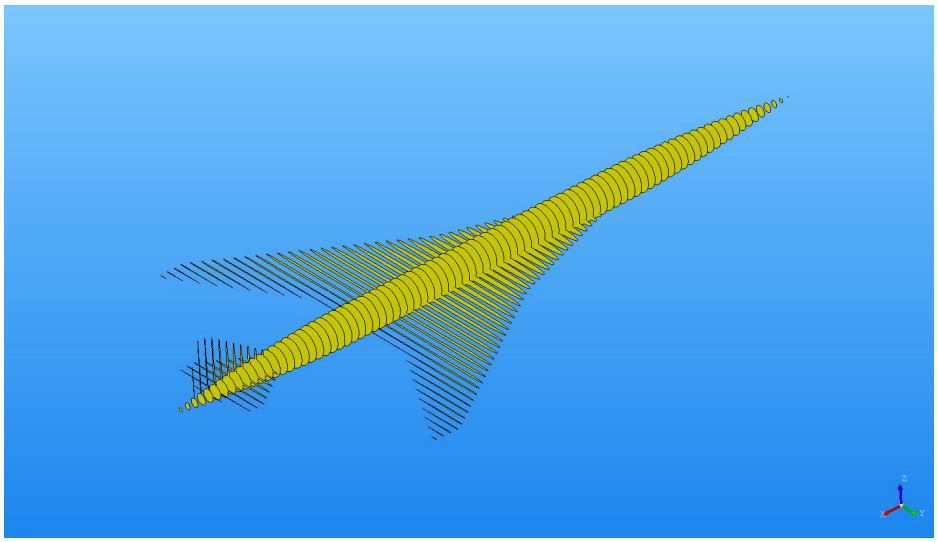

Figure C.18: Common areas of aircraft model and rectangles

By then combining the x-coordinate of each slice with its corresponding cross-sectional area, the distribution can be calculated for the aircraft, as shown in Figure C.19, where the distribution is compared to that of the NLR aircraft on which it is based. The comparison shows that there is a good match between the reference cross-sectional area distribution and that computed by using ParaPy, especially for the part left of the maximum value. The maximum cross-sectional area is underestimated by about 3.8%. This could be explained by a different airfoil being used for the reference aircraft wing and waisting of the fuselage cross-section. Towards the rear of the aircraft there is also some deviation which is caused by small differences in the shape and positioning of the horizontal and vertical tail.

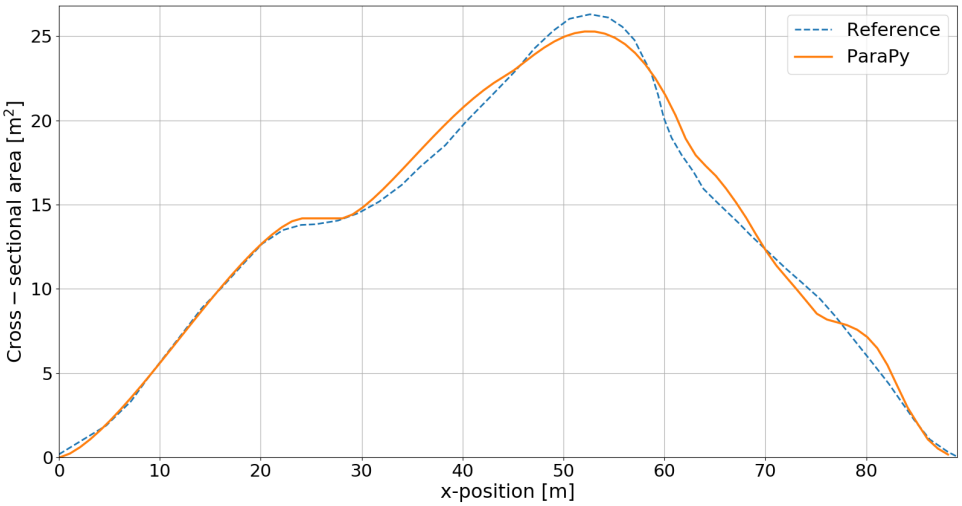

Figure C.19: Cross-sectional area curve comparison to reference [31]

After this is done, it is still necessary to account for the presence of the nacelles and the airflow through the engines. This airflow cross-sectional area has to be subtracted from the cross-sectional area along the nacelle position. To compensate for the added area of the nacelle, only 80% of the inlet area will be subtracted from A_{max}. The resulting maximum cross-sectional area is then provided to the drag program to generate the Sears-Haack body. In future research, this slicing method could be expanded to use it for the supersonic area rule as is briefly explained in the next section.

C.8. Future aerodynamic research

Due to the limited amount of time available for the setup of the aerodynamics module of the design program, not all literature and techniques that were found could be studied, implemented and tested. Also, the level of accuracy of the current method is not optimal for more detailed design than the early conceptual phase. Still, should there be interest in the future to expand the current program, it is useful to have some more ideas about things which could be looked into and improved. That is the purpose of this section. Below, a number of different techniques or specific design programs are listed and discussed which could be studied and tested. It was decided to not include these items in the recommendations chapter because together they are quite sizable and specific.

- *Apply panel methods capable of computing the lifting performance of an aircraft or wing in supersonic flight*

  For the current method, the lift is estimated by making use of the (digital) DATCOM method and program. While they are providing decent values, the prediction is still largely based on statistical data, and does not allow for detailed analysis of design choices like local changes in twist angle or camber. Also, the type of airfoil has a limited effect on the results. For this reason, a couple of programs have been built in the past, one of which is PANAIR [144], created at Boeing. This program requires a quite detailed input file, which has to be formatted properly. To aid in this, a different (pre-processing) program called PANIN has been created to help the user in setup the input file. Both programs are available for free[6] and are also provided with a list of additional literature which offer experimental applications of the program, and further information on the methods.

  Another set of programs which could be considered for this aspect is W12SC3[7], which can be combined with COREL [145]. They can be used for aerodynamic design of wings for supersonic maneuvering.

- *Improved zero-lift wave drag prediction*

  For the prediction of the zero-lift wave drag an important program to look at for comparison and possibly apply in the design procedure is that by Harris [146] which was created at Boeing. Since then more advanced models have been created which could also be investigated.

[6] http://www.pdas.com/ (accessed September 21 2018)
[7] http://www.pdas.com/w12sc3.html (accessed September 21 2019)

In Appendix C.7 a different approach was shown that used a 3D geometry defined inside a KBE framework, which allows for easy visualization. Now, instead of using a vertical cutting plane, the supersonic area rule can be applied where the cutting plane is rotated so that it is at the Mach angle μ. The drag is then computed by solving the following integral [31]:

$$D(\theta) = -\frac{\rho \cdot V^2}{4 \cdot \pi} \int_0^l \int_0^l A''(x_1) A''(x_2) \log|x_1 - x_2| dx_1 dx_2 \tag{C.33}$$

and the total drag is determined by integrating over the various equivalent bodies found for different angles θ as shown in Equation (C.34) and Figure C.20:

$$D = \frac{1}{2 \cdot \pi} \int_0^{2\pi} D(\theta) d\theta \tag{C.34}$$

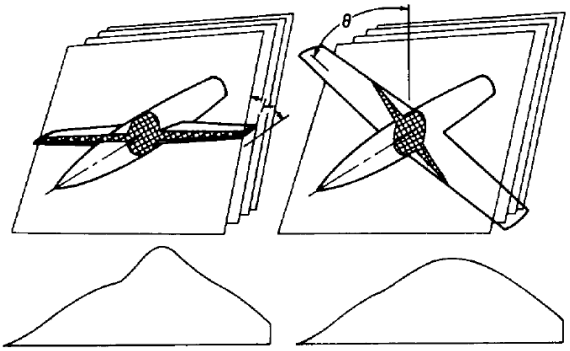

Figure C.20: Supersonic area rule slicing example [146]

Because this is a rather complex method, there is also the possibility to make use of a simplification through the method of Jumper [142]. It follows the same steps as the wave drag method described above, but makes use of a single equivalent body of revolution to represent the complete aircraft area distribution. Consequently, the amount of calculations required is less than for the full method.

As an alternative to building a custom wave drag prediction program the method currently available in OpenVSP[8] [147] can be used which was created by Waddington [148]. While it might not be ideal, it is possible to either create a 3D aircraft model in OpenVSP or use ParaPy's features to export the '.stl'-output of the geometry. This .stl-file can then be imported in OpenVSP and analyzed to find the supersonic zero-lift wave drag.

- *Subsonic lift and span efficiency prediction: Athena Vortex Lattice (AVL)*[9] *and Tornado*[10]

  Both programs are common to determine the subsonic lifting performance and lift-induced drag of wings alone or even full aircraft configurations. An added benefit of using AVL is that it has been integrated in ParaPy through an API which allows for defining the AVL inputs in ParaPy, and also running it from there. During the initial investigation an attempt was made at using AVL, but it seemed to be returning too high values for the lifting performance, overestimating by more than 10%. This could be due to the relatively high sweep angles and thin airfoils used on the supersonic aircraft wing, but should be further investigated.

  Tornado is a Matlab based program with a text based interface similar to AVL. Both can also be run in batch mode to analyze a large number of scenarios without the user having to interact with them each time. The programs can also estimate the span efficiency factor of the aircraft to allow for a better prediction of lift-induced drag than the current method. For this, it might also be useful to look at [62] to get a better overview of the different (semi-)empirical methods available for estimating the Oswald efficiency factor to determine which is the best.

[8] http://openvsp.org/ (accessed July 12 2018)
[9] http://web.mit.edu/drela/Public/web/avl/ (accessed September 17 2018)
[10] http://tornado.redhammer.se/ (accessed September 17 2018)

- *Application of CFD*

  To get a better prediction of the lift (and possibly drag) of the aircraft in all speed regimes CFD can be used. Recently, the option to create meshes using the aircraft geometry was added to ParaPy, and in the near future, it will also allow for direct interaction with the solver SU2 [149]. This solver is continually updated, free, available online[11], and is being contributed to by several universities including a group at TU Delft, so that there could be expertise available for support in case of questions. A disadvantage of using CFD is that it will take significantly more time to run and evaluate the results than for the simpler panel-based methods (e.g. PANAIR), although it will be more accurate. Because of the increased runtime an iterative design loop will take more time to complete, reducing the number of designs that can be studied. For this reason, it might be an option to only apply the CFD for several final designs to improve the knowledge about them, and check the accuracy of the lower fidelity panel methods.

  As a side project, it might also be an idea to look into using scaled models in a wind tunnel to check the accuracy of the results, although sufficient data is likely already available for a number of different geometries such as in [150]. This also discusses the boundary conditions and solver used, and indicates that half of the aircraft was simulated by applying a symmetrical boundary condition along the fuselage central plane.

- *Supersonic natural laminar flow research*

  As a more specific research topic it might be interesting to look into the creation of a design tool which can allow for estimating the portion of the aircraft that can feature laminar flow in supersonic flight. Having this ability, the amount of friction drag in the supersonic regime could be reduced as shown in [61]. However, because this is a very specific item it could be combined with the integration of CFD in the aerodynamics module.

- *More advanced high-lift device analysis and sizing*

  For the current version of the aerodynamics module, the high-lift devices are sized and their lift contribution is analyzed by making use of a set of low-fidelity equations, which is sufficient for now. However, in the case of supersonic aircraft with their low aspect ratio wings and thin airfoils, the lift contribution from high-lift devices can be very important in meeting the landing and takeoff requirements. Additionally, they could help allow the aircraft to use less thrust at takeoff by reducing the takeoff speed. This can help in reducing the amount of engine noise, but it should be ensured that the additional noise from more advanced high-lift devices does not outweigh this engine noise decrease. A recent thesis at TU Delft outlining a methodology for a medium-fidelity maximum lift estimation can be found in [151]. This item can be combined with the next step, but is mentioned separately because it is considered important enough to warrant a separate item.

- *Look at research related to the Initiator*

  For the design of subsonic transport configurations, a lot of research has already been completed at TU Delft, and part of that research has been combined in the Initiator aircraft design program [12]. In this program, a number of aerodynamic aspects which have only been analyzed at a low-fidelity in the current supersonic program or which were ignored, have been studied in much more detail such as the transonic drag rise in [152]. While these methods might not all be applicable to supersonic aircraft designs, it is a good place to start looking when attempting to improve the level of fidelity of the subsonic aerodynamic analyses in the supersonic program.

[11] https://su2code.github.io/ (accessed September 28 2018)

D
Class II support

D.1. Class II equations listings

In this section, the different equations used for each Class II component are listed. To make the equations easier to understand, all individual symbols used are listed at the end of this section. Note that the equations do not include the 5% growth factor, other penalties, or technology factors. These are only included in the Class II python module. Additionally, note that if more than one method is included, the component (e.g. electrical) weight will be the (weighted) average of those methods.

Structures group:

$$W_{wing,USAF} = 3.08 \cdot \left(\frac{K_{PIV} \cdot n_{ult} \cdot W_{TO}}{\mathrm{t/c_{w,max}}} \cdot \left[\left(\tan\left(\Lambda_{w,LE}\right) - \frac{2 \cdot (1-\lambda_w)}{AR_w \cdot (1+\lambda_w)} \right)^2 + 1 \right] \cdot 10^{-6} \right)^{0.593} \cdot [(1+\lambda_w) \cdot AR_w]^{0.89} \cdot S_w^{0.741} \tag{D.1}$$

$$W_{wing,Toren} = W_{TO} \cdot K_w \cdot b_s^{0.75} \cdot \left[1 + \sqrt{\frac{b_{ref}}{b_s}} \right] \cdot n_{ult}^{0.55} \cdot \left(\frac{\frac{b_s}{t_r}}{\frac{W_{TO}}{S_w}} \right)^{0.30} \tag{D.2}$$

$$W_{ht.kroo} = 5.25 \cdot S_{ht} + 0.8 \cdot 10^{-6} \cdot \frac{n_{ult} \cdot b_{ht}^3 \cdot W_{TO} \cdot \overline{c}_{ht} \cdot \sqrt{S_{ht}}}{t/c_{ht,avg} \cdot \cos\left(\Lambda_{ht,LE}\right)^2 \cdot L_{ht} \cdot S_{ht}^{1.5}} \tag{D.3}$$

$$W_{ht,FLOPS} = 0.53 \cdot S_{ht} \cdot W_{TO}^{0.2} \cdot (\lambda_{ht} + 0.5) \tag{D.4}$$

$$W_{fin} = 2.62 \cdot S_{vt} + 1.5 \cdot 10^{-5} \cdot \frac{n_{ult} \cdot b_{vt}^3 \cdot \left(8 + 0.44 \cdot \frac{W_{TO}}{S_w}\right)}{t/c_{vt,avg} \cdot \cos\left(\Lambda_{vt,LE}\right)^2} \tag{D.5}$$

$$W_{vt,kroo} = W_{fin} + W_{fin} \cdot \frac{S_r}{S_{vt}} \cdot 1.6 \tag{D.6}$$

$$W_{vt,FLOPS} = 0.32 \cdot W_{TO}^{0.3} \cdot (\lambda_{vt} + 0.5) \cdot S_{vt}^{0.85} \tag{D.7}$$

$$W_{fuse} = 1.35 \cdot \left(L_{fuse} \cdot D_{fuse,avg}\right)^{1.28} \cdot \left(1 + 0.05 \cdot N_{eng,\,fuse}\right) \cdot \left(1 + 0.38 \cdot C_{cargo}\right) \cdot N_{fuse} \tag{D.8}$$

$$W_{LG} = 20.44 \cdot \left(\frac{W_{TO}}{1{,}000} \right)^{1.125} \tag{D.9}$$

Propulsion group:

$$W_{eng} = N_{eng} \cdot W_{eng,dry} \tag{D.10}$$

$$W_{nac} = 0.25 \cdot N_{nac} \cdot D_{nac} \cdot L_{nac} \cdot T_{eng,rated}^{0.36} \tag{D.11}$$

$$W_{rev} = 0.034 \cdot T_{eng,rated} \cdot N_{nac} \tag{D.12}$$

$$W_{air\ induction} = W_{duct\ prov} + W_{int\ duct} + W_{var\ inlet} \tag{D.13}$$

$$W_{duct\ prov} = 0.32 \cdot N_{inl} \cdot L_{d,sub} \cdot A_{inl}^{0.65} \cdot p_{st,compr}^{0.6} \tag{D.14}$$

$$W_{int\ duct} = 1.735 \cdot \left(N_{inl} \cdot L_{d,sub} \cdot A_{inl}^{0.5} \cdot p_{st,compr} \cdot K_{GEO} \cdot K_M\right)^{0.7331} \tag{D.15}$$

$$W_{var\ inlet} = 4.079 \cdot \left(N_{inl} \cdot L_{ramp} \cdot A_{inl}^{0.5} \cdot K_{TE}\right)^{1.201} \tag{D.16}$$

$$W_{fuel\ sys} = 1.07 \cdot W_{f,max}^{0.58} \cdot N_{eng}^{0.43} \cdot M_{max}^{0.34} \tag{D.17}$$

$$W_{prop\ install} = 0.26 \cdot N_{eng} \cdot T_{eng,rated}^{0.5} + 11 \cdot N_{eng} \cdot M_{max}^{0.32} \cdot D_{nac}^{1.6} \tag{D.18}$$

Equipment group:

$$W_{IAE} = W_{instr} + W_{avionics} \tag{D.19}$$

$$W_{instr} = 0.48 \cdot S_{fuse,pf}^{0.57} \cdot M_{max}^{0.5} \cdot \left(10 + 2.5 \cdot N_{pilot} + N_{eng,wing} + 1.5 \cdot N_{eng,fuse}\right) \tag{D.20}$$

$$W_{avionics} = 15.8 \cdot R_{des}^{0.1} \cdot N_{pilot}^{0.7} \cdot S_{fuse,pf}^{0.43} \tag{D.21}$$

$$W_{surf\ contr} = K_{sc} \cdot W_{TO}^{2/3} \cdot K_{spoil} \cdot K_{LE} \tag{D.22}$$

$$W_{hydr} = 0.57 \cdot \left(S_{fuse,pf} + 0.27 \cdot S_w\right) \cdot \left(1 + 0.03 \cdot N_{eng,wing} + 0.05 \cdot N_{eng,fuse}\right) \cdot \left(\frac{3,000}{p_{hydr}}\right)^{0.35} \cdot (1 + 0.04 \cdot P_{var}) \cdot M_{max}^{0.33} \tag{D.23}$$

$$W_{elec,Raymer} = 7.291 \cdot R_{kva}^{0.782} \cdot L_{elec\ route}^{0.346} \cdot N_{gen}^{0.1} \tag{D.24}$$

$$W_{elec,Toren} = 36 \cdot R_{kva} \cdot \left(1 - 0.033 \cdot \sqrt{R_{kva}}\right) \tag{D.25}$$

$$W_{elec,FLOPS} = 92 \cdot L_{fuse}^{0.4} \cdot w_{fuse,max}^{0.14} \cdot N_{fuse}^{0.27} \cdot N_{eng}^{0.69} \cdot \left(1 + 0.044 \cdot N_{pilot} + 0.0015 \cdot N_{pax}\right) \tag{D.26}$$

$$W_{APU}{}^{1} = \frac{0.265}{100} \cdot W_{TO} \tag{D.27}$$

$$W_{ecs} = \frac{2}{3} \cdot \left[\frac{1}{2} \cdot \left(W_{ac,Raymer} + W_{ac,FLOPS}\right) + \frac{1}{2} \cdot \left(W_{antiice,Raymer} + W_{antiice,FLOPS}\right)\right] + \frac{1}{3} \cdot W_{ecs,Toren} \tag{D.28}$$

$$W_{ac,Raymer} = 62.36 \cdot \left(N_{pax} + N_{crew}\right)^{0.25} \cdot \left(\frac{V_{pres}}{1,000}\right)^{0.604} \cdot W_{uav}^{0.1} \tag{D.29}$$

$$W_{ac,FLOPS} = \left(3.2 \cdot \left(S_{fuse,pf} \cdot d_{fuse,max}\right)^{0.6} + 9 \cdot N_{pax}^{0.83}\right) \cdot M_{max} + 0.075 \cdot W_{avionics} \tag{D.30}$$

$$W_{antiice,Raymer} = 0.002 \cdot W_{TO} \tag{D.31}$$

$$W_{antiice,FLOPS} = \frac{b_w}{\cos \Lambda_{w,qc}} + 3.8 \cdot D_{eng,avg} \cdot N_{eng} + 1.5 \cdot w_{fuse,max} \tag{D.32}$$

$$W_{ecs,Toren} = 6.75 \cdot L_{pax\ comp}^{1.28} \tag{D.33}$$

$$W_{handling\ gear} = \left(3 \cdot 10^{-4}\right) \cdot W_{TO} \tag{D.34}$$

$$W_{furn} = 0.211 \cdot W_{MZF}^{0.91} \tag{D.35}$$

Operating items group:

$$W_{services} = W_{crew} + W_{unus\ fuel} + W_{eng\ oil} + W_{pax\ service} + W_{cargo\ cont} \tag{D.36}$$

$$W_{crew} = N_{attend} \cdot 155 + N_{pilot} \cdot 225 \tag{D.37}$$

$$W_{unus\ fuel} = 11.5 \cdot N_{eng} \cdot T_{eng,rated}^{0.2} + 0.07 \cdot S_w + 1.6 \cdot N_{tanks} \cdot W_{f,max}^{0.28} \tag{D.38}$$

[1] value for long-range, for short range use 0.471 instead of 0.265

$$W_{eng\ oil} = 0.082 \cdot N_{eng} \cdot T_{eng,rated}^{0.65} \tag{D.39}$$

$$W_{pax\ service} = \left(5.164 \cdot N_{pax,fc} + 3.846 \cdot N_{pax,bus} + 2.529 \cdot N_{pax,econ}\right) \cdot \left(\frac{R_{des}}{M_{max}}\right)^{0.225} \tag{D.40}$$

$$W_{cargo\ cont} = 175 \cdot \left[\frac{W_{cargo}}{950}\right] \tag{D.41}$$

All variables listed below require their values to be provided in **Imperial** units.

$\Lambda_{x,LE}$	leading edge sweep angle of component x
$\Lambda_{x,qc}$	quarter chord edge sweep angle of component x
λ_x	taper ratio of component x
A_{inl}	inlet area
AR_x	aspect ratio of component x
b_{ref}	reference span (6.25 ft)
b_s	structural wing span (span divided by cosine of mid-chord sweep)
b_x	span of component x
C_{cargo}	cargo factor (0 for passenger transport, 1 for military cargo transport)
$\overline{c}_x$	mean aerodynamic chord of component x
$D_{eng,avg}$	average engine diameter
$D_{fuse,avg}$	average fuselage diameter
D_{nac}	nacelle diameter
$d_{fuse,max}$	maximum fuselage depth
K_{GEO}	duct shape factor (1.33 if two relatively flat sides, 1 if round or one flat side)
K_{LE}	LE surface factor (1.2 if LE HLDs present, 1 otherwise)
K_M	duct material factor (1 if M_D<1.4, otherwise 1.5)
K_{PIV}	wing variable sweep structural factor (1 if fixed, 1.175 if variable sweep)
K_{sc}	surface control factor (assumed 0.64 as indicated by [34])
K_{spoil}	spoiler factor (1.15 if spoilers present, otherwise 1)
K_{TE}	temperature correction factor (1 if M_D<3, (M_D+2)/5 for 3 < M_D < 6)
K_w	wing factor of proportionality (depending on HLDs and landing gear position)
$L_{d,sub}$	subsonic duct length
$L_{elec\ route}$	electrical routing distance (generators to avionics to cockpit)
L_{fuse}	fuselage length
L_{ht}	tail length (distance wing quarter MAC to tail quarter MAC location)
L_{nac}	nacelle length
$L_{pax\ comp}$	passenger cabin length
L_{ramp}	variable ramp length
M_{max}	maximum Mach number
N_{attend}	number of cabin crew members
N_{crew}	number of crew members (flight and cabin crew)
N_{eng}	number of engines
$N_{eng,fuse}$	number of fuselage mounted engines
$N_{eng,wing}$	number of wing mounted engines
N_{fuse}	number of fuselages
N_{gen}	number of generators
N_{inl}	number of inlets
N_{nac}	number of nacelles
N_{pax}	number of passengers
$N_{pax,bus}$	number of business class passengers
$N_{pax,econ}$	number of economy class passengers
$N_{pax,fc}$	number of first class passengers
N_{pilot}	number of flight crew members
N_{tanks}	number of fuel tanks
n_{ult}	ultimate load factor
P_{var}	variable sweep penalty (value ranges from 0 for fixed-wing to 1 for full variable-sweep wing)

p_{hydr}	hydraulic system pressure
$p_{st,compr}$	maximum compressor face static pressure (typically 15-50 psi)
R_{des}	aircraft design range
R_{kva}	electrical system rating
S_x	area of component x
$T_{eng,rated}$	rated engine thrust
t_r	root wing thickness (at fuselage centerline)
$t/c_{x,max}$	maximum thickness-to-chord ratio of component x
$t/c_{x,avg}$	average thickness-to-chord ratio of component x
V_{pres}	pressurized fuselage volume
W_{cargo}	cargo weight
$W_{eng,dry}$	dry engine weight
$W_{f,max}$	maximum fuel weight
W_{MZF}	maximum zero fuel weight
W_{TO}	takeoff weight
W_{uav}	uninstalled avionics weight (typically 800-1400 lbs [50])
$w_{fuse,max}$	maximum fuselage width

Subscripts:

$fuse,\ pf$	fuselage planform
ht	horizontal tail
r	rudder
vt	vertical tail
w	wing

D.2. Weight breakdown output file example

Below, an example of the class II weight breakdown output file is shown for Concorde. All weights are listed in pounds (center column), and in kilograms (right column) in brackets.

Concorde.dat

```
Concorde

Weight breakdown

    Wing                                    30075.7 (13642.1)
    Horizontal tail                          0.0 ( 0.0)
    Vertical tail                           7127.8 (3233.1)
    Fuselage                                25729.5 (11670.7)
    Landing gear                            15820.1 (7175.9)
Structures                                 78753.0 (35721.7)
    Engines                                 27666.7 (12549.4)
    Nacelles                                6191.7 (2808.5)
    Air induction                           8570.3 (3887.4)
    Thrust reverser                         5208.6 (2362.6)
    Fuel system                             3134.0 (1421.6)
    Propulsion install                      687.5 (311.8)
Propulsion                                 51458.9 (23341.4)
    Instruments, Avionics and Electronics   4171.8 (1892.3)
    Flight controls                         5311.2 (2409.1)
    Hydraulics                              3564.1 (1616.6)
    Electrical                              5005.2 (2270.3)
    APU                                     1102.9 (500.2)
    Environmental control                   5430.6 (2463.3)
    Furnishings                             11821.6 (5362.2)
    Handling gear                           160.6 (72.8)
Equipment                                  35465.0 (16086.6)
-----------------------------------------------------------
Empty weight                               165676.9 (75149.7)
    Operations                              7823.2 (3548.5)
Operating empty weight                     173500.1 (78698.2)
```

D.3. Random technology factors

In order to come up with a sensitivity analysis for the Class II weight estimation, it was possible to simply select a less conservative set of technology factors and use them to create a design that represents further technological improvements. However, there can be variation in the amount of impact that a development has. For example, the engine weight might decrease by an additional 10%, but at the same time, the fuselage weight savings can be 5% less than predicted. To attempt to take such variation into account, the technology development factors can be randomized and used to produce a large number of aircraft operating empty weight scenarios using the inputs from Concorde (or other designs).

To produce randomized technology factors a probability distribution has to be selected. The first option is the symmetrical normal distribution. However, in that case it is necessary to select for each component a mean value (conservative value) and standard deviation. Also, because of the symmetry there is also a large probability that the random factor is larger than the conservative value used for the 'new' Concorde. Instead, a distribution is preferred which is skewed so that the technology factor will likely be relatively close to the conservative value, but that the probability is larger that the actual factor is lower than this conservative value. This will become more clear by the example shown later (Figure D.2).

The distribution that was selected is the beta-distribution. It is a continuous probability distribution in the interval [0, 1] that is defined by two shape parameters, 'a' and 'b' (also known as α and β). The selection of 'a' and 'b' was done by varying the values until a distribution was found that seemed to represent the expected technology distribution. The value selected for 'a' is 3.5, and 'b' is 2.0, and the resulting distribution is shown in Figure D.1. This distribution can be altered in the setup tab of the main input file by changing the values of 'a' and 'b'. Note that the distribution can be altered in the program.

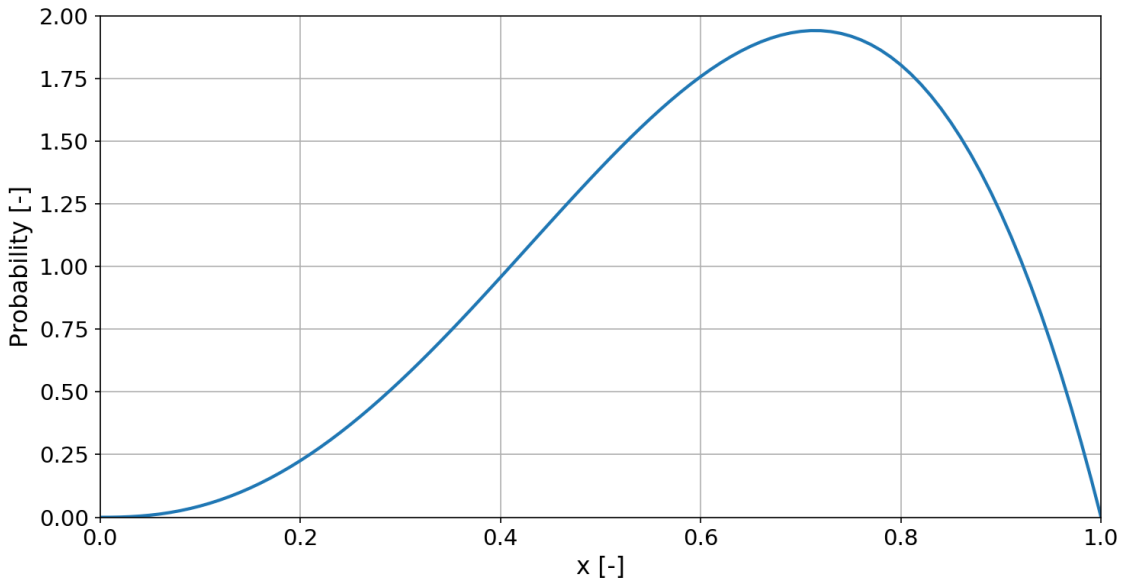

Figure D.1: Probability distribution for beta-distribution with 'a' of 3.5 and 'b' of 2

Since the real value of the technology factors are not in the range 0-1, but in a smaller range like 0.7-0.9, the random number has to be corrected for this. For this reason, the technology factor TF is equal to the following:

$$TF = \text{low limit} + \text{random} \cdot \left(\text{high limit} - \text{low limit}\right) = 0.7 + \text{random} \cdot (0.9 - 0.7) \tag{D.42}$$

where 'random' represents the random number in the range 0-1. A corrected probability distribution example with a lower limit of 0.75 and upper limit of 0.91 is shown in Figure D.2, which is the one that is used for the wing weight. It also shows a vertical line for the value of 0.85 that was used for the 'new' Concorde.

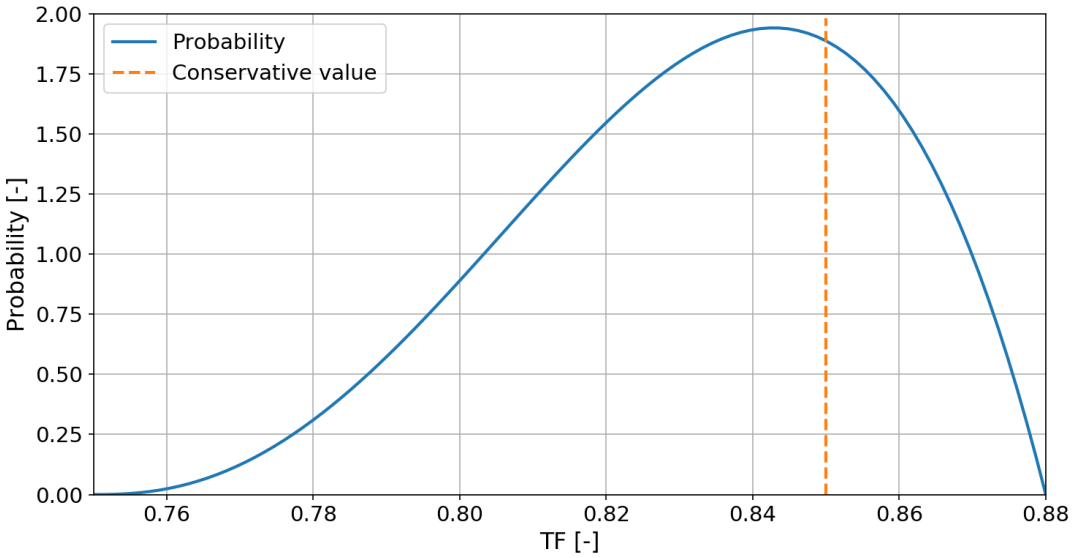

Figure D.2: Scaled beta-probability distribution with lower limit of 0.75 and upper limit 0.91

The graph shows that the largest area under the probability curve is located to the left of the value 0.85, meaning that there is a larger chance of the value falling in that region. This is desired to ensure that the operating empty weight values found are on average less conservative. Still, in some cases the technology factor is larger than 0.85 although the probability of this is smaller.

For the generation of the random number array, the 'random' module of Python's numpy[2] package is used. It should be noted that the values found are not random, but pseudo-random and that depending on the seed that is used, the random numbers are defined using the Mersenne Twister algorithm[3]. Each time the code is run, a different seed is selected by the program so that the values will be different from previous runs.

Now that this is explained, it is possible to look at the range of values within which the technology factors can fall. These ranges are listed in Table D.2 for each component. In most cases they have been defined in such a way that the conservative value used in Section 6.4 is on the right end of the range defined by the lower and upper limits. The lower limits have been based partially on the low values in Tables 6.6 and 6.7 from various sources, and also in some cases based on an educated guess. The upper limits are computed by adding a margin to the conservative value, which is usually in the range 0.01-0.03.

Table D.2: Upper and lower technology factor limits per component

Component	Conservative value [-]	Lower limit [-]	Upper limit [-]	Component	Conservative value [-]	Lower limit [-]	Upper limit [-]
Wing	0.85	0.75	0.88	Hydraulics	0.60	0.45	0.70
Vert. tail	0.85	0.78	0.88	IAE	0.86	0.76	0.89
Hor. tail	0.85	0.78	0.89	Electrical	0.92	0.85	0.94
Fuselage	0.85	0.78	0.88	Furnishings	0.85	0.80	0.87
Nacelle	0.85	0.78	0.88	ECS	0.86	0.76	0.90
Nose gear	0.88	0.83	0.90	APU	0.96	0.93	0.97
Main gear	0.85	0.78	0.88	Handling gear	0.86	0.82	0.88
Air induction	0.80	0.74	0.83	Crew	1.00	1.00	1.00
Engine weight	0.92[4]	0.86	0.94	Unusable fuel	0.85	0.82	0.86
Fuel system	0.90	0.85	0.92	Engine oil	0.90	0.84	0.92
Thrust reverser	0.88	0.82	0.90	Pax service	0.9	0.85	0.92
Engine install	0.88	0.82	0.90	Cargo container	0.85	0.80	0.86
Surface controls	0.86	0.76	0.90				

[2] http://www.numpy.org/ (accessed November 26 2018)
[3] https://docs.python.org/2/library/random.html (accessed March 20 2019)
[4] when using engine weight fit in Equation (4.3) this value is used. In Table 6.8 a larger factor of 0.78 was used.

E

Program testing & requirements support

This appendix is created to support the testing of the full design program, and the production of supersonic aircraft designs. First, Appendix E.1 describes and lists the top-level requirements and some inputs for the setup of the aircraft designs used to test the full program. Following this, Appendix E.2 describes the process leading to the top-level requirements for expected future supersonic transport aircraft.

E.1. Reference aircraft top-level requirements

In this section the top-level requirements and inputs used to generate the aircraft used for testing the full program as explained in Section 7.1 are briefly discussed. Since there is only limited information available in the aircraft design studies from which the data is extracted, many inputs are assumed. Since the goal is not to test whether the program will create virtually the same aircraft, but rather to show that the resulting takeoff and operating empty weights are similar, this is not deemed a large problem. Still, in some cases such as the Boom SST there is the issue that the cruise Mach number of 2.2 used in the design is too high for the current program, and consequently it is reduced to a lower Mach number for a modified Boom SST design.

The designs used and their key inputs and requirements are summarized in Table E.1. They are split in three groups, the requirements definition, some design inputs used by the aerodynamics and Class II analyses, and several engine parameters. Starting with the mission, the maximum number of passengers, load factor, and fraction of passengers with luggage, determine the payload weight. The design range is taken from literature, and can include out- or inbound subsonic segments. Similarly, the cruise Mach numbers, and takeoff and landing distances were taken from literature. In most cases, the stall speed at takeoff weight under sea-level conditions is unknown. Instead, the stall speeds were often selected such that the design wing loading was similar to the reference aircraft value. The new Concorde and Tu-144 are exceptions to this as their takeoff and landing distances, and stall speed were reduced to represent improvements in technology.

The wing aspect ratio and average thickness ratio are often taken from literature, although in some cases the aspect ratio had to be assumed. For example, the Aerion AS2 aircraft has a calculated aspect ratio of about 3.7, but this is in part due to its natural laminar flow wing design. Instead, a ratio of 2.2 was selected since the program uses a double delta wing, and this resulted in a good match of the takeoff weight. TF stands for the tech factor inclusion, and if it is True, the technology development factors are applied in the Class II analysis. C2growth is the Class II component weight growth factor, which normally is 1.05, except for two SSBJ designs where it was found to be necessary to increase the value to 1.1 and 1.15.

For the engine design, the most important top-level requirements are the overall pressure ratio (OPR) and bypass ratio (BPR). The values are taken from literature, and in case of the new Concorde, new Tu-144, and modified Boom SST, assumed by using a simple model where the combustor inlet temperature is limited. With the known ambient conditions in supersonic flight, it is then possible to determine what the maximum OPR would be so the maximum temperature is not exceeded. This is further explained in [7]. The engine count is taken from literature, although in case there are three engines, it is reduced to two (e.g. Aerion AS2) or increased to four (e.g. Boom SST). The last entry is the scaling factor for the specific fuel consumption at supersonic cruise, with respect to the subsonic value. Where possible, it is assumed to be 1.24, but in some cases (e.g. Boom SST and NLR M1.6) the value is assumed to be 1.16 as it is for Concorde. This value is the lower limit, and is further detailed in [7].

It should be noted that many other inputs like the seat pitch and width, engine component efficiency values, and reserve fuel segment definition, are not listed here. They can be found in the sample input files used to produce the aircraft which will be included in a folder within the design program. Aside from the inputs, the reference operating empty and takeoff weight are shown along with the results from the program, and their deviation. Lastly, at the bottom, the main sources are listed.

Table E.1: Full program validation aircraft data

Aircraft		Unit	Concorde	Concorde new	Tu-144	Tu-144 new	Boom SST	Boom SST mod	Aerion AS2	HELESA	Cranfield SSBJ	NLR M1.6	N+1 overwater
Requirements	Type	-	SST	SST	SST	SST	SST	SST	SSBJ	SSBJ	SSBJ	SST	SST
	$n_{pax,max}$	-	100	100	128[1]	128[1]	55	55	12	18	19	250	128
	load factor	-	0.88	0.88	1	1	1	1	1	1	1	1	1
	W_{PL}	kg	8,845	8,845	15,000	15,000	5,390[2]	5,390[2]	1,296[2]	1,890	2,000	23,750	12,800[2]
	R_{des}	NM	3,550	3,550	2,850	2,850	4,482	4,482	4,750	4,000	4,320	5,500[3]	3,720[4]
	M_{sup}	-	2.02	2.02	2.0	2.0	2.2	2.0	1.4	1.6	1.6	1.6	1.3
	M_{sub}	-	0.95	0.95	0.95	0.95	0.95	0.95	0.95	0.92	0.9	0.95	0.95
	s_{TO}	m	3,400	2,600	2,930	2,600	3,048	3,048	2,268	1,900	1,450	3,048	2,134
	s_{land}	m	2,200	2,100	2,570	2,200	2,500	2,500	1,850	1,150	1,200	2,00	1,736
	V_{stall}	m/s	92	85	86	84	82	82	80	84	83	78	89
Design	AR_w	-	1.829	1.829	1.64	1.64	1.39	1.83	2.2	2.0	2.25	2.8	2.7
	$t/c_{wing,avg}$	%	3.2	3.2	3.2	3.2	2.25	2.25	2.8	2.8	4.0	2.8	4.0
	n_{pilots}	-	3	2	3	2	2	2	2	2	2	2	2
	TF	-	False	True	False	True	True	True	True	True	True	True	True
	C2 growth	-	1.05	1.05	1.05	1.05	1.05	1.05	1.15	1.1	1.05	1.05	1.05
Engine	OPR	-	15.5	20	15.8	20	15.5	22	35	40	26	35	40
	BPR	-	0.0	2.0	0.0	2.0	3.0	3.0	3.0	3.0	2.0	2.5	1.0
	n_{eng}		4	4	4	4	4	4	2	2	2	4	2
	SFCscale	-	1.16	1.24	1.16	1.24	1.16	1.16	1.24	1.24	1.24	1.16	1.24
Results	$W_{TO,ref}$	kg	185,066	185,066	206,794	206,794	77,100	77,100	54,884	43,100	44,900	340,000	140,160
	$W_{TO,calc}$	kg	186,723	126,075	213,095	145,134	118,888	82,226	55,699	46,009	48,918	355,184	149,074
	Delta	**%**	**+0.90**	*-31.9*	**+3.05**	*-29.8*	**+54.2**	*+6.65*	**+1.49**	**+6.75**	**+8.95**	**+4.47**	**+6.36**
	$W_{OEW,ref}$	kg	79,264	79,264	99,199	99,199	34,464	34,464	26,218	19,577	21,000	136,000	62,489
	$W_{OEW,calc}$	kg	75,793	51,257	90,427	59,236	47,036	33,335	22,105	18,697	19,269	136,786	60,704
	Delta	**%**	**-4.38**	*-35.3*	**-8.84**	*-40.3*	**+36.5**	*-3.27*	**-15.7**	**-4.50**	**-8.24**	**+0.58**	**-2.86**
Sources			[5] [6] [21, 22]		[7] [8]		[93]	[93]	[9]	[26]	[25]	[31]	[32]

[1] passenger number smaller than 150 needed for design payload to keep fuselage closer to that of real Tu-144. Assumed that extra luggage and cargo compensates for the payload deficit.
[2] payload weight calculated by program
[3] includes 500 NM subsonic outbound segment
[4] includes 700 NM outbound and 1,100 NM inbound subsonic segments
[5] http://www.concordesst.com (accessed April 24 2018)
[6] IHS Markit, *Concorde*, https://janes.ihs.com/JAWAInServices/Display/1336723 (accessed June 26 2018)
[7] http://www.tu144sst.com/index.html (accessed April 24 2018)
[8] IHS Markit, *Saturn RD-36-51*, http://janes.ihs.com/AeroEngines/Display/1306317 (accessed April 24 2018)
[9] https://www.aerionsupersonic.com/performance/ (accessed April 30 2019)

E.2. SST top-level requirements

In this section, the different top-level requirements for the supersonic aircraft are discussed in more detail. These requirements include items like the design range and cruise Mach numbers, but the section starts with the payload in Appendix E.2.1 and concludes with some optional requirements in Appendix E.2.8.

E.2.1. Payload

The payload, together with the aircraft range, are among the most important top-level requirements to be specified for a new aircraft. For the supersonic aircraft, two aircraft classes are of interest, the supersonic business jet (SSBJ) and larger supersonic transport (SST). For the first generation, the focus will be on the transport of passengers, and not cargo. The latter could be an interesting niche market for high-end materials and express delivery of components required for quick repairs of broken machines critical to a large company. An added benefit of cargo transport is that the SST can be smaller for the same payload weight because of the higher cargo density [153]. Alternatively, a cargo version can be created by changing the internal configuration of the base SST [154].

The main segment of the air transportation market targeted by (smaller) SSTs is the premium market, which consists of passengers willing to pay the expected higher ticket prices, in exchange for a reduction of their travel time. In [155] the premium ticket market was studied to determine what size aircraft would be best for the first generation of SSTs. The result is shown in Figure E.1.

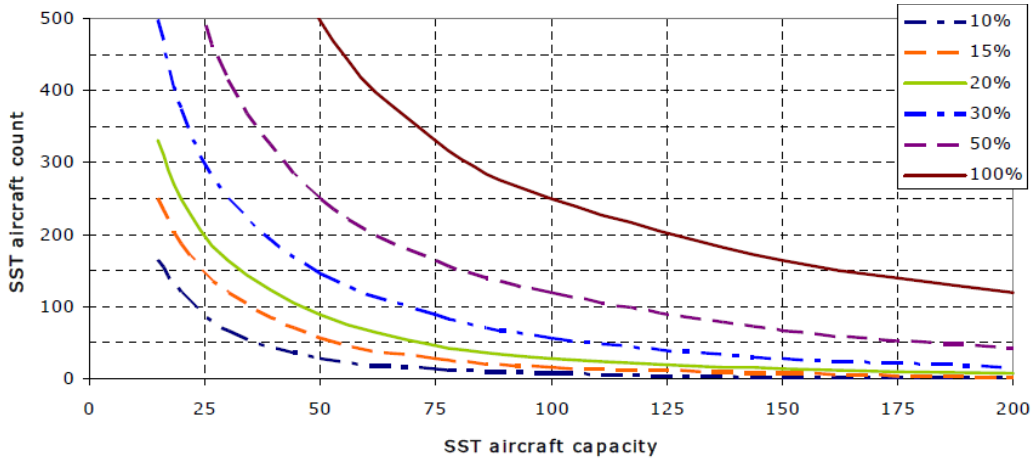

Figure E.1: Number of SSTs as a function of aircraft capacity and passenger switch percentage with overland boom restriction [155]

Note that in the graph, the percentage represents what part of the premium market passengers are convinced to switch from sub- to supersonic flight. The graph shows that the fleet size for SSTs is expected to be very small for large aircraft capacities (>100 passengers), unless over 50% of the passengers switch. It indicates that for SSTs, it is important to select the correct size so that the design has good sales potential and is not built for a non-existing market segment. Based on the findings, the most likely capacity for new SSTs are 50 (like the Boom Supersonic SST) and 90-120 (similar to Concorde and Tu-144). To further extend the capacity range, 170 and 250 passenger designs are also added, which will have a seating configuration similar to that of subsonic long-range aircraft. However, especially for the first generation of SSTs these aircraft are unlikely to be a success. Should the first SST generation be successful, then the second generation could feature these larger aircraft. A capacity of 300-320 passengers is currently seen as the upper limit, given the trend towards long-range widebody aircraft over the larger Boeing 747 and Airbus A380.

For the supersonic business jet market, a few market surveys have been performed to estimate the fleet size and their findings are listed in Table E.2 with their sources.

Table E.2: SSBJ fleet size forecast including period (if indicated by source)

Study	Gulfstream Aerospace study 1 & 2	Aerion	Supersonic Aerospace International
Fleet	180 & 350 (10 yr) [156]	600 (20 yr)[10]	300 [157]

[10] *Aerion unveils larger, three-engine supersonic business jet tailored to emerging global demand*, May 2014, https://www.aerionsupersonic.com/wp-content/uploads/2017/02/Aerion-Unveils-Larger-Supersonic-Business-Jet.pdf (accessed March 7 2018)

This shows that there is enough sales potential for SSBJs. The required SSBJ capacity is set to 18 which was on the higher end of the range found by looking at past design studies collected in [5] and similar to the HELESA [26] and Cranfield SSBJ [25] designs. Using a slightly different cabin seating configuration with more or less comfort and features, this amount can be increased to about 22 or reduced to less than ten.

E.2.2. Range and ETOPS

In order to determine the design range of the aircraft, it was decided to create a hypothetical network. This network is built up by making use of a number of large international airports which together cover most of the world, and is shown in Figure E.2. Note that for the first generation of supersonic aircraft, it is expected that the overland supersonic flight ban will not be lifted, at least not in the first five to ten years, so the majority of the airports are located close to a large body of water. Four city pairs require substantial amounts of overland flight, LHR-DXB, CDG-DXB, SIN-SYD and SIN-AKL. For these pairs, the aircraft will likely follow a different route so that the amount of supersonic flight achieved is increased. To a lesser degree the same applies to the pairs SIN-DXB, PEK-SEA, PEK LAX, and LHR-GRU. Also note that the city pair CDG-CCS (Paris-Caracas) was added as it is a route that Air France operated on with Concorde for a short period.

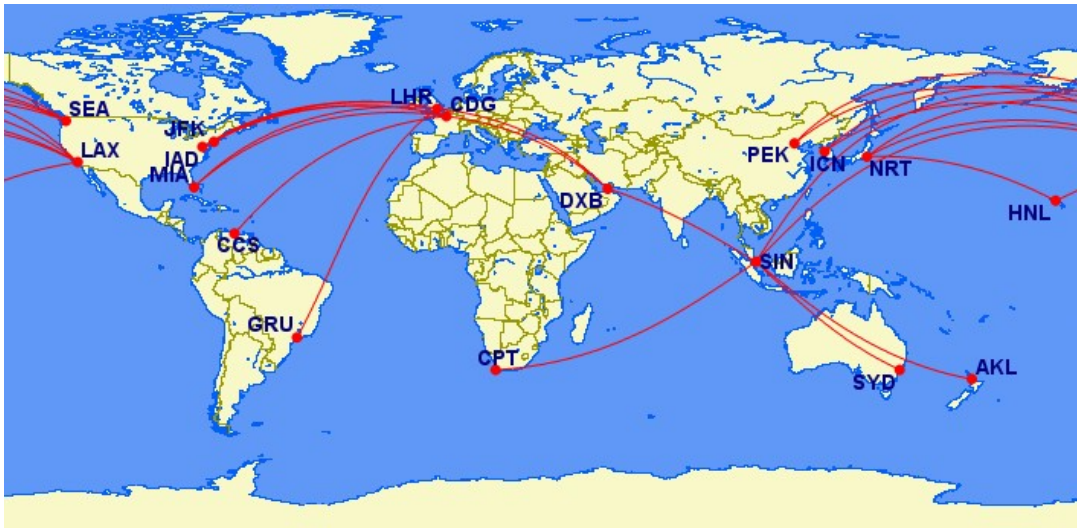

Figure E.2: Global network used for estimating flight distances[11]

For these 24 city pairs, the greater circle distance was measured using gcmap[11]. The findings are sorted by increasing distance and listed in Table E.3.

Table E.3: Great circle distance for 24 city pairs

City pair		Distance [NM]	City pair		Distance [NM]
Los Angeles	Honolulu	2,221	Paris	Caracas	4,123
Paris	Dubai	2,832	Seattle	Tokyo	4,144
London	Dubai	2,972	Seattle	Seoul	4,533
London	New York	2,999	Singapore	Auckland	4,541
Singapore	Dubai	3,157	Seattle	Beijing	4,698
Paris	New York	3,158	Los Angeles	Tokyo	4,737
London	Washington	3,195	London	Sao Paulo	5,095
Honolulu	Tokyo	3,318	Los Angeles	Seoul	5,209
Paris	Washington	3,355	Singapore	Cape Town	5,222
Singapore	Sydney	3,396	Los Angeles	Beijing	5,431
London	Miami	3,845	Seattle	Singapore	7,013
Paris	Miami	3,987	Los Angeles	Singapore	7,621

[11] gcmap.com (accessed January 3 2019)

Looking at the values, there is a clear distinction between the majority of the Transatlantic routes and those across the Pacific. Most Transatlantic routes go up to about 4,000 NM. A lot of city pairs in the Pacific region fall between roughly 4,000 and 5,500 NM. Looking at the past supersonic aircraft, and the design range of the Boom SST (4,500 NM[12]) and Aerion AS2 (4,750 NM[13]), the 5,500 NM seems like a too high range requirement. For such a distance, an intermediate stop will be required, or payload should be exchanged for fuel. A better design range would be 4,200 NM for Atlantic range, and roughly 5,000 NM for good Pacific coverage. In case 5,000 NM is too much, 4,600 NM could be used as an intermediate range to offer good Atlantic and partial Pacific coverage.

Aside from the range, a requirement can also be set on the ETOPS (Extended-range Twin-engine Operational Performance Standards) certification of the aircraft. However, it is not really possible to implement such a constraint in the current design program. Still, to be a bit more complete, it is discussed briefly. The ETOPS rating determines how far from the nearest compatible airport an aircraft can fly. It is expressed in minutes (e.g. ETOPS 120 means always flying within 120 minutes of the nearest compatible airport at one-engine inoperative cruise speed). Thus, ETOPS can limit the network an aircraft can operate on and in some cases, aircraft might not be allowed to operate in certain regions. The main region where this can be a problem is the Pacific, where the number of usable airports is limited. For example, to fly to Hawaii from the US mainland an ETOPS 180 rating is required. Also, for the city pair CDG-CCS, an ETOPS 180 rating would be required to operate on the optimal route. Other regions requiring high ETOPS are the Southern parts of the Oceans (Atlantic, Pacific, Indian), but these regions have very low air traffic so it is not really an issue. To provide a good operating network, an ETOPS 180 rating is expected, and introduced as a requirement, although it cannot be checked at this stage.

E.2.3. Landing and takeoff distance

The landing and takeoff distances are another set of important requirements. They are used in the wing loading diagram and therefore can affect the wing area and required engine thrust, if the constraints are critical. To get a feel for the different conditions which can be encountered a small survey was performed by looking at 32 international airports. The airports were selected to provide a good coverage of the world with the main focus on the US, Europe and Asia-Pacific region, complemented with some airports in South America and Africa. The airport locations are visualized in Figure E.3 and their elevation and maximum runway length are listed in Table E.4.

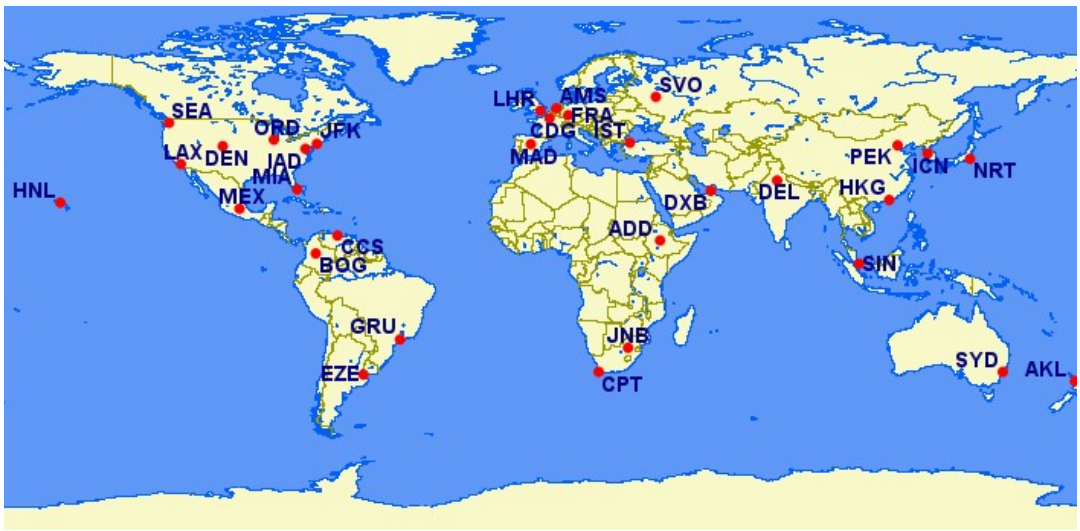

Figure E.3: Global airport network used for runway distances and elevation[11]

Since the first generation of SSTs is expected to be restricted by the overland supersonic flight ban, the majority of the airports operated on will be located close to large bodies of water. Consequently, their elevation is limited and often less than 100 meters. For this reason, the elevation used for the landing and takeoff requirements is sea-level altitude. Looking at the runway length values, the minimum value is 3,201 m, which is still

[12] https://boomsupersonic.com/airliner (accessed January 3 2019)
[13] fully supersonic flight https://www.aerionsupersonic.com/ (accessed January 3 2019)

Table E.4: Airport elevation and maximum runway distance for 32 airports

Code	City	Elevation [m]	Max runway length [m]	Code	City	Elevation [m]	Max runway length [m]
ADD	Addis Abeba	2,334	3,800	ICN	Seoul	7	4,000
AKL	Auckland	7	3,635	IST	Istanbul	99	4,100
AMS	Amsterdam	-3	3,800	JFK	New York	4	4,423
BOG	Bogota	2,548	3,800	JNB	Johanesburg	1,694	4,421
CCS	Caracas	72	3,610	LAX	Los Angeles	39	3,939
CDG	Paris	119	4,215	LHR	London	25	3,902
CPT	Cape Town	46	3,201	MAD	Madrid	610	4,350
DEL	Delhi	237	4,430	MEX	Mexico City	2,230	3,952
DEN	Denver	1,655	4,877	MIA	Miami	3	3,967
DXB	Dubai	19	4,450	NRT	Tokyo	41	4,000
EZE	Buenos Aires	21	3,300	ORD	Chicago	204	3,962
FRA	Frankfurt	111	4,000	PEK	Beijing	35	3,810
GRU	Sao Paulo	750	3,700	SEA	Seattle	132	3,627
HKG	Hong Kong	9	3,800	SIN	Singapore	7	4,000
HNL	Honolulu	4	3,753	SVO	Moscow	192	3,700
IAD	Washington	95	3,505	SYD	Sydney	6	3,962

over three kilometers. Should the aircraft take off from higher elevation airports like DEN and MEX, then it will have access to longer runways, and in many cases a reduced payload to enable safe takeoff. This can for example be seen when looking at the takeoff graphs of a 737 in [82].

If higher airport elevations are desired it is best to select a maximum of about 1,800 meter so airports like DEN and JNB can be served. Even higher elevations will result in a further increase of the takeoff constraint, and will result in increased thrust loading. Consequently, the engines and aircraft will be heavier, noisier and worse for the climate, making it less appealing to potential customers. To get a feel for the performance of other aircraft a small survey was again performed with the results listed in Table E.5.

Table E.5: Takeoff and landing distances for several aircraft

Aircraft	MTOW [kg]	Takeoff distance [m]	MLW [kg]	Dry landing distance [m]	Wet landing distance [m]	Source
Boeing 737-800	79,016	2,362	66,361	1,753	2,042	[82]
Boeing 787-8	227,980	3,078	172,365	1,615	1,890	[130]
Gulfstream G650	45,178	1,786	37,875	817	-	[14,15]
Bombardier Global 6000	45,132	1,974	-	682	-	[16]
Bombardier Global 7500	48,194	1,768	-	768	-	[17]
Boom SST		3,048[18]	-			[19]
Concorde		3,426		2,200	-	[20]

From the data it can be seen that the takeoff and especially landing distances for subsonic business jets are less than 2,000 meters, with landing distances of less than 1,000 meters. For SSBJs these values are expected to be slightly worse due to the poorer low-speed lift. Also, for aircraft to take off from the same airfield at maximum takeoff weight, the takeoff distance is often critical as it is larger than the landing distance. The same also applies to the other subsonic aircraft and Concorde. Based on these findings and the airport runway

[14] http://www.gulfstream.com/aircraft/gulfstream-g650 (accessed January 4 2019)
[15] https://www.jetcraft.com/jetstream/2016/06/gulfstream-g650-overview-2012-present/ (accessed January 4 2019)
[16] https://businessaircraft.bombardier.com/en/aircraft/global-6000#!#bba-pdp-section-5 (accessed January 4 2019)
[17] https://businessaircraft.bombardier.com/en/aircraft/global-7500#!#bba-pdp-section-5 (accessed January 4 2019)
[18] balanced field length
[19] https://boomsupersonic.com/airliner (accessed January 4 2019)
[20] https://www.aircraftcompare.com/helicopter-airplane/Aerospatiale-BAC-Concorde/431 (accessed January 4 2019)

lengths, the takeoff distance for SSTs is expected to be in the range 2,300-3,200 meters, with the larger SSTs being on the high end of that range, and for SSBJs 1,700-2,100 meters. Similarly, the landing distances are expected to be in the range 1,800-2,600 meters for SSTs and 1,200-1,500 meters for SSBJs. Note that reducing the takeoff distance will likely result in heavier and more noisy engines, which are studied in [7].

E.2.4. Cruise speed and altitude

For supersonic aircraft the main selling point is the increased speed and reduced travel time. Therefore, it is necessary to define the Mach numbers at which the aircraft should operate. Looking at a compilation of past SSBJ designs [5] and more recent designs [4], the typical Mach number range for supersonic flight is 1.4 to 2.5, with the more recent designs showing a narrower range of 1.4-1.8. At these lower speeds, the complexity of the engine inlet is reduced as a variable inlet is not necessarily required for good performance. Also, aerodynamic heating is less important as can be seen from the values in Table E.6. For new SSBJs the Mach number is therefore expected to be about 1.6.

Table E.6: Aerodynamic heating values [158]

Cruise Mach	Surface temperature °C	
	Peak	Average
1.6	65	40
1.8	85	65
2.0	120	95
2.2	155	125

For the larger SSTs, the aircraft characteristics used in the validation of the Class I module are used to get a feeling for the Mach number range. This is found to be between 1.3 and 2.62, although the aircraft with high Mach numbers of 2+ are often old designs from the 20th century. The more recent designs are more concentrated at Mach 1.6, with the Boom SST being an exception at Mach 2.2. For SST designs the expected range used for the requirement is Mach 1.6-1.8. This provides good time savings while limiting the complexity of the design, and need for more advanced materials.

Aside from the supersonic cruise Mach number, SSTs and SSBJs also have the possibility of flying efficiently at slightly higher subsonic Mach numbers than subsonic aircraft. During the Class I investigation the majority of the aircraft have a subsonic cruise Mach number of 0.9-0.95 with one exception being the Edge SST at 0.7. To offer an additional speed benefit over subsonic aircraft, the subsonic cruise Mach number requirement is set to 0.95.

The supersonic cruise altitudes are expected to be in the range 14-18 km with higher Mach numbers operating at the higher end of this range. Note that with the increased importance of climate impact, it is better to fly in the lower end of the range indicated because it can aid in limiting the climate impact of a supersonic aircraft, as is further detailed in Chapter 8. The subsonic cruise altitudes were also used in the Class I validation aircraft and are expected to be around 10-12 km for both SSBJs and SSTs.

E.2.5. Sonic boom

The sonic boom is the first environmental issue related to supersonic aircraft, and is important because it restricts the network of SSTs. Currently, many national aviation authorities have rules in effect which ban overland supersonic flight such as regulation 14 CFR 91.817[21] in the US since 1973. It states that all sonic boom noise is unacceptable and it forbids civil supersonic flight over the US, as well as any supersonic operation to and from US airports which would result in a sonic boom reaching the ground in US territory. In Germany, a slightly different rule applies as supersonic flight is allowed so long as the aircraft flies above 15 km [159].

In the past, several large studies have been performed where groups of subjects and even small communities were exposed to sonic booms over a period of time, to try to determine what sonic boom levels are acceptable [160–164]. Despite these studies, no uniform definition of an acceptable sonic boom noise level is currently available. It is also unlikely that in the near future, a clear rule is defined. A new project related to this is the X-59, an experimental aircraft being developed by NASA and Lockheed Martin Skunk Works aiming to produce a sonic boom with a noise level of 75 PLdB[22]. This is similar to the sound of a car door closing.

[21] https://www.law.cornell.edu/cfr/text/14/91.817 (accessed April 4 2019)
[22] https://www.lockheedmartin.com/en-us/products/quesst.html (accessed January 4 2019)

Supersonic Aerospace International (SAI) is also aiming for a 65 dBA ground signature when cruising at Mach 1.6 at 60,000 feet (≈18.3 km)[23].

Because of the uncertainty in the sonic boom regulations, the top-level requirements are indicative based on requirements set in other design projects. Furthermore, since the sonic boom analysis is currently not used in the design routine, but only for the final set of designs so it does not affect the direction of the design process. In [7], more information on the sonic boom requirements of the aircraft designs can be found.

E.2.6. Airport noise

This is the second noise related top-level requirement to be applied to new supersonic aircraft. It is related to the noise produced by the aircraft while it is performing its approach and takeoff, and is quantified by measuring the noise levels in the following three locations [165]:

- *Fly-over*: 6.5 km from the brake release point, directly underneath the takeoff flight path.
- *Sideline*: the highest noise measurement recorded at any location 450 m from the runway axis during takeoff.
- *Approach*: 2 km from the runway threshold, underneath the approach flight path.

The measured values are then summed, and used as noise metric. The current regulation in effect for new aircraft of at least 55 tonnes is ICAO Chapter 14, which defines the cumulative noise level that cannot be exceeded. For lighter aircraft, Chapter 14 will be applicable from 2021 onward [165]. There is an exception possible here, as for the US and some other countries, the flight noise certification tests can be held up to five years after the application date, meaning that an aircraft weighing less than 55 tonnes could be certified using the older Chapter 4 (Stage 4) until 2025 [166]. However, for the aircraft to be competitive and not run into noise issues in the near future, the decision is made to set the requirements to Chapter 14. This regulation is also referred to as Stage 5 by the FAA [167]. The difference in noise levels for the different noise chapters is visualized in Figure E.4. As with the sonic boom, more information can be found in [7].

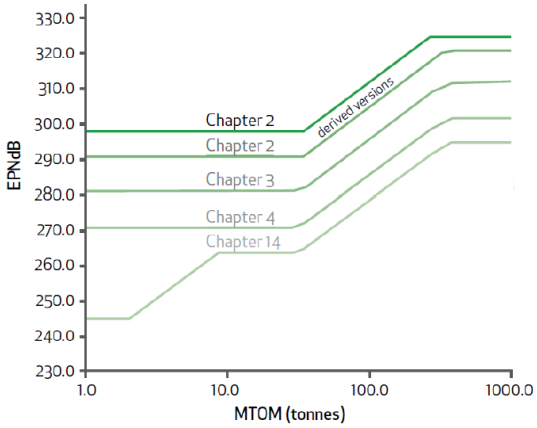

Figure E.4: ICAO noise levels for different chapters as a function of MTOW [165]

E.2.7. Emissions

Emissions are an important part of this thesis as they are key to one of the two research goals. For this reason, the amount of depth in this text is limited as more details are provided in Chapter 8. For the top level requirements, values found in other studies are currently used. For emissions these requirements apply to the emission indices for nitrogen oxides and water vapour for the supersonic cruise segment. In [4], it is indicated that an acceptable emission index for NO_x is 15 g/kg when flying less than Mach two, but for NASA's N+2 and N+3 projects, the goals are in the range 5-10 g/kg [33]. For water, an upper limit of 1,400 g/kg was defined by a National Research Council study [168], which should not be a problem for standard kerosene (approximated as $C_{12}H_{23}$) which under ideal combustion produces about 1,240 g/kg.

These values should be aimed for but are not part of the design process itself. Rather, the emission study is performed for a few final designs which are also used to study the sensitivity to variables like the emission index values.

[23] http://www.sai-qsstx.com/quiet.html (accessed January 4 2019)

E.2.8. Other possible requirements

Aside from the requirements discussed so far, there are more potential requirements which could be included in the future once the design program has been expanded with new modules. These are briefly described below in a list and include the following:

- Unit cost of an aircraft. Important because for an aircraft to be successful, it should not be much more expensive than its subsonic competitors so long as it does not make up for it by the time savings offered to customers.
- Operating costs of an aircraft, expressed through ticket costs for a certain route, or as the cost per seat mile. For supersonic aircraft to be competitive, these costs should not be much higher than for subsonic aircraft when flying in the same seat class, or offer sufficient reduction of travel time as compensation.
- Service and absolute flight ceilings for the aircraft, to further define the flight envelope of the aircraft design. However, aircraft will hardly ever operate at those altitudes so it is not currently implemented.
- Ground handling of the aircraft. Especially for supersonic aircraft with longer landing gear struts the turning performance on the ground can be problematic and should be considered during the positioning and sizing of the landing gear.
- Aircraft should be compatible with current airport infrastructure, meaning that its dimensions should not be dissimilar to that of subsonic aircraft designed for similar missions.

F
Climate support

In this appendix, additional information is provided about the climate analyses performed during the research. This includes information about the atmosphere, and climate and emitted species in Appendices F.1 and F.2, respectively. Then, Appendices F.3 and F.4 go into the LTO and CO_2 certification process before Appendix F.5 goes into emission index prediction. Lastly, Appendix F.6 describes the fleet setup and Appendix F.7 the AirClim model.

F.1. Atmosphere

Earth's atmosphere is often said to extend up to the Kármán line at 100 km altitude. It is built up from four principal layers as shown in Figure F.1, which with increasing altitude are: troposphere, stratosphere, mesosphere and thermosphere. The troposphere extends from sea-level up to a height of 8 to 16 km. The exact boundary height depends on latitude and season, but in general the troposphere is thinner at the poles than at the equator [169]. In the troposphere, the air temperature decreases at a lapse rate of -6.5 K/km, as defined in the International Standard Atmosphere (ISA) [170]. The stratosphere can be split into smaller regions based on the temperature gradient. The lower stratosphere extends from the tropopause, which is the boundary with the troposphere, up to roughly 20 km altitude and has a nearly constant temperature. Above 20 km the temperature starts to increase again. As the supersonic aircraft to be designed will not operate above 20 km, this region, and the meso- and thermosphere are not of interest and are not discussed in more detail.

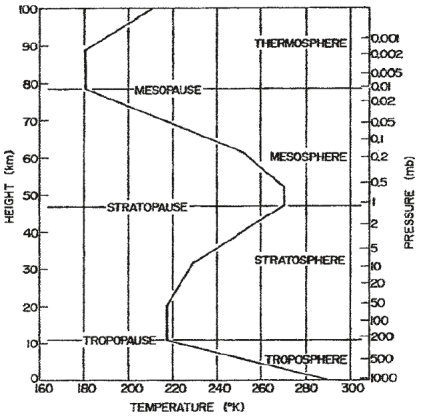

Figure F.1: Atmosphere buildup [169]

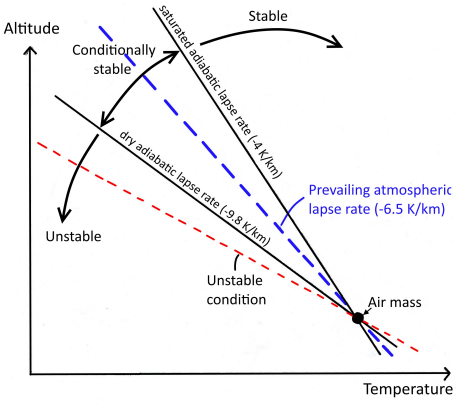

Figure F.2: Atmospheric stability

Now that the tropo- and stratosphere have been defined, it is possible to look at their stability. For an atmospheric layer to be stable, a rising air pocket has to cool down more quickly than the surrounding air, forcing the air pocket to descent again because of its higher density, staying in approximately the same position. The natural lapse rate of air varies based on its saturation level, from -10 K/km when unsaturated (dry adiabatic lapse rate) to -6 [169] or even -4.5 K/km when fully saturated (moist adiabatic lapse rate). As the prevailing lapse rate in the troposphere is -6.5 K/km, it depends on the local saturation of the layer whether it is stable or not. This is visualized in Figure F.2.

Different from the troposphere, the lower stratosphere has a near zero temperature gradient, which indicates that it is a very stable region of the atmosphere with little mixing. As a result of this, any emitted species in the lower stratosphere are likely to have a much longer lifetime than they would have when emitted in the

troposphere, where mixing and precipitation increases the removal rate. This affects the impact that these emissions have on the climate.

For the majority of the analyses being performed, it is assumed that the atmosphere is the International Standard Atmosphere (ISA). However, for some situations such as takeoff and landing constraints, and for engine sizing routines it might be necessary to use different scenarios. These scenarios are the cold, hot and tropic atmosphere, and are reflected by the temperature profiles shown in Figure F.3.

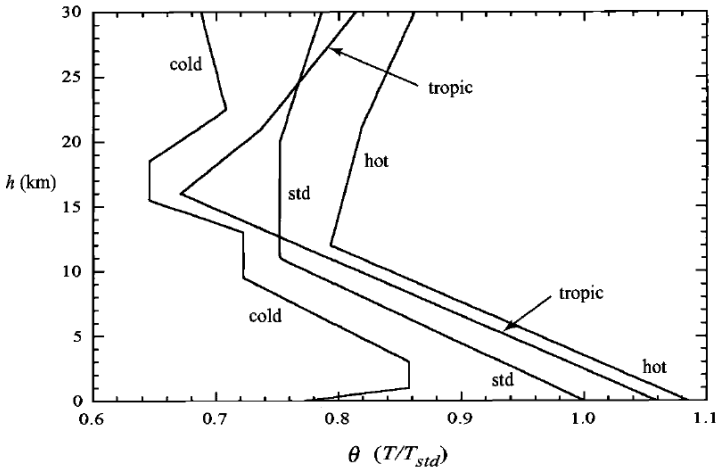

Figure F.3: Atmospheric temperature profiles for four scenarios [38]

F.2. Species and climate effects

Aircraft engines burn fuel during operations and because the combustion is not ideal, there are several unwanted products. From complete combustion, carbon dioxide and water will be produced, while incomplete combustion results in carbon-monoxide, unburned hydrocarbons (UHC) and soot particles. Aside from this, there are by-products like NO_x and SO_x, which are also formed for complete combustion. The emission quantities of CO_2 and water are proportional to the amount of fuel burnt, while the amount of UHC, NO_x, CO and soot is dependent on the type of engine, its thrust setting, altitude and airspeed. The key NO_x formation process is that of thermal-NO_x. At full thrust, the largest amount of soot and NO_x is produced, while at idle the amount of CO and UHC will be large. Balancing these issues should be considered during the engine design process. The emission index (EI) of most species can be predicted for engines to quantify their performance, and were also set as top-level requirements for several supersonic aircraft projects.

To get a feel for the radiative forcing (RF) contribution of aviation Figure F.4 depicts the RF-values for several emitted species. It also shows that the level of scientific understanding (LOSU) is still low for many species. The total aviation induced radiative forcing is estimated at 55 mW/m^2 [101]. In the following subsections, the different species used in the temperature change estimation of Section 8.1.3 and LTO cycle, their characteristics will be briefly discussed.

F.2.1. Carbon dioxide

CO_2 is the best known greenhouse gas to the general public. It is well-mixed within the atmosphere which allows for using the method by Sausen and Schumann [171] to compute its concentration change and radiative forcing. Since CO_2 has a long atmospheric lifetime compared to the other species considered here, the location where it is emitted does not matter much for its climate impact. Because of the long lifetime and lag of the earth ocean system, an emissions reduction will only result in a temperature change reduction around 30-50 years after the reduction takes place. For subsonic aviation, CO_2 is the biggest contributor to radiative forcing changes, excluding the contrail cirrus for which the impact is not yet fully understood, and ozone, which is partially negated by methane reduction [172]. For supersonic aircraft it was found that water vapor is actually a much larger contributor, in some case greater than carbon dioxide [99].

F.2.2. Ozone

Ozone is a greenhouse gas which is not directly emitted by aircraft, but is indirectly formed and broken down chemically by other aircraft emissions like NO_x, and water vapor. The full process of ozone production and

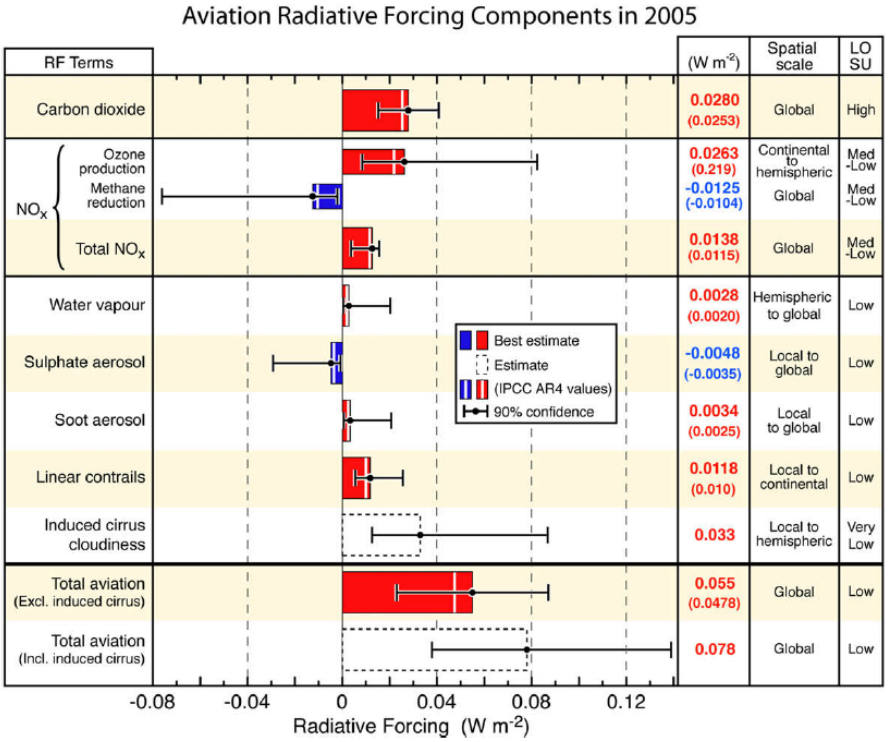

Figure F.4: Radiative forcing components from global aviation as evaluated from preindustrial times until 2005 [3]

breakdown is too complex to fully discuss here, and more information can be found in [173, 174]. The concentration of ozone is larger in the stratosphere, where supersonic aircraft will mostly be operating. At higher altitudes the chemical destruction cycle of ozone also has a higher efficiency, increasing the potential impact [99]. Research in [175] found that ozone depletion varies almost linearly with fuel burn for the cases studied. The ozone layer in the stratosphere also acts as a UV-shield, and has in the past been severely harmed by chlorofluorocarbons (CFCs), adding extra motivation to reduce the amount of harmful emissions.

F.2.3. Methane

The greenhouse gas methane is indirectly affected by emissions of nitrogen oxides and water. These will through changes in the OH-concentration lead to a reduction of the lifetime of methane. As a result of the reduced lifetime the climate impact of methane is reduced, causing a negative radiative forcing, partially offsetting the increase in RF by ozone production. This can be seen in Figure F.4 where the negative RF from methane partially negates the positive RF from ozone production. The reduction in lifetime was found to range between 0.01% and 0.44% for the SCENIC project [99].

F.2.4. Water vapor

Water is a greenhouse gas because it captures incoming solar radiation. As the climate becomes warmer the air becomes capable of holding a larger amount of water, which in turn increases the potential temperature change. As each kg of kerosene burnt produces roughly 1.25 kg of water this can be an important contributor to the climate impact. For tropospheric emissions, the majority of the water will rain out after a relatively short time due to the unstable atmosphere (see Appendix F.1). Only stratospheric emissions of water vapour are likely to strongly perturb the atmospheric humidity, and add radiative forcing due to their long lifetime and the low ambient humidity [176]. For supersonic aircraft in particular this is true because of the higher altitudes where they operate. In fact, it was found that the contribution of water vapor resulted in the largest climate impact of supersonic aircraft from the SCENIC project [99]. Similarly, for the HISAC project with smaller supersonic aircraft, which also operate at lower altitudes, it was found that roughly 20% of the climate impact came from water vapor [100].

F.2.5. Unburned hydrocarbons

Unburned hydrocarbons (UHC) are a group representing any chemical compounds which solely consist of carbon (C) and hydrogen (H). They often remain after the combustion (and any further reactions in turbine and exhaust) have been completed. These can be pure fuel molecules which simply were not broken down, or smaller hydrocarbons resulting from the partial breakdown of the fuel during combustion. While the majority of the hydrocarbons in the atmosphere are not dangerous, some are important because of their carcinogenic properties. Additionally, UHC has been shown to attribute to the formation of tropospheric ozone [177], and can increase smog occurrence. It is therefore particularly important for emissions near the ground.

F.2.6. Smoke (soot)

The performance of an aircraft engine in terms of smoke is generally defined by the smoke number, which quantifies the opacity of the exhaust plume and has a value between 0 and 100. For smoke number measurements, a filter is positioned in the nozzle and exhaust jet using a probe and subjected to a specified exhaust gas mass (12-21 kg per square meter of filter) [178]. The smoke number is then determined using the following equation:

$$SN = 100 \cdot \left(1 - \frac{R_f}{R_0}\right) \tag{F.1}$$

with R_0 and R_f being the absolute reflectance of the filter before and after sampling, respectively [178]. However, the smoke number only provides a qualitative estimation of particle emission and shown to be strongly dependent on sampling conditions, soot characteristics and morphology. An investigation also showed that particles smaller than 300 nm were not caught by the filter, lowering the accuracy of the measurements [177]. Consequently, it was assumed to have little value for the atmospheric impact estimation [179]. Other measurement techniques have been investigated but no agreement has been reached on which should be used as of yet.

F.2.7. Carbon monoxide

Carbon monoxide is the lesser known variant of carbon dioxide, and is produced during incomplete combustion. It is a colorless and odorless gas, and it is oxidized to carbon dioxide in the atmosphere through a reaction triggered by UV-radiation and heat [177]. This means that it indirectly increases the radiative forcing of carbon dioxide. Aside from the climate effect, carbon monoxide is a highly toxic substance to humans because it prevents the hemoglobin in blood from absorbing oxygen. This reduces the oxygen capacity of people and in the worst case even suffocation. Even in smaller concentrations encountered by jet fuel combustion it can cause health issues, but it is highly unlikely that people are exposed to it either on the ground or in the cabin.

F.2.8. Sulfur oxides

Sulphur dioxide (SO_2) is the most abundant sulfur-containing gas in aircraft exhaust plumes. Through further chemical reactions with hydroxyl-radicals, the SO_2 is oxidized to SO_3, which when reacting with water vapour, forms H_2SO_4 [101]. This compound is known as sulphuric acid. This and other acidic compounds can reach the ground through wet deposition, which is also termed "acid rain". There, it can have damaging effects on nature (e.g. plants, aquatic animals) through changes in the pH-values. It can also damage buildings resulting in additional costs for the general population. Inhalation of the sulphur oxides can also cause headaches and in high concentration damage the lungs [177].

F.3. LTO cycle calculation

In this section, a detailed example LTO cycle emissions analysis will be shown along with the results for several other engines. The engine used for the example is the CFM56-7B27E and all data is taken from the Emissions Databank[1]. From this databank, the fuel flow and emission indices for the four segments are extracted and combined into Equation (F.2) with the known segment operating times, resulting in the values in Table F.1. Note that in the table, for each species the top row contains the values computed numerically, and the bottom row (with * in the first total value) the reference values from the databank.

[1] *ICAO Aircraft Engine Emissions Databank* , https://www.easa.europa.eu/easa-and-you/environment/icao-aircraft-engine-emissions-databank (accessed January 24 2019)

$$M_X = \sum_{segments} EI(X) \cdot \dot{m}_f \cdot \Delta t \tag{F.2}$$

Table F.1: LTO cycle values for CFM56-7B27E from Emissions Databank

Species	Takeoff		Climbout		Approach		Taxi		Total	M_X/T_{TO} [g/kN]	Correction (# eng) [-]	M_X/T_{TO} char[2] [g/kg]
	EI [g/kg]	$\dot{m}_f$ [kg/s]	EI [g/kg]	$\dot{m}_f$ [kg/s]	EI [g/kg]	$\dot{m}_f$ [kg/s]	EI [g/kg]	$\dot{m}_f$ [kg/s]	M_X [g]			
HC	0.03	1.293	0.02	1.031	0.02	0.343	1.54	0.110	272.7	2.25	0.8572	2.62
									273*	2.25*	(3)	2.62*
CO	0.31		0.17		2.82		29.39		5,315	43.78	0.9246	47.36
									5,320*	43.80*	(3)	47.4*
NO_x	23.94		17.89		9.09		4.36		5,231	43.09	0.9442	45.64
									5,231*	43.09*	(3)	45.6*

Looking at the values in the last four columns, the total weight of the emitted species is nearly the same. Consequently, the ratio of the mass divided by the takeoff thrust also match closely. These values were then checked against the different regulations, where the same percentages were found as in the databank. To further support the method, four more engines were analyzed with the results shown in Table F.2.

Table F.2: LTO cycle calculation comparison for five subsonic engines to their reference values from Emissions Databank

Species	M_{HC}/T_{TO}			M_{CO}/T_{TO}			M_{NO_x}/T_{TO}		
Engine	Ref [g/kN]	Calc [g/kN]	Delta [%]	Ref [g/kN]	Calc [g/kN]	Delta [%]	Ref [g/kN]	Calc [g/kN]	Delta [%]
V2527-A5	0.4	0.446	+11.5	30.6	30.5	-0.33	56.2	56.1	-0.18
RR Trent XWB-84	1.44	1.45	+0.69	28.9	28.9	0	55.62	55.63	+0.18
PW JT8D-11	39.5	39.5	0	139.8	139.7	-0.07	57.6	57.6	0
GE GEnx-2B67B	1.07	1.08	+0.93	28.21	28.26	+0.18	42.44	42.84	+0.94
CFM56-7B27E	2.62	2.62	0	47.4	47.36	-0.08	45.6	45.64	+0.09
Average			**+2.63**			**-0.06**			**+0.17**

This again shows that the difference between the thrust corrected characteristic (=corrected) values of the emissions masses are very small. One clear exception is the HC ratio for the V2527-A5 engine where the difference is 11.5%. The most likely cause for this is that the reference value is rounded of to nearest decimal and would in reality be about 0.43-0.45. In that case the difference would be much smaller. The other differences are also likely caused by round-off errors, but this could not be checked because no other sources were found than the databank. It can be concluded that the method will return accurate results so long as the emission index estimates and fuel flows are reliable.

F.4. CO_2 certification methodology

For the CO_2 certification of the new supersonic aircraft, the first item is to check the calculations of the reference geometric factor (RGF). After this the method applied for supersonic aircraft is detailed in Appendix F.4.2. In order to be able to relate the performance of the supersonic aircraft it is useful to try to analyze a set of subsonic aircraft to show whether they conform with the regulations. This is shown in Appendix F.4.3.

F.4.1. Reference Geometric Factor calculations

The reference geometric factor (RGF) has been mentioned in Section 8.1.2, and is implemented in the CO_2 metric to negate the difference in SAR between aircraft of different sizes. As mentioned, the RGF is approximated in the design program using the following equation, and is non-dimensional:

$$RGF \approx \frac{L_{cabin} \cdot w_{max}}{1m^2} \tag{F.3}$$

Because the RGF has an impact on the CO_2 metric it was decided that the method used to determine it in the design program should be tested. To this end, 13 aircraft were selected, of which two are supersonic designs as listed in Table F.3. For all subsonic aircraft, the lengths and widths were measured by using aircraft

[2] characteristic value used for certification

dimension sheets from websites or manufacturer airport planning manuals, and used to estimate the RGF. These are listed in italic font. The reference RGF values were taken from the Piano-X website[3], which has a large database of values. Note that these values are not completely accurate. The non-italic row contains the outputs from the supersonic aircraft design program, which again are used for the RGF calculation.

Table F.3: Reference geometric factor (RGF) calculation check

Aircraft	n_{pax} [-]	L_{cabin} [m]	w_{cabin} [m]	RGF_{calc} [-]	RGF_{pianoX} [-]	**Deviation [%]**	**Source**
Gulfstream G650	19	*14.27*	*2.49*	*35.5*	43.9	*-19.1*	[4]
		14.14	1.86	26.3		-40.1	
Gulfstream G550	19	*13.39*	*2.13*	*28.5*	28.5	*+0.1*	[5]
		14.14	1.86	26.3		-7.7	
Dassault Falcon 7X	16	*11.91*	*2.25*	*26.8*	25.2	*+6.6*	[6]
		12.1	1.86	22.5		-10.5	
Embraer 190	100	*29.1*	*2.7*	*78.5*	77	*+2.0*	[180]
		31.3	2.75	86.1		+11.8	
Airbus A319neo[7]	140	*23.2*	*3.95*	*91.6*	92.7	*-1.1*	[181]
		28.3	3.85	108.8		+17.4	
Airbus A320neo[7]	165	*26.5*	*3.95*	*104.7*	107.6	*-2.7*	[182]
		33.7	3.85	129.7		+20.6	
Airbus A321neo[7]	206	*33.4*	*3.95*	*131.9*	135.3	*-2.5*	[129]
		40.8	3.85	157.1		+16.1	
Boeing 737-8NG[7]	155	*27.0*	*3.76*	*101.5*	104.3	*-2.7*	[82]
		31.1	3.85	119.7		+14.8	
Boeing 787-8	219	*39.0*	*5.77*	*225.0*	233.4	*-3.6*	[130]
		44.7	3.85	171.9		-26.3	
Airbus A350-9XWB	268	*46.5*	*5.96*	*276.8*	299.4	*-7.5*	[183]
		51.5	3.85	198.3		-33.8	
Airbus A340-642	308	*55.5*	*5.75*	*319.1*	330.0	*-3.3*	[184]
		59.5	3.85	229.1		-30.6	
Boom SST	55	*27.5*	*2.40*	*66.0*	80.0[8]	-17.5	[93]
		21.8	2.36	51.5		-35.7	
NLR M1.6	250	*41.0*	*4.25*	*174.2*	-	-	[31]
		48.9	3.85	188.3		-	

Looking at the table, starting with the three business jets, it can be seen that apart from the G650, the program deviation is less than 11%. The main reason for the difference is the smaller cabin width for the supersonic aircraft which is the result of the more narrow aisle and seats used, compared to the subsonic jets. For the G650 the difference is larger since its reference RGF is larger (43.9). This deviation can be explained by Piano-X using ambiguous RGFs for some aircraft, mostly for small business jets due to geometrical issues like intricate rear bulkhead arrangements[3].

Looking at the second group (narrow-body aircraft), the RGF found by measuring the aircraft on the airport planning manuals results in values close to the values in Piano-X. For the design program, the RGF found are on average 15.8% higher, which is mainly due to the longer cabin found by the program. This extra length can be explained by the longer range supersonic aircraft having a larger seat pitch than the short-range subsonic aircraft. Note that for the Airbus A319neo and A320neo, and Boeing 737-8NG, the number of seats abreast was fixed to six in the program so that it matches the layout of the subsonic aircraft. Without this, the number of seats abreast would have been four (A319neo) or five (A320, 737-8NG). In that case the RGF for the A319neo is 106.3 which is 2.3% less. For the A320neo (106.3) and 737-8NG (121.4) the RGF increases by 0.2% and 1.4%, respectively, when compared to the value for six seats abreast. This shows that the impact of the seating arrangement on the RGF is small.

[3] http://www.lissys.demon.co.uk/co2metricdata-update1.html (accessed May 8 2019)
[4] http://www.gulfstream.com/aircraft/gulfstream-g650 (accessed May 5 2019)
[5] http://www.gulfstream.com/aircraft/gulfstream-g550 (accessed May 5 2019)
[6] https://www.dassaultfalcon.com/en/Aircraft/Models/7X/pages/overview.aspx (accessed May 5 2019)
[7] supersonic design program modified so that it has six seats abreast like the reference aircraft
[8] reference value from [93] and not Piano-X

For the smaller wide-body aircraft, the RGF values found by measuring the aircraft are again quite close to the reference values in Piano-X. However, the design program will return substantially lower RGF (on average 30.2% lower) values. It can be seen that the supersonic aircraft all have the same cabin width, which corresponds to the maximum of six seats abreast. The subsonic aircraft, which feature two aisles, have more seats abreast, and consequently have a wider but also shorter cabin. Additionally, the subsonic aircraft could feature a larger galley space because of their increased flight time, which can add a bit of length to the cabin, further increasing the RGF.

From the three groups combined, it is found that the program has deviations, but that these can be explained by the design choices. Therefore, it is decided that the program can be used to estimate the RGF of (supersonic) aircraft. To further substantiate this, two supersonic aircraft were analyzed, the Boom SST and NLR M1.6 aircraft. For the former, the reference RGF was taken from [93], but it seems that the value of 80 is a bit too high when comparing it to the aircraft dimensions in the reference. The supersonic program will also return a lower RGF which is partially explained by the program using less luxurious seats than the actual aircraft. Consequently, the width and length of the cabin, and RGF are smaller. For the NLR design, the difference between the reference and the program are small in absolute terms, although the width is under- and length overestimated. No definitive reason for these differences could be provided because a detailed description of the seating arrangement is not provided in the reference literature.

F.4.2. Supersonic aircraft methodology

For the CO_2 certification it is necessary that the specific air range is computed for the thee weights. To compute the SAR (in km/kg of fuel) for a particular segment the following equation is used:

$$SAR = \frac{1}{W} \cdot \frac{V}{c_j} \cdot \frac{L}{D} \tag{F.4}$$

In the current program version, the weight used is the mid-segment weight in kilogram, V is the cruise speed in km/hr, c_j is the specific fuel consumption in kg/kg/hr or lbm/lb/hr, and L/D the lift-to-drag ratio for the segment. SAR needs to be evaluated for the cruise segment, which in this case is the supersonic segment. In order to calculate the variables needed for the SAR calculation, the fuel fraction method from the Class I analysis is applied but in a slightly different manner such that the mid-segment weight can be estimated.

For the calculations it is assumed that the payload weight is the same as that at the design point of the aircraft used for the Class I calculations. Combined with the operating empty weight this represents the aircraft weight once all segments used in the Class I analysis are completed (i.e. zero fuel weight). The takeoff weight is also known because it was defined by the CO_2 regulations for all three cases. By assuming that the reserve fuel requirements do not change, meaning that only the supersonic cruise segment is altered, all other fuel fractions remain unchanged with respect to the design point values. Consequently, it becomes possible to apply the fuel fractions to the takeoff weight to determine the weight at the start of the supersonic cruise. Similarly, by working backwards from the zero-fuel weight, the weight at the end of the supersonic cruise can be calculated. The average value of these weights then represents the mid-cruise weight needed for SAR determination.

The flight speed V is simply the supersonic cruise speed only multiplied by 3.6 to convert from m/s to km/hr. For the lift-to-drag estimation it would be possible to simply use the same value as for the design point. However, as the average cruise weight is reduced it is possible for the aircraft to fly higher, which affects the aerodynamic performance. To estimate the altitude change it is assumed that the aircraft is again operating at the design lift coefficient (see Equation (C.30)). Since the wing area, flight speed and lift coefficient are the same, the density will vary by the ratio of the mid-cruise weight for the case X investigated and that for the design point, i.e.:

$$\rho_X = \frac{W_{mid,X}}{W_{mid,design}} \cdot \rho_{cr,design} \tag{F.5}$$

With this density and an atmospheric model the new average cruise altitude can be estimated to within several meters. Combining this with the aircraft geometry, the aerodynamics model is applied to determine the new lift-to-drag ratio. During preliminary investigations it was found that the ratio decreased slightly when the aircraft became lighter but the changes were limited to an order of several tenths of a percent. This is due to the different cruise altitude, which affects the drag values.

Then, using this lift-to-drag ratio with the mid-segment weight, the mid-segment thrust can be estimated if steady cruise flight is assumed with lift equal to weight and thrust equal to drag. The supersonic specific

fuel consumption is then calculated by scaling the subsonic specific fuel consumption. The specific air range value can then be determined for all three scenarios.

An investigation in [93] of an aircraft approximating the new Boom SST showed that the aircraft will unlikely meet the new requirement as it was found to exceed its regulatory CO_2 values by 57% in the most optimistic situation, and 115% for the worst-case scenario. To test the results from the program two aircraft was created for the same mission as that defined in the report, one with a cruise number of Mach 2.2 and a modified version at Mach 2.0. These were also listed in Table 7.1. A comparison of the results found to those from the reference are shown in Table F.4.

Table F.4: CO_2 certification of Boom SST-like aircraft with comparison to reference analysis [93]

Source	SST program		Reference		
Scenario	Unmodified	Modified	Best	Most likely	Worst
MTOM [kg]	119,458	82,226	77,000		
Standard [kg/km]	1.0325	0.8336	0.80		
1/SARavg [kg/km]	5.386	3.513	3.464	3.807	4.923
RGF [-]	51.3	51.3	80		
Metric [kg/km]	2.093	1.361	1.21	1.33	1.72
Exceedance [%]	**+103.3**	**+63.8**	**+52%**	**+67%**	**+115%**

From the comparison to the reference values it can be seen that the unmodified design exceeds the regulations by 103.3%, which falls between the most likely and worst case scenarios of the reference. However, as was shown during the program validation, the Mach number of 2.2 causes the aircraft weight to be much higher, which consequently increases the regulatory limit. For this reason, despite having a worse specific air range than the worst case scenario from the reference, it has a smaller margin. Additionally, as shown in the previous subsection, the RGF is lower because of the different seat pitch and arrangement.

Looking at the modified Boom SST aircraft, the results are more similar to the reference. Although the takeoff weight is about 5.2 tonnes greater, the regulatory limit and specific air range values are closer. The amount by which the regulations are exceeded falls in between the best and most likely scenarios. This is seen as a reasonable finding , but it should be noted that the aircraft designed by the program is not designed for the exact same mission. Still, it shows that the CO_2 regulation analysis works for supersonic aircraft. In the future, more tests should be performed once more reference data becomes available for other supersonic aircraft studies.

F.4.3. Subsonic aircraft analysis using Piano-X

For subsonic aircraft the Piano-X software[9] is used, rather than the method described previously. The payload weight is fixed to 100% of the payload defined in Piano-X, and the three takeoff weights are defined in accordance with the CO_2 regulations. By adjusting the value of the maximum takeoff weight it is possible to use Piano-X to analyze the high takeoff weight scenario by running a block range analysis. For the mid gross mass it is often not possible and for the low gross mass scenario it is never possible to perform a mission analysis this way, because it is not possible to select such low weights in Piano-X.

To overcome this issue, the point performance of the aircraft will be used where the Mach number, altitude and weight are needed. For the weight estimation it was necessary to study the aircraft fuel weight buildup which was found to be as follows:

$$W_{f,total} = W_{f,takeoff} + W_{f,climb} + W_{f,cruise} + W_{f,descent} + W_{f,approach} + W_{f,reserves} \tag{F.6}$$

By then selecting six takeoff weights and performing a block range analysis, the values for each of these fuel components were found and used to find correlations to predict the values. This showed that $W_{f,takeoff}$ and Wf, approach were constants regardless of the takeoff weight. $W_{f,descent}$ was found to vary very slightly by an order of ten to twenty kilograms. For the climb fuel $W_{f,climb}$ ($R^2 > 0.9$), $W_{f,cruise}$ ($R^2 > 0.99$) and $W_{f,reserves}$ ($R^2 = 1.0$) accurate linear fits were produced against the aircraft takeoff weight. By combining these values with the known takeoff weight for the three scenarios, it is possible to estimate the aircraft weight at the end, and at the start of cruise, and consequently the mid-cruise weight.

[9] http://www.lissys.demon.co.uk/PianoX.html (accessed January 15 2019)

The cruise Mach number is assumed to be the one found for the block mission analysis and falls in the range 0.78 (e.g. A300) to 0.85 (e.g. 787-8). For the altitude estimation the detailed flight profile analysis at high gross mass is run in Piano-X such that the average cruise altitude can be estimated. For the mid- and low gross mass scenarios this altitude is increased by 500 and 1,000 ft, respectively. Together, the three required parameters for the point performance calculation are now available. The point performance for the high and if possible mid-gross weight scenarios were then compared to the SAR found by dividing the cruise distance and cruise fuel calculated by a block range analysis. Although they were close (often within 1-2%), it was decided to scale the point performance by the block range SAR value because it represents the performance over a longer flight time. For the low gross weight scenario the scaling factor for the mid gross weight was used if available, and otherwise that for the high gross weight was used.

Combining these three values the average SAR was found, and then inverted for the CO_2 metric. As a last step the Reference Geometric Factor (RGF) had to be estimated by making use of airport planning manuals provided by Airbus and Boeing. This was done best as possible, but it can be that the values are deviating from the real values, for which no official sources were found. The results found for five aircraft are shown in Table F.5 including the regulatory limits and margin.

Table F.5: CO_2 certification analysis of five subsonic aircraft with reference data from [92]

Aircraft	B787-8	A380-800	B767-300ERW	A300-600R	A340-642
SAR_{high} [km/kg]	0.19057	0.06840	0.17954	0.15793	0.10288
SAR_{mid} [km/kg]	0.20424	0.07379	0.19207	0.16832	0.11069
SAR_{low} [km/kg]	0.21897	0.07956	0.20524	0.18067	0.11914
$1/SAR_{avg}$ [kg/km]	4.8878	13.5285	5.2007	5.9181	9.0170
RGF [-]	219	620	194	210	320
Metric [kg/km]	1.3323	2.8912	1.4689	1.6400	2.2585
Max allowed [kg/km]	1.4858	2.7291	1.3469	1.2744	2.0543
Margin	-10.3%	+5.94%	+9.06%	+28.7%	+9.94%
Reference margin	-14 to -10%	+2 to +7%	+10 to +15%	-[10]	-[10]

Looking at the margins found for the aircraft it can be seen that only the 787-8 is capable of meeting the requirements, while the A380-800 would require some small improvements. For the relatively old A300-600R it is clear that its performance is poor. However, as it has been out of production for a long time this is not an issue. It can be seen that the newer A340-600 series aircraft is almost on par with the 767-300ERW, which is still being produced. Additionally, looking at the A380 it can be seen that despite its lower SAR, it is closer to meeting the regulations than the smaller aircraft, indicating that the regulations are not necessarily biased towards smaller aircraft. This is termed as being transport capability neutral and means that aircraft types with diverse transport capabilities, but similar levels of fuel efficiency technology/design, have similar margins to the limit line, which was achieved by the RGF introduction[11].

In a study published by the ICCT [92], a range by which different aircraft types exceed or meet the CO_2 requirements is shown. Looking at the values for the 787-8 and A380-800 both fall within the range provided. The 767-300ERW value found is lower than the the range listed by the ICCT, but the aircraft listed there is the regular 767-300ER without winglets, which could to some extent explain the difference as winglets help improve performance. For the remaining Airbus aircraft no data is provided, but overall the data conforms with the Piano-X results. It should be noted that in [92], it is shown that the majority of the subsonic aircraft from the major manufacturers (e.g. Airbus, Boeing, Bombardier and Embraer) expected to be in production in 2023 will meet the CO_2 regulations. Additionally, the full version of Piano-X also includes the CO_2 regulations with the results listed on the website[12]. Looking at the values there and comparing them to those shown in Table F.5, there is some difference visible with the RGF-values being a few percent lower and the metric values slightly different. This can be explained by Piano-X using a method to find the optimum SAR values, while for the analysis performed here, point performance is used to represent the full cruise phase. The difference in RGF can vary a bit depending on the method used to measure the different dimensions.

[10] no data available in reference

[11] Dickson, N. *Progress on the development of the ICAO CO_2 Standard*, https://www.icao.int/Meetings/Green/Documents/day%201pdf/session%203/3-Dickson.pdf (accessed January 22 2019)

[12] http://www.lissys.demon.co.uk/co2metricdata-update1.html (accessed March 8 2019)

F.5. Emission index estimation

In order to be able to evaluate the climate impact of an aircraft, it is necessary to determine the amount of emissions produced during missions. The main species of interest at this stage are the nitrogen oxides, because those are needed for the global climate impact analysis and were found to cause issues with LTO certification. For the estimation of the emission index of nitrogen oxides, there a number of options available as shown in Figure F.5, and they are briefly discussed below.

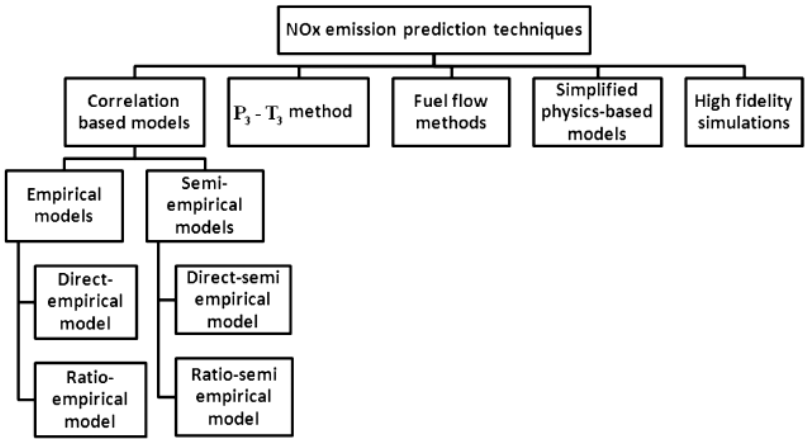

Figure F.5: Overview of NO_x emission prediction technique categories [185]

- The correlation-based (or direct) models are (semi-)empirical relationships which require engine data to calculate an emission index value. This data can include engine variables like p_3, T_3, T_4 and the water-to-air ratio, but also combustor related parameters like the flame and primary zone temperatures as well as the residence times. A key issue with the correlation methods is that they are often created using a set of underlying assumptions and design choices for the engines upon which they are based. These are often considered company secrets making the direct correlations difficult to use properly. When going outside of the range for which the methods are created, the results will likely deviate because of sensitivity to inputs. Still, in a number of aircraft design studies (e.g. [186, 187]) such direct methods are applied to estimate the emission index value.

- The p_3-T_3 method is the most dependable and preferred method for the industry [185]. It requires information from the engine cycle which can be estimated using gas turbine simulation software (e.g. GSP [112] or GasTurb [111]) for the LTO cycle points, but also proprietary engine information such as component pressure ratios, and the pressure exponent "n" and fuel-to-air ratio (FAR) exponent "m". However, when these exponents are unknown one can use $m = 0$ and $n = 0.4$ [185] as a starting point.

- Fuel flow (or relative) methods use LTO cycle emissions data of an existing engine from a database[13] to create curve fits as a function of fuel flow. For a specific flight condition where the fuel flow is known, it is then possible to determine a corrected fuel flow, for which the fit is evaluated. The value found can then be uncorrected for the flight conditions. While this would work well in case the engine studied is similar to that in the database, for supersonic aircraft it is less straightforward because no engines for that regime are included (e.g. most modern reference engines have much larger bypass ratios). Still, given the large amount of engine data available, decent accuracy of the results, and the relatively low complexity, this method is certainly an interesting option. An example method is the DLR fuel flow method [188].

- Simplified physics-based models divide the combustor into zones that contain ideal reactors within which reduced-order physics and chemistry are used to try to get useful results [185, 189]. Because of the lower complexity, the computational effort required is limited. Despite this lower computational effort, the method is not commonly applied because it is possible to have good estimates without having a good representation of the physics and chemistry involved [189]. It is also necessary to have a combustor geometry available to set up the zones. As there is no data available for the combustor geometry

[13] *ICAO Aircraft Engine Emissions Databank* , https://www.easa.europa.eu/easa-and-you/environment/icao-aircraft-engine-emissions-databank (accessed January 24 2019)

and because of the complexity of the method, it is not applied for this research.

- High fidelity simulation can provide the most accurate results of all options so long as the combustor is correctly and accurately modeled by making use of a large number of cells and kinetic mechanisms [185]. It is necessary to know the full geometry of the combustor, which again often is proprietary information of engine manufacturers. A flow modelling technique that can be applied is large-eddy simualation (LES) [189] which uses a model for the small-scale behavior of turbulence in combustion, as compared to direct numerical simulation (DNS) which models all changes, but requires much more computational effort. As a result of the high computational cost, DNS is not an option at this time. LES, despite it also requiring large computational efforts, can be used for emission estimation as done in [190] for the GE90 engine. However, in light of the complexity and need for combustor geometry data, it is not considered an option for this investigation.

Based on the list above, the correlation-based methods and fuel flow methods were deemed feasible within the available time frame. The former are discussed in Appendix F.5.1 for NO_x and CO/HC. For the fuel flow methods the Boeing Fuel Flow Method 2 (BFFM2) and DLR fuel flow methods were selected, and they are discussed in Appendices F.5.2 and F.5.3, respectively. For the fuel flow methods, an attempt was also made to reduce issues caused by the lack of reference engines as explained in Appendix F.5.4.

F.5.1. Correlation-based models

For the direct methods there are a large number of relationships available for NO_x. In [185] a large number of these methods were compiled to study their accuracy and applicability. Two such methods are shown next to give some understanding of the fidelity level used, being that of Lipfert [185] and NASA [191]:

$$\text{Lipfert} \qquad \mathrm{EI}(\mathrm{NO}_x) = 0.17282 \cdot \mathrm{e}^{0.00676593 \cdot \mathrm{T}_3} \tag{F.7}$$

$$\text{NASA} \qquad \mathrm{EI}(\mathrm{NO}_x) = 2 + 28.5 \cdot \sqrt{\frac{\mathrm{p}_3}{3,100}} \cdot \mathrm{e}^{\frac{\mathrm{T}_3 - 825}{250}} \tag{F.8}$$

with p_3 in kPa and T_3 in K. It was found that all methods either over- or underestimated the emission index values when compared to the p_3-T_3 method [185]. An example is the Lipfert method included earlier which due to its exponential dependency on T_3 will strongly over-predict NO_x emissions as the temperature is increased. In an attempt to overcome the shortcomings of the different methods, a new method was proposed based on the method used in GasTurb [111] as described in which uses the severity parameter S_{NO_x} [185]:

$$S_{NO_x} = \left(\frac{p_3}{2,965}\right)^{0.4} \cdot e^{\left(\frac{T_3 - 826}{194} + \frac{6.29 \cdot 100 \cdot WAR}{53.2}\right)} \tag{F.9}$$

In the original method [192], a curve of shape $EI(NO_x)_{SL} = C \cdot S_{NO_x}$ is fit through the origin and the reference engine LTO cycle points. The values of T_3, p_3 and war need to be calculated for the LTO points by making use of an engine model like GasTurb, and the emission indices are taken from the engine databank. As an example, in [192] the constant is found to be about 18.8 for modern dual annular combustors.

In the revised method [185], it is no longer assumed that the linear fit goes through the origin, making the fit: $EI(NO_x)_{SL} = C_1 \cdot S_{NO_x} + C_2$. Once the fit is made, it is possible to estimate the emission index at a specific flight condition by computing the value of the severity parameter S_{NO_x} through use of an engine model. By then applying the severity parameter value in the fit, the emission index is determined. The benefit of the new method is that it does not require proprietary engine information and its predictions compare well to that of the p_3-T_3 method. Note that it is also stated that when no engine simulation software is available, the fuel flow methods can offer the best compromise [185].

For future studies some more sources of direct prediction methods were found which were not included in [185]. These include the SNECMA and AERONOx methods in [94], and the method for modern RQL combustors in [193]. An important note about direct methods is that each method can use a different set of units, with some requiring temperatures in Kelvin, but also in Rankine or Fahrenheit. Similarly, pressure can be in Pa, but also in kPa or psi.

As with NO_x there are also direct methods for the emission index of CO and HC, although it seems that the amount of literature on them is much smaller, meaning that there are fewer methods available. Given the relative importance of good NO_x prediction for the global climate impact, these two species which are mainly of interest for the LTO cycle are ignored and will be analyzed using fuel flow methods. Still, it was decided

to show an example method for CO and HC based on the CFM56-engines which is applied in the GasTurb program [111]:

$$100 - \eta = 0.1 \cdot (0.232 \cdot EI\,(CO) + EI\,(HC)) \tag{F.10}$$

$$\log_1 0\,(EI\,(HC)) = C_1 \cdot \log_{10}\,(EI\,(CO)) + C_2 \tag{F.11}$$

where for the CFM56 engines the constants in the equations are C_1 = 3.15 and C_2 = -4.3 [111]. Note also that η is the combustion efficiency of the engine. The emission indices for both species can then be found by solving the two equations simultaneously. Other methods found can be found in [194].

F.5.2. Boeing Fuel Flow Method 2 (BFFM2)

The Boeing Fuel Flow Method 2 (BFFM2) is an empirical method which was developed during an emission inventory study [96]. It is an advancement of the first Boeing method which accounted for ambient pressure, temperature and humidity, and introduces a Mach number dependency. The method uses engine emissions data from the ICAO defined LTO cycles listed in sources like the ICAO Engine Emissions Databank[14]. Note that BFFM2 uses Imperial units so that fuel flow values are in lbs/hr and EI in lbs/1,000lbs.

In the first step the measured fuel flow values from the ICAO engine data have to be adjusted for aircraft installation effects:

$$w_f = w_{f,unadjusted} \cdot r \tag{F.12}$$

where the correction value r differs for each segment (takeoff 1.01, climbout 1.013, approach 1.02, idle 1.1). With these corrected fuel flows and the emission indices a log-log graph is created with the fuel flow on the x-axis and emission index on the y-axis. Starting with the NO_x-curve a linear regression fit (which is a power fit on log-log scale) should be created through the four measurement points. For the HC and CO-species a slightly different fit is applied, namely a bi-linear fit. For this fit, a linear regression is created through the 7% and 30% thrust points. Another line is drawn horizontally and positioned exactly in between the 85% and 100% thrust points. Both curves are extended until they intersect, resulting in the bi-linear fit. Examples are shown in Figures F.6 and F.7.

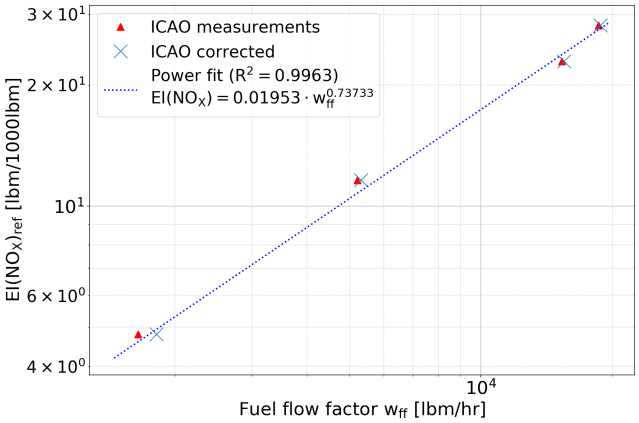

Figure F.6: NO_x emission index fit example from [96]

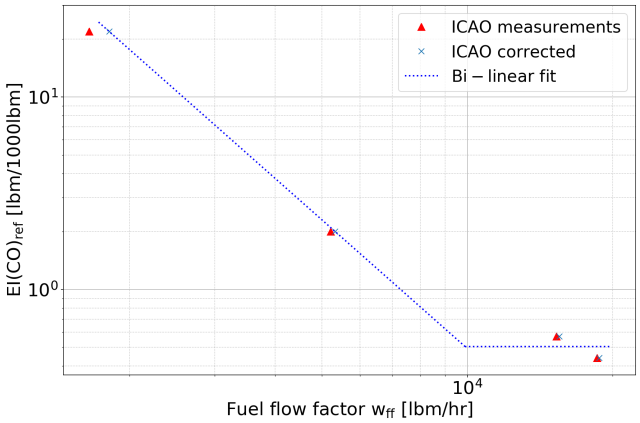

Figure F.7: CO emission index bi-linear fit example from [96]

These graphs are based on the examples provided in Appendix D of [96], and were found to closely approximate the reference graphs. Next, for the situation in which the emission index is to be estimated, the known fuel flow w_f is corrected using Equation (F.13).

$$w_{ff} = \frac{w_f}{\delta_{amb}} \cdot \theta_{amb}^{3.8} \cdot e^{0.2 \cdot M^2} \tag{F.13}$$

where θ_{amb} is the ratio of ambient pressure to sea-level pressure, and δ_{amb} the ratio of ambient temperature and sea-level temperature (288.16 K), and M the Mach number. Using this value and the curve fits produced earlier, the emission index can be estimated. As a last step, these emission index values have to be uncorrected by using Equations (F.14) to (F.16) so that they reflect the at-altitude flight conditions.

[14] https://www.easa.europa.eu/easa-and-you/environment/icao-aircraft-engine-emissions-databank (accessed January 8 2019)

$$EI(HC) = EI(HC)_{ref} \cdot \frac{\theta_{amb}^{3.3}}{\delta_{amb}^{1.02}} \tag{F.14}$$

$$EI(CO) = EI(CO)_{ref} \cdot \frac{\theta_{amb}^{3.3}}{\delta_{amb}^{1.02}} \tag{F.15}$$

$$EI(NO_x) = EI(NO_x)_{ref} \cdot e^{H} \cdot \left(\frac{\delta_{amb}^{1.02}}{\theta_{amb}^{3.3}} \right)^{0.5} \tag{F.16}$$

where the following equations are used to find some of the so-far undefined variables.

$$H = -19.0 \cdot (\omega - 0.00634) \tag{F.17}$$

$$\omega = \frac{0.62197058 \cdot \phi \cdot p_v}{p_{amb} - \phi \cdot p_v} \tag{F.18}$$

$$p_v = 0.014504 \cdot 10^{\beta} \tag{F.19}$$

$$\begin{aligned} \beta = 7.90298 \cdot \left(1 - \frac{373.16}{T_{amb} + 273.16}\right) + 3.00571 + 5.02808 \cdot \log\left(\frac{373.16}{T_{amb} + 273.15}\right) + \\ \left(1.3816 \cdot 10^{-7}\right) \cdot \left[1 - 10^{11.344 \cdot \left(1 - \frac{T_{amb} + 273.16}{373.16}\right)}\right] + \left(8.1328 \cdot 10^{-3}\right) \cdot \left[10^{3.49149 \cdot \left(1 - \frac{373.16}{T_{amb} + 273.16}\right)} - 1\right] \end{aligned} \tag{F.20}$$

Note that in [195] a different version of the specific humidity calculation (Equation (F.18)) is used, which has a factor 0.37802 in the denominator. This change would be correct if the specific humidity referred to moist air, but because BFFM2 uses dry air as reference so the factor should not be implemented [188]. The relative humidity ϕ is often assumed to be 60% for the entire flight as done in the example of [96]. Using that example, the program created was found to return the expected values for the sea-level conditions. The assumption of 60% relative humidity will hardly affect the NO_x emission index at cruise altitudes (<0.1% change) as is shown in Table 13 of [195].

BFFM2 is used in a number of different studies and programs such as PianoX[15] and SAGE [196]. Although it is accurate, especially when combined with good aircraft performance data, little to no engine data for SSTs is available because no engines have been certified for that purpose. The one group of engines for supersonic flight, those of fighter jets, are not in the databases. However, new engines such as the GE Affinity for Aerion AS2, are a strongly modified versions of higher bypass (subsonic) engines, so it is possible to use data for such engines instead. An example of this is the HISAC study where engines similar to the V2527-A5 were used [94]. A similar assumption was made in [93] where three scenarios were analyzed, two of which featured a derivative of a recent turbofan, and one a military engine for which no data was available. Additionally, it should be noted that with introduction of new technologies, the amount of emitted species can be further reduced.

In an attempt to test the application of the method on more accurate aircraft operational data, Piano-X was used because it too uses the BFFM2, albeit with a different method for the reference emission index fit. While the regular BFFM2 uses a log-log plot, Piano-X uses a regular plot and quadratic spline. This is displayed in Figures F.8 and F.9 where the example from the Piano-X manual is used to show the similarity of the graphs. Note that all other steps are the same, except that Piano-X uses SI units. Additionally, for CO and HC a linear fit is uses rather than a bi-linear one.

The comparison of the graphs shows that the fits are the same when using a quadratic spline between the individual LTO measurement point. From Piano-X, the emission index data of each aircraft for the LTO cycle could be extracted and used to produce similar fits to those shown in Figures F.6 and F.7. By then selecting several point performance analyses, the flight conditions and actual fuel mass flow are calculated by Piano-X. These can then be used in the fuel flow methods to estimate the NO_x emission index. Note that the emission indices of CO and HC could also be determined but these are only of direct importance during the low thrust operations of the LTO cycle. The results of the NO_x emission index estimation analyses are summarized in Tables F.6 and F.7 for the Boeing 787-8 and Airbus A380-800, respectively. In the tables the first five columns contain the inputs for the point performance in Piano-X as well as the emission index returned. The remaining columns show the emission index found for the same scenario by using the regular and Piano-X version of

[15] http://www.lissys.demon.co.uk/PianoX.html (accessed January 15 2019)

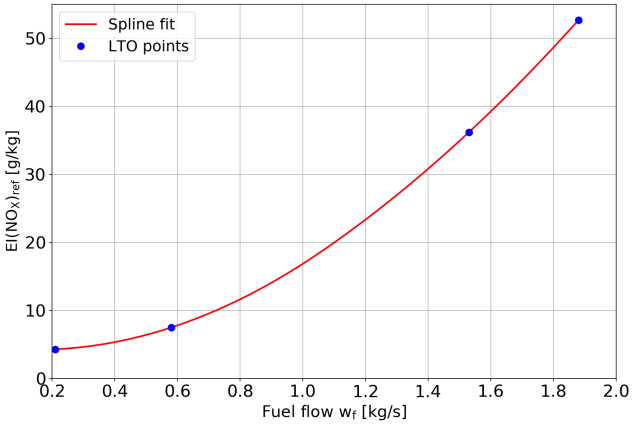

Figure F.8: NO_x emission index fit using Piano-X example

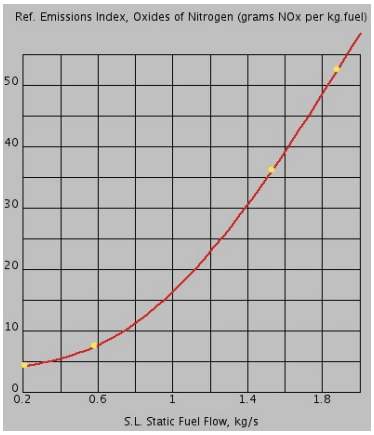

Figure F.9: NO_x emission index fit from Piano-X manual[a]

[a] http://www.lissys.demon.co.uk/pug/c12.html (accessed February 26 2019)

BFFM2 and the DLR method (see Appendix F.5.3) in combination with the LTO cycle data defined in Piano-X, as well as the deviation.

Table F.6: Scenarios and corresponding NO_x emission indices found by Piano-X, BFFM2 and DLR method for Boeing 787-8

Mach [-]	Altitude [ft]	Weight [kg]	Flow per engine [kg/hr]	EI(NO_x) Piano-X [g/kg]	EI(NO_x) BFFM2[16] [g/kg]	Delta [%]	EI(NO_x) BFFM2[17] [g/kg]	Delta [%]	EI(NO_x) DLR [g/kg]	Delta [%]
0.2	0	219,000	3,378	12.90	11.72	-9.18	13.00	+ 0.79	11.37	-11.9
0.3	0	219,000	2,582	11.24	9.78	-13.0	11.13	-1.02	9.75	-13.3
0.5	10,000	178,600	2,353	11.57	10.11	-12.6	11.49	-0.72	9.50	-17.9
0.6	10,000	178,600	2,935	13.10	11.98	-8.55	13.23	+0.97	11.41	-12.9
0.7	35,000	178,600	2,024	10.84	9.79	-9.66	10.91	+0.63	7.73	-28.7
0.8	35,000	178,600	2,218	11.40	10.66	-6.49	11.57	+1.49	8.59	-24.6
0.85	35,000	178,600	2,384	11.77	11.34	-3.66	11.97	+1.73	9.27	-21.2
0.7	40,000	150,000	1,705	9.88	9.00	-8.93	9.97	+0.90	7.23	-26.8
0.8	40,000	150,000	1,848	10.33	9.72	-5.89	10.49	+1.58	7.96	-22.9
0.85	40,000	150,000	1,983	10.65	10.33	-3.00	10.83	+1.73	8.57	-19.5
Abs. avg.						**8.09**		**1.16**		**20.0**

Looking at the tables it can be seen that for the Boeing 787-8, the emission index is always underestimated by the standard BFFM2, while for the Airbus A380-800 it is consistently overestimated. The average deviations are less than ±10%, which shows that the deviation is not too large. When using the Piano-X BFFM2 method, the deviations are much smaller, consistently within ±2% and the absolute average deviations are 1.16 and 1.32%. This improvement was expected because it more closely matches the method applied by Piano-X. For the remaining difference, no additional explanations could be found.

The DLR method explained in the next subsection was also applied to the points generated by Piano-X and are shown in the last two columns of Tables F.6 and F.7. It can be seen that for the situations considered, the DLR method on average has a larger deviation than BFFM2. However, because the difference varies quite drastically it is possible that for an alternate set of points the DLR method performs better.

Aside from the comparison made earlier, a previous study in [197] has shown that BFFM2 has excellent performance for NO_x emission prediction when compared to the p_3-T_3 method, which is the best option. For CO and HC the method is somewhat less accurate, in particular for low thrust settings. As these are less important for non-LTO conditions the reduced accuracy is not a direct issue.

[16] with linear regression in log-log space as in [96]
[17] with quadratic fit similar to Piano-X

Table F.7: Scenarios and corresponding NO_x emission indices found by Piano-X, BFFM2 and DLR method for Airbus A380-800

Mach [-]	Altitude [ft]	Weight [kg]	Flow per engine [kg/hr]	EI(NO_x) Piano-X [g/kg]	EI(NO_x) BFFM2 [g/kg]	Delta [%]	EI(NO_x) BFFM2 [g/kg]	Delta [%]	EI(NO_x) DLR [g/kg]	Delta [%]
0.2	0	569,000	6,452	23.33	25.43	+9.01	22.87	-1.98	24.70	+5.87
0.3	0	569,000	4,348	17.39	17.81	+2.40	17.63	+1.36	16.89	-2.88
0.5	10,000	520,000	3,533	16.61	16.72	+0.66	16.83	+1.34	15.68	-5.60
0.6	10,000	520,000	4,072	18.60	19.46	+4.63	18.76	+0.87	17.97	-3.39
0.7	35,000	453,400	2,962	15.78	16.53	+4.76	15.91	+0.82	16.31	+3.36
0.8	35,000	453,400	3,012	16.31	17.27	+5.86	16.36	+0.28	16.55	+1.47
0.85	35,000	453,400	3,221	17.35	18.65	+7.51	17.16	-1.10	17.82	+2.71
0.7	40,000	420,000	3,014	16.76	18.23	+8.77	16.46	-1.82	19.71	+17.6
0.8	40,000	420,000	2,838	16.35	17.73	+8.42	16.08	-1.68	18.11	+10.8
0.85	40,000	420,000	2,962	17.19	18.73	+8.95	16.86	-1.93	18.96	+10.3
Abs. avg.						**6.10**		**1.32**		**6.39**

F.5.3. DLR Fuel Flow Correction method

The DLR Fuel Flow Correction method is relative method similar to BFFM2 discussed previously. It also makes use of the LTO cycle engine data from the Emissions Databank, but unlike BFFM2 it can only be used for NO_x, and not for CO and HC. In the first step of the method, a parabolic fit is produced through the four measurement points with the fuel flow (note, in kg/s) on the x-axis and the emission index on the y-axis. An example is shown in Figure F.10 by using the CFM56-5A3 engine. The graph was compared to that in [188] which looked similar for the same inputs.

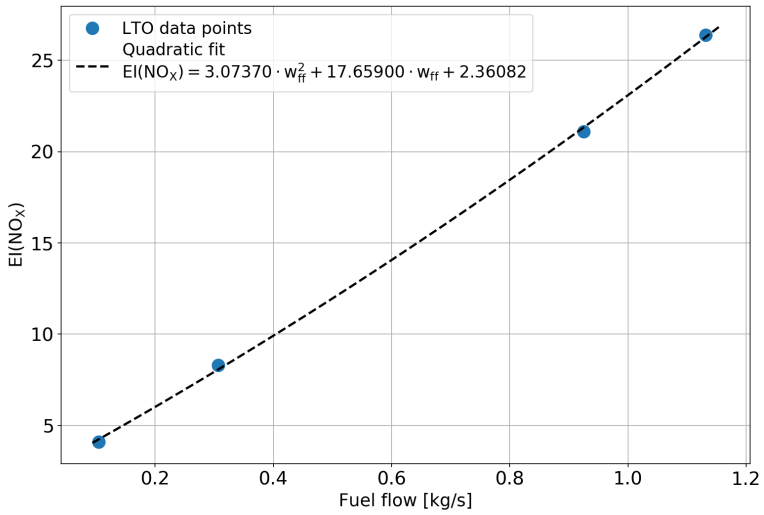

Figure F.10: DLR Fuel Flow correction fit for CFM56-5A3 engine

Following this, the flight conditions at the point where the emission index is to be estimated are used to correct the (actual) fuel flow to the ISA reference conditions by using the following equation:

$$w_{f,corr} = \frac{w_{f,actual}}{\delta_{tot} \cdot \sqrt{\theta_{tot}}} \tag{F.21}$$

where δ_{tot} and θ_{tot} are similar to those for BFFM2 but now in SI units (Pa and K) instead of Imperial units:

$$\delta_{tot} = \frac{p_{total}}{101{,}325} \qquad \theta_{tot} = \frac{T_{tot}}{288.15} \tag{F.22}$$

and with the total pressure and temperature values depending on the flight Mach number M:

$$p_{total} = p_{amb} \cdot \left(1 + 0.2 \cdot M^2\right)^{3.5} \qquad T_{total} = T_{amb} \cdot \left(1 + 0.2 \cdot M^2\right) \tag{F.23}$$

This corrected fuel flow can then be used with the parabolic fit on the reference conditions to determine the reference emission index value. Then, as a last step the emission index under reference conditions has to be re-corrected for the operating altitude by application of the following equation:

$$EI(NO_x) = EI(NO_x)_{ref} \cdot \delta_{tot}^{0.4} \cdot \theta_{tot}^{3} \cdot e^{H} \tag{F.24}$$

with:

$$H = -19.0 \cdot (\omega - 0.00634) \qquad \omega = 10^{-3} \cdot e^{-0.0001426 \cdot (h - 12{,}900)} \tag{F.25}$$

Note that in this last equation the altitude h should be provided in feet rather than meters. Results found for the DLR method are shown in the results of the previous subsection. More detailed information on the theory and validity of the method can be found in [198].

F.5.4. Supersonic engine LTO data generation

For the relative emission index estimation methods the reference engine emission indices (NO_x, CO, HC, SN_{max}) and fuel flows have to be known at the LTO cycle points. However, for the low bypass ratios in SST-engines no recent subsonic reference engines exist. Additionally, the fuel flow at takeoff for the supersonic engine is often larger than that of engines with similar thrust due to the lower bypass ratio. This causes issues with the relative fuel flow methods because for cruise conditions, it was found that the corrected fuel flow is often greater than that at takeoff conditions which results in unrealistic (high) emission index values.

To attempt to resolve these issues, a different dataset will be used where the emission index and smoke number values are determined by using fits through the emission index values for several engine series. This methodology is similar to that which was applied in [93] for a Boom SST like aircraft, where the NO_x performance in the LTO cycle was based on a fit for CFM56 and LEAP series engines. The exact method was also confirmed with one of the authors. In that method, the emission index values for several engines from a series are taken from the Emissions Databank and plotted against the engine overall pressure ratio (OPR) for each of the LTO segments. For a number of engine series it is then possible to find good exponential and polynomial fits, meaning that for a known SST engine OPR, the emission index values for each segment can be estimated under the assumption that the SST engine features a combustor similar to the reference engine. Examples are shown in Figures F.11 and F.12 for the CFM56 engine series with the CO and NO_x species, respectively.

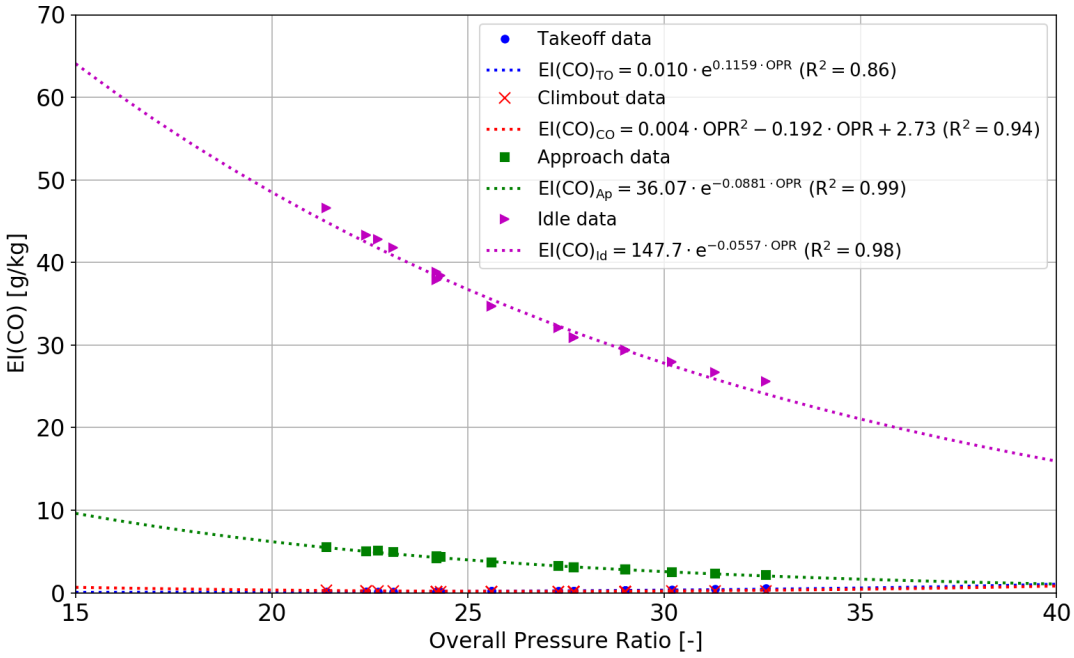

Figure F.11: CO emission index fit as function of engine OPR for CFM56-series

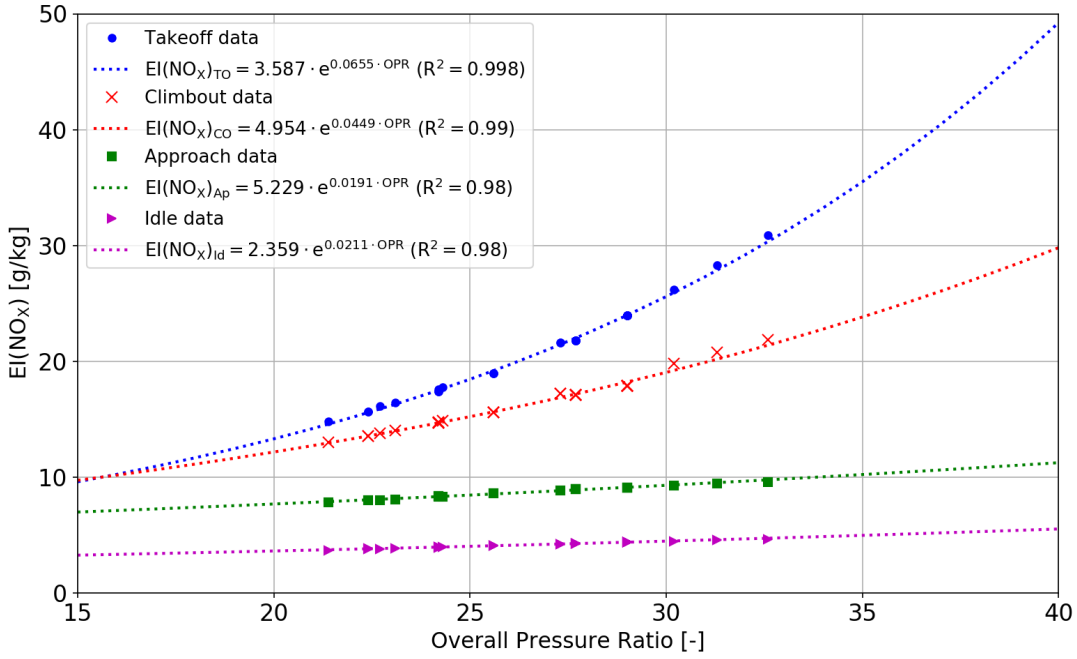

Figure F.12: NO_x emission index fit as function of engine OPR for CFM56-series

Similar graphs were also made for the HC and smoke number values. This was done for a number of engines series, but it should be noted that it is not possible to create good fits for all engine series in the Emissions Databank. To limit the amount of fits, four engine series are considered:

- CFM56: used in [93], and has similar thrust to that expected for the smaller SSTs, but has lower OPR than expected of new SSTs (30-40). For the fit creation 31 engines are used.
- LEAP: used in [93], and meant to replace the CFM56 engines for new subsonic narrow-body aircraft. It has higher OPR values and features TAPS II (Twin-Annular Pre-mixing Swirler) combustors, but the number of engines in the fit is limited at just four.
- CF6: engine series selected to represent old performance as the test data used was produced in 1987. Primary reason to use this series is to show the effect of combustion technology improvement over time. For the fit creation thirteen engines are used.
- GenX: series to represent the current higher OPR engines, and tested in the early 2010s. This series is anticipated to give an indication of the best possible performance and features a TAPS combustor. For the creation of the fits nine engines are used.

The databases containing the engine data and emission index fits are included with the rest of the program.

The remaining unknowns are the LTO fuel flows for which a statistical relation will be used. That relationship was established by using all engines from the emission databank certified after 1989. Engines from before that year are left out because they are considered too old to be representative of current engines. For the roughly 440 remaining engines, the fuel flows at the LTO points were normalized by dividing them by the takeoff fuel flow. For each of the LTO points, the average of these normalized values was then calculated, and a quadratic curve was fit through the points. The resulting fit is shown in Figure F.13 and displays the ratio of the fuel flow at a thrust level to that at takeoff as a function of the thrust level.

For the LTO points the following ratios are then found: climbout = 0.81884 ; approach = 0.28067 ; idle = 0.10108. Now, for the resulting aircraft design, the fuel flow at the design point (takeoff) is known. Then, using this value and the ratios it is possible to estimate the expected fuel flow at the remaining LTO points. It should be noted that especially for the idle condition, the standard deviation is 0.0171, which is rather large (≈17%). However, given that the statistical basis of the method is about 440 engines the average is still considered a good approximation.

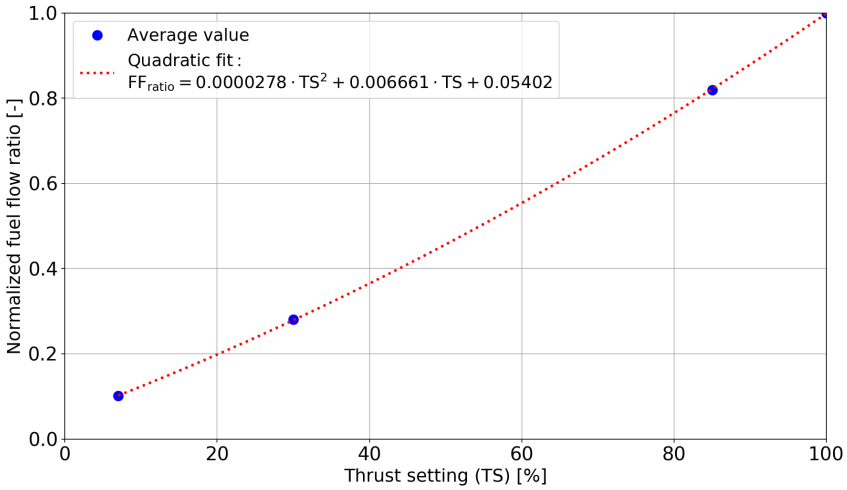

Figure F.13: Normalized fuel flow ratio versus thrust setting

F.6. Fleet setup

For the global temperature change estimation method employed in the thesis, the annual fuel consumption for the entire supersonic fleet in the year 2050 has to be known. Since the Class I analysis will only return the (cruise) fuel consumption of a single aircraft, which is not representative, it is necessary to come up with a definition of the supersonic fleet. Additionally, to allow for comparing supersonic and subsonic aircraft, a subsonic fleet should be defined which is roughly equivalent to the supersonic fleet. As a metric to make the two fleets similar, the number of revenue passenger kilometers (RPK) is selected. It is defined here as the product of the annual number of flights per aircraft, the average distance flown per flight, the average number of passengers transported, and the size of the fleet. This value is typically lower than the available passenger kilometers (APK) because the aircraft are often not filled completely.

Note that the fleets are based on a number of assumptions. A more detailed analysis could offer better insight into the fleet but would require setting up a complete flight routing network which required too many resources. The main assumptions used in the fleet definition are the following:

- Load factors:
  - The load factor for Transatlantic flights on subsonic aircraft is on average about 81% as found in [199]. To account for expected growth of air traffic an 85% load factor is assumed for all subsonic flights in 2050. This is still less than the load factors for some airlines such as KLM and similar to Norwegian [199]. For Transpacific flights on subsonic aircraft the average load factor was found to be 82% [200]. Similar to the Transatlantic flights, an 85% load factor is assumed for all subsonic flights in 2050. For the larger SST of more than 120 passengers, it is assumed that they feature a similar seating arrangement to subsonic aircraft and also have an 85% load factor.
  - For the smaller SSTs (up to 100 pax) it is expected that they focus on the premium market. In [201] an average load factor of 40% is assumed for first class and 60% for business class in 2008. The SSTs will not provide first-class seating, but be more akin to business-class. Additionally, because supersonic transport could be a real time-saver a higher factor of about 70-75% is assumed for 2050, so long as the ticket prices do not differ significantly between sub- and supersonic flight as is predicted by Boom. It is assumed that this number could go up to 80% for the SST100, but this requires the SSTs to be successful and depends on market conditions.
  - For the super- and subsonic business jets no clear data could be found on the average load factors from literature. Therefore, it is assumed that the load factors will be about 70% as for the small SSTs. An additional issue for business jets is that they are often operated using fractional ownership such that the load factors can vary from day-to-day.
- The performance of the subsonic aircraft will be estimated by making use of Piano-X as it features a large aircraft database, and is commonly used in studies on aircraft climate effects. The aircraft used for comparison in the three supersonic categories are:

  - For the large SST250 the subsonic aircraft available for comparison are the Boeing 767-300ER(W), 767-400, 777-300ER, 787-8, and Airbus A330-200, A340-642, A350-800XWB and A380-800.
  - For the smaller SST50 and SST100, it is difficult to find a comparable subsonic aircraft since subsonic aircraft in that range are mainly designed for operations on smaller range (continental, up to 3,000-3,500 NM) flight like the 737 and A320-families. There are potential exceptions like the new A321LR, but this aircraft is currently not available in Piano-X, and is likely too large to properly compare. An aircraft capable of a 4,200 NM flight is the A319neo with a load of 95 passengers. However, it is questionable whether this would result in a good comparison since the aircraft is analyzed for a mission, it was not really designed for. For the SST50, the Boeing 737BBJ business aircraft and Airbus Corporate jet which were analyzed with a 35 and 44 passenger load, respectively. In both cases, the design payload of Piano-X was taken and multiplied with the 70% load factor. Still, these aircraft are not seen as very reliable because the payloads seem to be relatively high for a business jet, although they represent modified versions of the 737 and A320.
  - For the SSBJ it was easier to find a set of subsonic aircraft as they often have a larger design range than that of the SSBJ. The reference aircraft currently included are the Gulfstream G550 and G650, and the Dassault Falcon 7X.

- For the flight frequencies several city pairs were looked at with estimated flight times depending on the cruise Mach number. This showed that for some Transatlantic city pairs (e.g. LHR-JFK), supersonic flight at Mach 1.6 or higher could offer the option of flying a stretch at least three times a day compared to subsonic aircraft only being capable of flying it twice a day. Note that the level of detail in this analysis was very low with turnaround times ranging from 1 to 1.5 hours. Maintenance could be performed during the overnight stay. However, flying three times a day might also affect crew planning and other aspects. For Transpacific flight supersonic aircraft could allow for operating flights twice in 24 hours while a subsonic aircraft would require just over 24 hours. All in all, this shows that supersonic aircraft could offer an increased aircraft utilization, and it is assumed that SSTs and SSBJs offer a 20% higher utilization than an equivalent subsonic fleet.

- The fleet size is the last key item as well as the number of flights performed per aircraft each year. For the SSBJ the fleet size is assumed to be 250 aircraft with 100 flights per year each, as used in the HISAC study [100]. For the SST50/100 a fleet size of 200 aircraft is assumed with an average of 500 flights per year per aircraft. This fleet size is smaller as the 50 to 100 segment looks less attractive than the smaller business jet in the current market. Lastly, for the SST170/250 the fleet sizes are slightly larger at 250 aircraft which again operate 500 flights annually. Note that this fleet size is about half that of the standard fleet size used in the SCENIC investigation [99]. However, the main purpose of this investigation is to compare a similar sub- and supersonic fleet for one point. Because of the linearity of the climate functions with fuel consumption, a doubling of the supersonic fleet or doubling of productivity would result in a doubling of the temperature change.

Now that these assumptions and choices have been detailed, it is possible to determine the size of a subsonic fleet. In this example the SST250 will be used with 250 aircraft operating 500 flights each every year (in 2050) with an average flight distance of 4,200 NM (or 7,778.4 km) and 85% load factor. Then the number of RPKs is:

$$RPK_{SST250} = (250 \cdot 0.85) \cdot 7,778.4 \cdot 500 \cdot 250 = 2.066 \cdot 10^{11} \text{pax} \cdot \text{km} \tag{F.26}$$

Now, using the Boeing 787-8 baseline design defined in Piano-X which has a 242 passenger capacity for the same distance can perform 20% less flights, or 500/1.2 = 416.7 per year. By setting the number of subsonic RPKs equal to the supersonic amount the fleet size can then be estimated:

$$RPK_{787} = (242 \cdot 0.85) \cdot 7,778.4 \cdot 416.7 \cdot n_{ac} = 2.066 \cdot 10^{11} \longrightarrow n_{ac} = 309.92 \approx 310 \tag{F.27}$$

This shows that about 310 787-8 aircraft would be needed to fly same number of RPKs as 250 SST250 aircraft. This value can then be used to determine the total fuel consumption of the subsonic fleet in the climate impact analysis. The same will be done for the other subsonic aircraft.

F.7. AirClim model

In order to accurately analyze the climate impact of certain emission scenarios on a global scale complex climate models are needed. These require a lot of computation power and a runtime in the order of days to weeks, and include models like E39/C, OsloCTM2 , ULAQ and SLIMCAT [202]. While this might be acceptable for complex situations where the goal is to get high resolutions and detailed breakdowns of the different contributions, for short-term situations where decisions need to be made quickly, this is undesirable. With the increased importance of aviation climate impact, it is much more important to properly estimate climate effects of different aircraft designs. In order to enable a proper climate impact estimation without requiring powerful computers and advanced models, the AirClim model [203] was created at DLR.

AirClim is a climate model capable of analyzing emission scenarios within minutes on simple desktop computers, meaning that it can be included in the design routine for climate sensitive aircraft design solutions. This short runtime is achieved through the linearization of the climate response to emissions. The overall program structure of AirClim is shown in Figure F.14, and contains three large groups: the pre-calculated input data (red), the emission input data (yellow) and the AirClim model (blue).

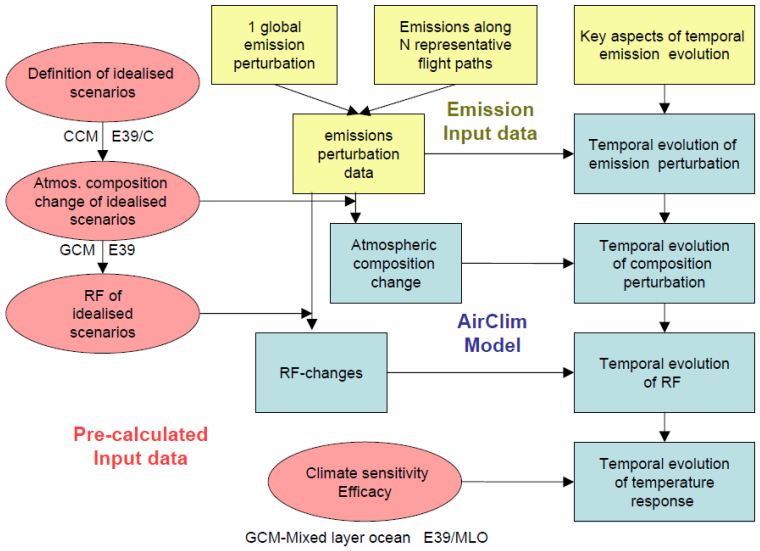

Figure F.14: Overview of climate modeling in AirClim [203]

For the generation of the pre-calculated input data, the atmosphere is approximated by 24 grid points, six in the vertical (altitude) and four in latitudinal direction. The definitions of the six altitude regions are:

- Climb Low: 967 hPa (≈0.4 km)
- Climb High: 499 hPa (≈5.6 km)
- Subsonic Cruise Level: 198 hPa (≈11.85 km)
- Superosnic Cruise Level-Low: 132 hPa (≈14.4 km)
- Supersonic Cruise Level-Medium: 89 hPa (≈16.9 km)
- Supersonic Cruise Level-High: 52 hPa (≈20.3 km)

For the latitudinal regions, the following definitions were used:

- 60°N-90°N: Northern high latitudes (pole)
- 30°N-60°N: Northern-mid-latitudes (midlat)
- 30°S-30°N: Tropical region (tropic)
- 45°S-30°S: Southern-mid-latitudes (south)

The remaining latitudinal range towards the South pole is not included in the grid because the amount of air traffic in that region is negligible compared to the other regions. At each of the 24 locations uniform emission

quantities of nitrogen oxides and water vapor were introduced into the atmosphere, and analyzed using a steady-state simulation of the E39/C climate-chemistry model [204] for the year 2050. The resulting changes of the atmospheric composition and radiative forcing form the pre-calculated input data for AirClim [203].

Second, there is the emission input data which has to be provided by the user and represents the emission scenario to be analyzed by the model. The data contains information about the flight routing of the aircraft, and the local emissions produced along the route. The values used depend on factors like the routing, altitude, engine efficiency and aerodynamic characteristics. When setting up the scenarios it is important that there is always a base scenario included which is used to compare the other scenarios (where something was modified in e.g. design or fleet size) to. The scenarios should be representative of the expected traffic densities (e.g. the routing and flight frequency has to be accurate). If this is not done properly, the results will not be representative for the design and lose their value.

The last component is the linear response model of AirClim, which combines the pre-calculated data and emissions data to determine the composition changes in the atmosphere and the resulting radiative forcing changes. These are then converted to a near surface temperature change (or other climate metric) through summation of the contributions of the different emitted species. For computing the temperature changes the method that was defined by Sausen and Schumann [171] is used [203].

Through the application of the AirClim model to a set of different scenarios, the accuracy of the results found were tested by comparing them to the outputs provided by the more advanced climate models. The comparison showed that the values for the species concentration changes, radiative forcing, and temperature changes calculated by AirClim show a reasonable agreement with the other models. A scenario featuring a supersonic aircraft fleet showed that the value found by AirClim was within 10%, and that the main contributor to the temperature change was water vapor [203].

F.8. CO_2 fits from Piano-X

This section shows two fits for the CO_2 certification metric taken from the Piano-X website for a large number of subsonic aircraft. The metric is plotted against the maximum takeoff weight and span loading in Figures F.15 and F.16, respectively.

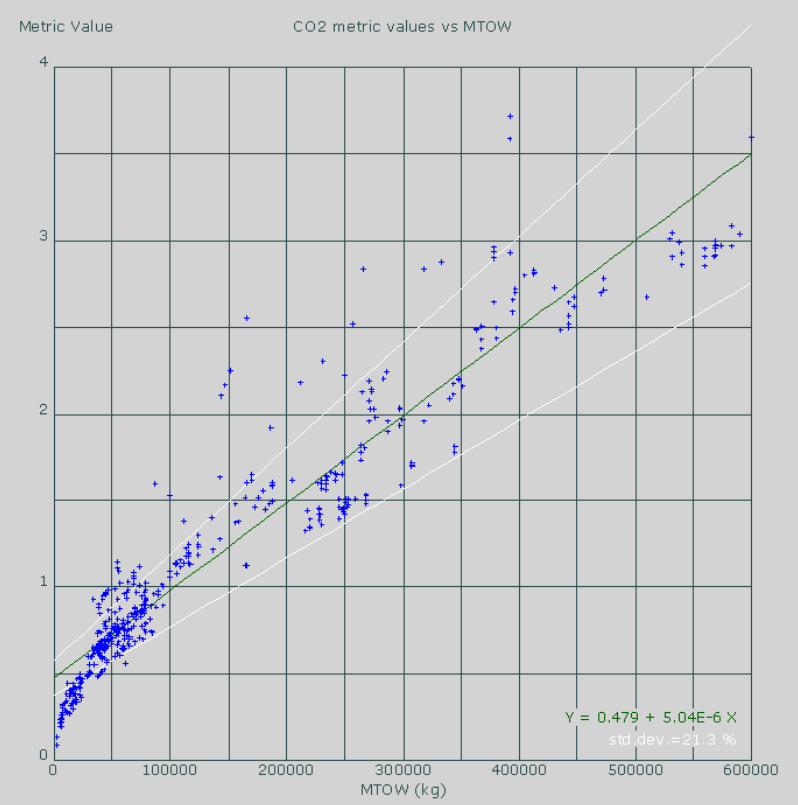

Figure F.15: CO_2 metric fit against takeoff weight for subsonic aircraft[18]

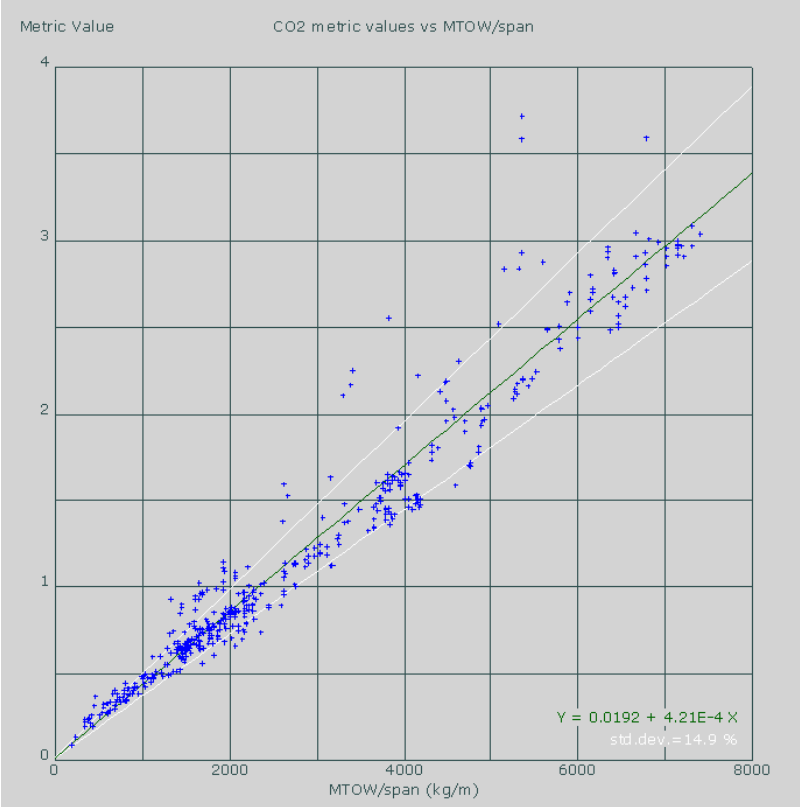

Figure F.16: CO_2 metric fit against span loading for subsonic aircraft[19]

The corresponding fits are for takeoff weight:

$$CO_2\text{metric} = 0.479 + 5.04 \cdot 10^{-6} \cdot \text{MTOW} \tag{F.28}$$

and for span loading:

$$CO_2\text{metric} = 0.0192 + 4.21 \cdot 10^{-4} \cdot \text{MTOW/span} \tag{F.29}$$

G
Output example

This appendix contains an example output file as produced by the program. Note that this version is produced when ParaPy is installed, and without random technology factors. The design shown was produced by for the following key design parameters:

- Maximum payload: 250 passengers
- Number of flight attendants: 7
- Design point load factor: 0.85
- Design range: 5,000 NM
- Supersonic cruise Mach number: 1.6
- Supersonic cruise altitude: 16,000 m
- Subsonic cruise Mach number: 0.95
- Subsonic cruise altitude: 10,200 m outbound and 11,500 m inbound
- Wing aspect ratio: 2.5
- Takeoff distance: 3,200 m at elevation of 0 m
- Landing distance: 2,500 m at elevation of 0 m
- Clean sea-level stall speed of 80 m/s at MTOM
- Fowler flaps at the trailing edge both inboard and outboard
- Technology factors included
- Reference engine series for LTO cycle is the GenX-series
- Subsonic reference aircraft are the Boeing 787-8 and Airbus A350-800XWB

Output created: Sat May 25 11:00:53 2019
Runtime for design routine: 159.7 seconds and 11 iterations
Runtime for ParaPy images and area distribution: 27.7 seconds

The SST250 aircraft is capable of transporting a maximum of 250 passengers. The design point is a range of 5,000 NM (9,260 km) with an outbound subsonic segment of 0 NM at 10,200 m, and inbound subsonic segment of 0 NM at 11,500 m, at a load factor of 0.85, which results in a payload mass of 21,675 kg. The supersonic cruise at Mach 1.60 is performed at an altitude of 16,000 m (52,493 ft). Subsonic cruise is performed at Mach 0.95 at 10,200 m (33,465 ft) altitude. The aircraft has an aspect ratio of 2.50. For the design mission the nominal fuel efficiency (assuming no fuel reserves used) is 11.61 passenger kilometer per kg of fuel. Harmonic fuel efficiency is 13.50 passenger kilometer per kg of fuel.

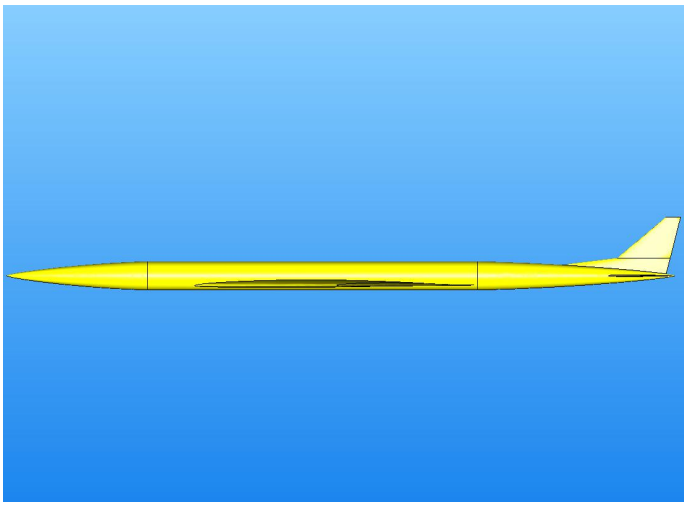

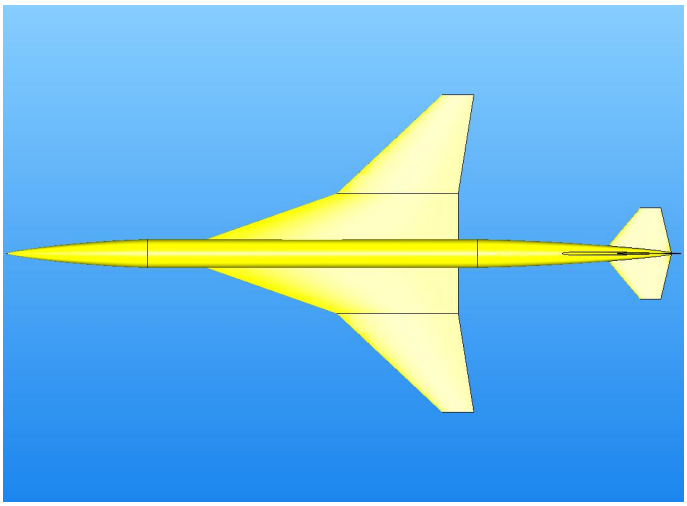

Note: x- and y-scale for images can be different due to scaling

Payload-range performance

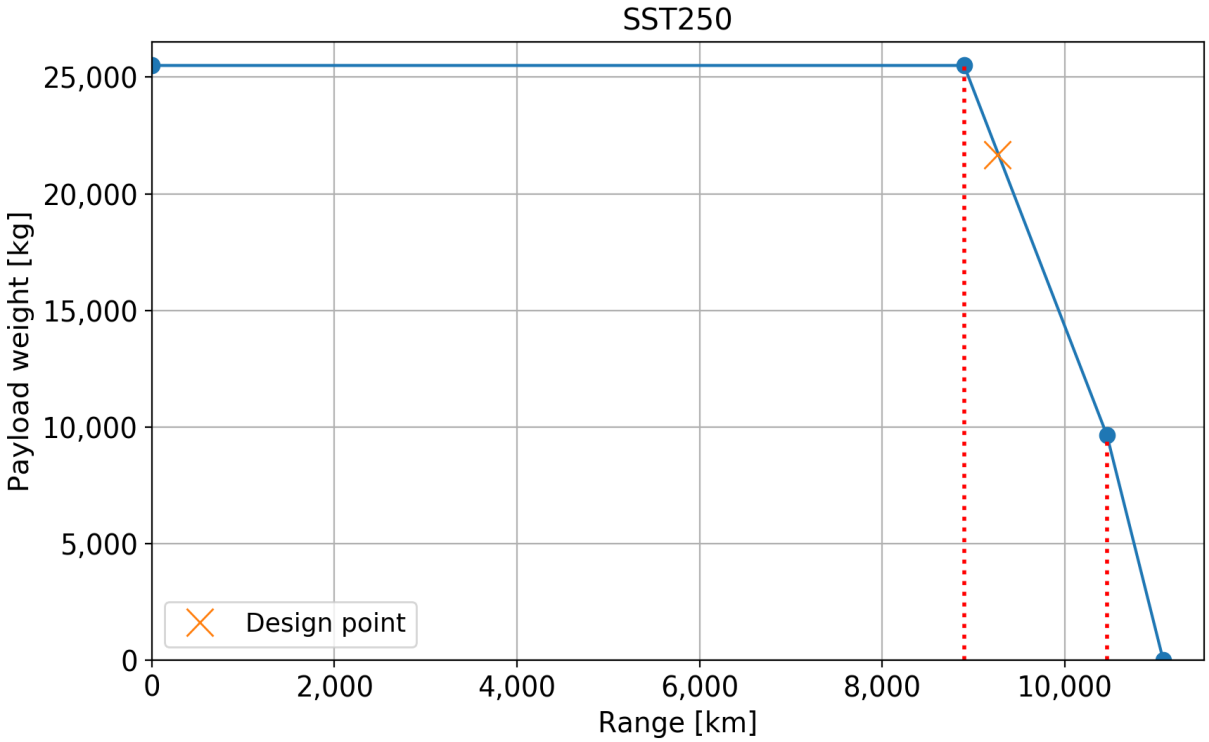

Maximum takeoff mass	332,721.5	kg
Operating empty mass	129,042.2	kg
Maximum landing mass	191,492.1	kg
Maximum ramp mass	337,771.2	kg
Maximum fuel mass	194,037.3	kg
Harmonic mission		
Harmonic range	4,804.3	NM
Harmonic payload	25,500.0	kg
Harmonic fuel	178,179.4	kg
Design point		
Design range	5,000.0	NM
Design payload	21,675.0	kg
Design fuel	182,004.4	kg
Point C		
Range C	5,649.6	NM
Payload C	9,642.0	kg
Fuel at C	194,037.3	kg
Ferry mission		
Ferry range	5,982.7	NM
Ferry takeoff mass	323,079.5	kg

Wing loading and aircraft dimensions

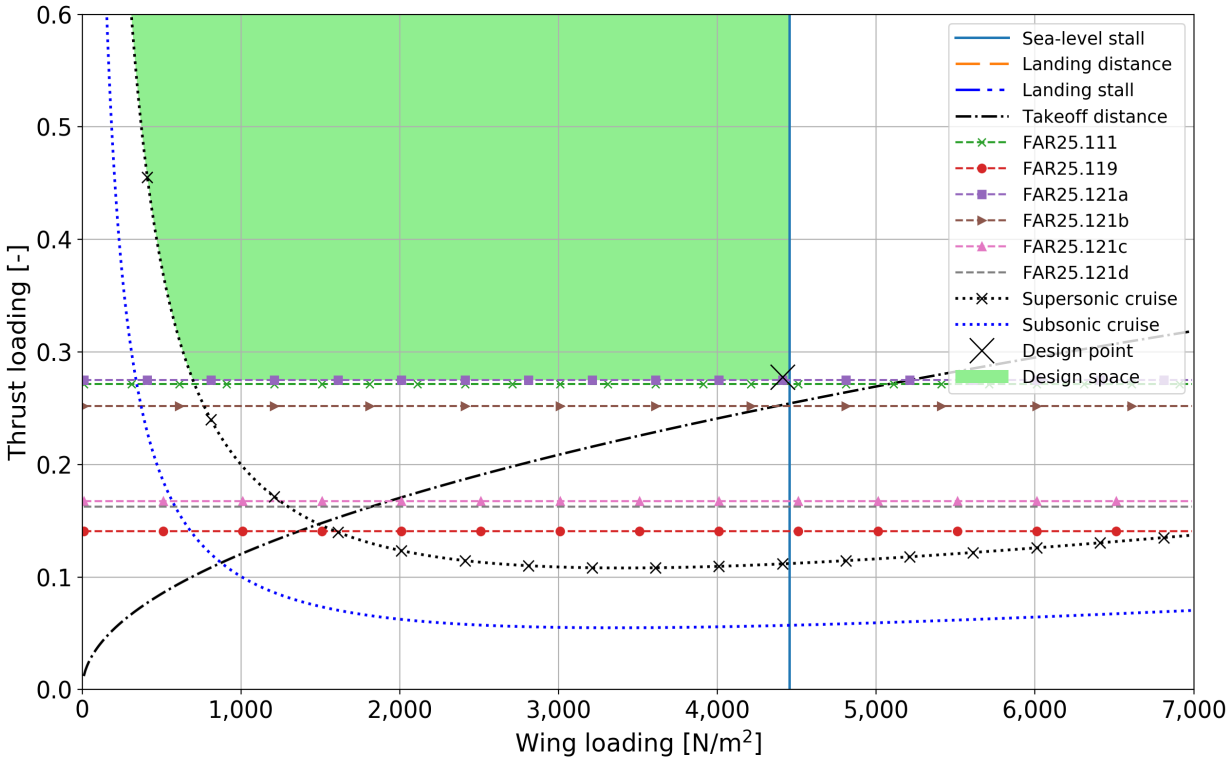

Design point	W/S [N/m^2]	T/W [-]
Value [-]	4,409.4	0.278

Fuselage		
Length	91.11	m
Diameter	3.85	m
Slenderness	23.66	-
Forebody length	19.25	m
Cylindrical length	44.91	m
Aftbody length	26.95	m
Seats abreast	6	-
Wetted area	784.4	m^2

Wing		
Area	740.6	m^2
Span	43.0	m
MAC	22.99	m
Root chord (centerline)	39.92	m
Kink chord	16.54	m
Tip chord	4.37	m
Aspect ratio	2.50	-
Wetted area	1155.4	m^2

Horizontal tail		
Area	76.19	m^2
Span	12.34	m
Root chord	9.50	m
Tip chord	2.85	m
LE sweep	40.0	deg
Wetted area	137.1	m^2

Vertical tail		
Area	59.54	m^2
Height	7.72	m
Root chord	24.14	m
Tip chord	2.85	m
LE sweep	60.0	deg
Wetted area	113.1	m^2

Aerodynamic characteristics

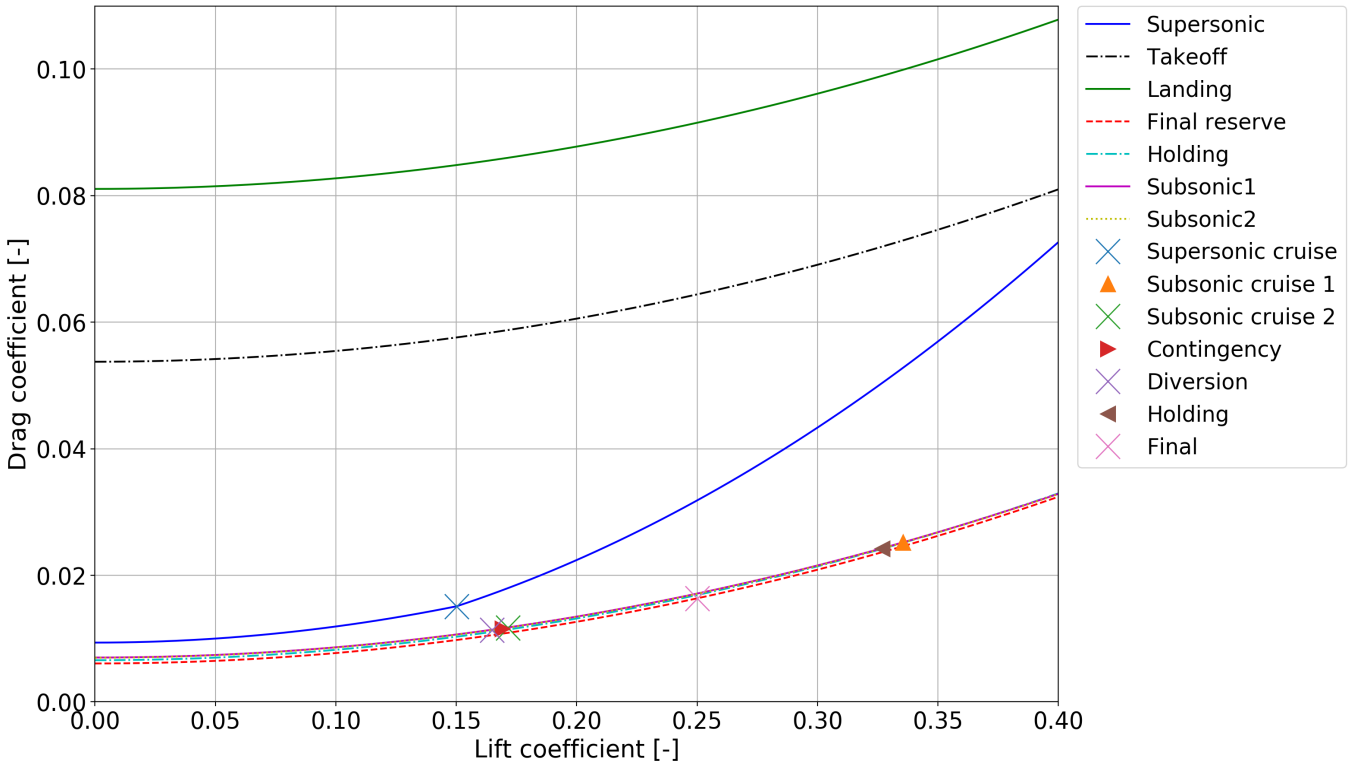

Key aerodynamic parameters

Parameter	*Value*	*Unit*
$C_{L,cruise}$	0.150	-
$C_{D,cruise}$	149.5	cts
$L/D_{max,cruise}$	10.044	-
$C_{L,\alpha}$	2.388	rad^{-1}
$C_{L,max,TO}$	1.226	-
$C_{L,max,landing}$	1.338	-

Lift coefficient and aerodynamic efficiency per flight segment

Condition	$C_{L,mid}$ *[-]*	*L/D [-]*
Sub1	0.263	14.62
Sub2	0.170	14.63
Contingency	0.169	14.59
Diversion	0.165	14.51
Loiter	0.327	13.50
Final reserve	0.250	15.28

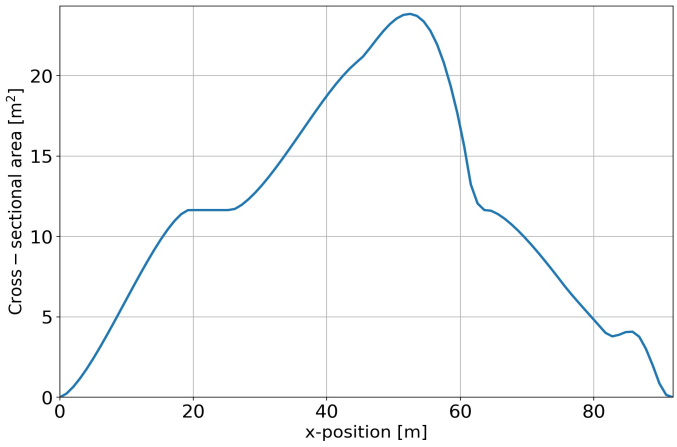

TE HLDs are fowler flaps inboard and fowler flaps outboard.
At LE no HLD included in design.

Maximum area:

23.84 m^2 with 92 slices

Engine characteristics

Parameter	Value	Unit	
Maximum thrust (per engine)	226.7	kN	
Bypass ratio	3.0	-	
Overall pressure ratio	35.0	-	
Length	4.02	m	
Diameter	1.80	m	
Dry mass	4,020	kg	
Thrust-to-weight ratio	5.75	-	
Fuel mass flow (T/O)	3.37	kg/s	
Air mass flow (T/O)	435.1	kg/s	
Fuel type	Jet A1		
Fuel LHV	43.1	MJ/kg	
Fan pressure ratio	2.0	-	using 2 stages
HPC pressure ratio	17.9	-	using 9 stages
TIT	2,037	K	
Inlet type	fixed		
T/O SFC	14.88	g/kN.s	
Number of engines	4		

Segment	Fuel flow kg/s	SFC g/kN.s	SFC 1/hr
Subsonic 1	1.28	23.85	0.842
Supersonic	1.92	28.38	1.002
Subsonic 2	0.64	22.24	0.785
Contingency	0.63	22.21	0.784
Diversion	0.62	22.16	0.782
Loiter	0.71	24.37	0.861
Final reserve	0.62	24.82	0.876

Fuel volume information

Component	Wing/Center fuselage	Forebody	Tail	HT	Total	Required	Margin
Volume [m^3]	297.59	0.00	76.32	0.00	373.91	241.42	132.49

Engine cycle graph at T/O

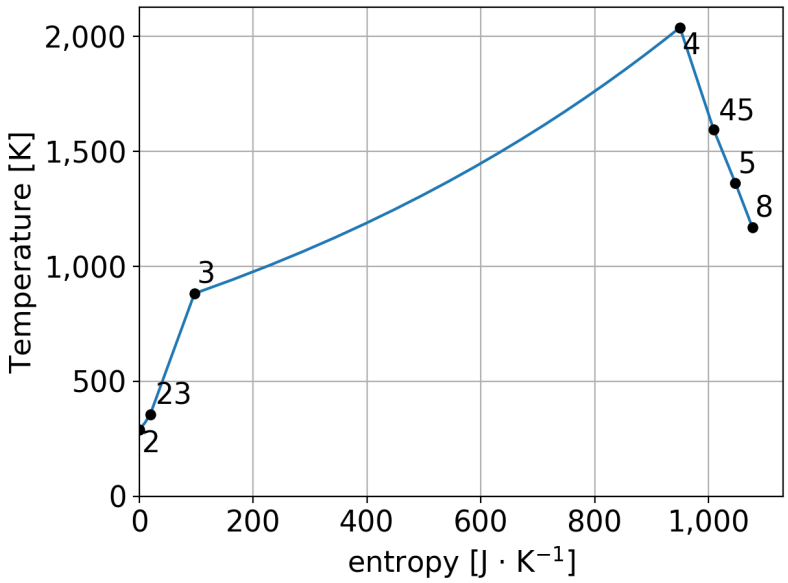

Operating empty weight breakdown

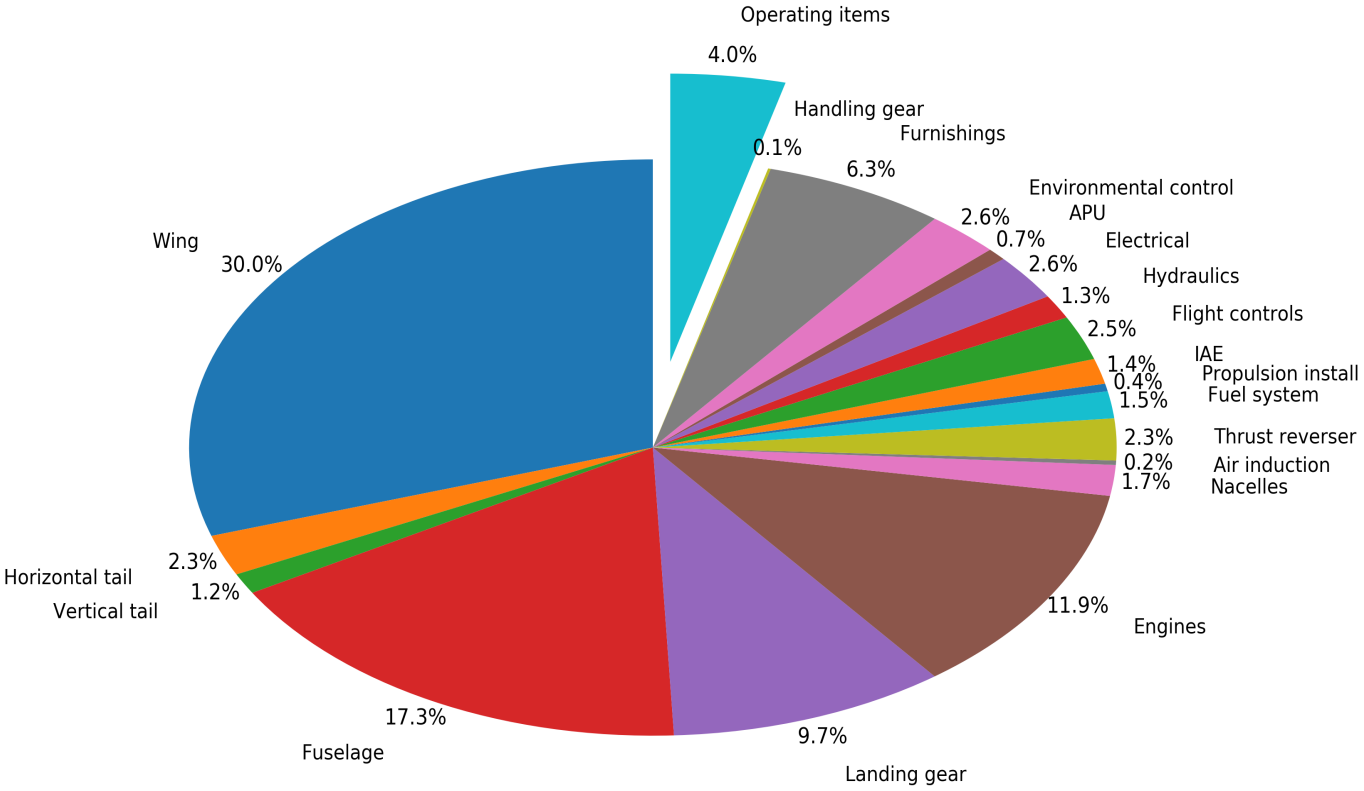

Group/Component	Weight [kg]
Wing	38,663.3
Horizontal tail	2,960.6
Vertical tail	1,491.3
Fuselage	22,342.9
Landing gear	12,477.5
Structures	**77,935.6**
Engines	15,380.1
Nacelles	2,221.8
Air induction	318.2
Thrust reverser	3,019.6
Fuel system	1,951.0
Propulsion install	550.0
Propulsion	**23,440.7**
IAE	1,825.8
Flight controls	3,201.6
Hydraulics	1,719.9
Electrical	3,311.9
APU	889.2
Environmental control	3,293.7
Furnishings	8,146.0
Handling gear	117.7
Equipment	**22,505.9**
Empty weight	**123,882.3**
Operating items	5,160.0
Operating empty weight	**129,042.2**

Environmental impact

LTO cycle data using Modified GenX/P1 engine as reference for EI

Mode	Power setting [% FN]	Time [min]	Fuel flow [kg/s]	EI HC [g/kg]	EI CO [g/kg]	EI NO_x [g/kg]	Smoke number [-]
Takeoff	100%	0.7	3.367	0.016	0.36	15.33	0.0
Climbout	85%	2.2	2.770	0.020	1.38	9.79	0.0
Approach	30%	4.0	0.941	0.078	4.10	8.10	0.0
Idle	7%	26.0	0.344	0.993	23.48	4.12	0.0
Total mass [g] or max smoke number				560.2	14,084.2	9,785	7.60
Number of engines tested				1	1	1	1
Characteristic values Dp [g] or smoke number				862.8	17,287.6	11,341.8	9.78
Dp/F0 [g/kN]				3.81	76.25	50.03	-
Regulatory limit [g/kN]				19.60	118.00	60.12	18.91
Exceedance [%]				**-80.58**	**-35.38**	**-16.79**	**-48.28**

CO_2-certification results

Specific Air Range

High [km/kg]	Mid [km/kg]	Low [km/kg]	1/avg [kg/km]
0.0648	0.0703	0.0768	14.2262
RGF [-]			188.3
Metric value [kg/km]			4.0469
Regulatory limit [kg/km]			1.9264
Exceedance [%]			**110.1**

Global impact overview

Scenario	Aircraft	Fleet size [-]	Mach [-]	Range [NM]	Pax count [-]	Cruise altitude [m]	RPK [10^{10} pax km]	FC_{2050} [10^9 kg]	EI(NO_x) [g/kg]	ΔT_{2050} [mK]	dT [mK]
SupPes	SST250	250	1.60	5,000	212	16,000	24.539	16.932	18.00	10.688	1.402
SupML	SST250	250	1.60	5,000	212	16,000	24.539	16.932	10.00	9.286	-
SupOpt	SST250	250	1.60	5,000	212	16,000	24.539	16.932	5.00	8.410	-0.876
SupBFFM	SST250	250	1.60	5,000	212	16,000	24.539	16.932	13.25	9.855	0.569
Sub1	B788	308	0.85	5,000	206	12,619	24.500	5.160	10.67	2.106	-7.180
SupFS1	SST250	57	1.60	5,000	212	16,000	5.565	3.840	10.00	2.106	-7.180
Sub2	A358XWB	288	0.85	5,000	221	12,924	24.577	5.253	10.79	2.231	-7.055
SupFS2	SST250	60	1.60	5,000	212	16,000	5.896	4.068	10.00	2.231	-7.055
SupAltM	SST250	250	1.60	5,000	212	15,500	24.539	16.932	10.00	8.944	-0.341
SupAltP2	SST250	250	1.60	5,000	212	16,500	24.539	16.932	10.00	9.611	0.325

Weight convergence history

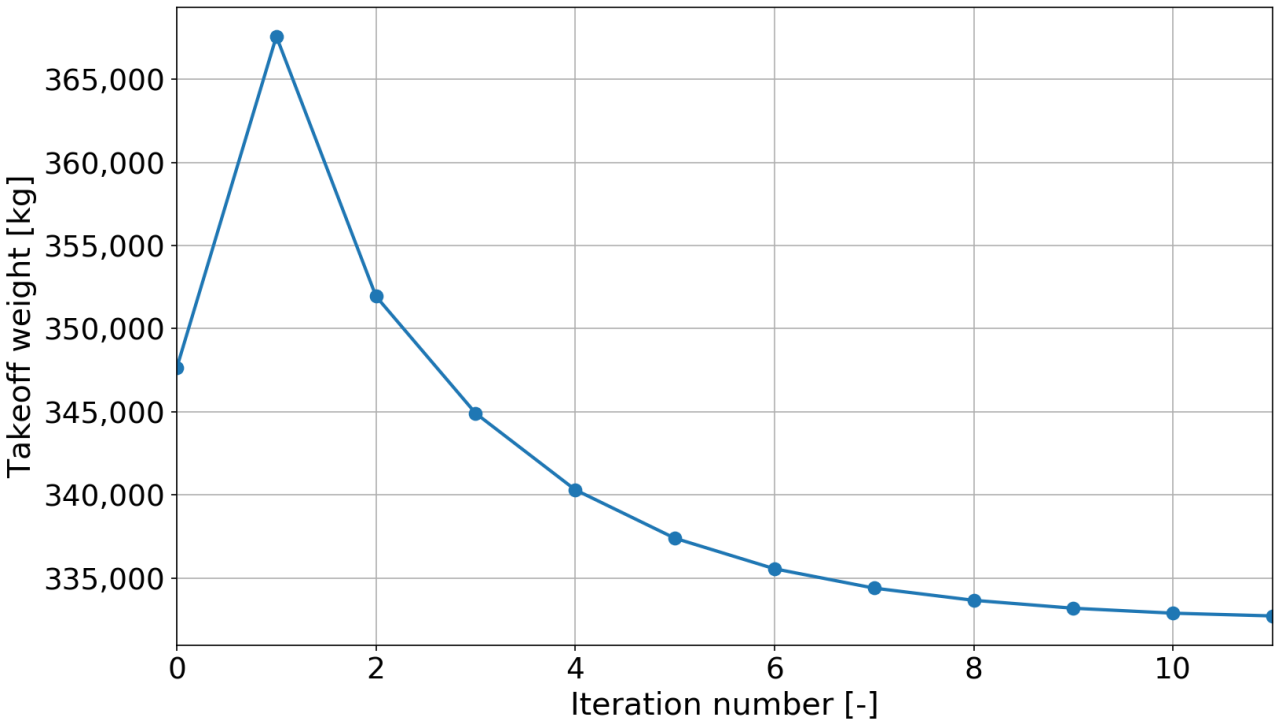

H

Sidenote: Oblique Flying Wing

From discussions with Egbert Torenbeek it was concluded that for supersonic transports to become successful, the currently applied double delta wing concept might not be the best. Instead, the oblique flying wing (OFW) could be considered, but given the limited resources available, the OFW not being a common SST concept, and the limited studies on the configuration, it was not used in the research. Still, it was considered interesting to write a small sidenote about the concept for interested readers.

The oblique flying wing, also known as oblique all wing (OAW), is different from the configurations commonly studied in aircraft design projects. It can be seen as a combination of the blended-wing-body (BWB) and oblique wing (as studied by Jones [205]) configurations, and is shown in Figure H.1. The passenger cabin is positioned inside the wing and no fuselage or empennage is present, although vertical tail(s) will be needed. Engines will likely be podded underneath the wing, along with cockpit and should be capable of rotating with the wing such that the engines and pilots are always facing in the direction of travel (and airflow).

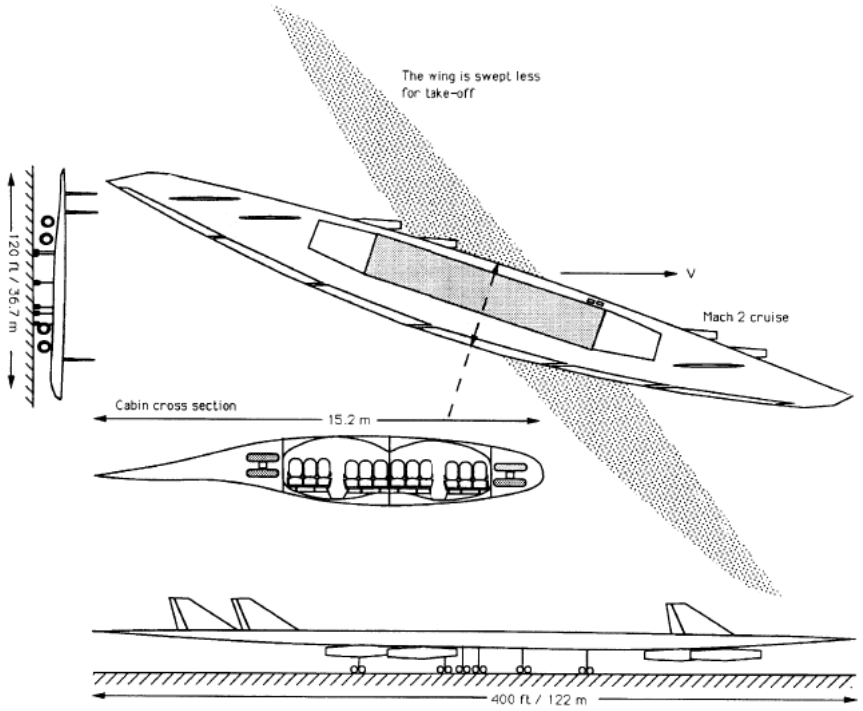

Figure H.1: Oblique flying wing design sketch [206]

A project which was worked on by Northrop Grumman for DARPA (Defense Advanced Research Projects Agency) in the mid-2000s was termed 'Switchblade', and looked to design an experimental UAV capable of bombing targets[1]. However, after many test runs DARPA decided not to continue the funding of a flight demonstrator aircraft, because the preliminary results were not satisfactory.

Looking at some of the findings from several studies combined with the knowledge gathered on supersonic aircraft design during this research, a number of key advantages of the OFW concept can be listed:

[1] Shachtman, N., *DARPA Kills Shape-shifting, Supersonic Bomber*, 2008, https://www.wired.com/2008/10/the-pentagons-s/ (accessed January 24 2019)

- The wing structural efficiency is higher because of the increased wing thickness. Also, since the cabin is located inside the wing, an additional download is generated which cancels out part of the lift. For conventional aircraft this download would be primarily caused by the fuel stored in the wing tanks. Overall, these factors improve the resistance to bending and reduce the overall bending moment, allowing for a lighter structure.
- The relatively smooth area distribution results in relatively low volume wave drag for the aircraft, and can be tweaked further through the positioning of the engines. For the design produced in [206] it was found that the OFW design had lower volume-dependent drag than delta wing designs below Mach 2. Above that speed its drag would start to rise sharply, while for conventional delta wing designs the volume drag component continued to decrease. In [206] it was also shown that the drag due to lift for oblique elliptic wings is lower than for delta wings.
- As with a variable sweep wing, the OFW can change its "sweep angle" depending on the speed at which it is flying. For low speeds the orientation will be similar to that shown in grey in the sketch on the previous page, while for higher (supersonic) speeds it will be oriented at a higher sweep angle. As a result of this ability, the OFW can offer higher lift-to-drag ratios than most existing configuration up to Mach 2.0 [206]. This is visualized in Figure H.2. Note that since the time of that study, there have been improvements to conventional aircraft aerodynamics, but it is still expected that the OFW will offer better performance, especially when compared to regular SSTs. This is particularly true for the subsonic flight regime where regular SSTs have relatively poor performance.

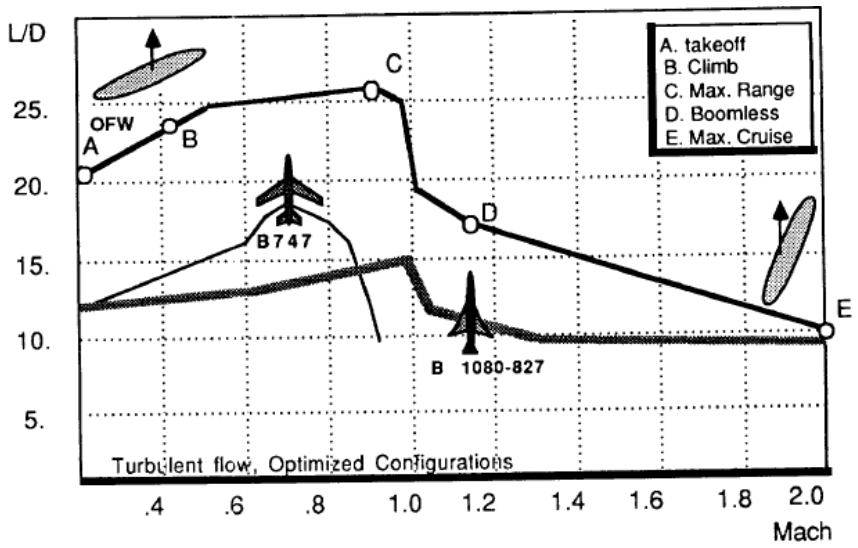

Figure H.2: Oblique flying wing L/D versus Mach number [206]

- As a result of the improved lift-to-drag ratios achieved by the OFW concept, the aircraft can have lower fuel fractions, and thus lower fuel quantities than conventional SSTs designed for the same mission. From an environmental point of view this is especially important given the reduced climate impact. An extra benefit of the reduced fuel fraction is that the payload fraction is higher for supersonic OFW aircraft, and was even found to be close to that of subsonic aircraft with similar payloads [206]. This is substantially better than the conventional supersonic transports which often cannot even offer half that payload fraction.
- Because of the smaller sweep angle at low-speeds, the OFW concept can be operated from shorter runways than comparable conventional SST aircraft, which have much worse low-speed performance [206]. This can also reduce airport noise since engines can be operated at lower throttle settings or be less powerful [207].

While these benefits offer a nice prospect, the OFW also has a number of issues which would have to be resolved before it becomes a promising option for future designs:

- The aircraft will have a larger span than current subsonic aircraft and even blended-wing-body aircraft

designs. Consequently, it is likely incompatible with the majority of the current infrastructure like runways and taxiways. Modifying these will be very costly and complex, and might require entirely new terminal buildings or even new airports to be built. The way the aircraft is boarded will also require different positioning of the doors and a change to existing jet bridges. Additionally, positioning the landing gears will be more complex, because it is not an option to have a single nose gear [208]. Instead, it is more likely that there will be about four struts in front of, and four behind the cabin to better spread the loading on the pavement. It is also important to consider the ability of the aircraft to perform ground maneuvers, which is more difficult with more forward struts.

- Passengers are used to flying inside a mostly cylindrical fuselage, while being seated facing the direction of flight. In an OFW they will likely not have any or at least fewer windows to look outside. This could be seen as similar to the situation for BWB-aircraft but there the passenger are still positioned facing in the flight direction. This is also safer during incidents such as emergency landings because the seats are more capable of dealing with any forces encountered. For the reasons provided, it might be harder to convince passengers to travel on OFW aircraft.
- There has been very little research into the OFW configuration compared to most other designs. As a result, there are still many unknown factors at play which cannot be foreseen, and which make the prediction of the performance difficult.
- The flight control system required for the OFW concept to be properly operated is complex. According to Ilan Kroo, an aeronautics professor who worked on an OFW project at Burt Rutan, they did not have the flight control systems and computer stability augmentations available to meet the requirements[1]. Note that since then there have been major developments in flight control systems so it is unclear whether this is still an issue.
- Positioning all of the different components such as the passenger cabin, fuel tanks and cargo holds within a single structure can be complex because they all have to be accessible but also separated. In [208] it was indicated that for the design studied, more than enough room was available for the systems, meaning that there was sufficient freedom available.
- From a sonic boom perspective it might be harder to reduce the boom strength as is indicated in [209]. However, the article assumes an aircraft with a takeoff weight much greater than what is expected of new SSTs. Still, this should be investigated to determine the importance of the sonic boom.

Another interesting concept which is an extension of the oblique flying wing is the so-called bi-directional flying wing [210]. It is symmetric about both longitudinal and span axes (see Figure H.3). For supersonic flight it will have a low aspect ratio and high sweep, and for subsonic flight it rotates 90° to get a lower sweep angle and higher aspect ratio. The study also showed that this concept has the potential to largely remove, or at least strongly reduce the sonic boom strength.

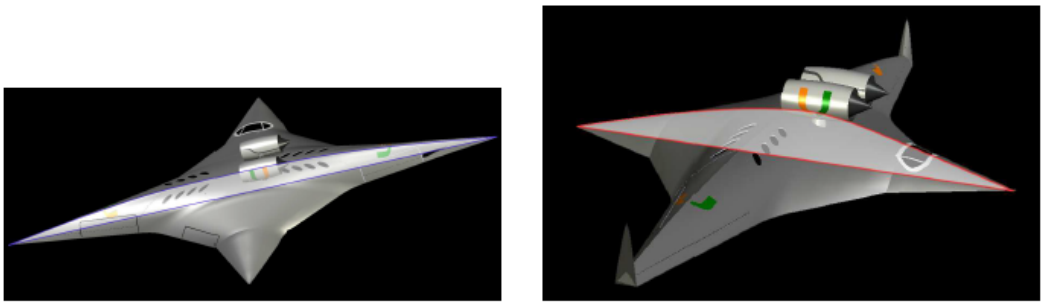

Figure H.3: Bi-directional flying wing moving from left to right (left image supersonic configuration with thin airfoil outlined, and right image in subsonic configuration with thick airfoil outlined) [210]

In conclusion, it can be stated that the oblique (and bi-directional) flying wing concepts are certainly interesting options for future supersonic transports, albeit more complex and challenging, in particular due to the relative lack of research performed and incompatibility with existing infrastructure.